

Application of Plasma Phenomena



Po-Yu Chang

Institute of Space and Plasma Sciences, National Cheng Kung University

Lecture 9

2024 spring semester

Tuesday 9:10-12:00

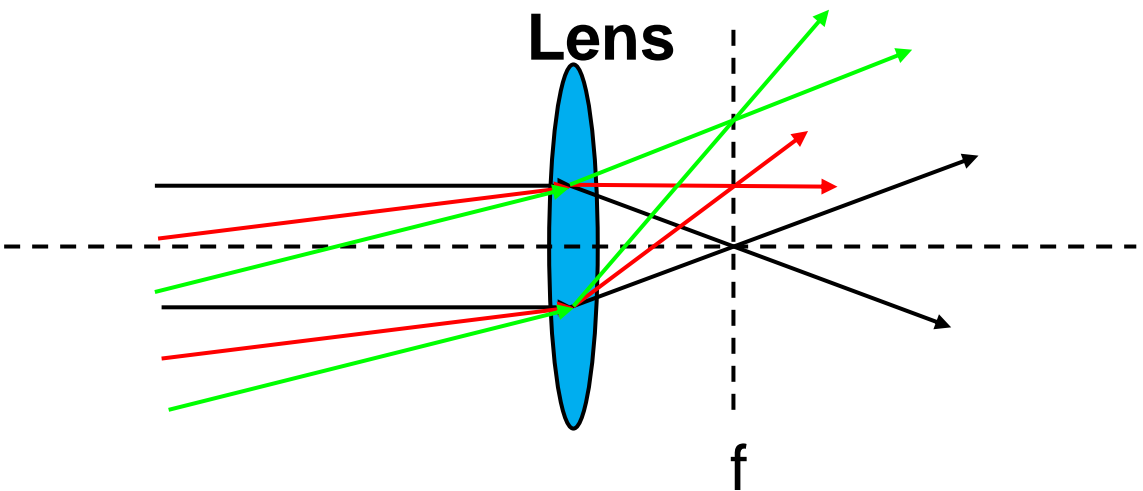
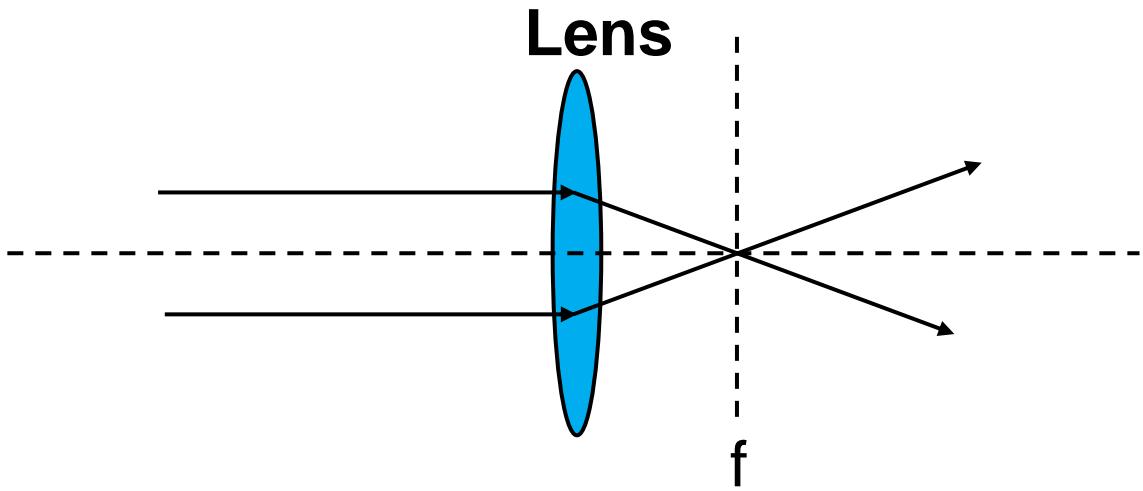
Materials:

<https://capst.ncku.edu.tw/PGS/index.php/teaching/>

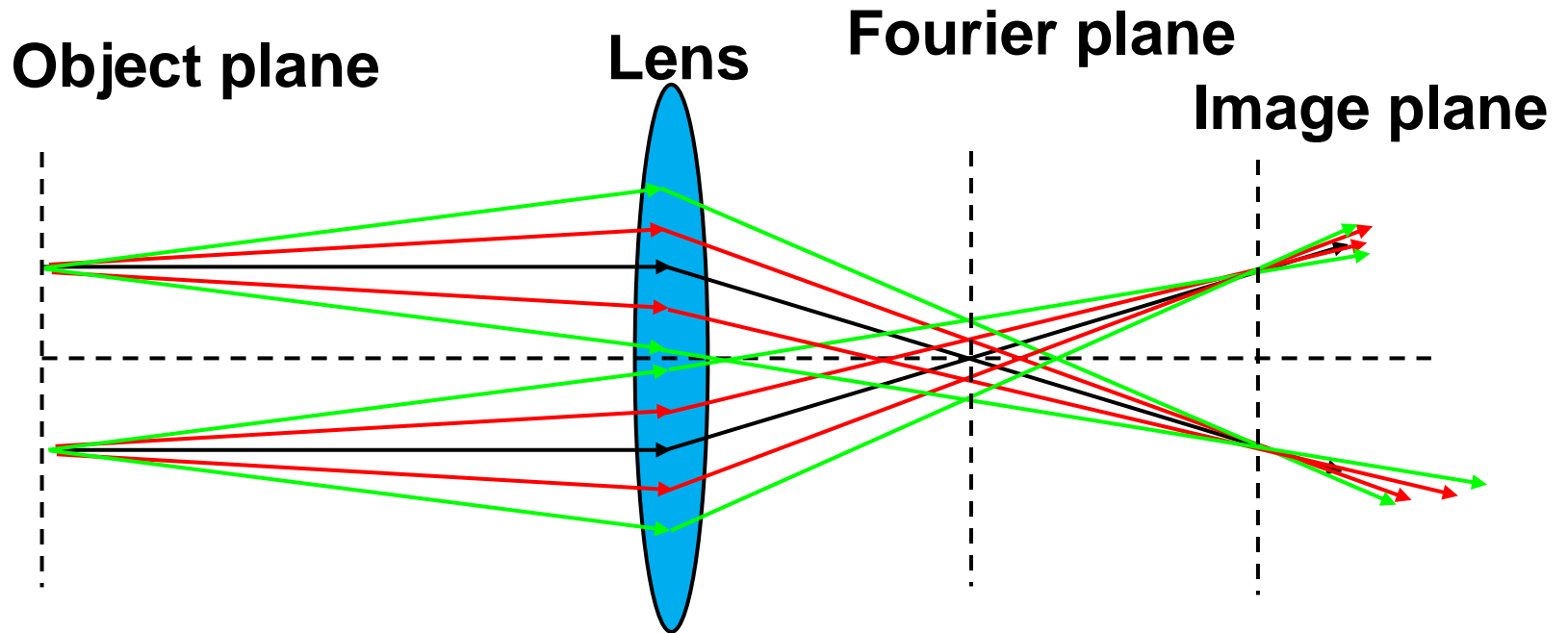
Online courses:

<https://nckucc.webex.com/nckucc/j.php?MTID=m4082f23c59af0571015416f6e58dd803>

Angular spectrum of plane waves can be used for diagnostic



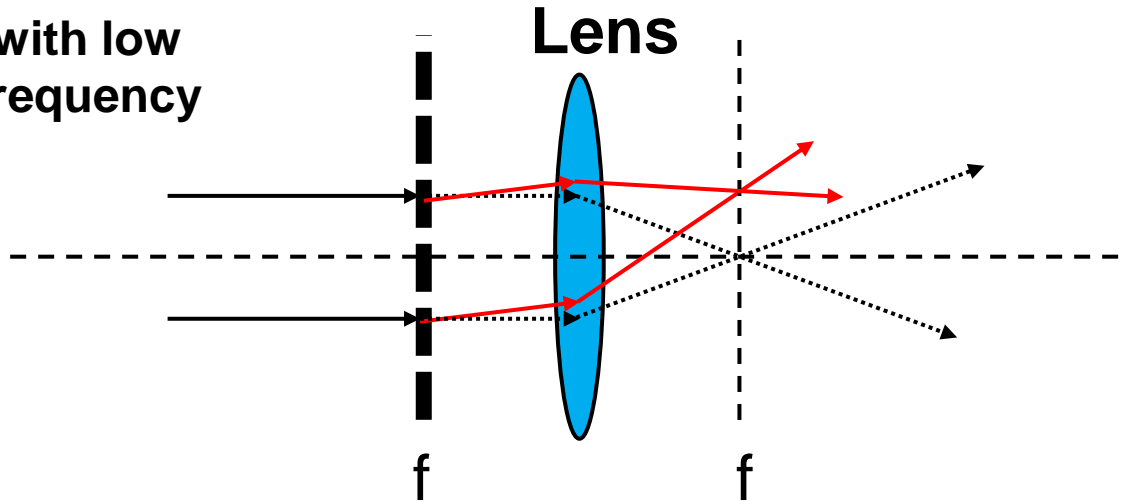
Rays with different angles go through different focal points on the focal points



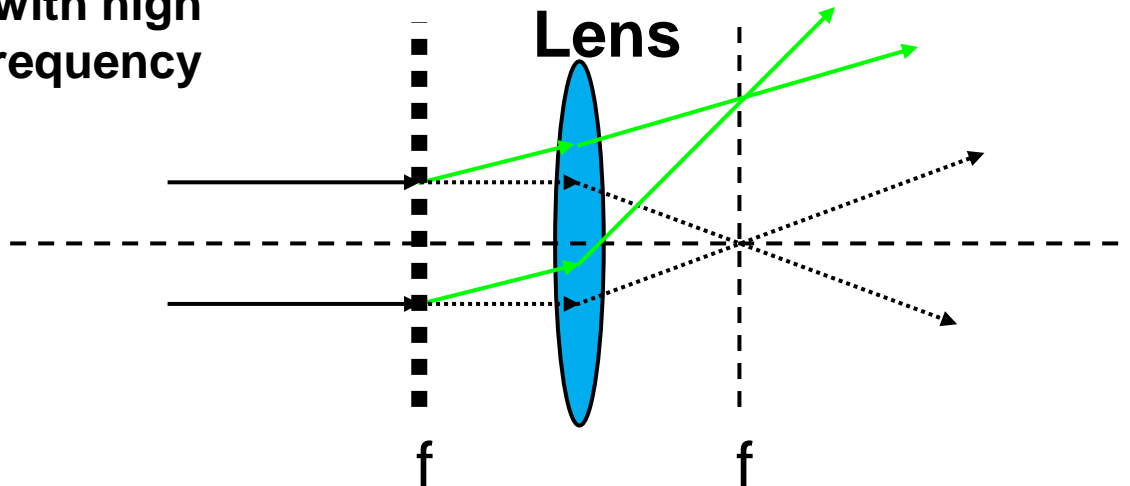
Parallel beams are deflected to different angles with grating with different spatial frequencies



- Grating with low spatial frequency



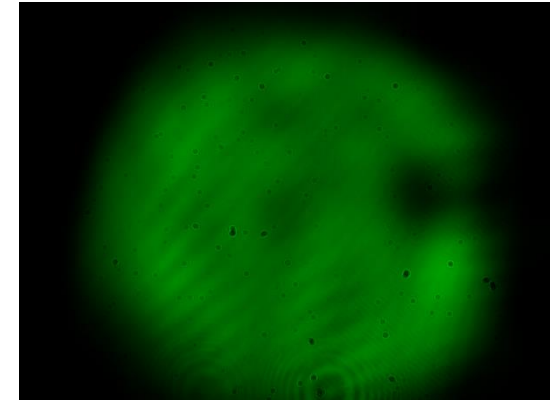
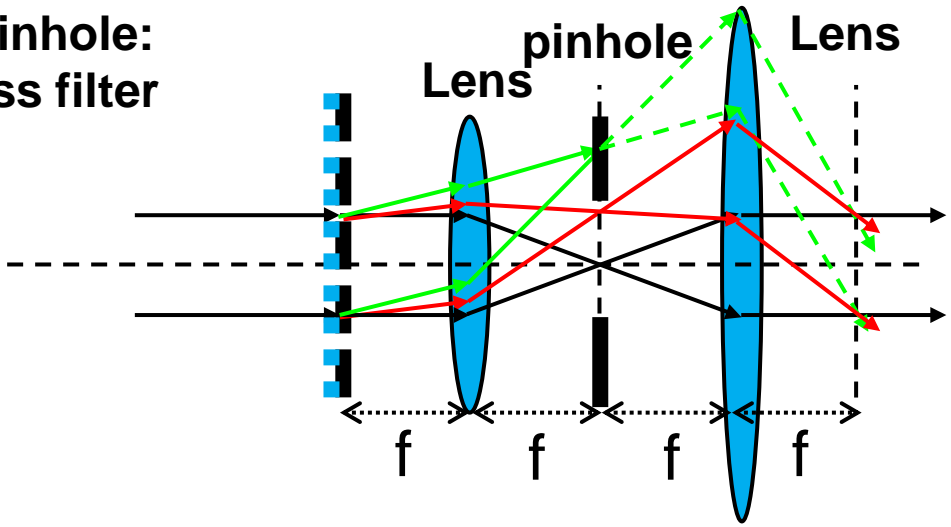
- Grating with high spatial frequency



A pinhole or a dot acts like a low-pass / high-pass filter

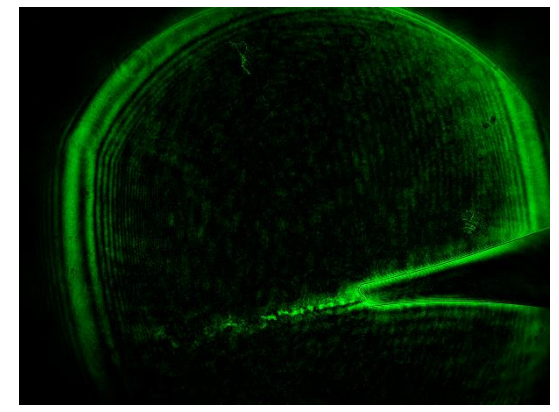
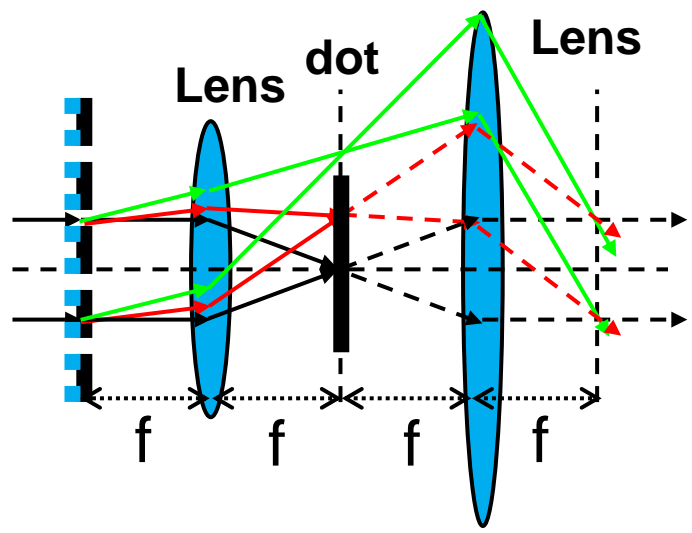
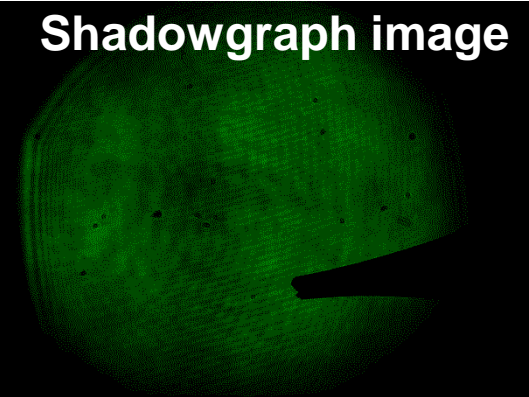


- Using pinhole:
Low-pass filter



- Using dot:
High-pass filter

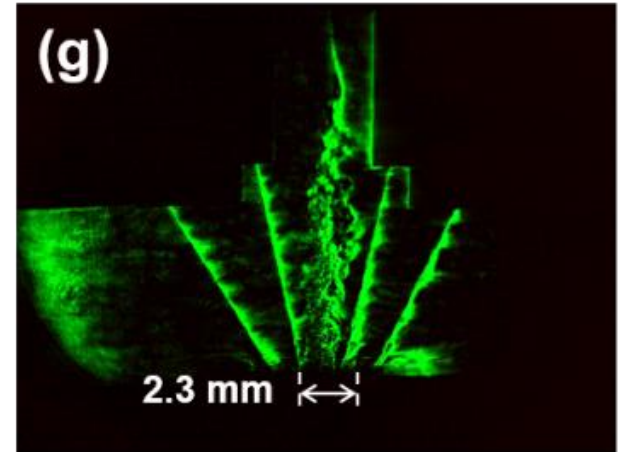
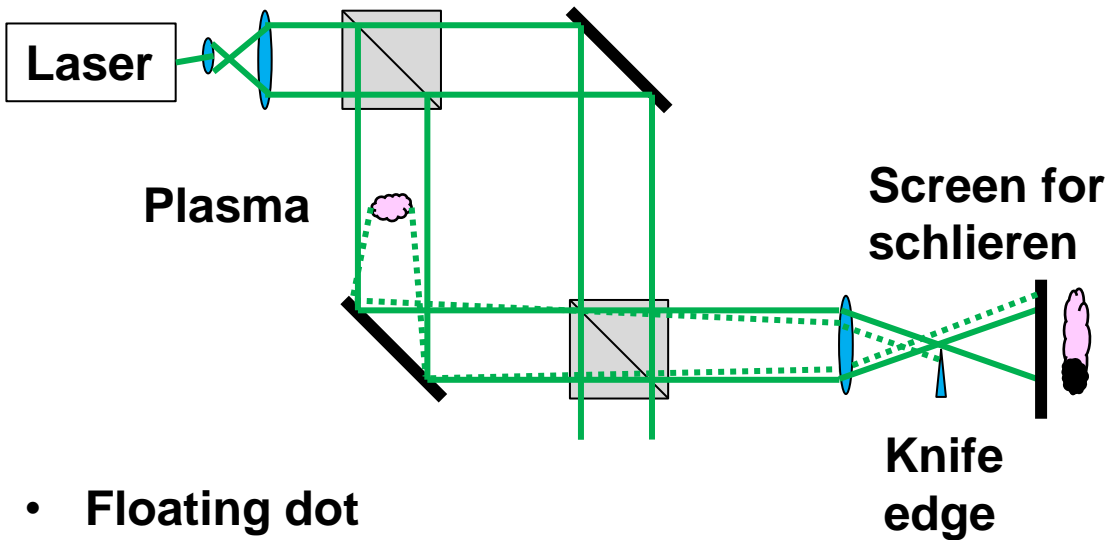
Shadowgraph image



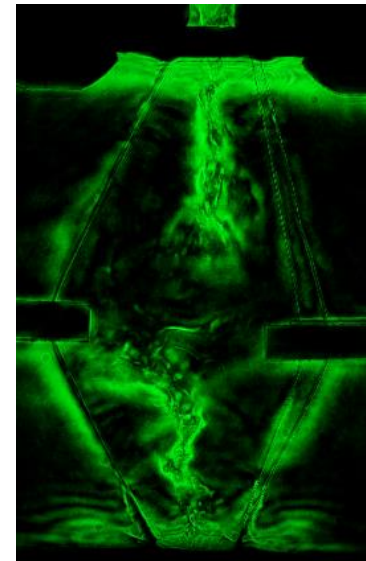
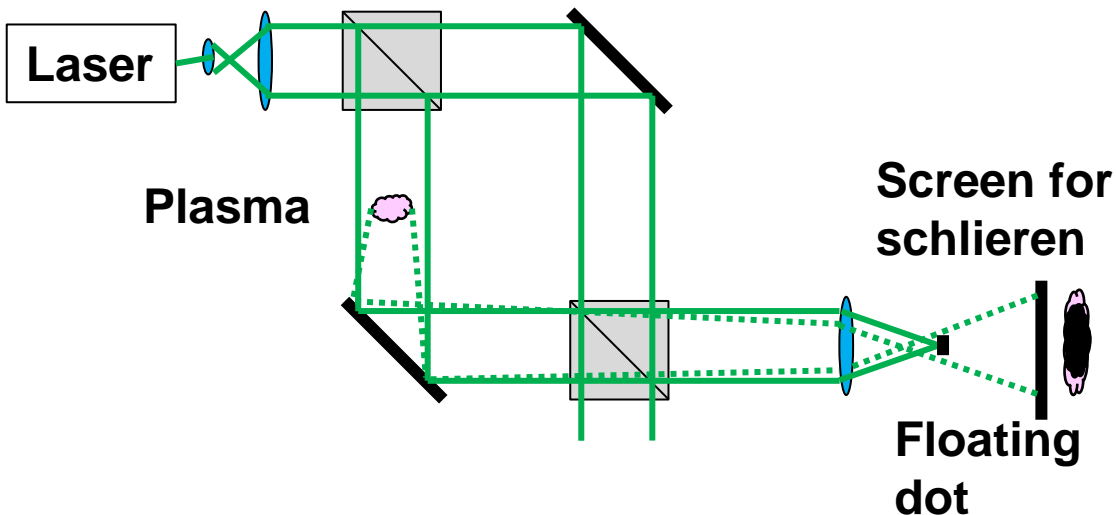
A symmetric Schlieren image can be obtained if the knife edge is replaced by a “floating dot”



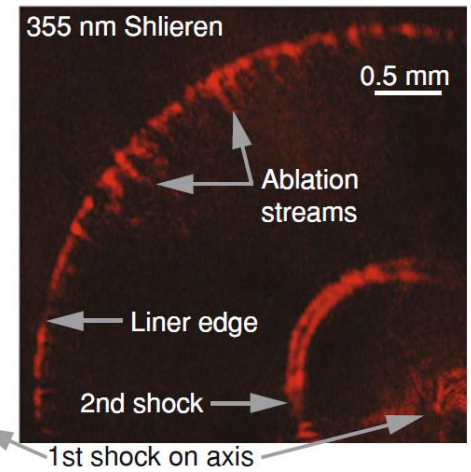
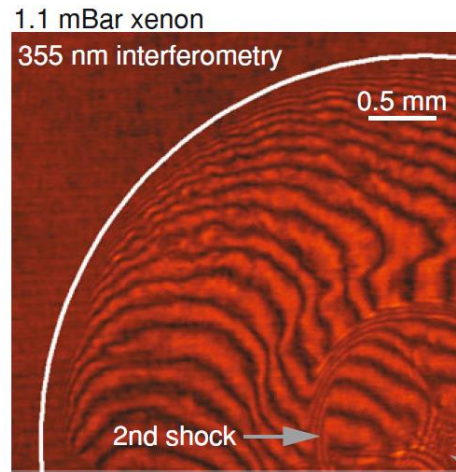
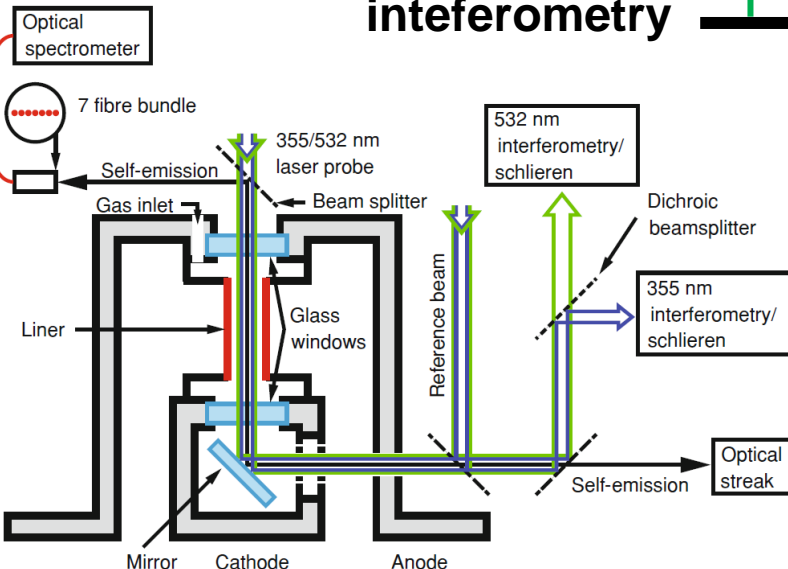
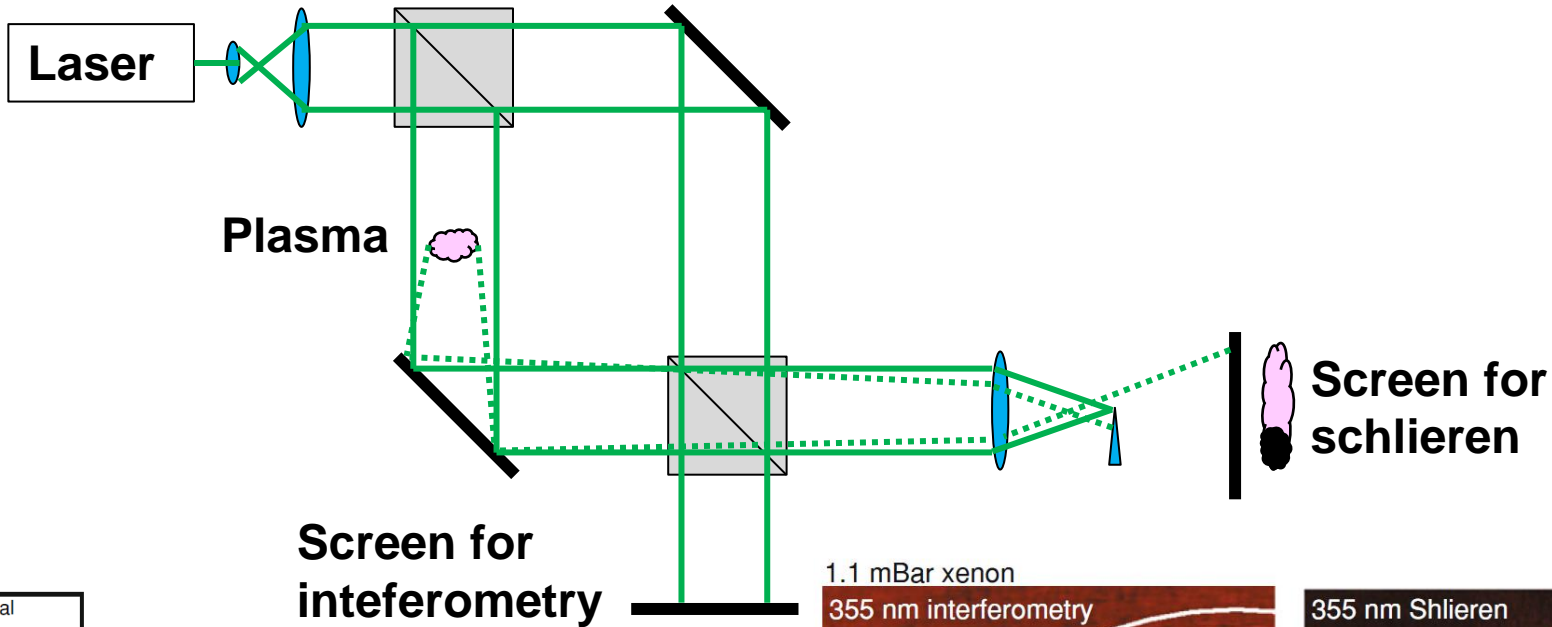
- Knife edge



- Floating dot

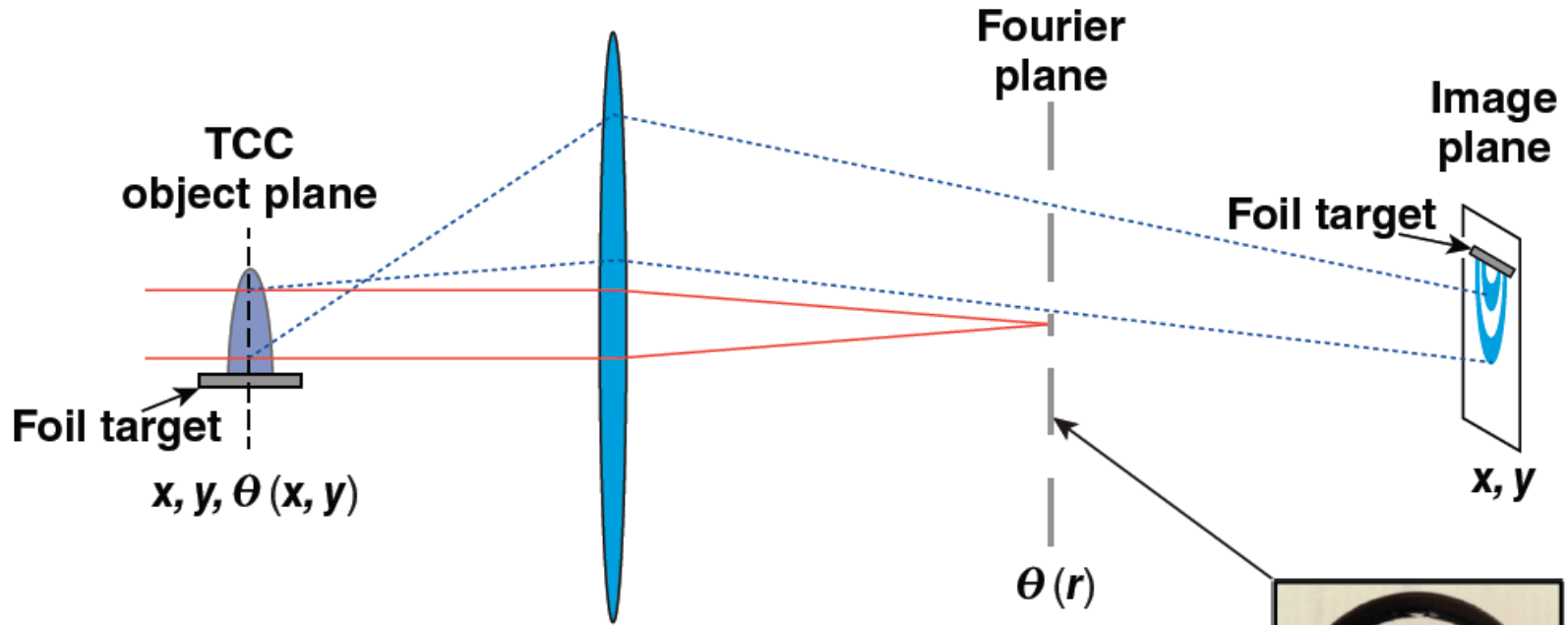


Schlieren imaging system can detect density gradient



G. C. Burdiak, Cylindrical liner z-pinch as drivers for converging strong shock experiments

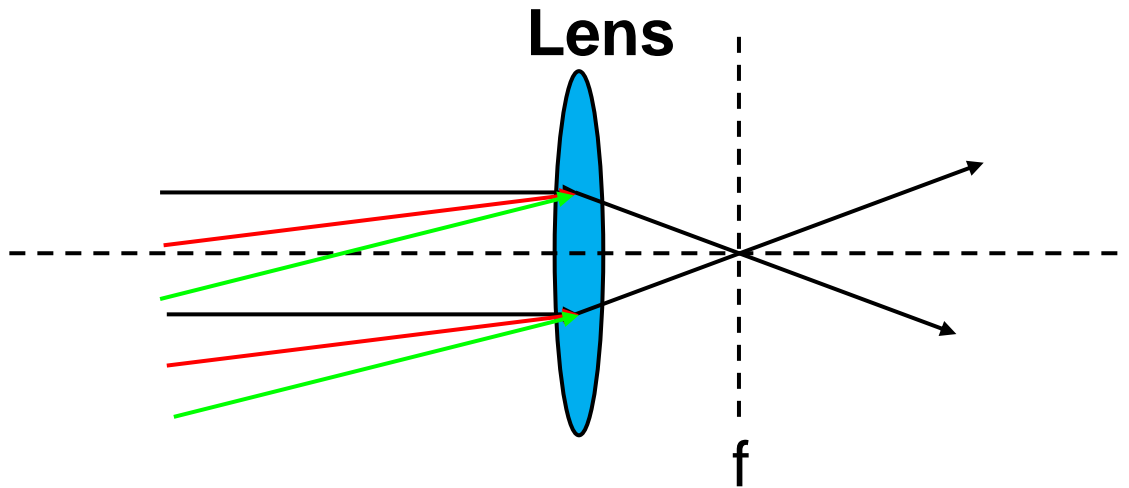
Angular filter refractometry (AFR) maps the refraction of the probe beam at TCC to contours in the image plane



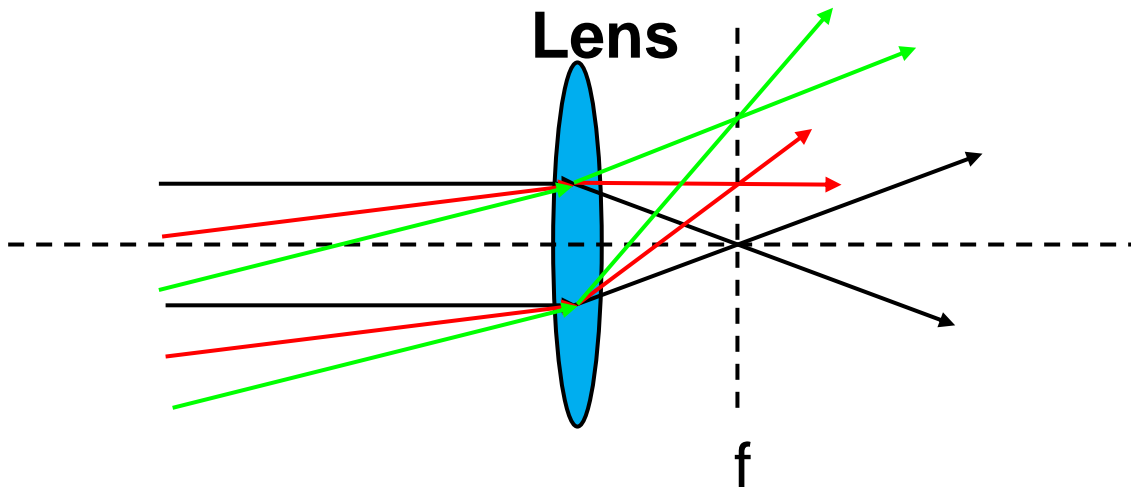
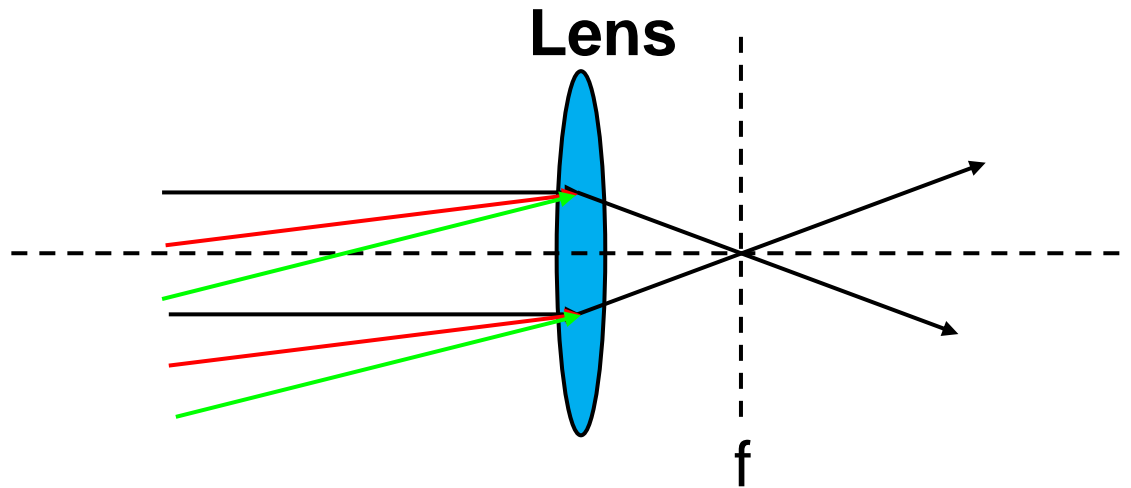
The edges of the rings map a certain refraction angle to the spatial location in the object plane.



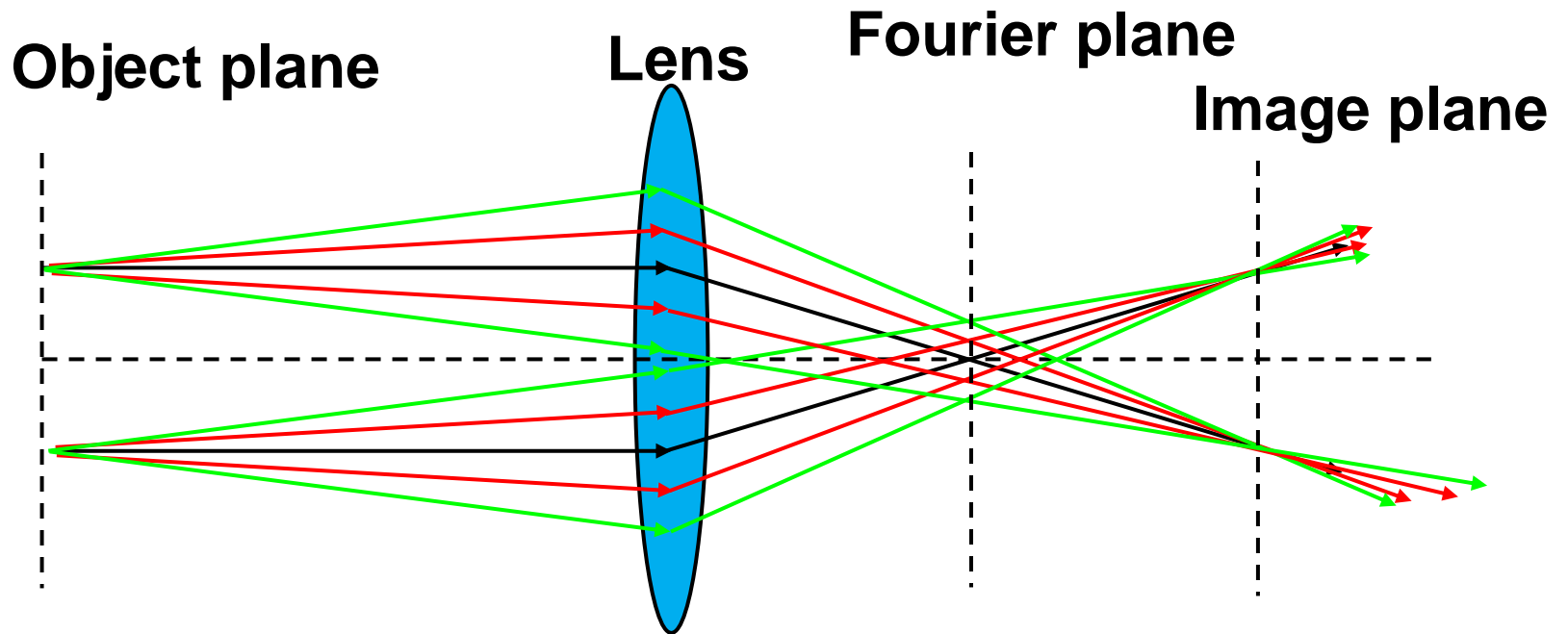
Angular spectrum of plane waves can be used for diagnostic



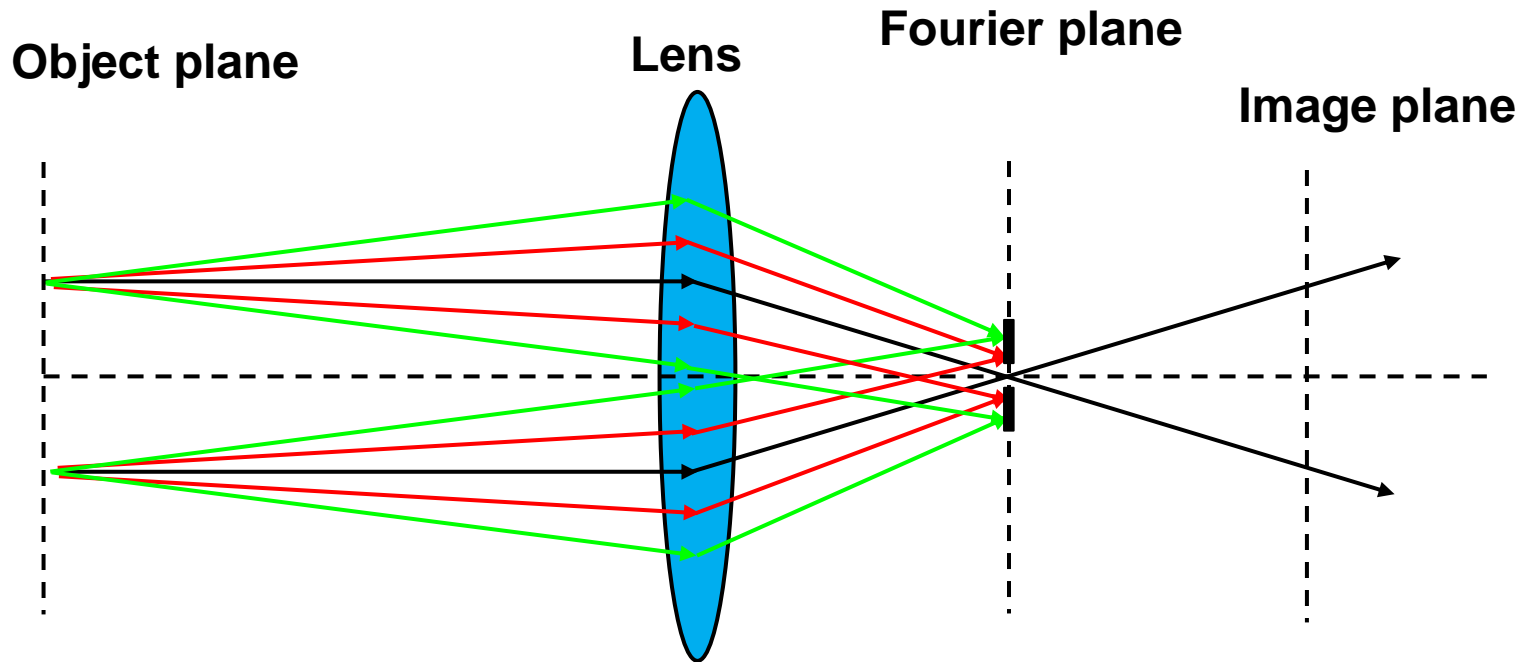
Angular spectrum of plane waves can be used for diagnostic



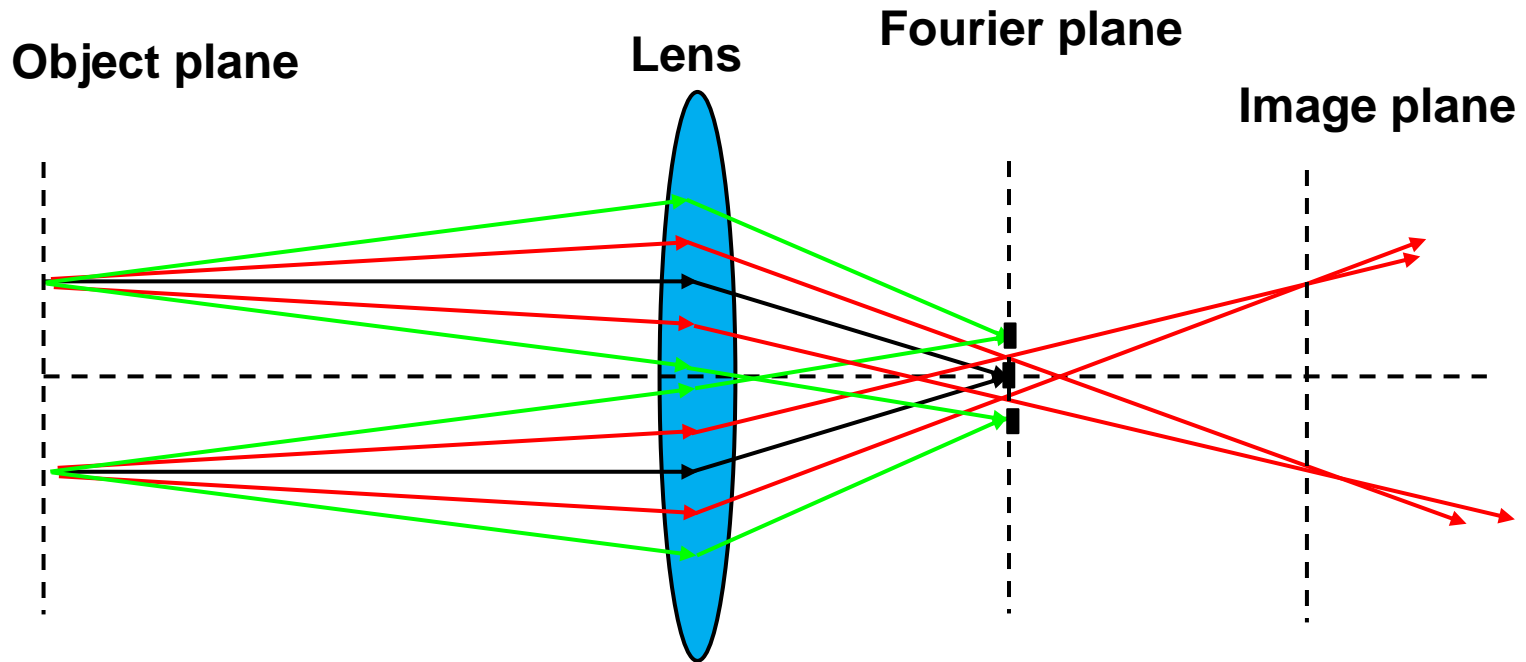
Rays with different angles go through different focal points on the focal points



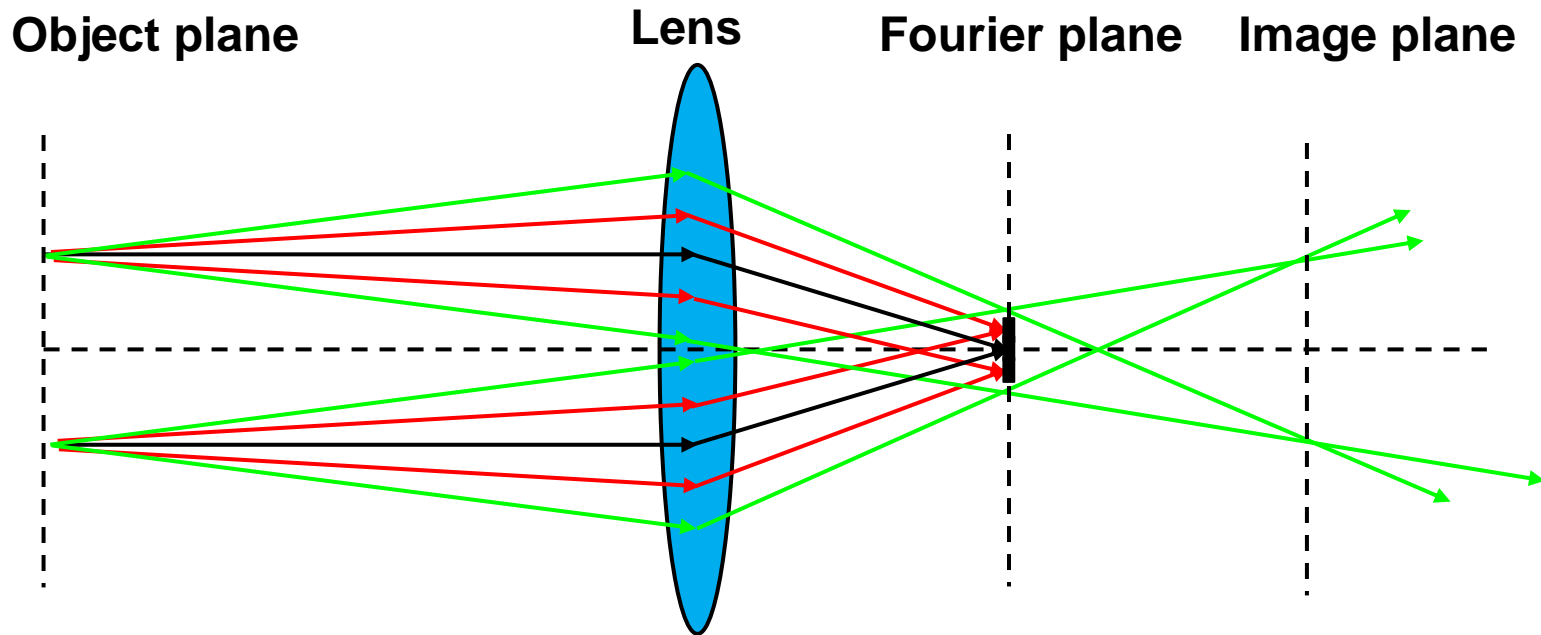
Rays with different angles can be selected by blocking different focal points



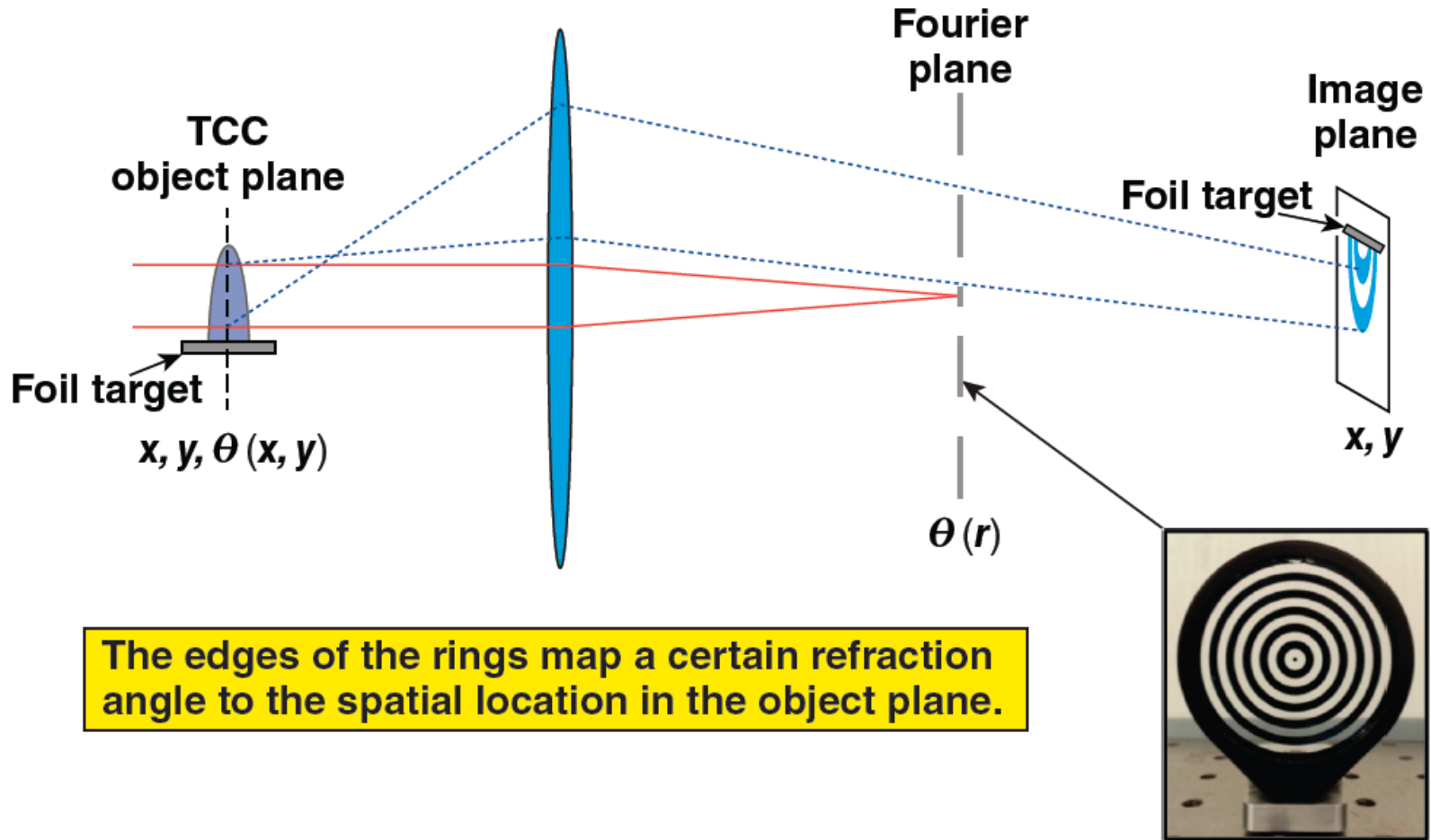
Rays with different angles go through different focal points on the focal points



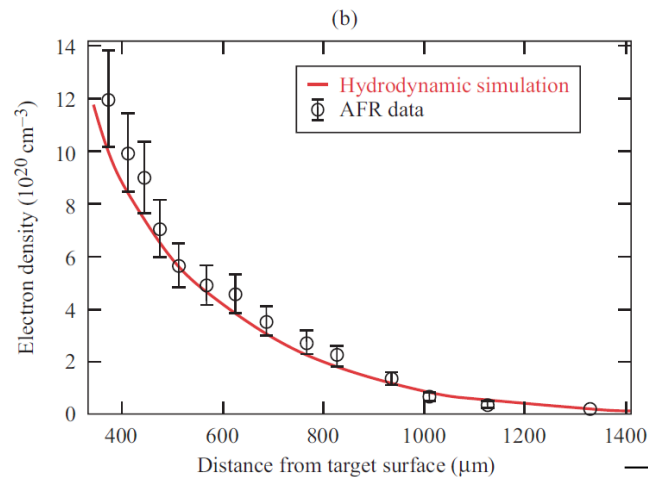
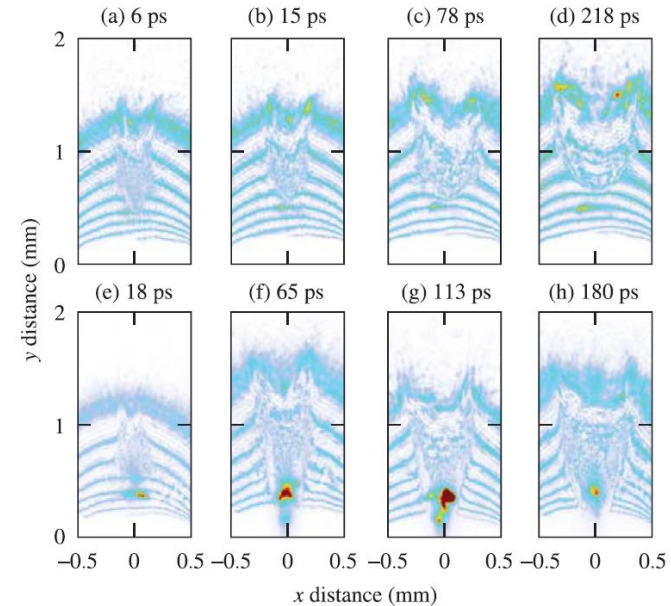
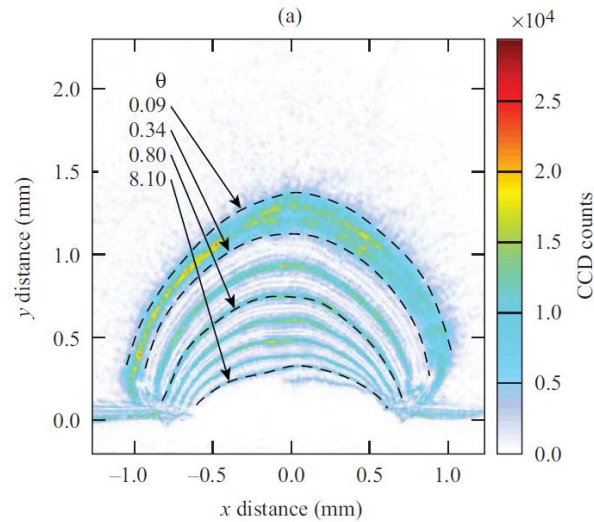
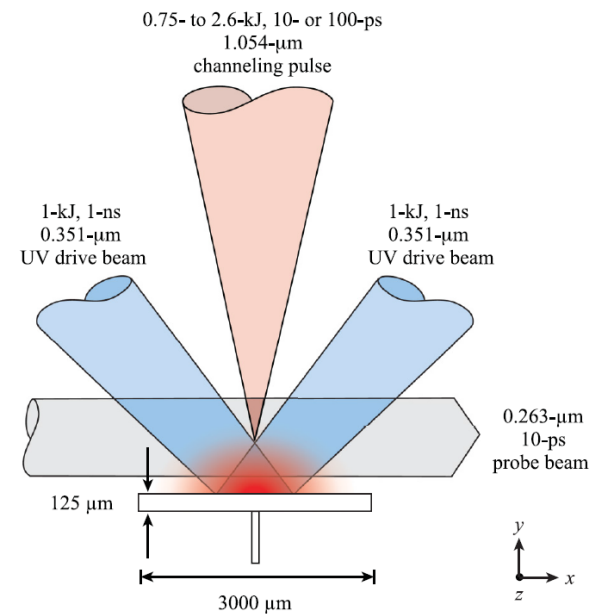
Rays with different angles go through different focal points on the focal points



Angular filter refractometry (AFR) maps the refraction of the probe beam at TCC to contours in the image plane



Channeling of multi-kilojoule high-intensity laser beams in an inhomogeneous plasma was observed using AFR



Electromagnetic wave can be used to measure the density or the magnetic field in the plasma



- Nonmagnetized isotropic plasma (interferometer needed):

$$n^2 = 1 - \frac{X(1-X)}{1 - X - \frac{1}{2}Y^2 \sin^2 \theta \pm \left[\left(\frac{1}{2}Y^2 \sin^2 \theta \right)^2 + (1-X)^2 Y^2 \cos^2 \theta \right]^{1/2}}$$

$$= 1 - X = 1 - \frac{\omega_p^2}{\omega^2} = 1 - \frac{n_e}{n_{cr}} \quad \left(Y \equiv \frac{\Omega}{\omega} \equiv 0 \right)$$

Note: $\omega_p^2 = \frac{n_e e^2}{\epsilon_0 m_e}$ $n_{cr} = \frac{\epsilon_0 m_e \omega^2}{e^2}$

- Magnetized isotropic plasma (Polarization detected needed):

Parallel to B_0

$$n^2 = 1 - \frac{\omega_p^2}{\omega(\omega \pm \Omega)} \quad \frac{E_x}{E_y} = \pm i \quad \Omega \equiv \frac{eB_0}{m_e}$$

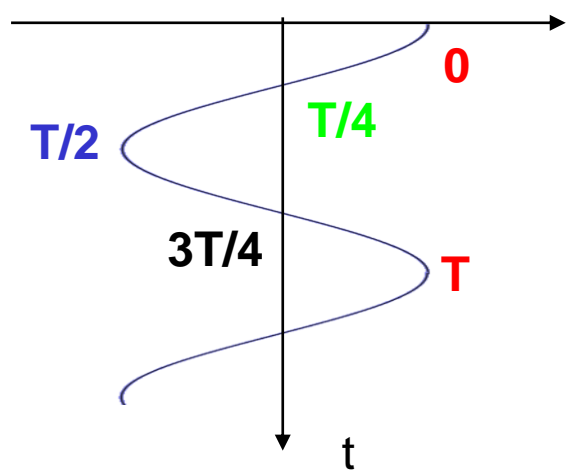
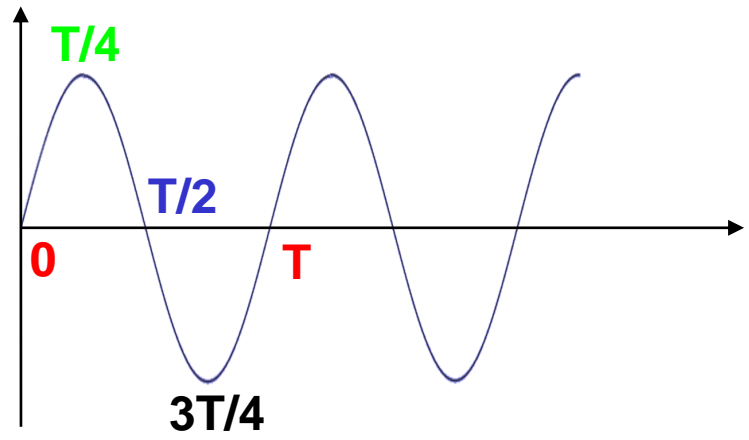
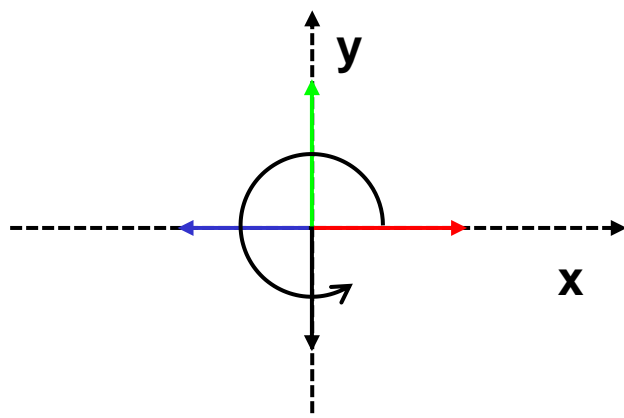
Faraday rotation: linear polarization rotation caused by the difference between the speed of LHC and RHC polarized wave.

Circular polarization



$$E_x = E_0 \exp(-i\omega t)$$

$$E_y = iE_x = iE_0 \exp(-i\omega t) = E_0 \exp\left(i\frac{\pi}{2}\right) \exp(-i\omega t) = E_0 \exp\left[-i\left(\omega t - \frac{\pi}{2}\right)\right]$$



Linear polarization rotates as the wave propagates with different speed in LHC and RHC polarization



$$\vec{E} = E_0 \hat{x} = \frac{E_0}{2} [(\hat{x} + i\hat{y}) + (\hat{x} - i\hat{y})] \quad \vec{E}(z) = \vec{E} \exp(i\phi) \quad \phi_R \neq \phi_L$$

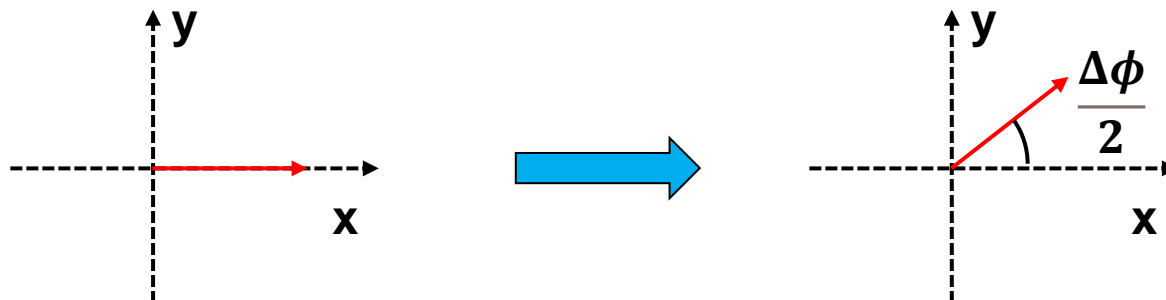
$$\vec{E}(z) = \frac{E_0}{2} [(\hat{x} + i\hat{y})e^{i\phi_R} + (\hat{x} - i\hat{y})e^{i\phi_L}] \quad \bar{\phi} \equiv \frac{\phi_R + \phi_L}{2} \quad \Delta\phi \equiv \frac{\phi_R - \phi_L}{2}$$

$$= \frac{E_0}{2} [\hat{x}(e^{i\phi_R} + e^{i\phi_L}) + \hat{y}i(e^{i\phi_R} - e^{i\phi_L})]$$

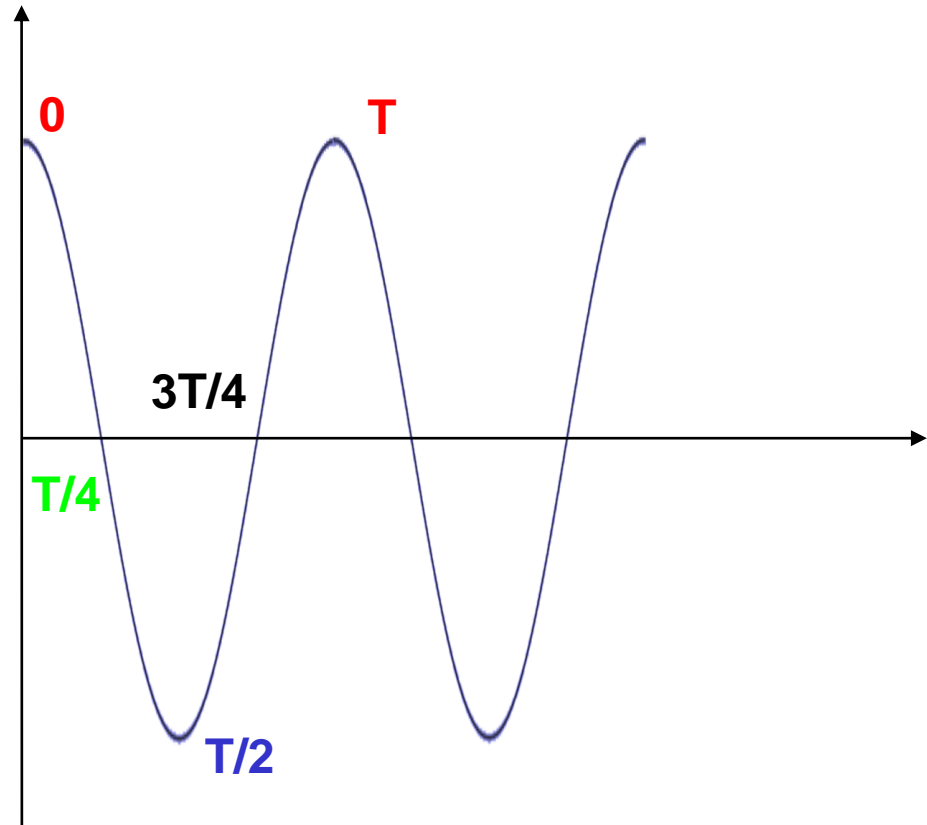
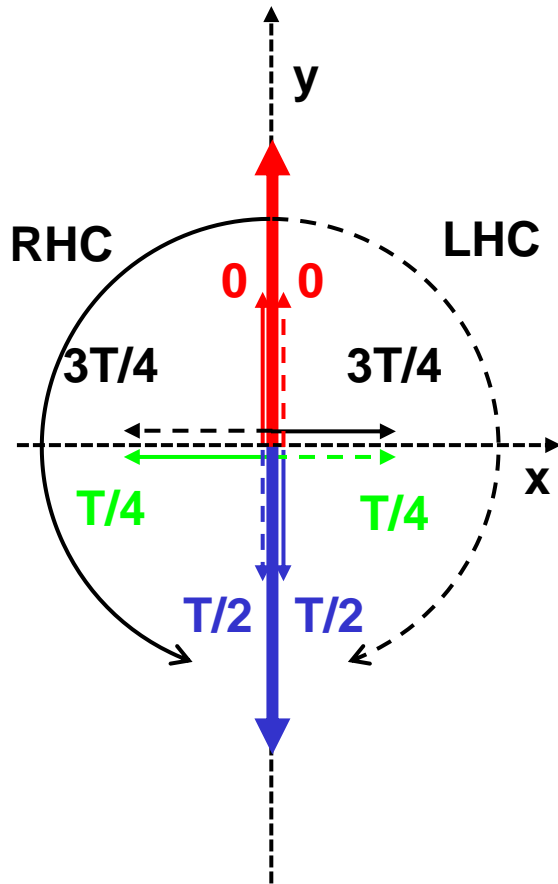
$$= \frac{E_0}{2} \left[\hat{x} \left(e^{i(\bar{\phi} + \frac{\Delta\phi}{2})} + e^{i(\bar{\phi} - \frac{\Delta\phi}{2})} \right) + \hat{y}i \left(e^{i(\bar{\phi} + \frac{\Delta\phi}{2})} - e^{i(\bar{\phi} - \frac{\Delta\phi}{2})} \right) \right]$$

$$= E_0 e^{i\bar{\phi}} \left[\hat{x} \left(\frac{e^{i\frac{\Delta\phi}{2}} + e^{-i\frac{\Delta\phi}{2}}}{2} \right) + \hat{y}i \left(\frac{e^{i\frac{\Delta\phi}{2}} - e^{-i\frac{\Delta\phi}{2}}}{2} \right) \right]$$

$$= E_0 e^{i\bar{\phi}} \left[\hat{x} \cos\left(\frac{\Delta\phi}{2}\right) + \hat{y} \sin\left(\frac{\Delta\phi}{2}\right) \right]$$



A linear polarized wave can be decomposed into one left-handed circular polarized wave and a right-handed circular polarized wave



The rotation angle of the polarization depends on the linear integral of magnetic field and electron density



$$\phi = \int k dl = \int n \frac{\omega}{c} dl \quad \alpha = \frac{\Delta\phi}{2} = \frac{\omega}{2c} \int (n_R - n_L) dl$$

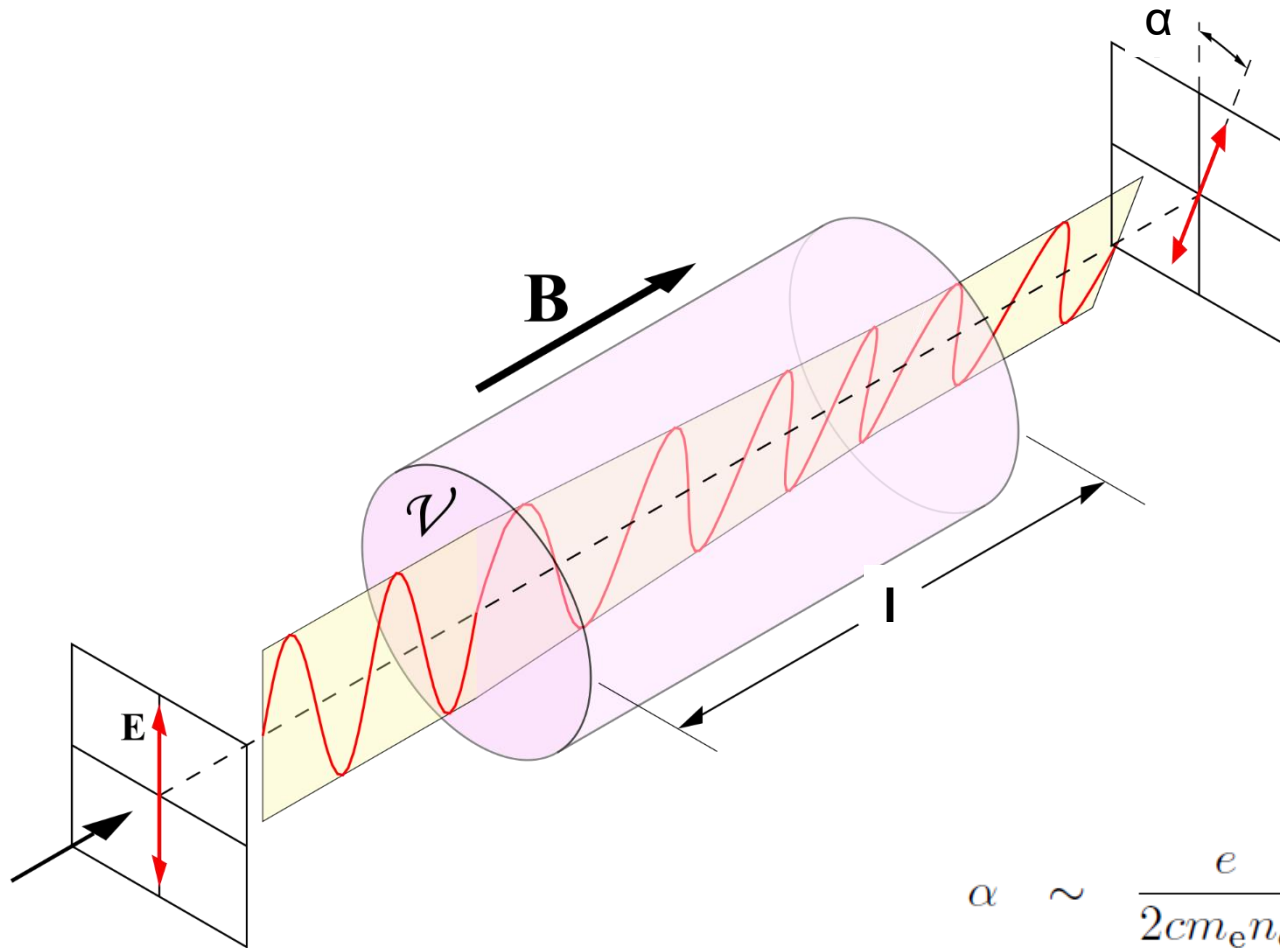
$$n_R = \sqrt{1 - \frac{X}{1+Y}} \sim 1 - \frac{1}{2} \frac{X}{1+Y} \quad X, Y \ll 1$$

$$n_L \sim 1 - \frac{1}{2} \frac{X}{1-Y} \quad \frac{X}{1 \pm Y} \ll 1$$

$$n_R - n_L \sim \frac{X}{2} \left(\frac{1}{1-Y} - \frac{1}{1+Y} \right) = \frac{XY}{1-Y^2} \sim XY$$

$$\begin{aligned} \alpha &\sim \frac{\omega}{2c} \int XY dl = \frac{\omega}{2c} \int \frac{\omega_p^2}{\omega^2} \frac{\Omega}{\omega} dl = \frac{1}{2c} \int \frac{n_e}{n_{cr}} \frac{eB}{m_e} dl \\ &= \frac{e}{2cm_e n_{cr}} \int n_e B dl \end{aligned}$$

The rotation angle of the polarization depends on the linear integral of magnetic field and electron density



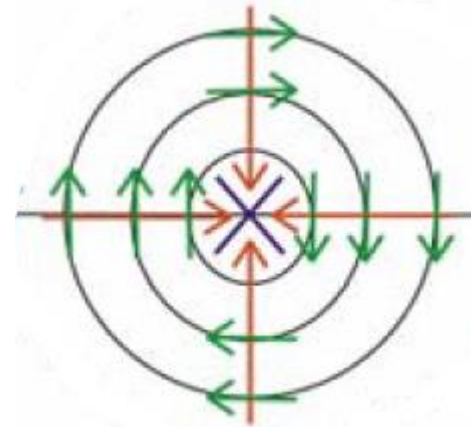
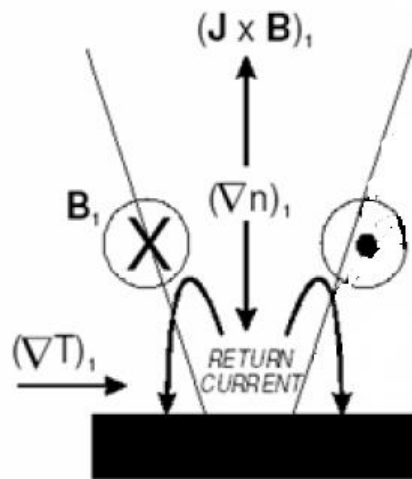
$$\alpha \sim \frac{e}{2cm_e n_{cr}} \int n_e B dl$$

Magnetic field can be generated when the temperature and density gradients are not parallel to each other



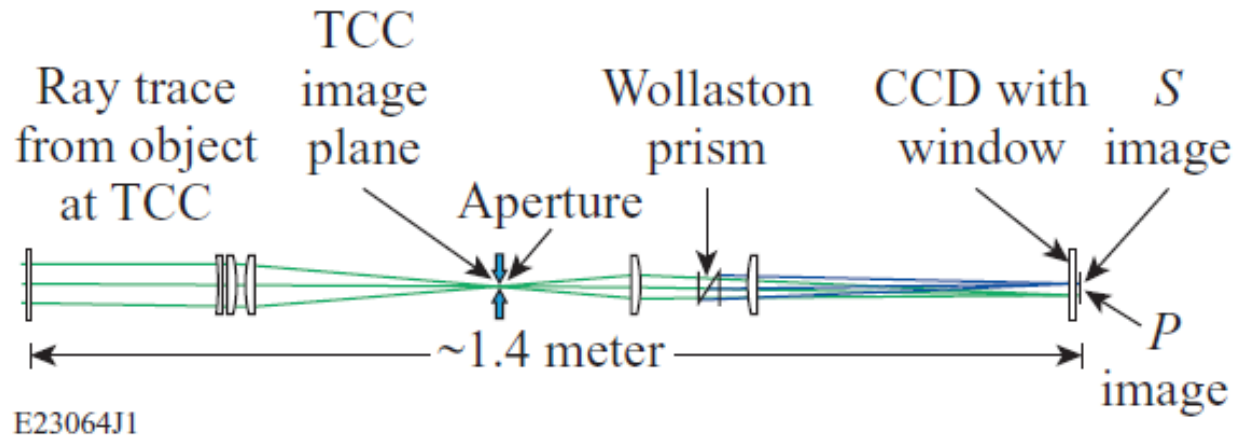
$$\frac{\partial \vec{B}}{\partial t} = \nabla \times \left[\underbrace{\vec{u} \times \vec{B}}_{\text{Convection term}} + \underbrace{\frac{1}{\sigma \mu_0} \nabla \times \vec{B}}_{\text{Diffusion term}} + \underbrace{\frac{\nabla p_e}{n_e e}}_{\text{self generated field}} - \underbrace{\frac{1}{\mu_0} \left(\frac{\nabla \times \vec{B}}{n_e e} \times \vec{B} \right)}_{\text{Hall term}} \right]$$

$$\nabla \times \frac{\nabla p_e}{n_e e} = - \frac{k_B}{e} \frac{\nabla n_e \times \nabla T_e}{n_e}$$

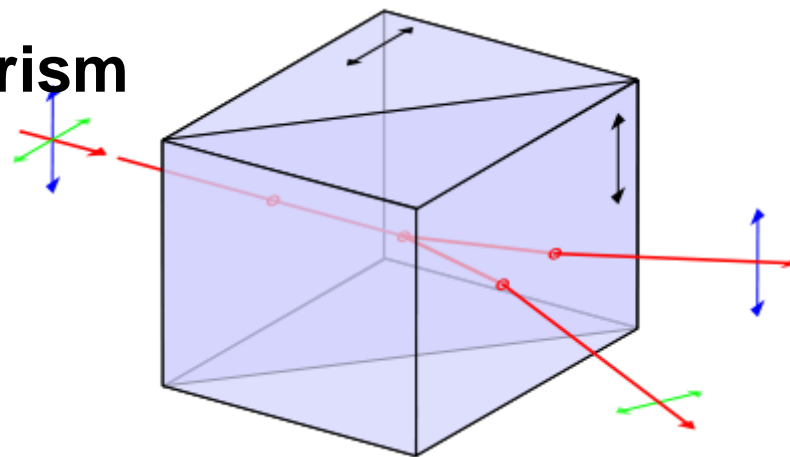


$$(\text{grad } n_e) \times (\text{grad } T_e) \longrightarrow \text{B field} \longrightarrow$$

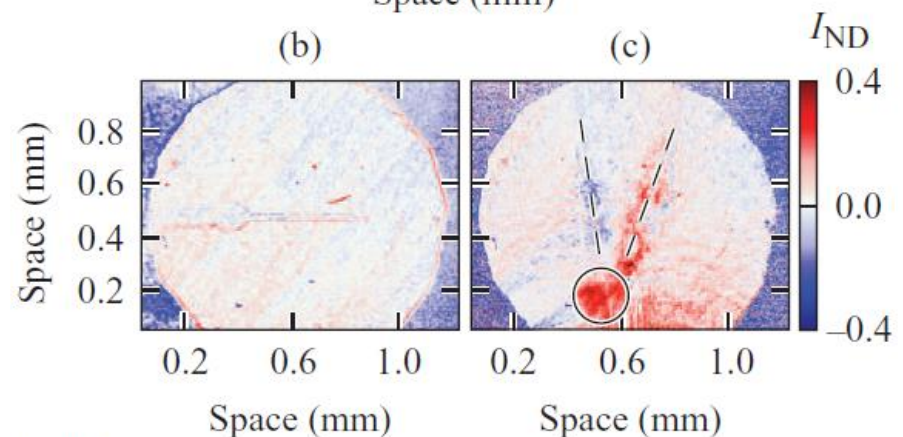
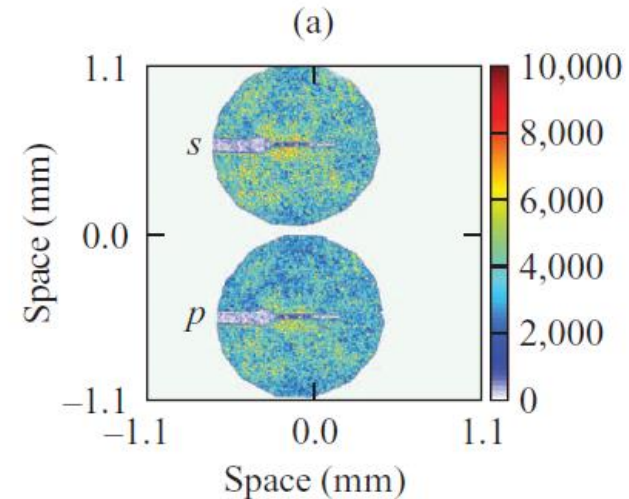
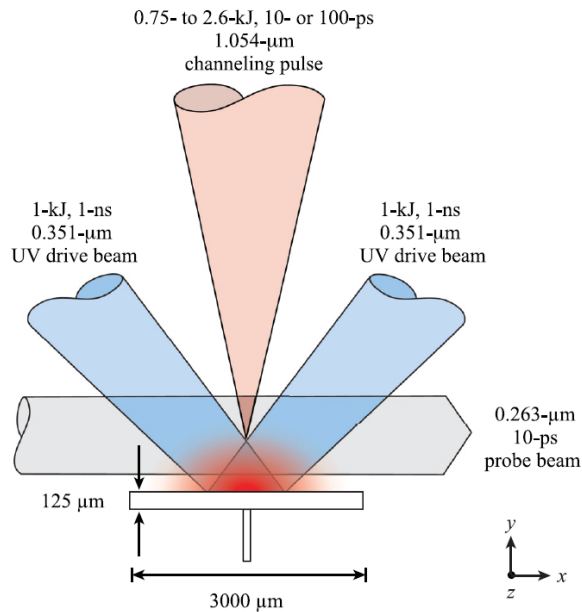
Polarimetry diagnostic can be used to measure the magnetic field



Wollaston prism

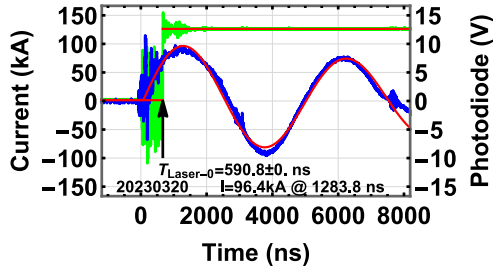


Self-generated field was suggested when multi-kilojoule high-intensity laser beams illuminated on an inhomogeneous plasma

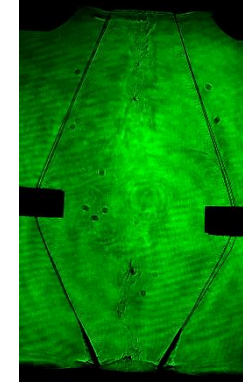
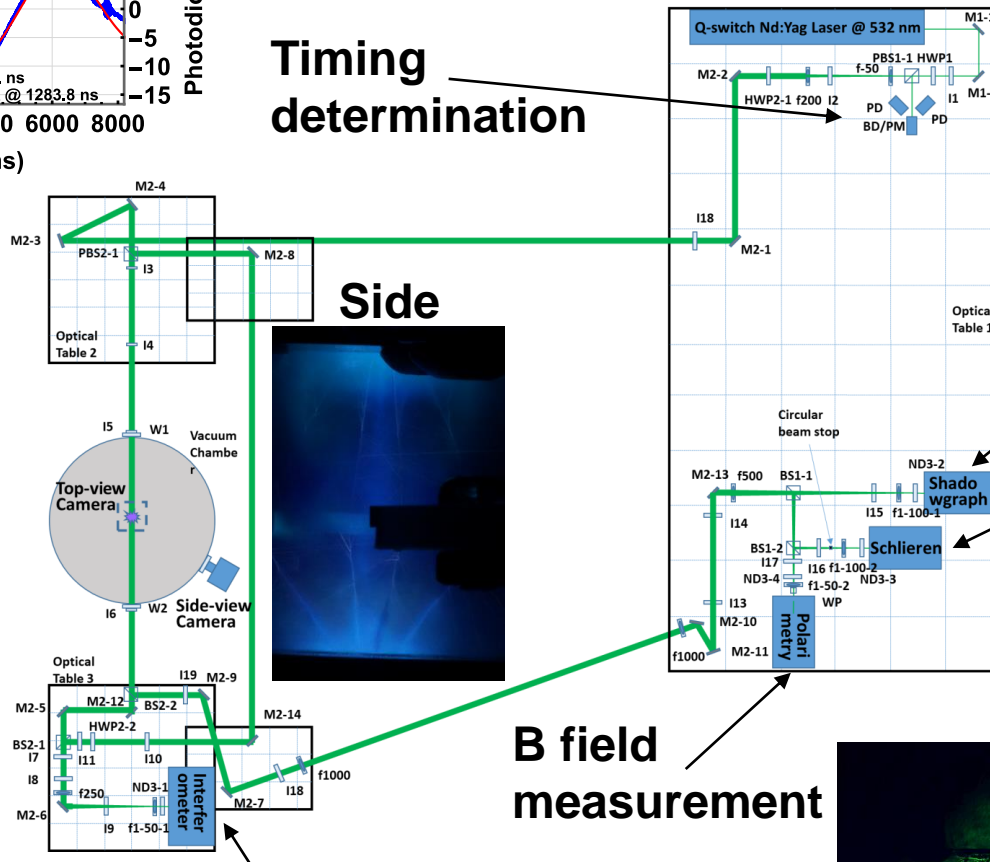


E23066J1

Time-resolved imaging system with temporal resolution in the order of nanoseconds was implemented

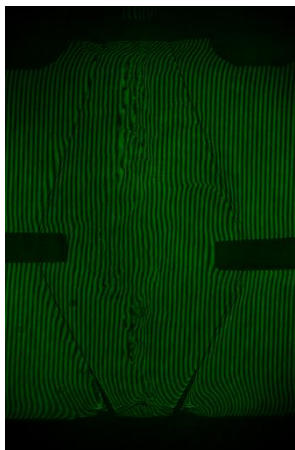
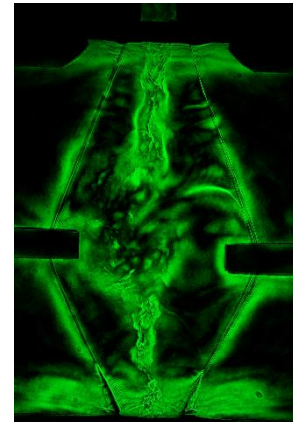


Timing determination

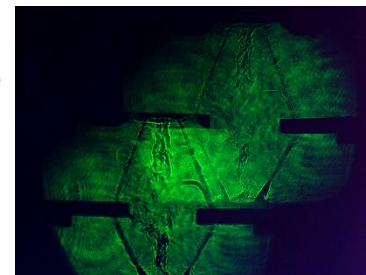


Plasma image

Plasma edge detection

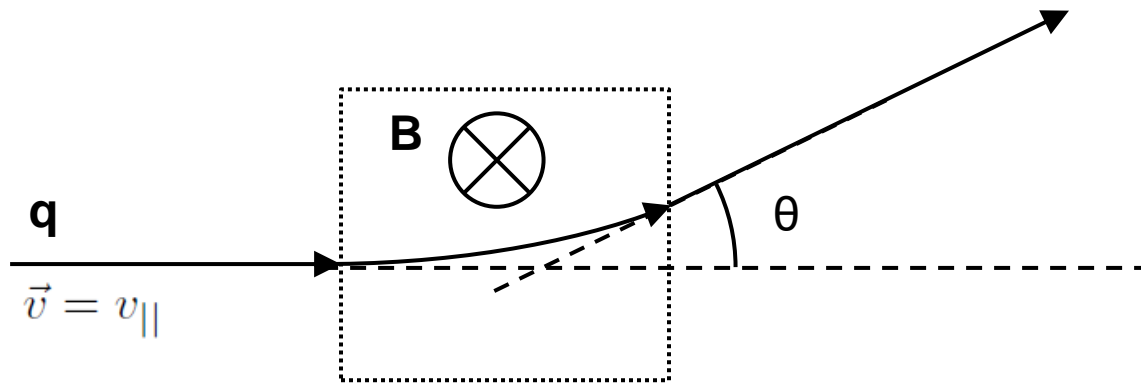


Density measurement



B field measurement

The magnetic field can be measured by measuring the deflected angle of charged particles

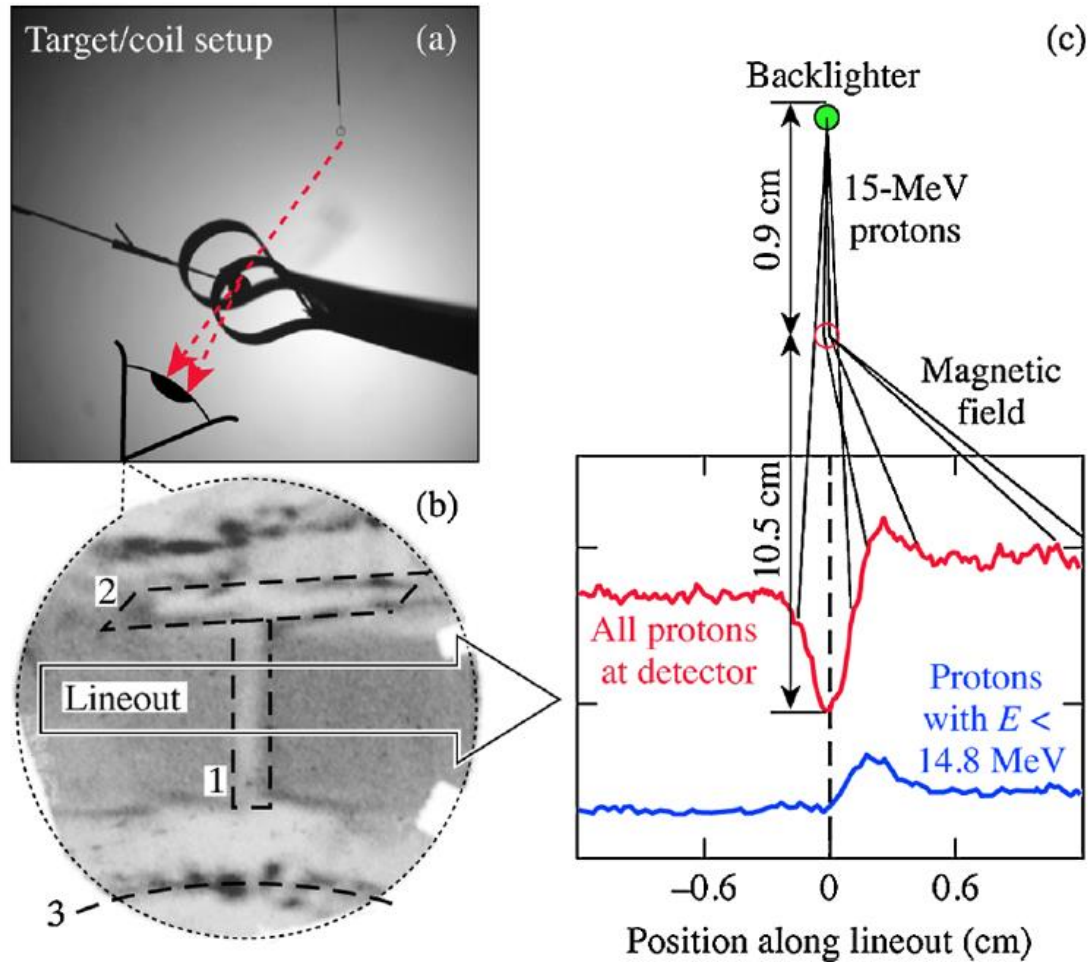


$$F_{\perp} = q\vec{v} \times \vec{B} = qv_{\parallel}B = m\frac{dv_{\perp}}{dt}$$

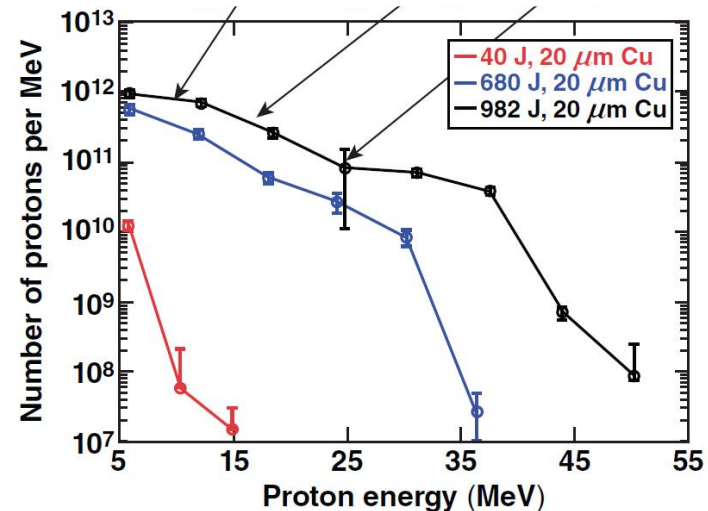
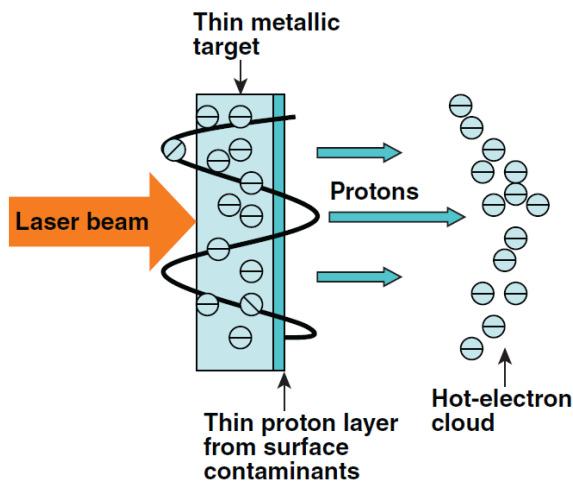
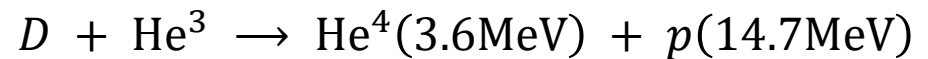
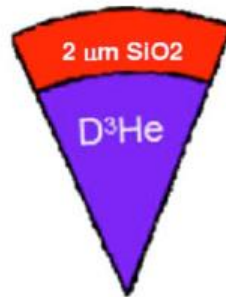
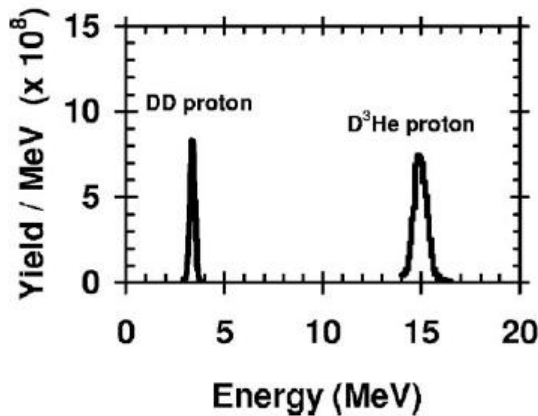
$$v_{\perp} = \int \frac{qv_{\parallel}B}{m} dt = \frac{qv_{\parallel}}{m} \int B dt \frac{dx}{dx} = \frac{qv_{\parallel}}{m} \int \frac{B}{v_{\parallel}} dx = \frac{q}{m} \int B dx$$

$$\tan \theta = \frac{v_{\perp}}{v_{\parallel}} = \frac{q}{mv_{\parallel}} \int B dx = \frac{q}{\sqrt{2mE}} \int B dx \quad \int B dx = \frac{\sqrt{2mE}}{q} \tan \theta$$

Magnetic field was measured using protons



Protons can be generated from fusion product or copper foil illuminated by short pulse laser



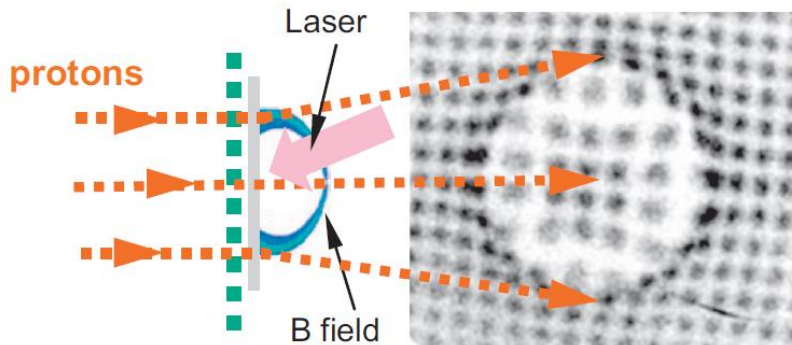
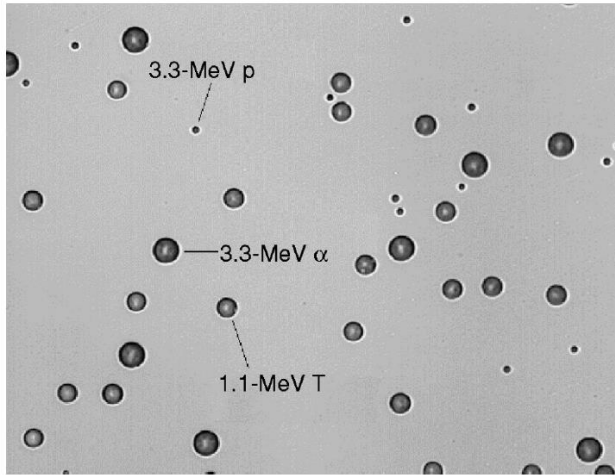
Target normal sheath acceleration (TNSA)

C. K. Li *et al.*, Rev. Sci. Instrum. **77**, 10E725 (2006)
L. Gao, PhD Thesis

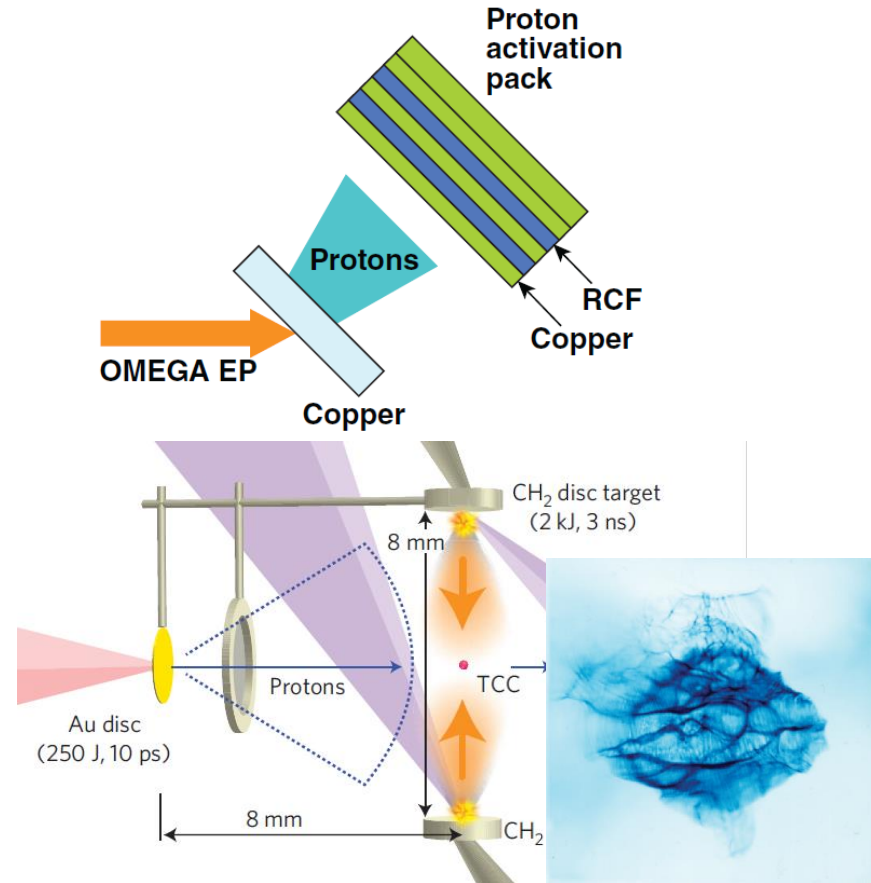
Protons can leave tracks on CR39 or film



CR 39



Radiochromic film pack



F. H. Seguin *et al.*, *Rev. Sci. Instrum.* **74**, 975 (2003)

C. K. Li *et al.*, *Phys. Plasmas* **16**, 056304 (2009)

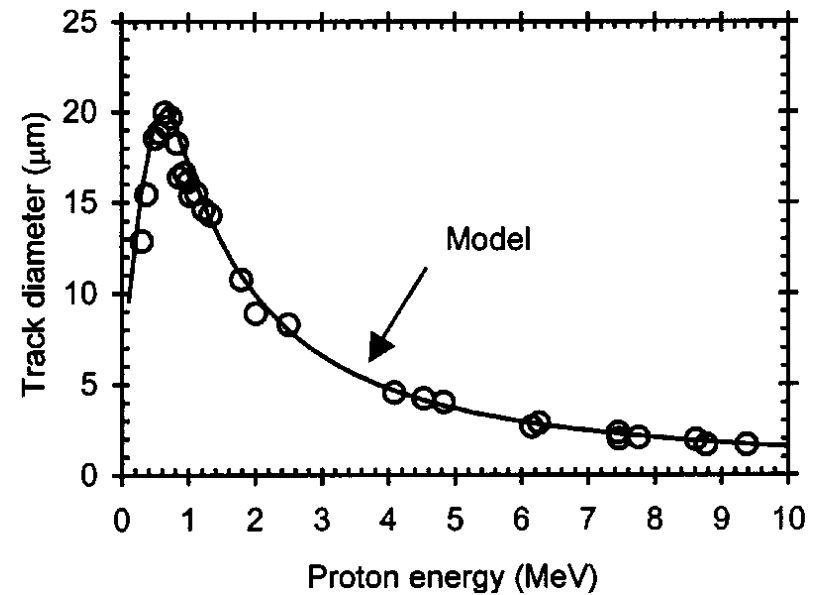
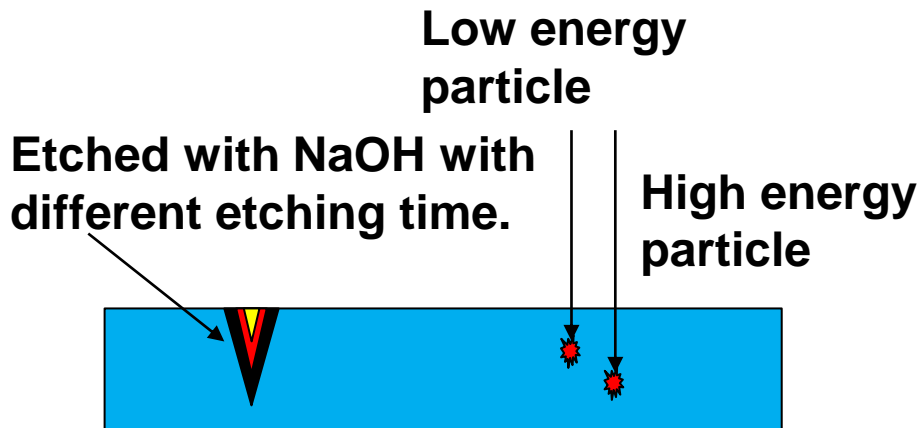
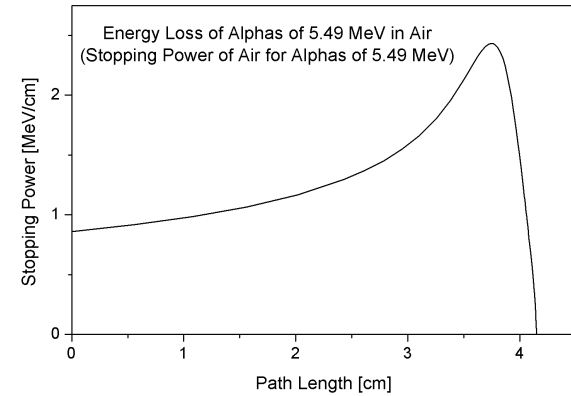
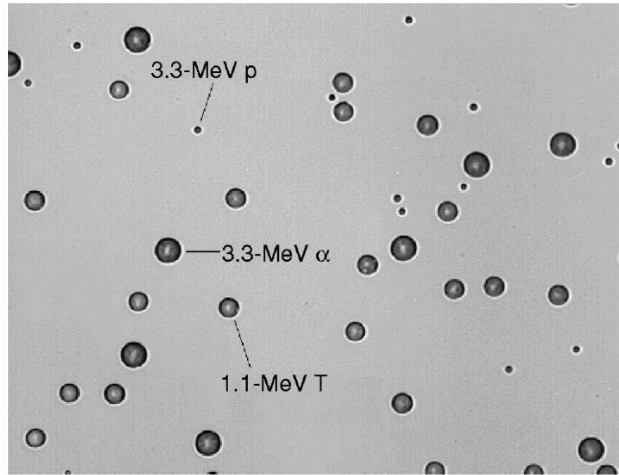
L. Gao, PhD Thesis

N. L. Kugland *et al.*, *Nature Phys.* **8**, 809 (2012)

Track diameter on the CR39 is depended on the particle energy that incidents



CR 39



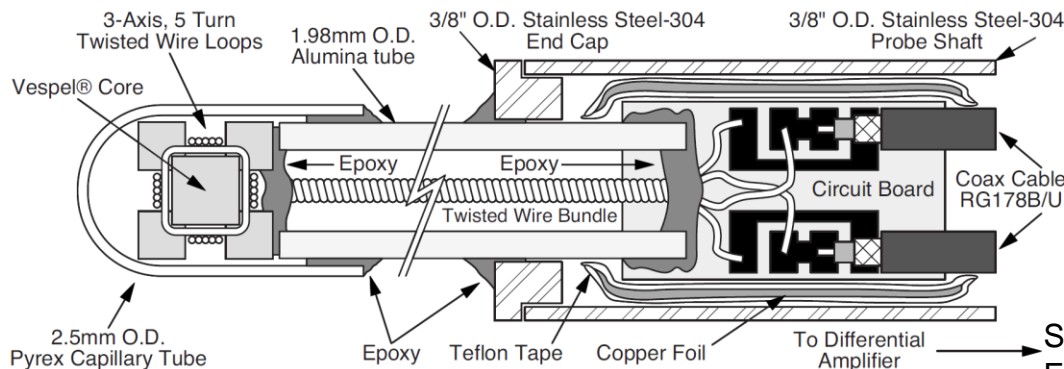
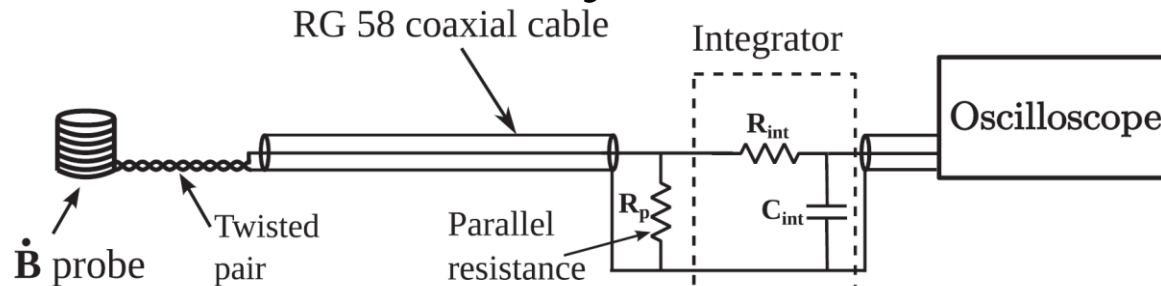
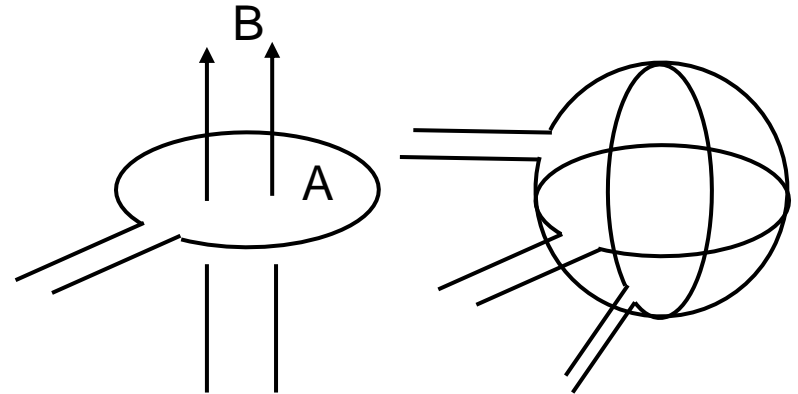
Time dependent magnetic field can be measured using B-dot probe



$$\vec{B} = \vec{B}(t) \quad \nabla \times \vec{E} = -\frac{\partial \vec{B}}{\partial t}$$

$$\int d\vec{A} \nabla \times \vec{E} = \oint \vec{E} d\vec{l} = V = -\int d\vec{A} \frac{\partial \vec{B}}{\partial t}$$

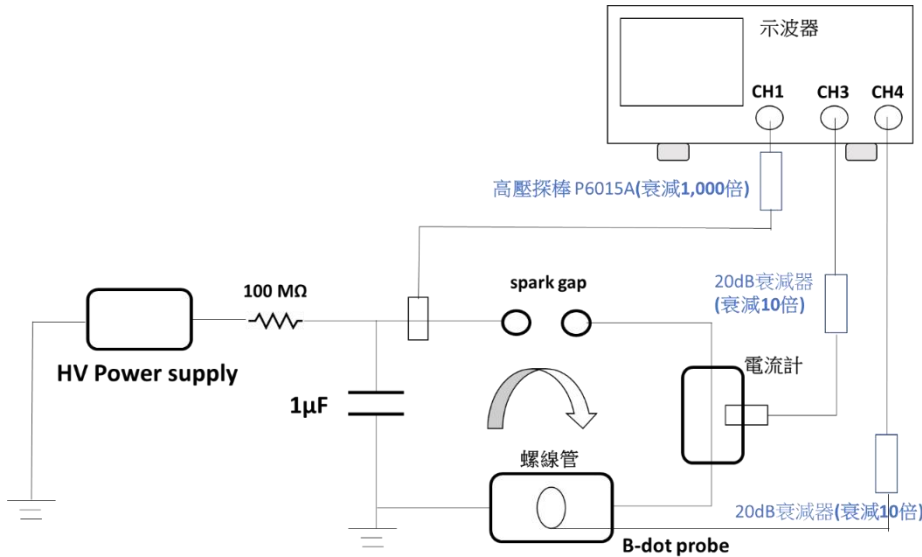
$$V \sim -A \frac{\partial B}{\partial t} \quad B = -\int \frac{V}{A} dt \sim -\frac{1}{A} \int V dt$$



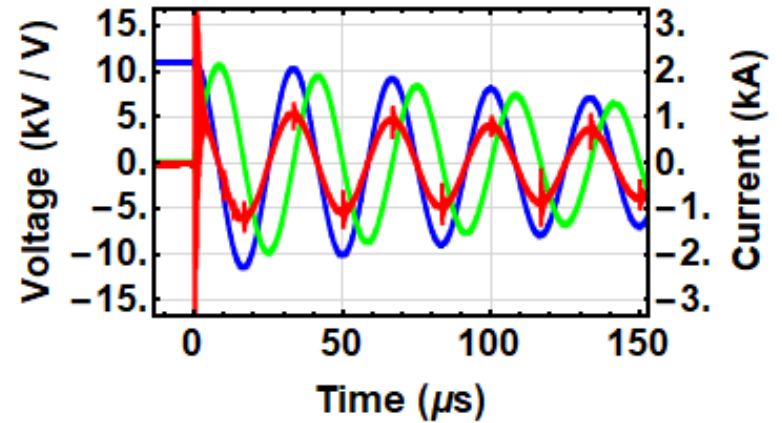
S. Bose *et al.*, *Eur. J. Phys.* **40**, 015803 (2019)

E. T. Everson *et al.*, *Rev. Sci. Instrum.* **80**, 113505 (2009)

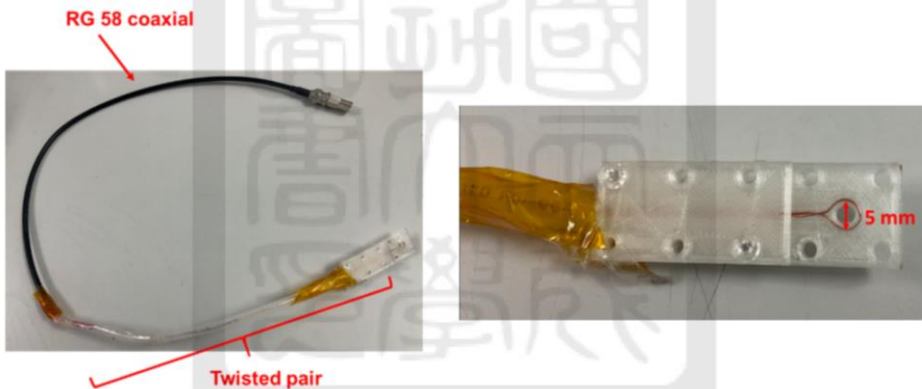
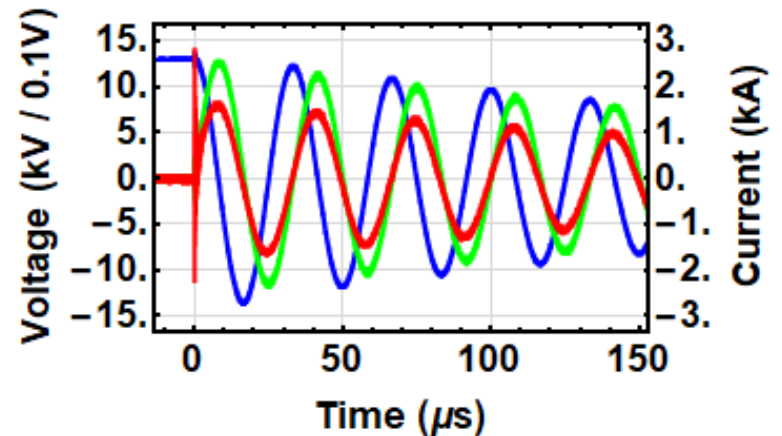
B-dot probe experiments



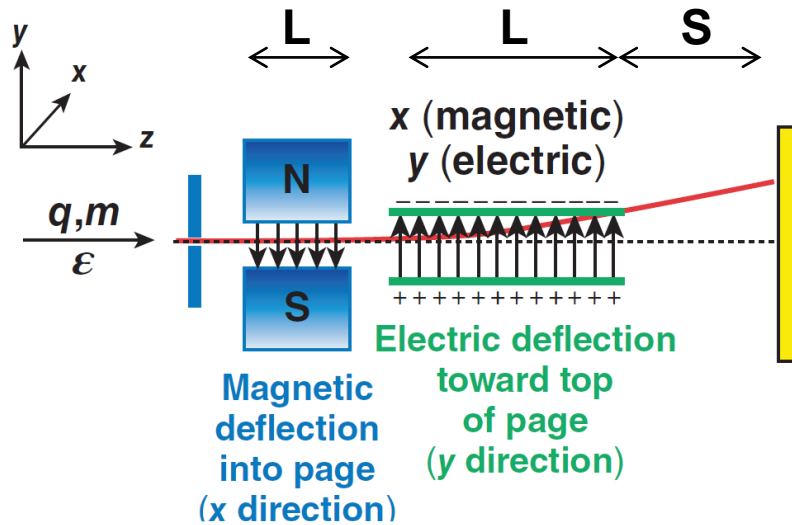
- Without integrator



- With integrator



A Thomson parabola uses parallel electric and magnetic fields to deflect particles onto parabolic curves that resolve q/m



- Deflection caused by magnetic field $\sim q/p$
- Deflection caused by electric field $\sim q/KE$
- Ion traces form parabolic curves on detector plane

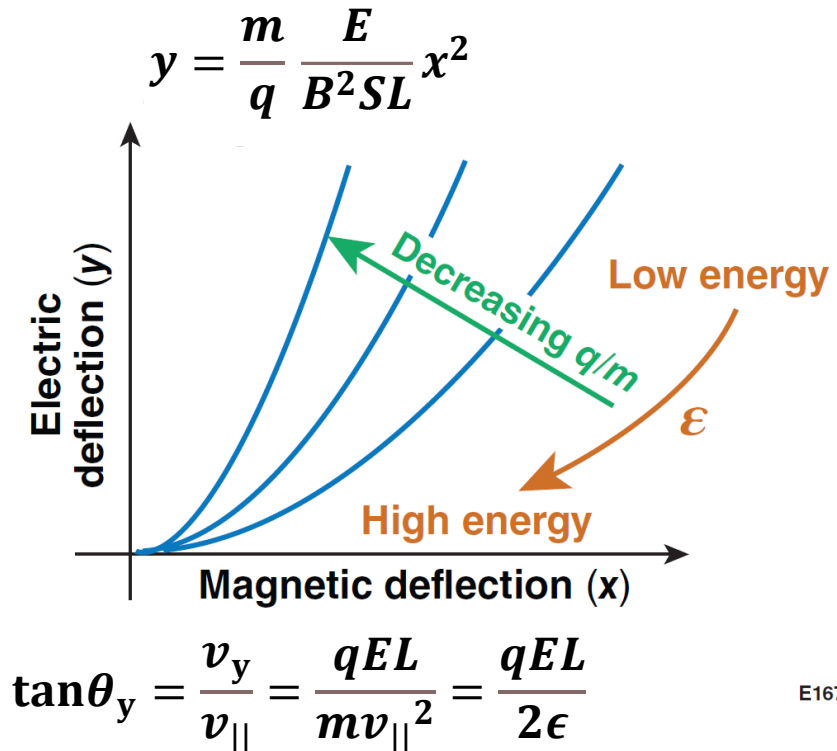
$$F_x = qv_{\parallel}B = m \frac{dv_x}{dt}$$

$$v_x = \frac{q}{m} v_{\parallel} B \Delta t = \frac{q}{m} v_{\parallel} B \frac{L}{v_{\parallel}} = \frac{qBL}{m}$$

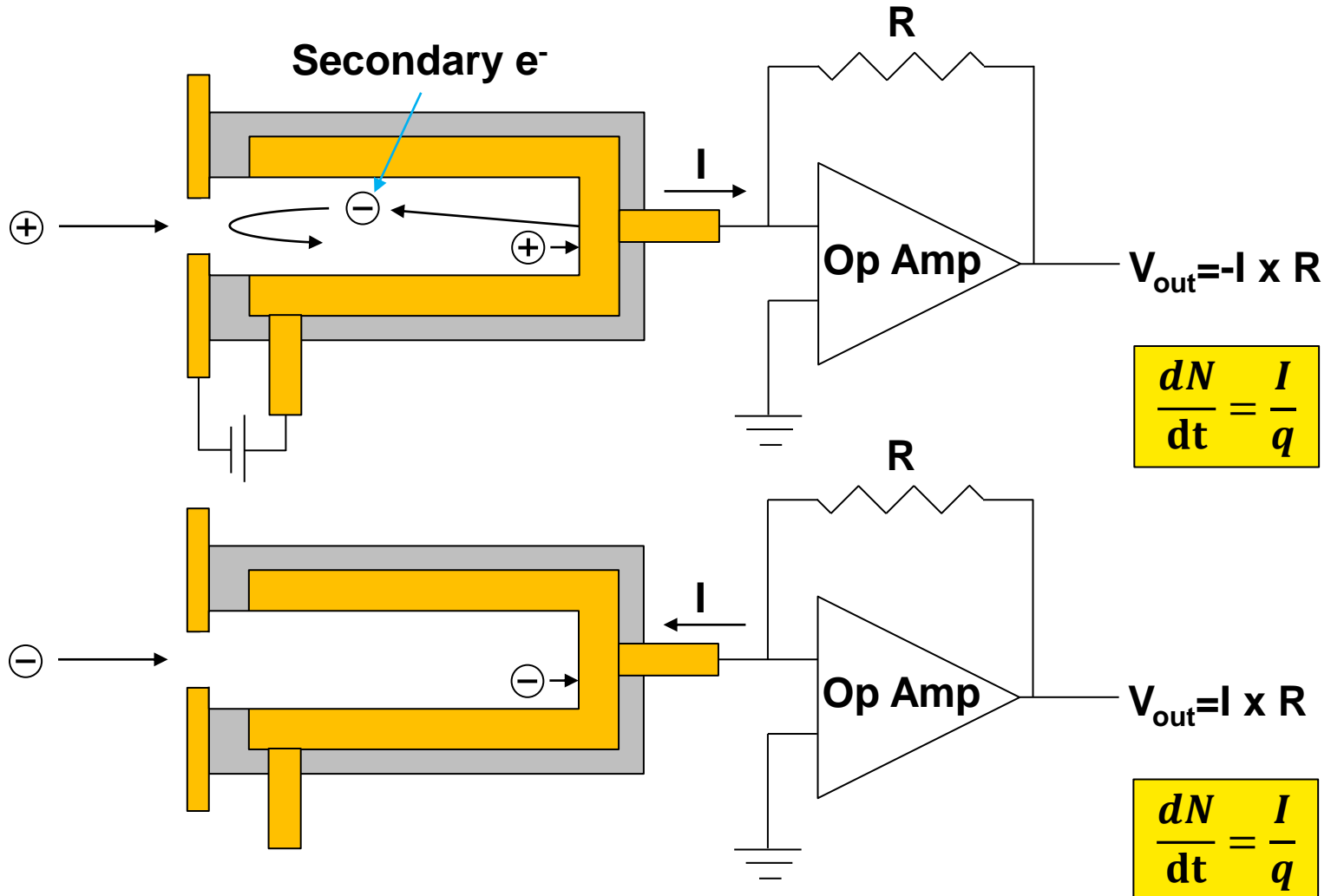
$$\tan\theta_x = \frac{v_x}{v_{\parallel}} = \frac{qBL}{mv_{\parallel}} = \frac{qBL}{\sqrt{2m\epsilon}}$$

$$F_y = qE = m \frac{dv_y}{dt}$$

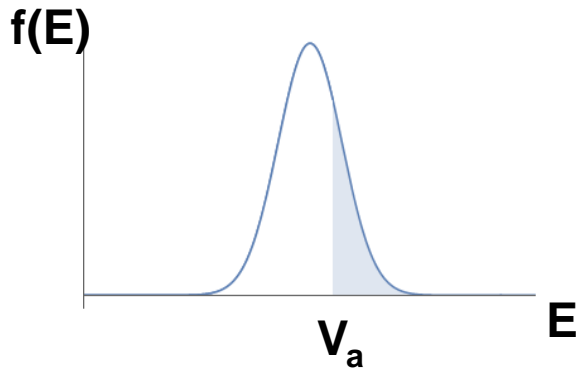
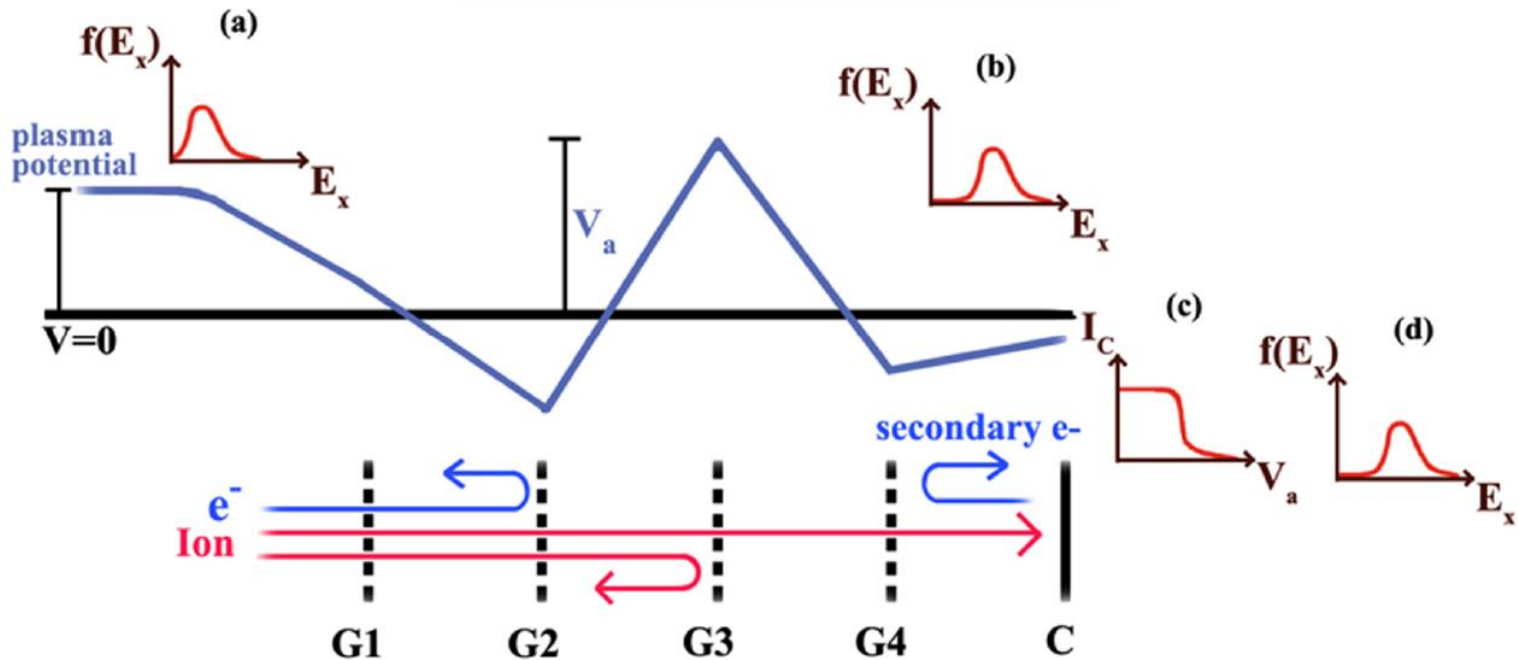
$$v_y = \frac{q}{m} E \Delta t = \frac{q}{m} E \frac{L}{v_{\parallel}} = \frac{qEL}{mv_{\parallel}}$$



A faraday cup measures the flux of charge particles



Retarding potential analyzer measures the energy / velocity distribution function



The photon energy spectrum provides valuable information

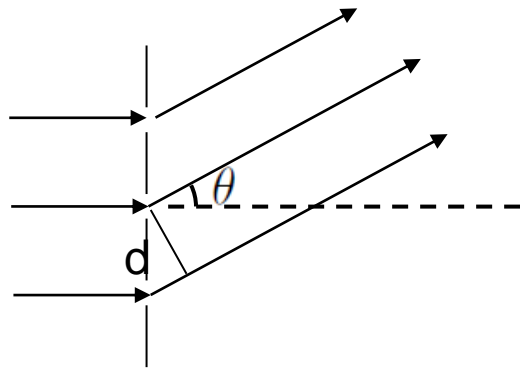


- **Plasma conditions can be determined from the photon spectrum**
 - **visible light: absorption and laser-plasma interactions**
 - **x rays: electron temperature, density, plasma flow, material mixing**
- **There are three basic tools for determining the spectrum detected**
 - **filtering**
 - **grating spectrometer**
 - **Bragg spectrometer**

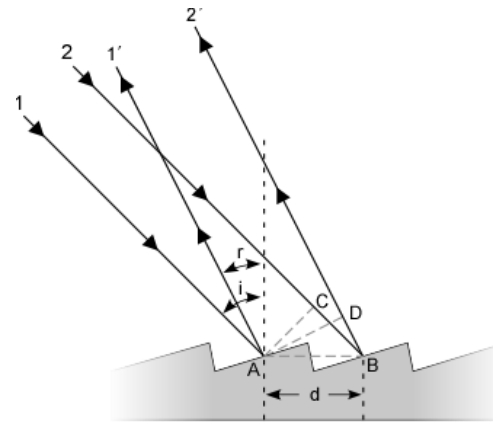
Spectrum can be obtained using grating



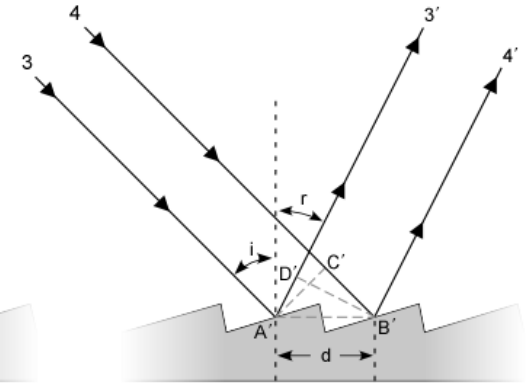
- Grating is used to disperse the light



$$d \sin \theta = m\lambda$$

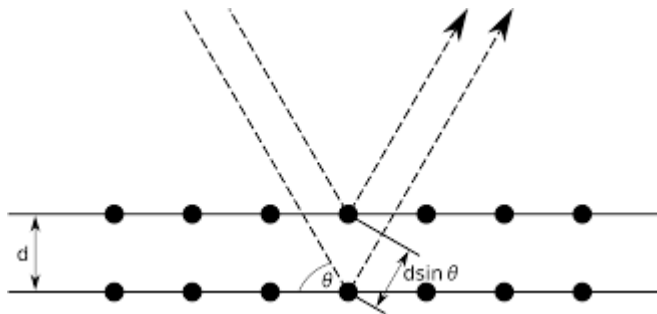


$$n\lambda = d(\sin(i) + \sin(r))$$



$$n\lambda = d(\sin(i) - \sin(r))$$

- Bragg condition in the crystal is used for X-ray.

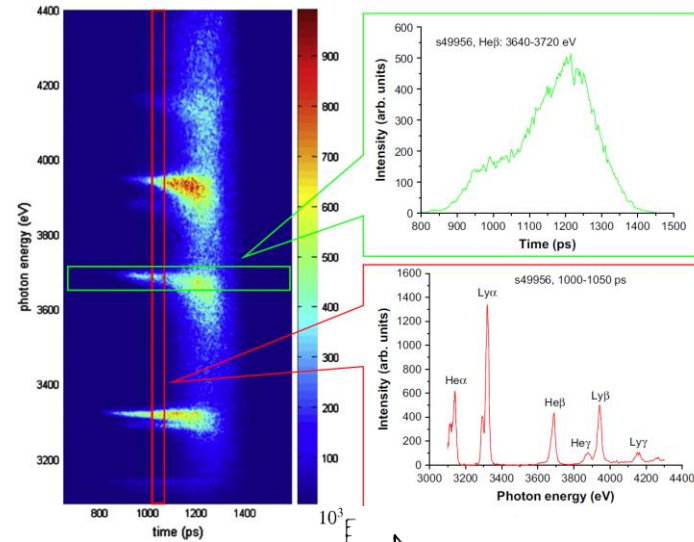
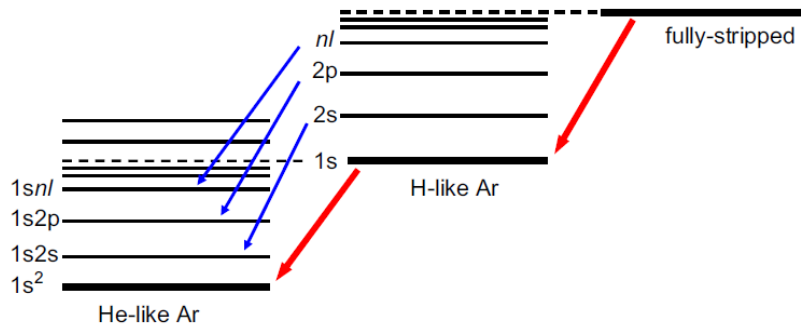


$$2d \sin \theta = m\lambda$$

Temperature and density can be obtained from the emission

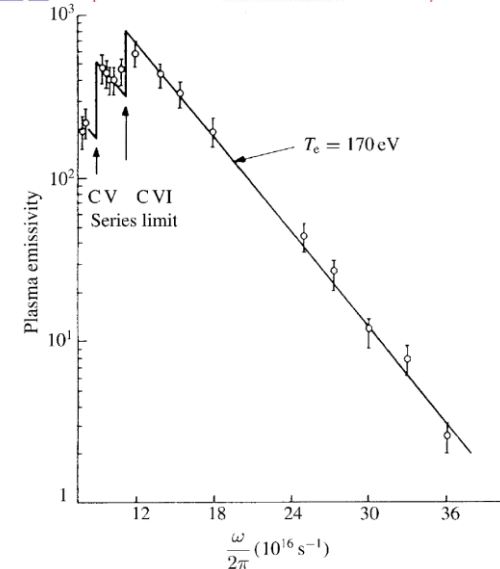


Line emission



Bremsstrahlung emission

$$\eta_\nu = \frac{16\pi}{3\sqrt{6\pi}} \frac{e^6}{m_e^2 c^3} \frac{Z_i^2 n_e}{\sqrt{k_B T_e / m_e A m_p}} \exp\left(-\frac{h\nu}{k_B T_e}\right)$$



Information of x-ray transmission or reflectivity over a surface can be obtained from the Center for X-Ray Optics



- http://henke.lbl.gov/optical_constants/



X-Ray Database

- Nanomagnetism
- X-Ray Microscopy
- EUV Lithography
- EUV Mask Imaging
- Reflectometry
- Zoneplate Lenses
- Coherent Optics
- Nanofabrication
- Optical Coatings
- Engineering
- Education
- Publications
- Contact



The Center for X-Ray Optics is a multi-disciplined research group within Lawrence Berkeley National Laboratory's (LBNL)

X-Ray Interactions With Matter

Introduction

Access the [atomic scattering factor](#) files.

Look up [x-ray properties of the elements](#).

The [index of refraction](#) for a compound material.

The x-ray [attenuation length](#) of a solid.

X-ray transmission

- Of a [solid](#).
- Of a [gas](#).

X-ray reflectivity

- Of a [thick mirror](#).
- Of a [single layer](#).
- Of a [bilayer](#).
- Of a [multilayer](#).

The diffraction efficiency of a [transmission grating](#).

Related calculations:

- [Synchrotron bend magnet radiation](#).

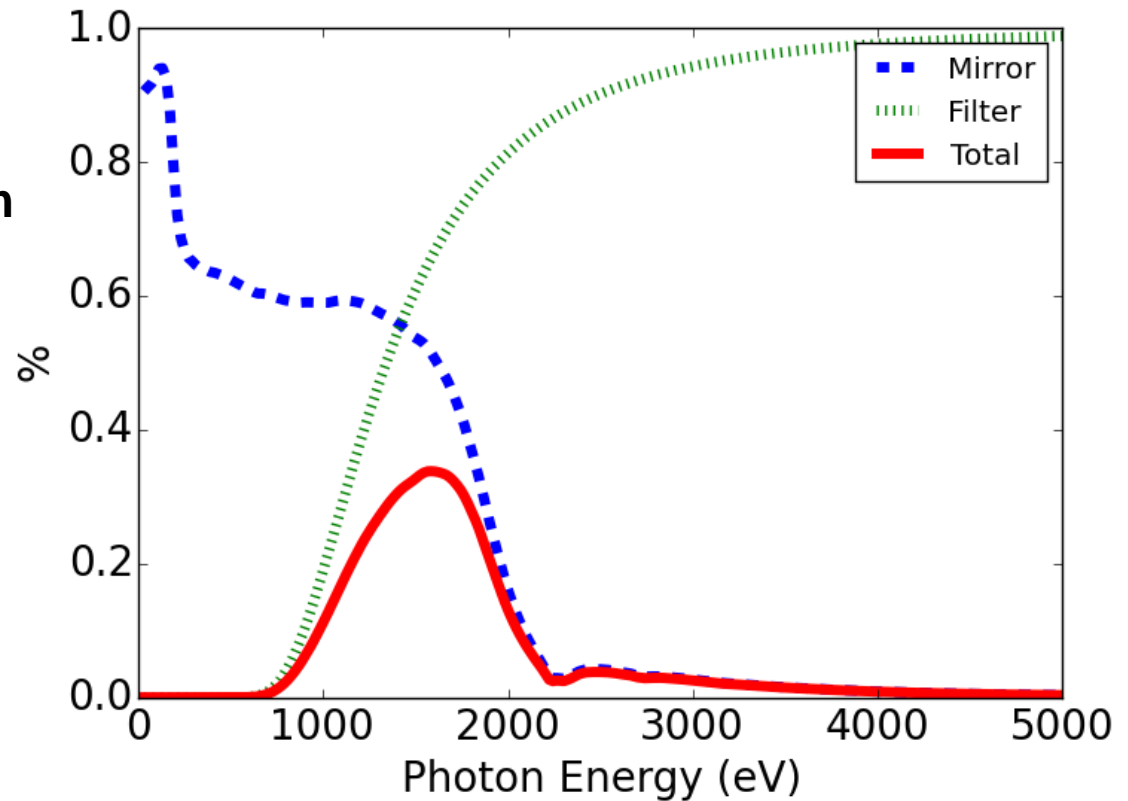
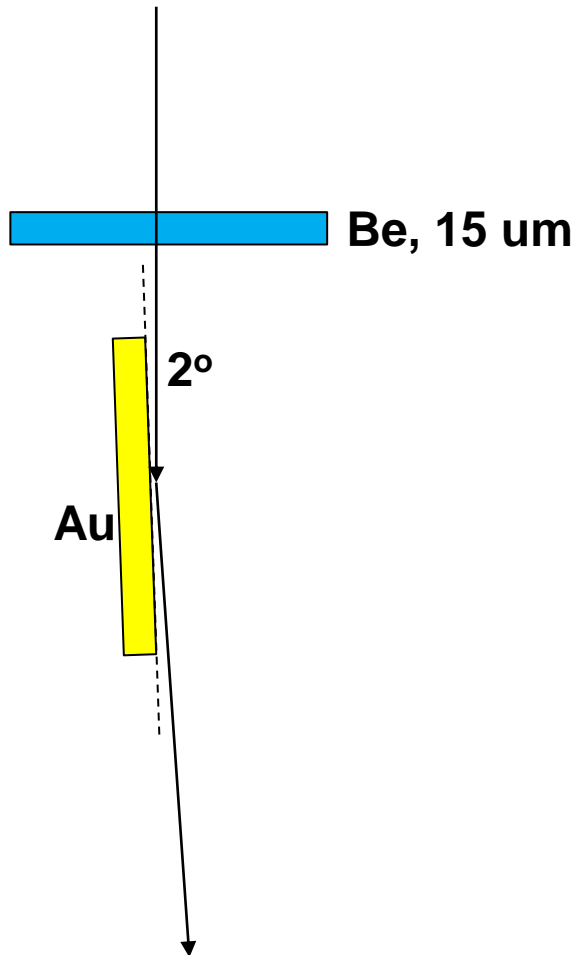
[Other x-ray web resources](#).

[X-ray Data Booklet](#)

Reference

B.L. Henke, E.M. Gullikson, and J.C. Davis. *X-ray interactions: photoabsorption, scattering, transmission, and reflection at E=50-30000 eV, Z=1-92*, Atomic Data and Nuclear Data Tables Vol. **54** (no.2), 181-342 (July 1993).

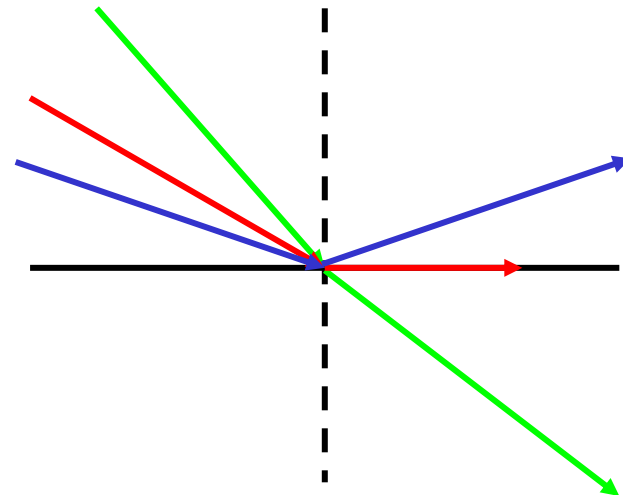
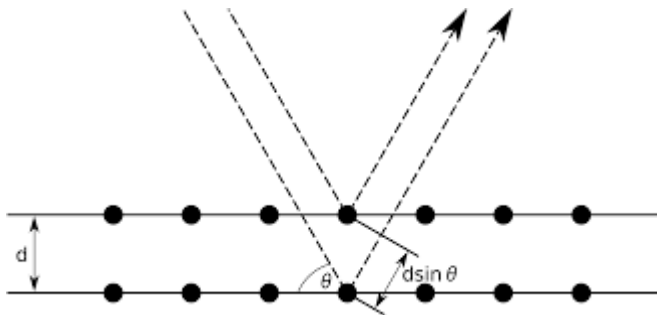
A band pass filter is obtained by combining a filter and a mirror



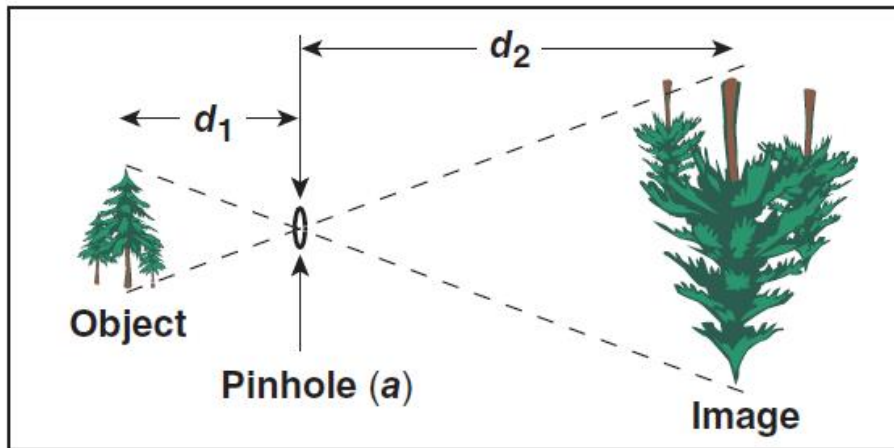
X rays can not be concentrated by lenses



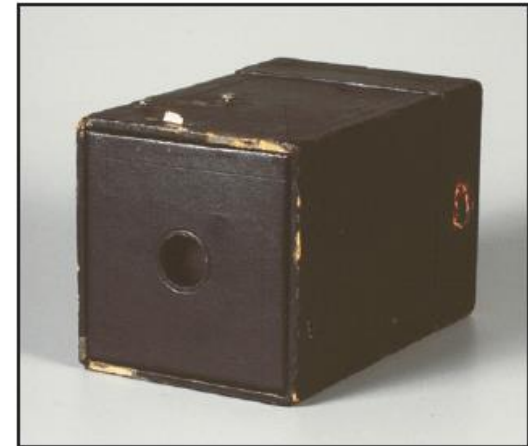
- X-ray refractive indices are less than unity, $n \lesssim 1$
- For those with lower refractive indices, the absorption is also strong
- X-ray mirrors can be made through
 - Bragg reflection
 - External total reflection with a small grazing angle



The simplest imaging device is a pinhole camera



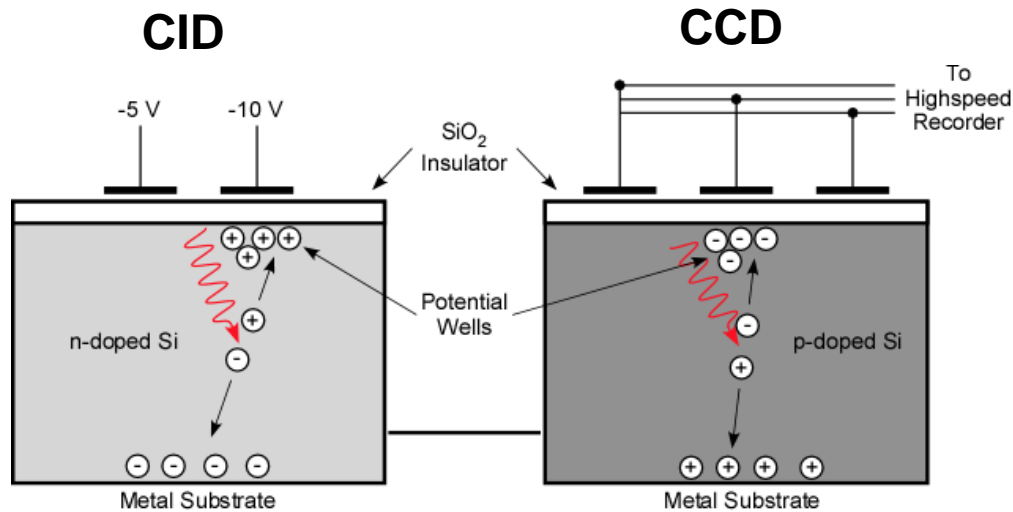
Kodak Brownie camera



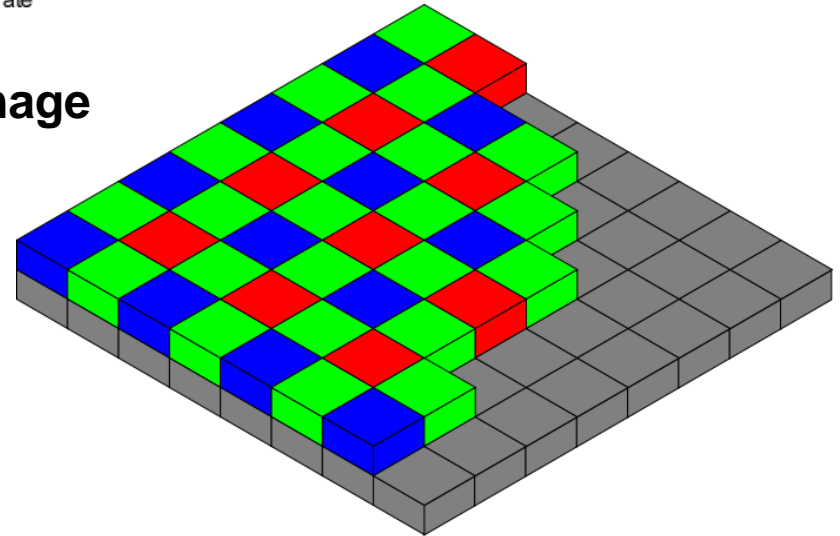
- Magnification = $\frac{d_2}{d_1}$
- Infinite depth of field (variable magnification)
- Pinhole diameter determines
 - resolution $\sim a$
 - light collection: $\Delta\Omega = \frac{\pi}{4} \frac{a^2}{d_1^2}$

Imaging optics (e.g., lenses) can be used for higher resolutions with larger solid angles.

2D images can be taken using charge injection device (CID) or charge coupled device (CCD)



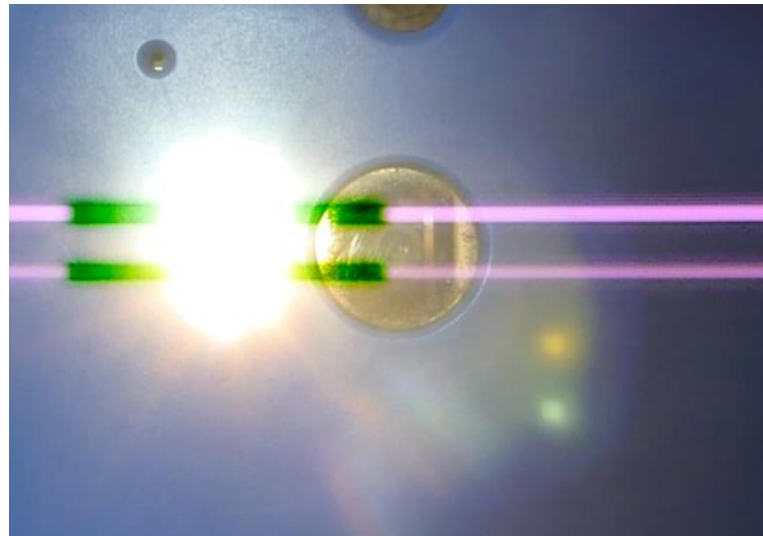
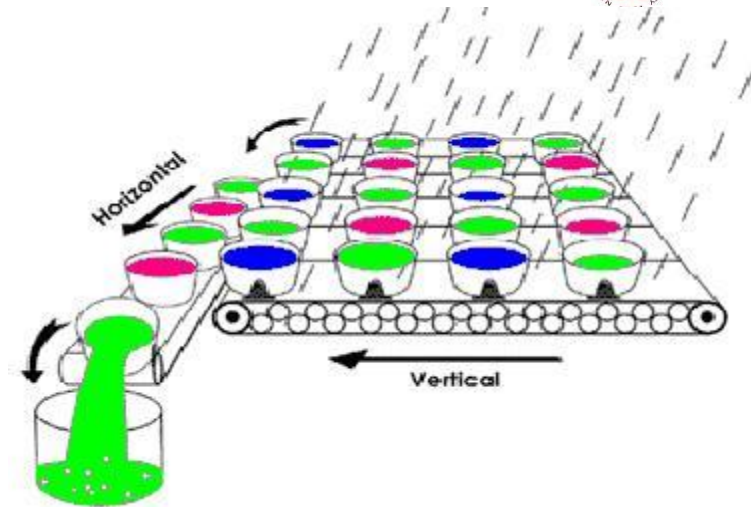
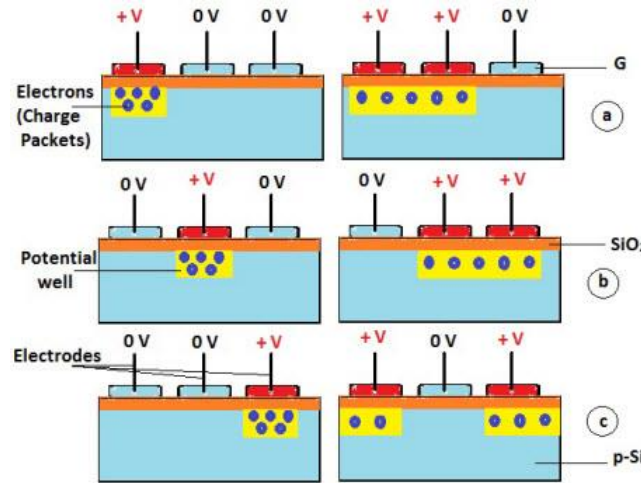
- Color mask is used for color image



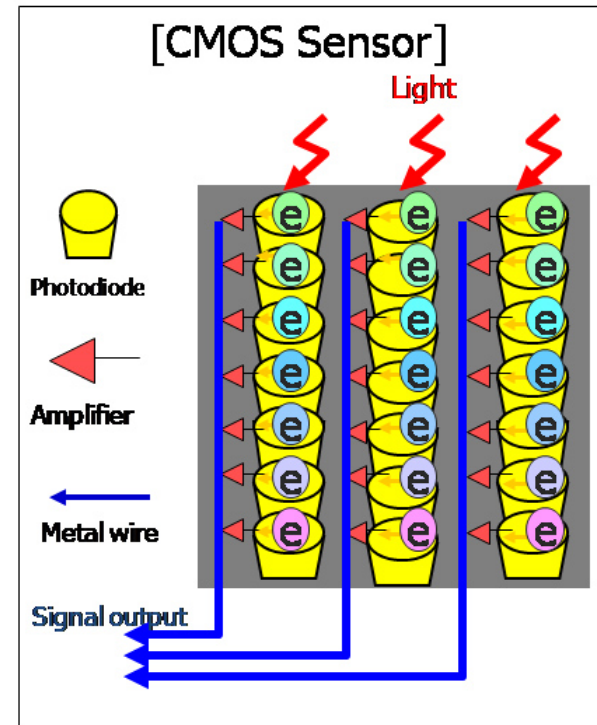
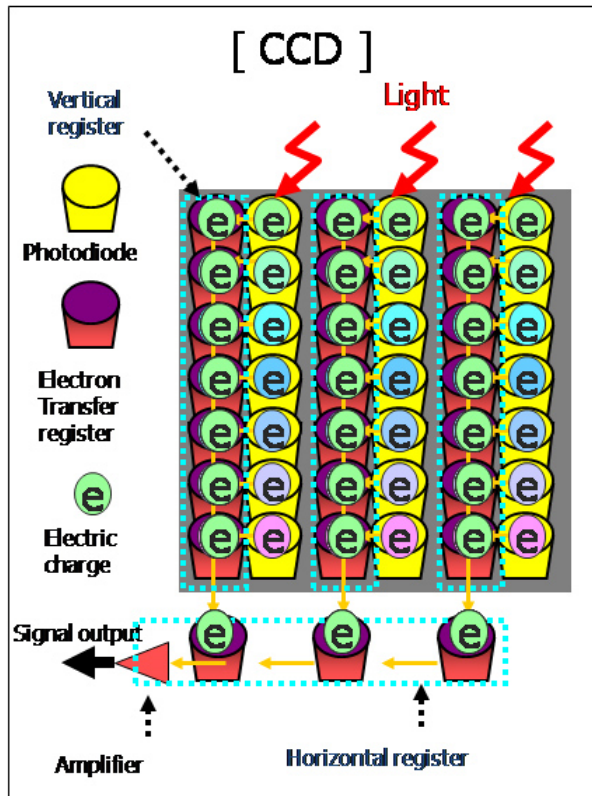
Charges are transferred along the array for readout in CCD



CCD readout:



Signal is readout individually in CMOS sensor

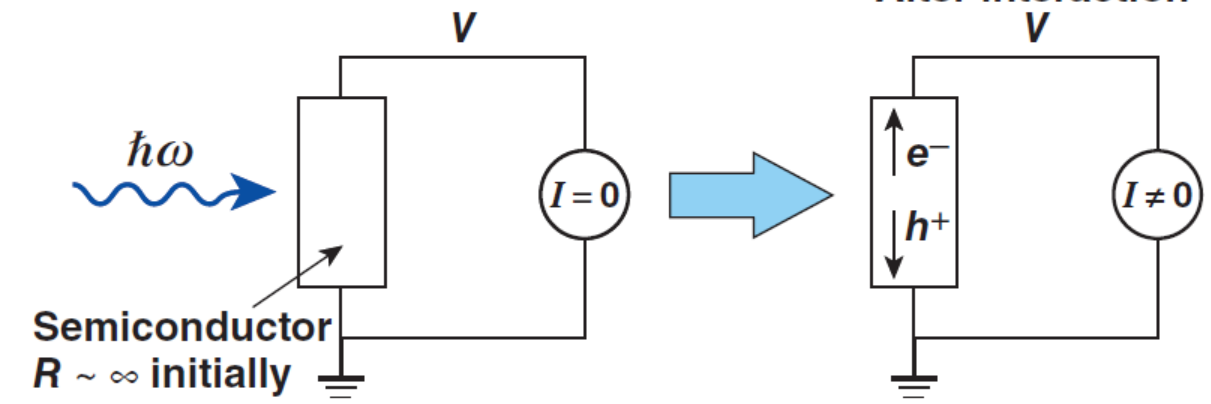


Electronic detectors provide rapid readout

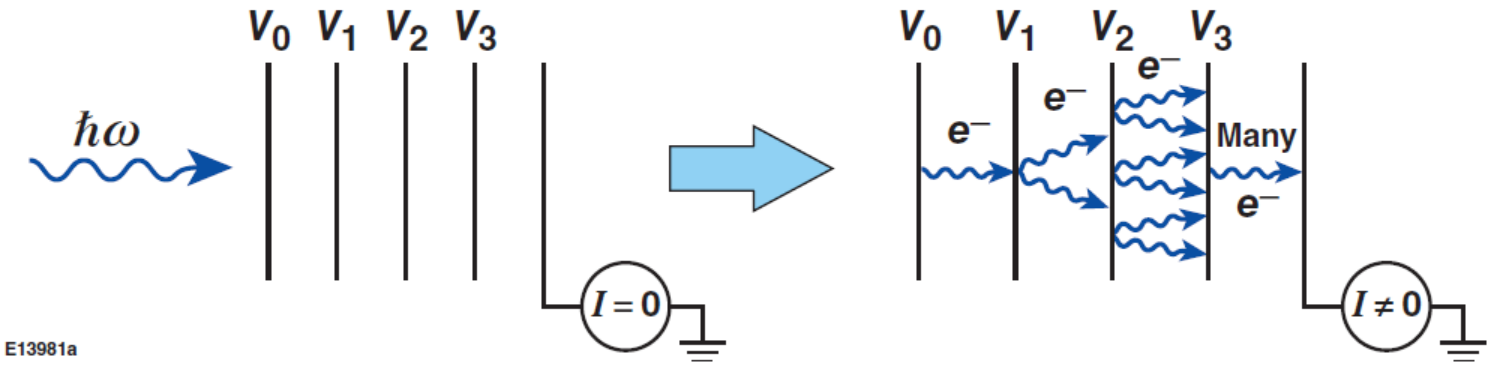


- Electronic detectors are typically semiconductors or ionization-based stacks (e.g., photomultipliers)

Semiconductor detectors

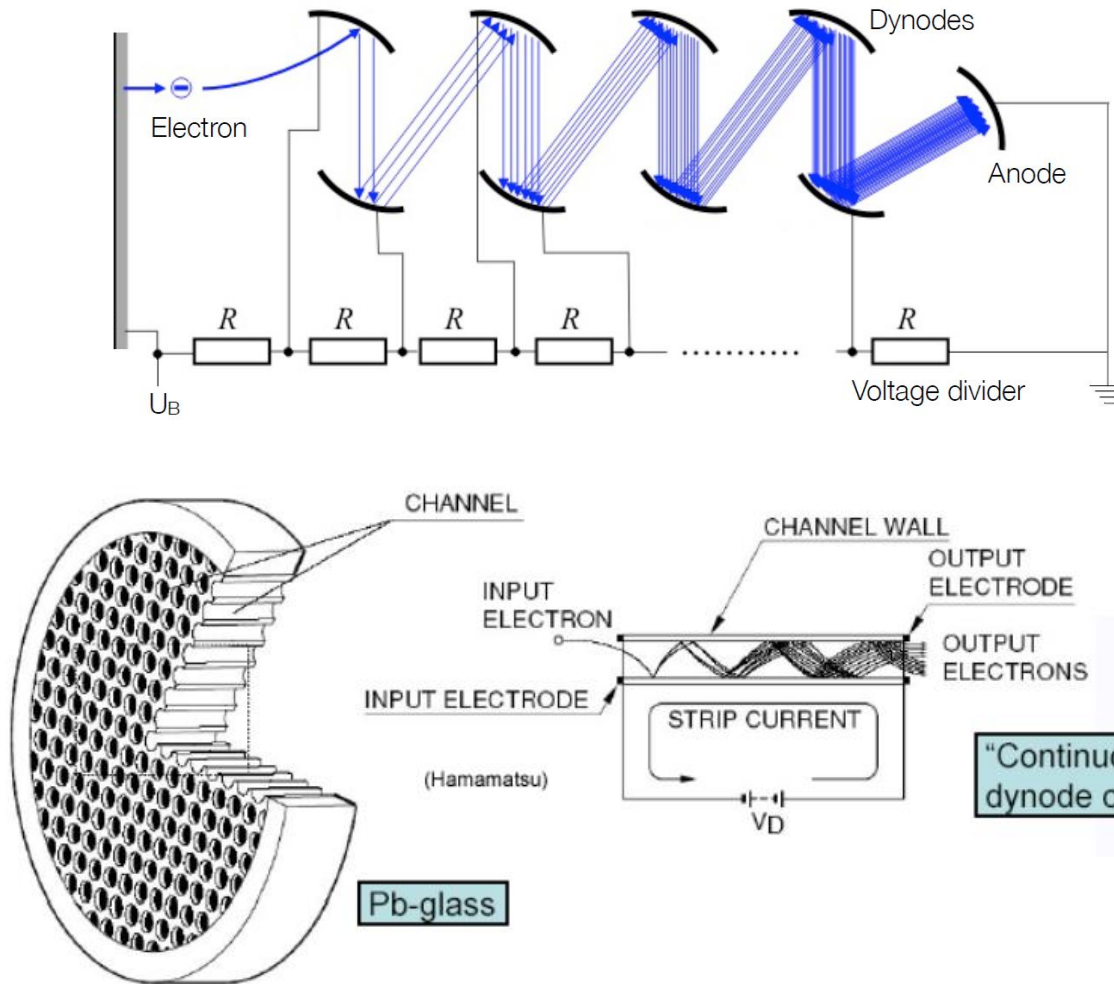


Ionization detectors

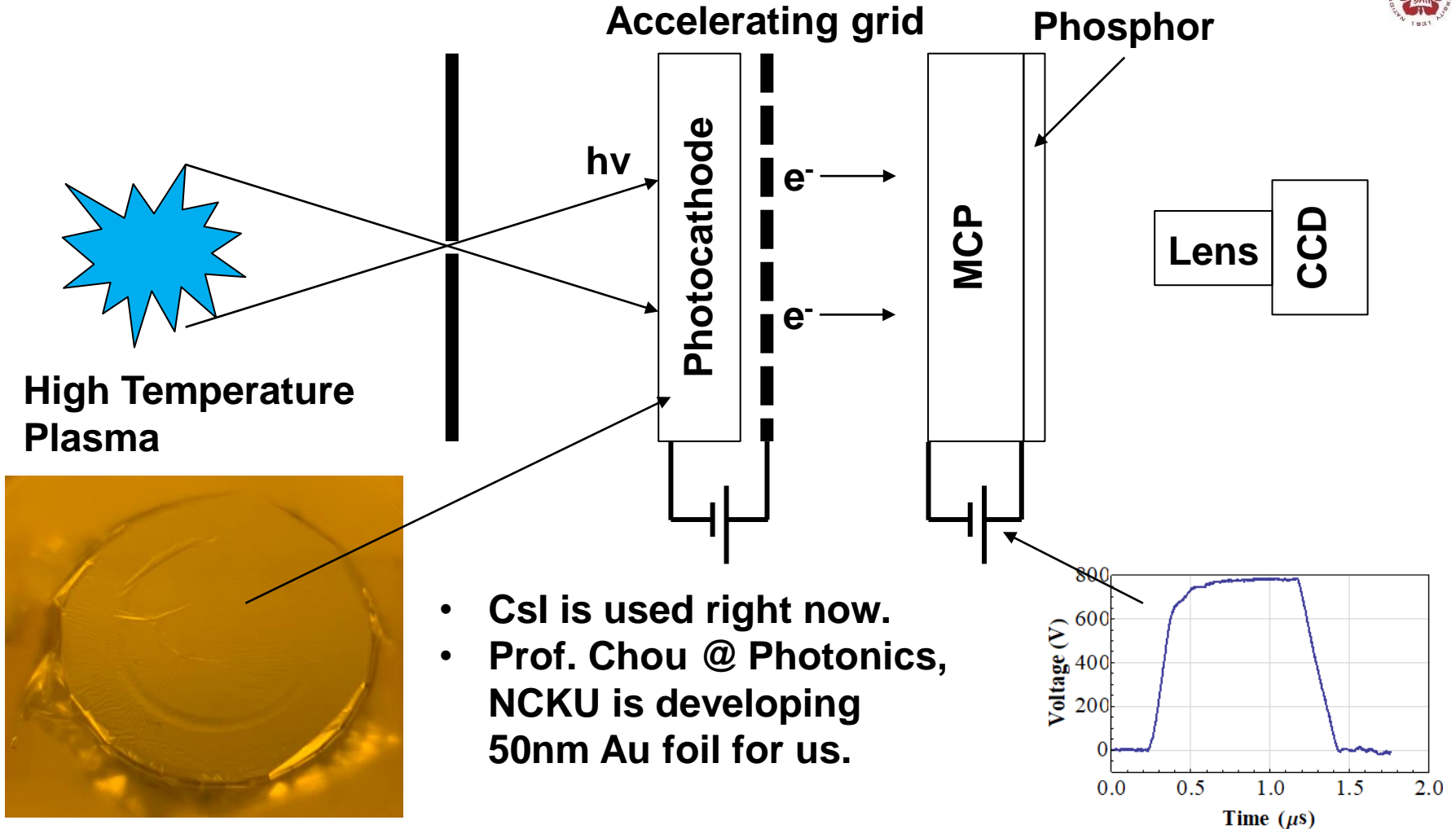


E13981a

The number of electrons can be increased through photomultipliers or microchannel plate (MCP)

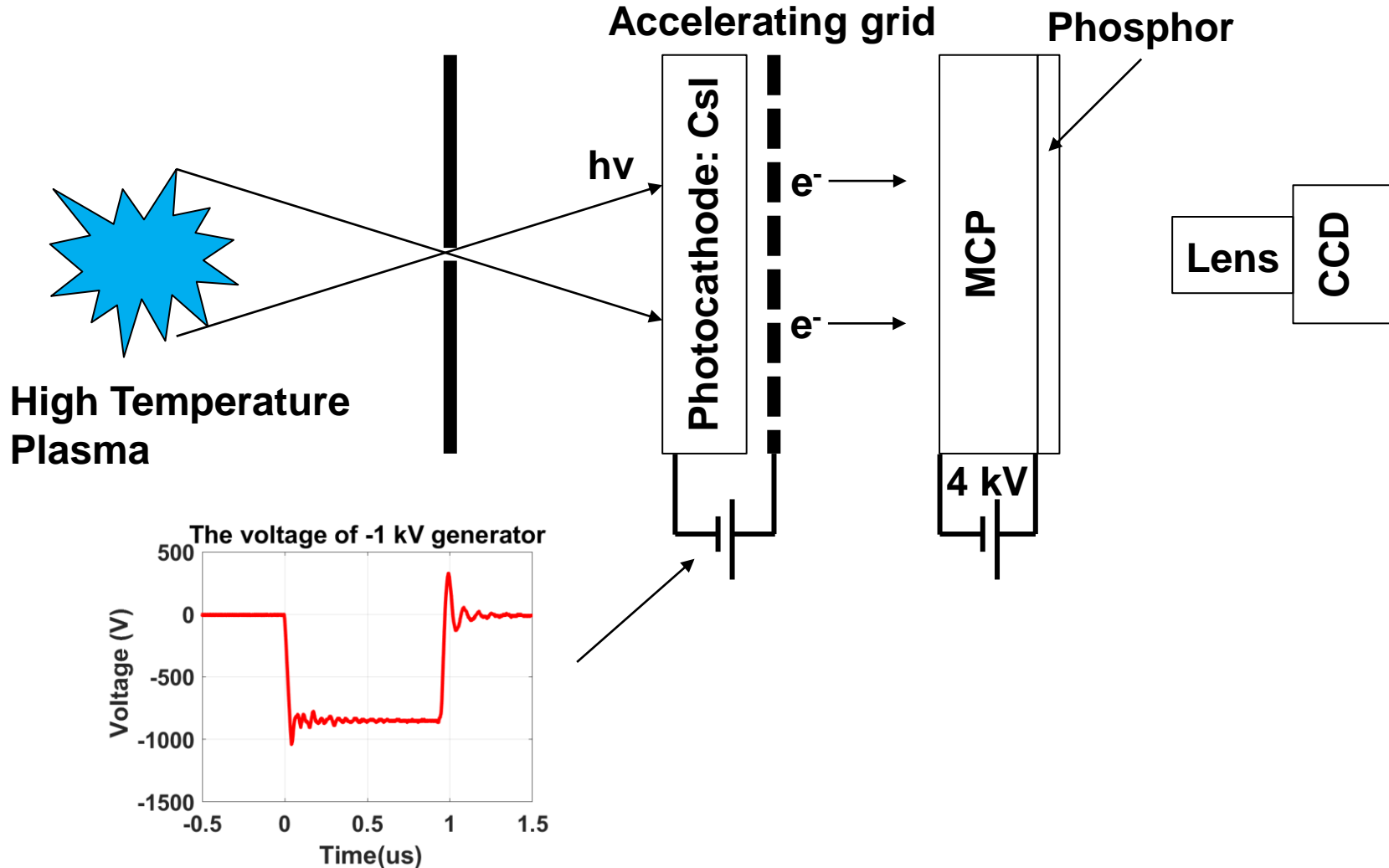


X-rays are imaged using photocathode, MCP, phosphor, and CCD



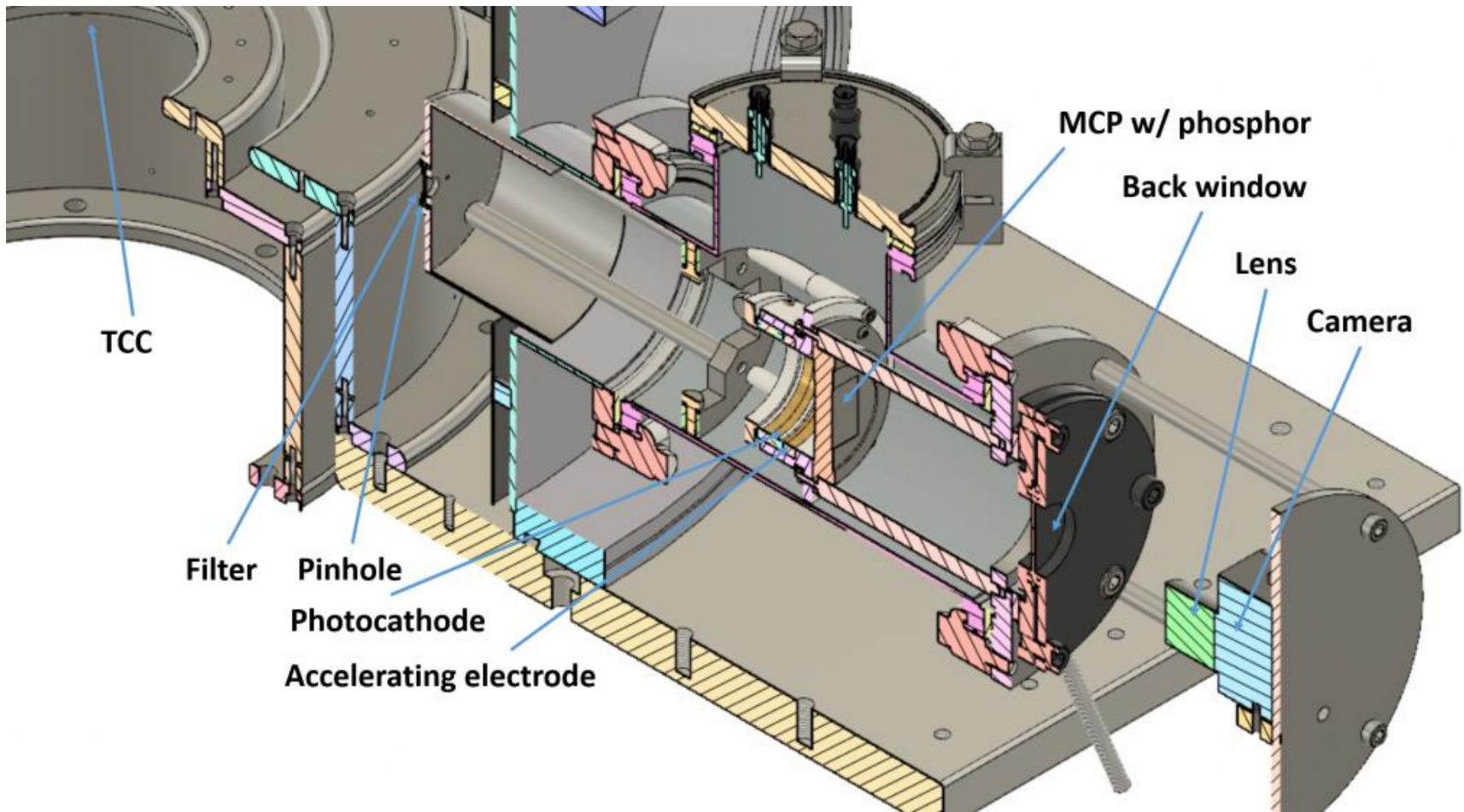
• Images can be gated using fast high voltage pulses.

A negative high-voltage pulse is used in our x-ray pinhole camera

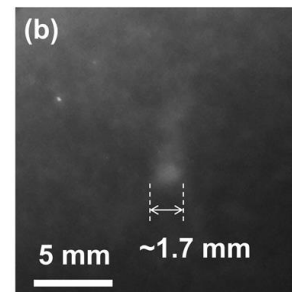
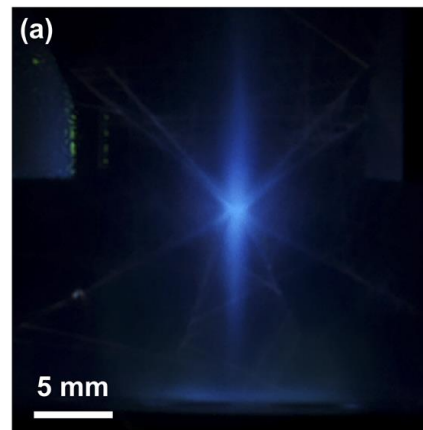
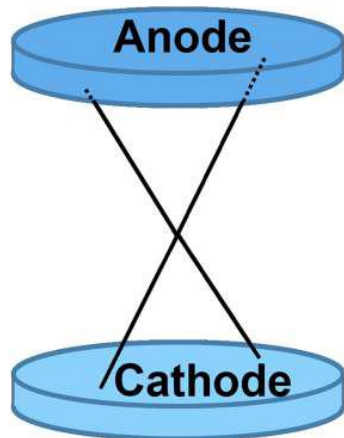
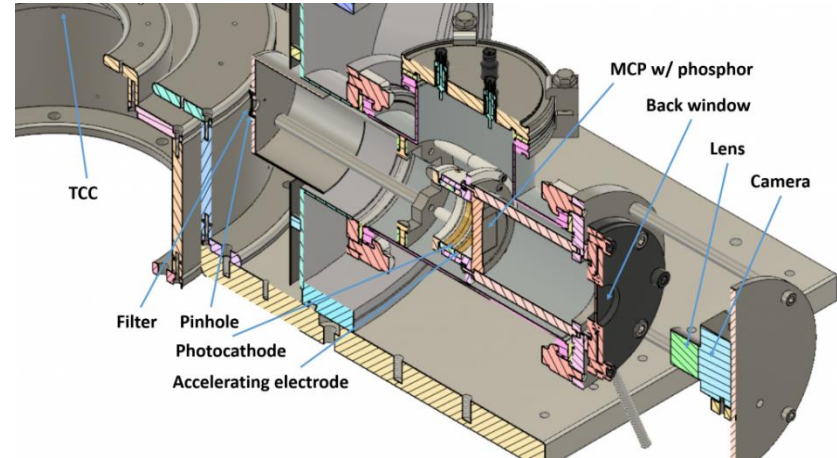
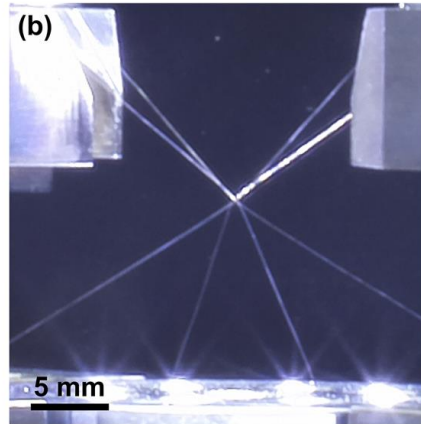
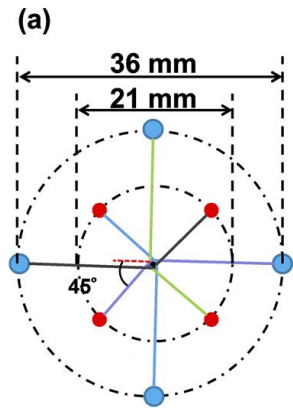


- The x-ray camera with a shutter opening time of ≤ 10 ns will be built.

A pinhole camera was designed and was built



We demonstrated using x-ray pinhole camera to capture the radiation from an imploded x pinch

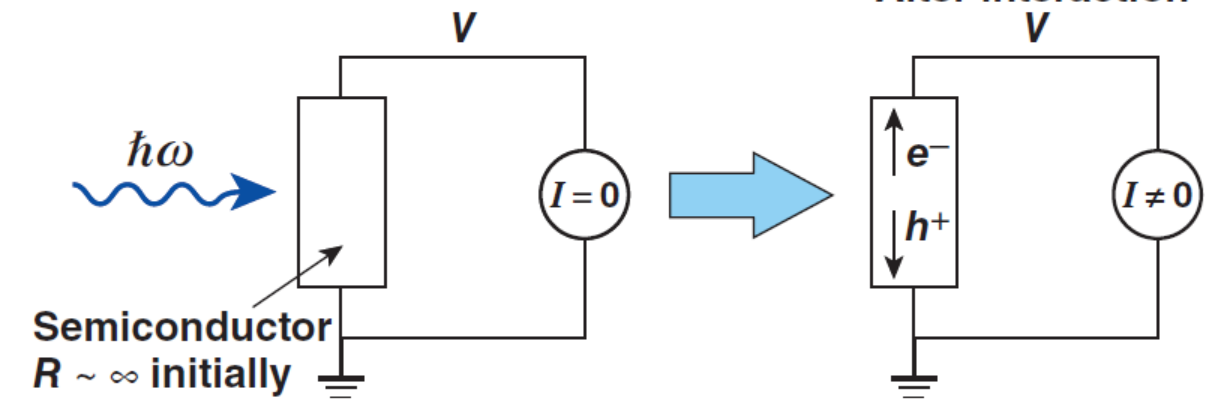


Electronic detectors provide rapid readout

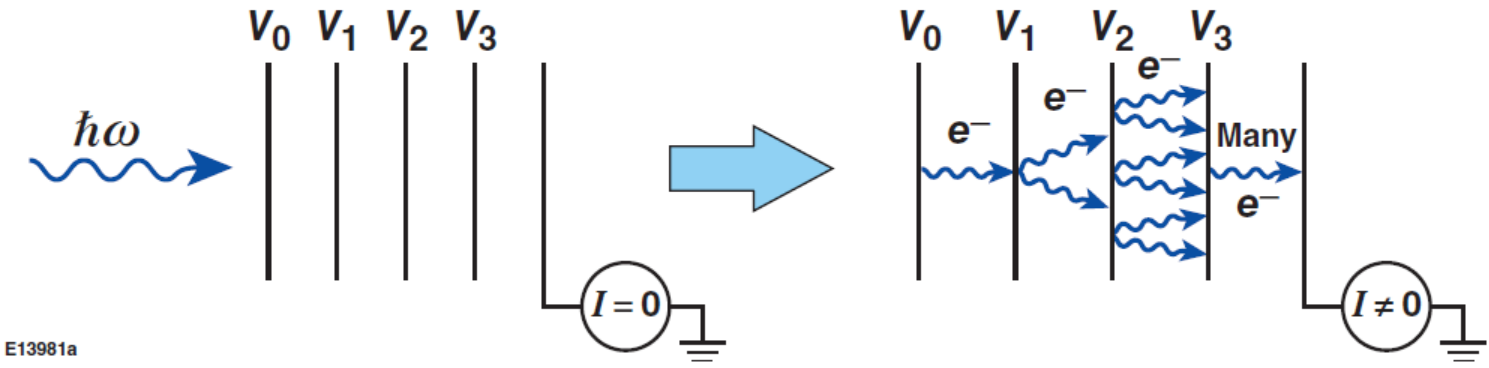


- Electronic detectors are typically semiconductors or ionization-based stacks (e.g., photomultipliers)

Semiconductor detectors



Ionization detectors

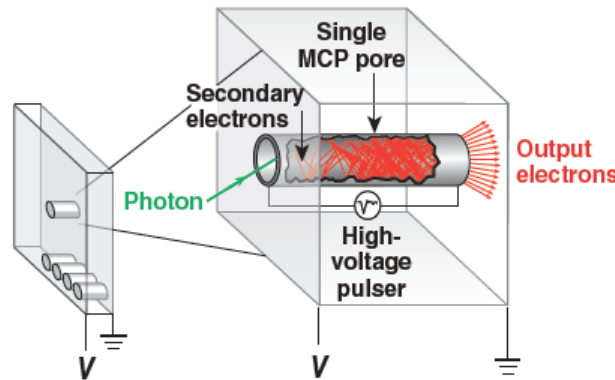


E13981a

A framing camera provides a series of time-gated 2-D images, similar to a movie camera

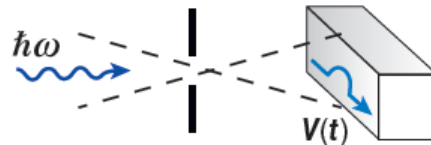


- The building block of a framing camera is a gated microchannel-plate (MCP) detector
- An MCP is a plate covered with small holes, each acts as a photomultiplier



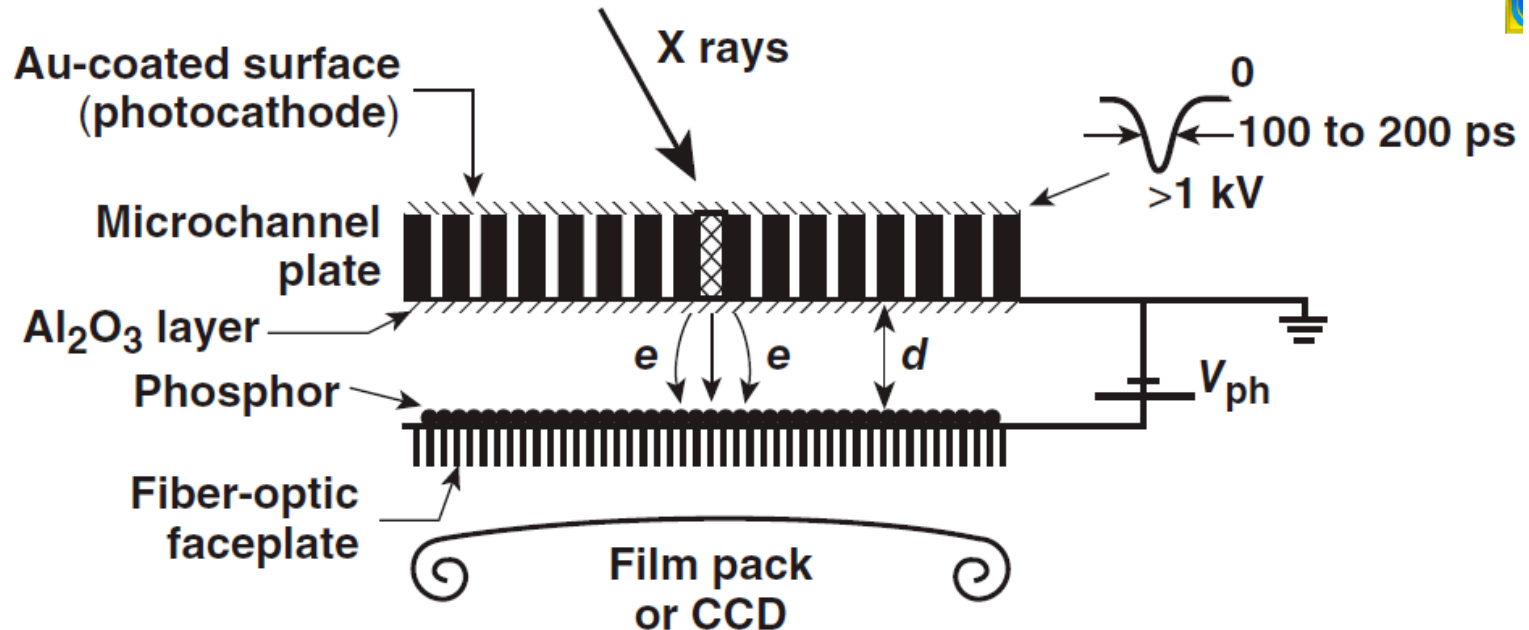
Multiple electrons are produced each time an electron or photon hits the wall

- A voltage pulse is sent down the plate, gating the detector



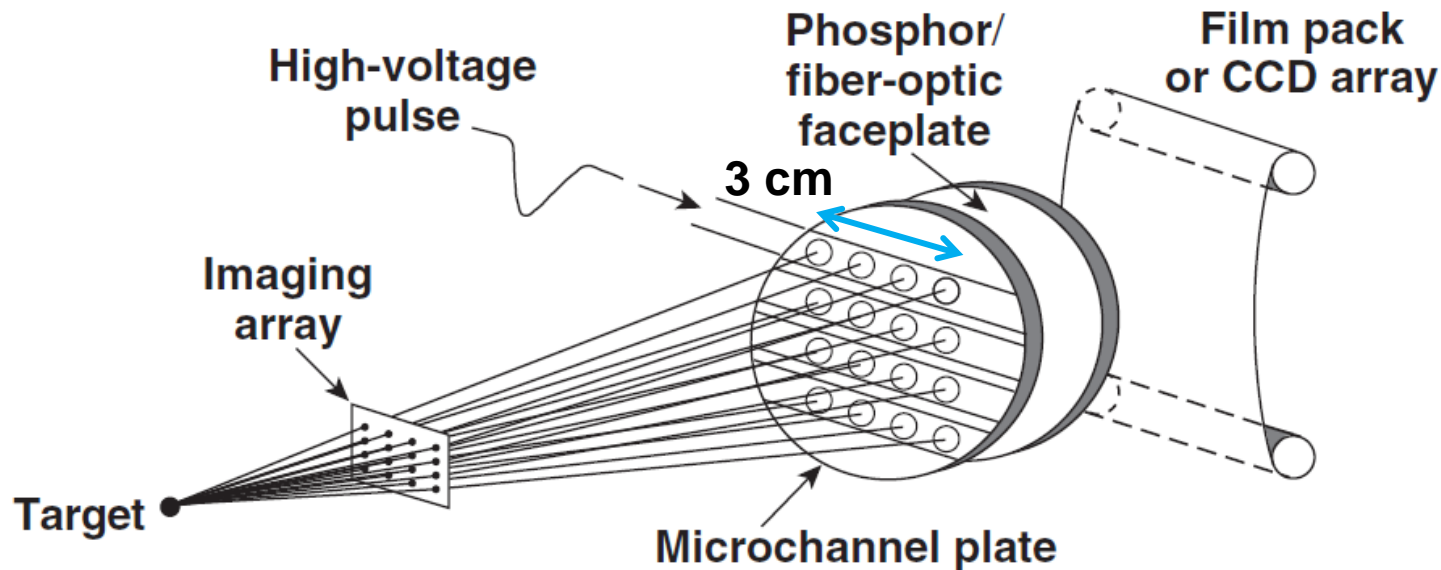
The detector is only on when the voltage pulse is present

A framing camera detector consists of a microchannel plate (MCP) in front of a phosphor screen



- Electrons are multiplied through MCP by voltage V_C
- Images are recorded on film behind phosphor
- Insulating Al_2O_3 layer allows for V_{ph} to be increased, thereby improving the spatial resolution of phosphor

Two-dimensional time-resolved images are recorded using x-ray framing cameras

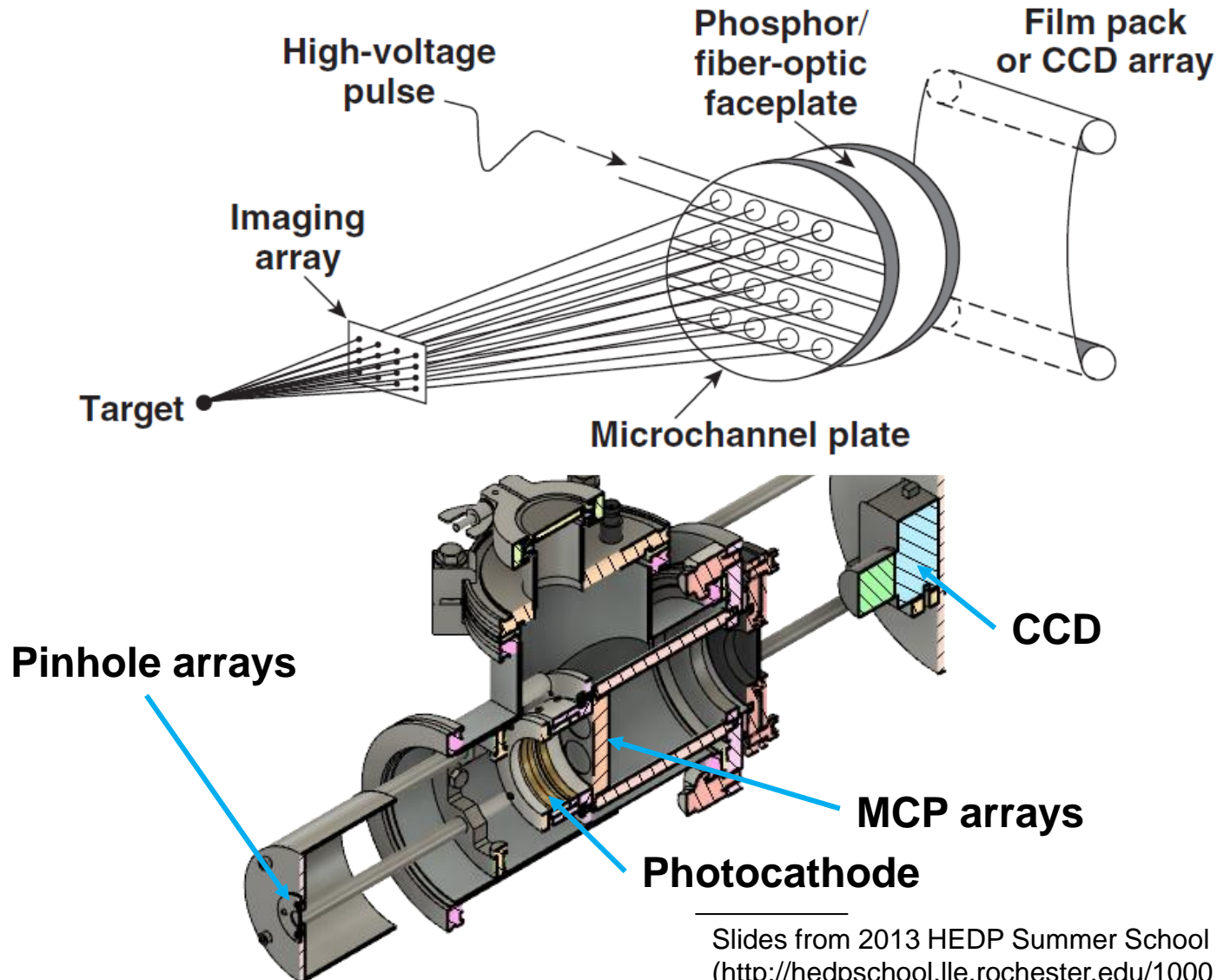


- Temporal resolution = 35 to 40 ps
- Imaging array: Pinholes: 10- to 12- μm resolution, 1 to 4 keV
- Space-resolved x-ray spectra can be obtained by using Bragg crystals and imaging slits

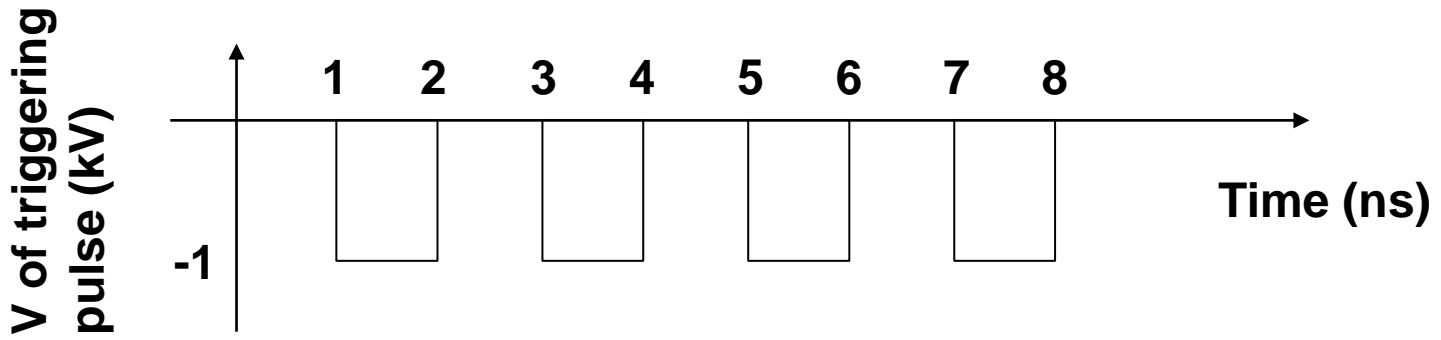
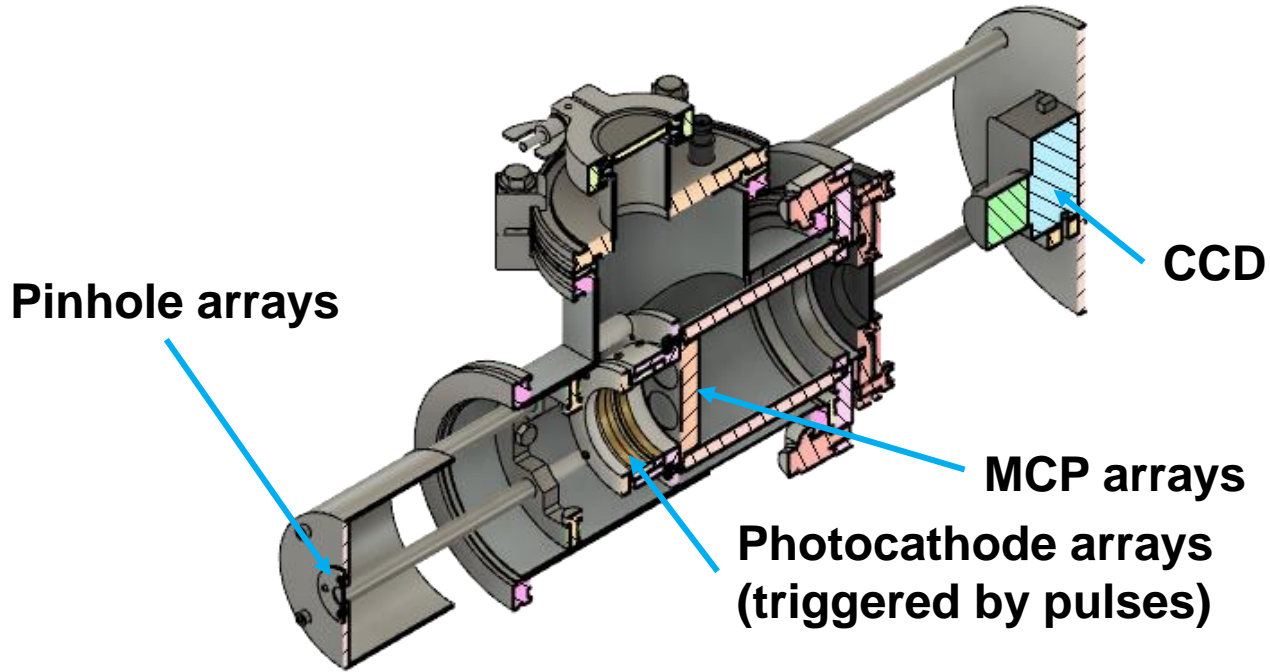
E7105b

$$\text{Ex: } \Delta t = \frac{3 \text{ cm}/3}{3 \times 10^{10} \text{ cm/s}} = 33 \text{ ps}$$

X-ray framing cameras for recording two-dimensional time-resolved images will be built by the end of 2021



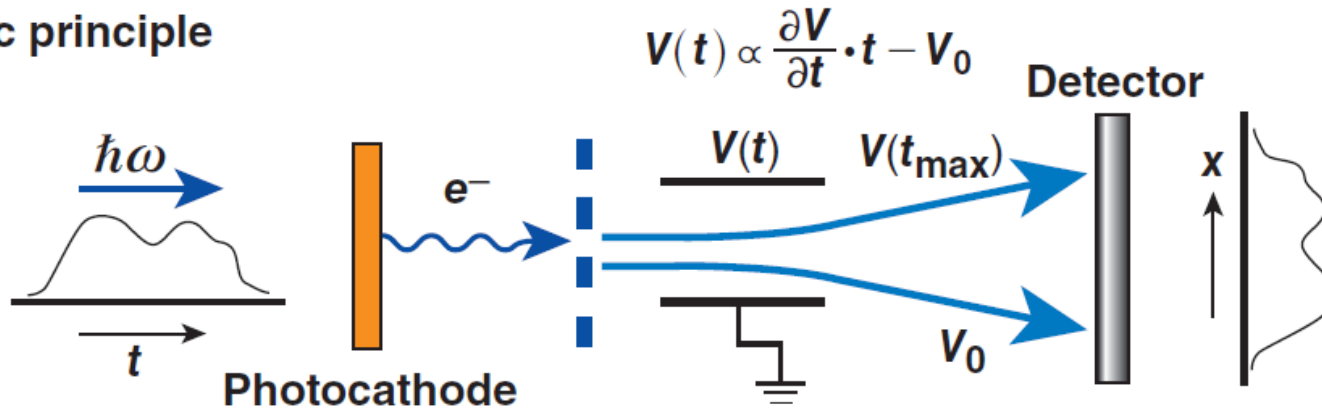
Each pinhole camera will be triggered separately



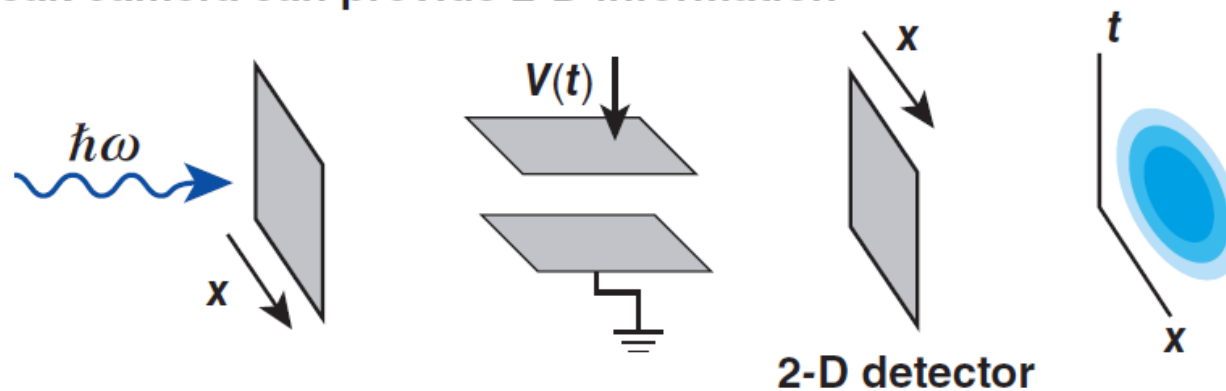
A streak camera provides temporal resolution of 1-D data



Basic principle



A streak camera can provide 2-D information

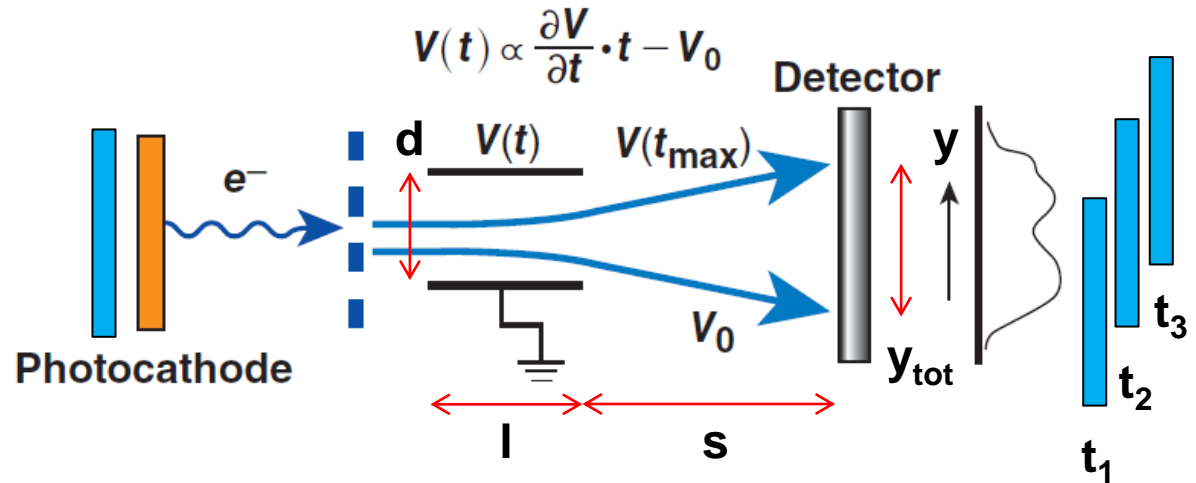


A slit is to prevent spatial information at different times interfering with each other



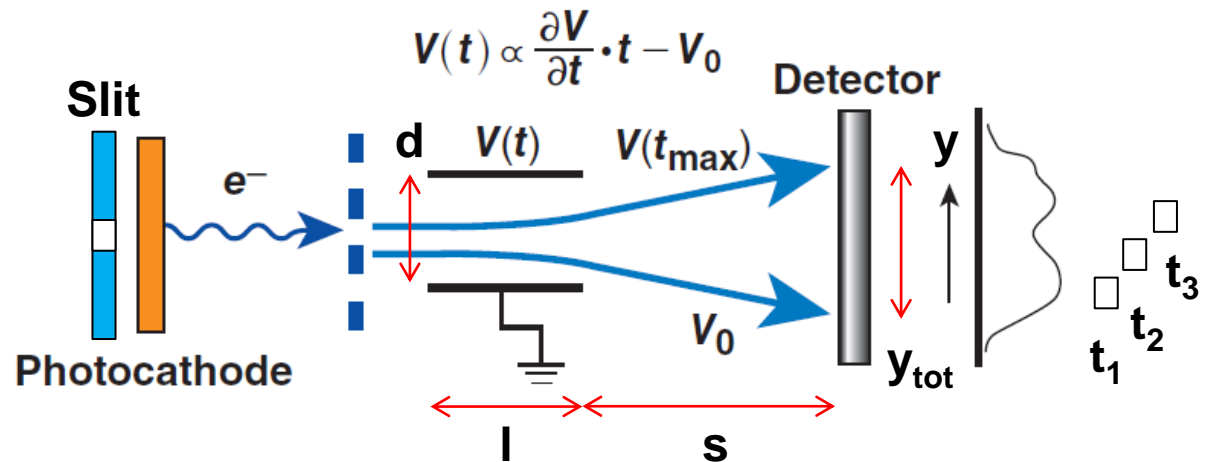
Imaging system

- Visible light: regular lens
- X rays: pinhole



Imaging system

- Visible light: regular lens
- X rays: pinhole

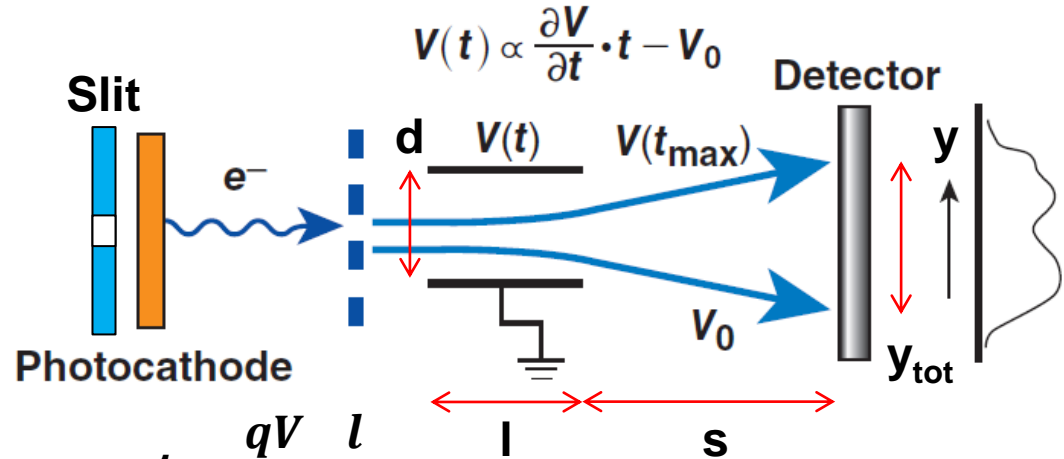


A temporal resolution higher than 15 ps is expected



Imaging system

- Visible light: regular lens
- X rays: pinhole



$$a = \frac{F}{m} = \frac{qE}{m} = \frac{qV}{md}$$

$$v_{\perp} = at = \frac{qV}{md} \frac{l}{v_{\parallel}}$$

$$y = s \tan \theta = s \frac{v_{\perp}}{v_{\parallel}} = \frac{1}{2E_k} \frac{l}{d} sqV = \frac{1}{2E_k} \frac{l}{d} sq(V_0 + V't)$$

- Let $d=10$ mm, $l=20$ mm, $s=50$ mm, $E_k=1$ keV, $V=-200 \sim 200$ V

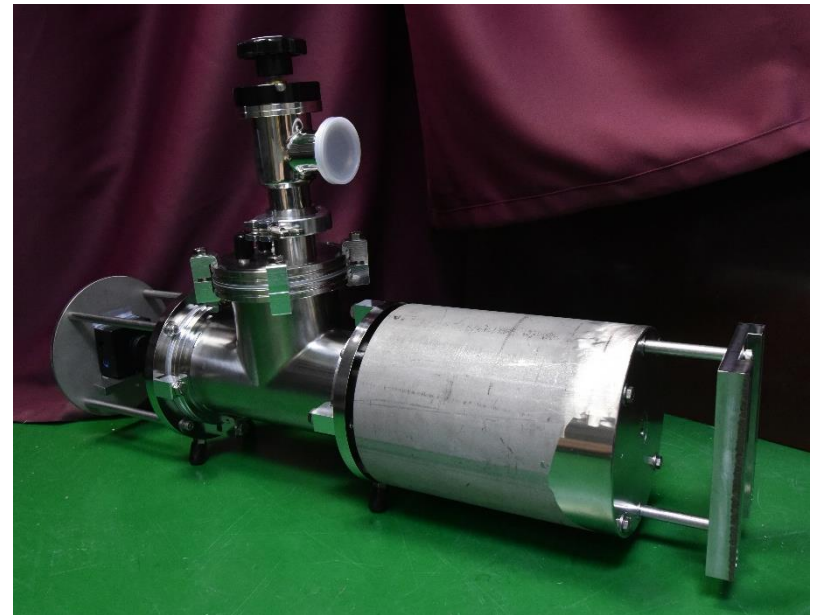
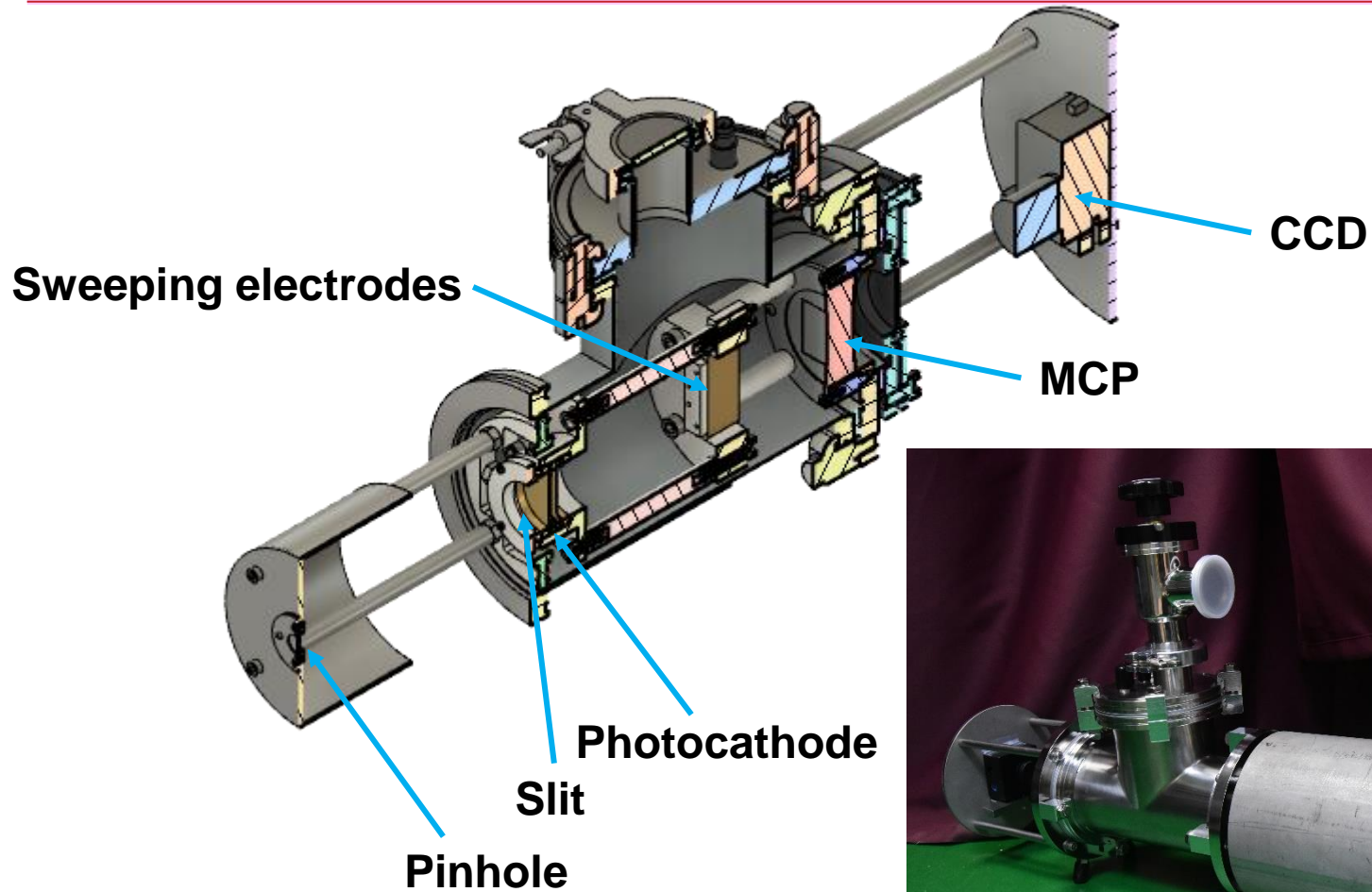
$$V' \equiv \frac{V_{\text{tot}}}{t_{\text{tot}}} = 0.06 \text{ kV/ns} \quad y_{\text{tot}} = 15\text{mm} \quad y_{\text{tot}} = 15\text{mm}$$

- Temporal resolution:

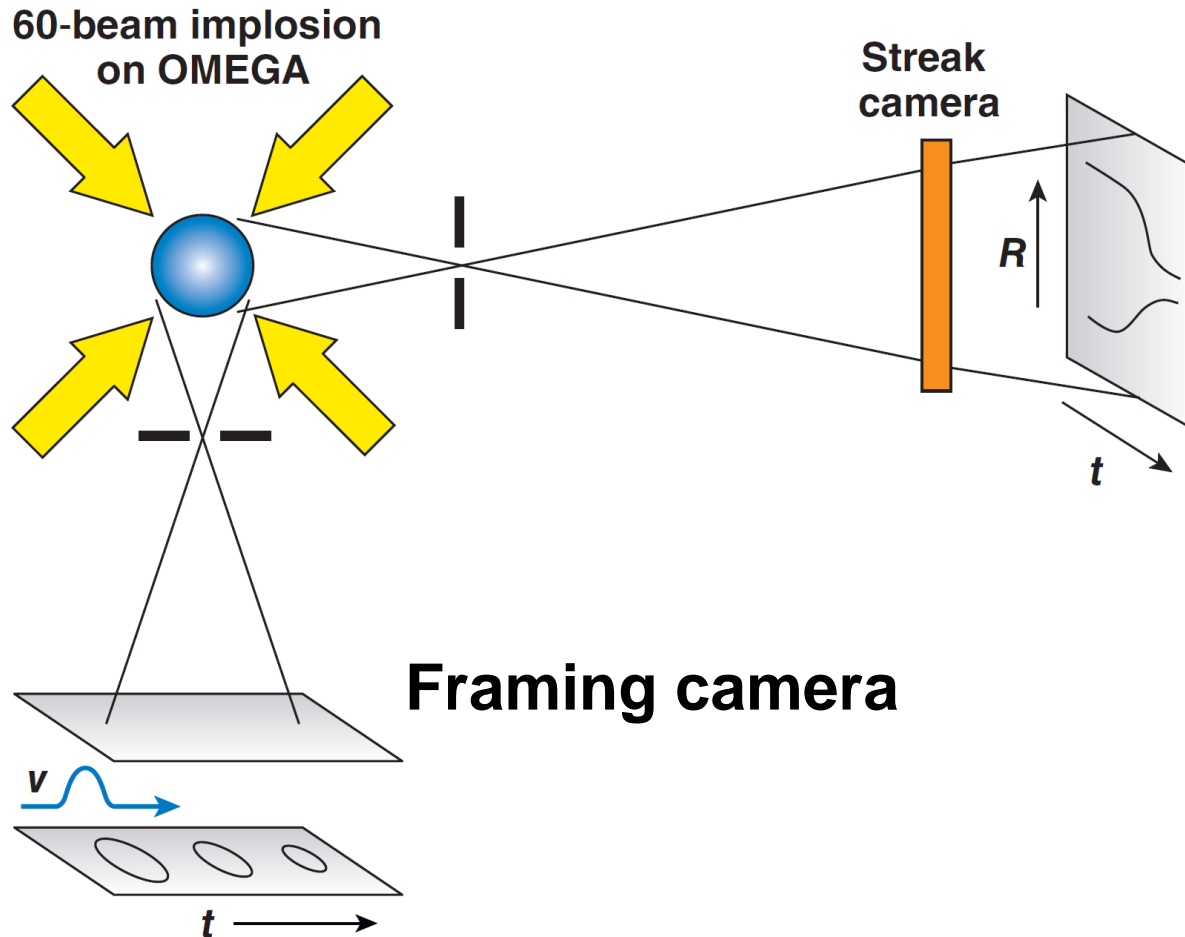
$$\delta t = \delta y \frac{2E_k d}{lsqV'} = 15 \text{ ps for } \delta y = 45\mu\text{m}$$

- δt will be adjusted by changing E_k .

A streak camera with temporal resolution of 15 ps has been developed



Shell trajectories can be measured using framing camera or streak camera

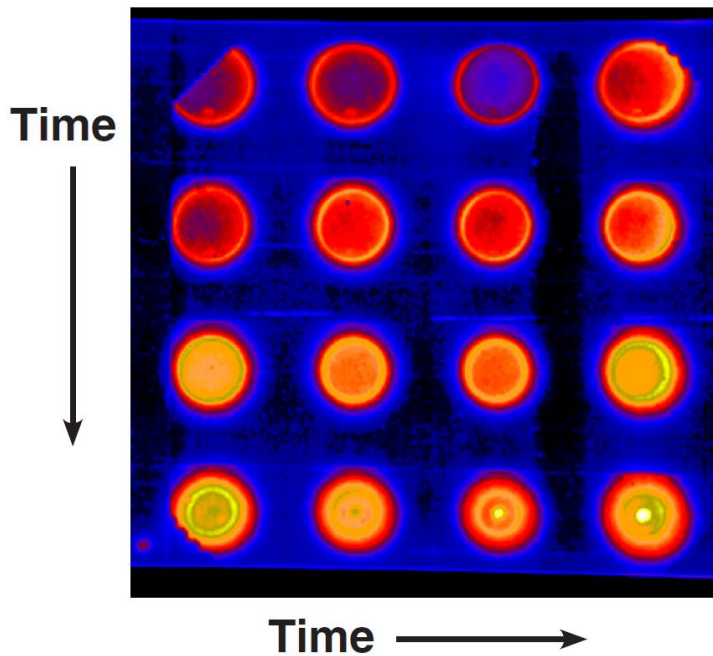


Comparison of images from framing camera versus streak camera



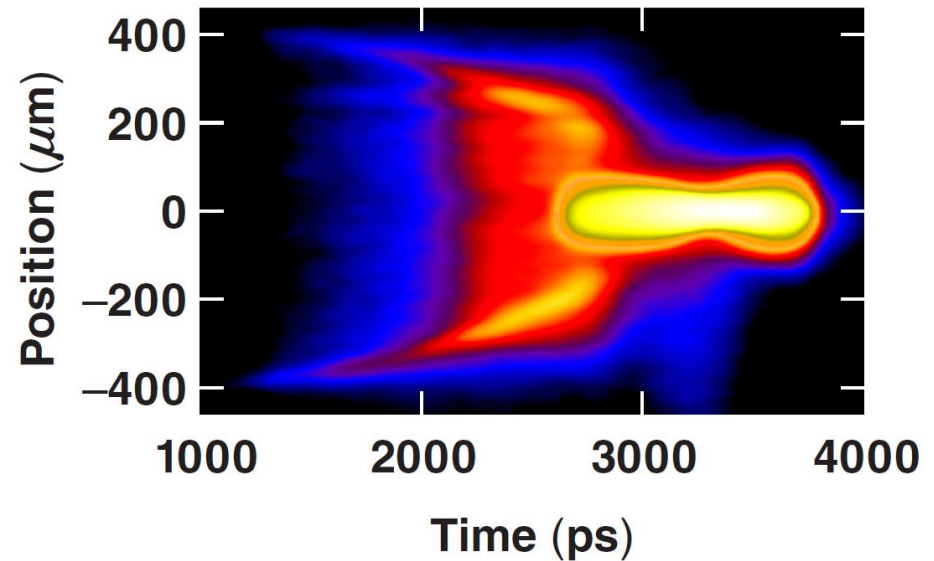
Framing-camera image
6× magnification

Shot 13377

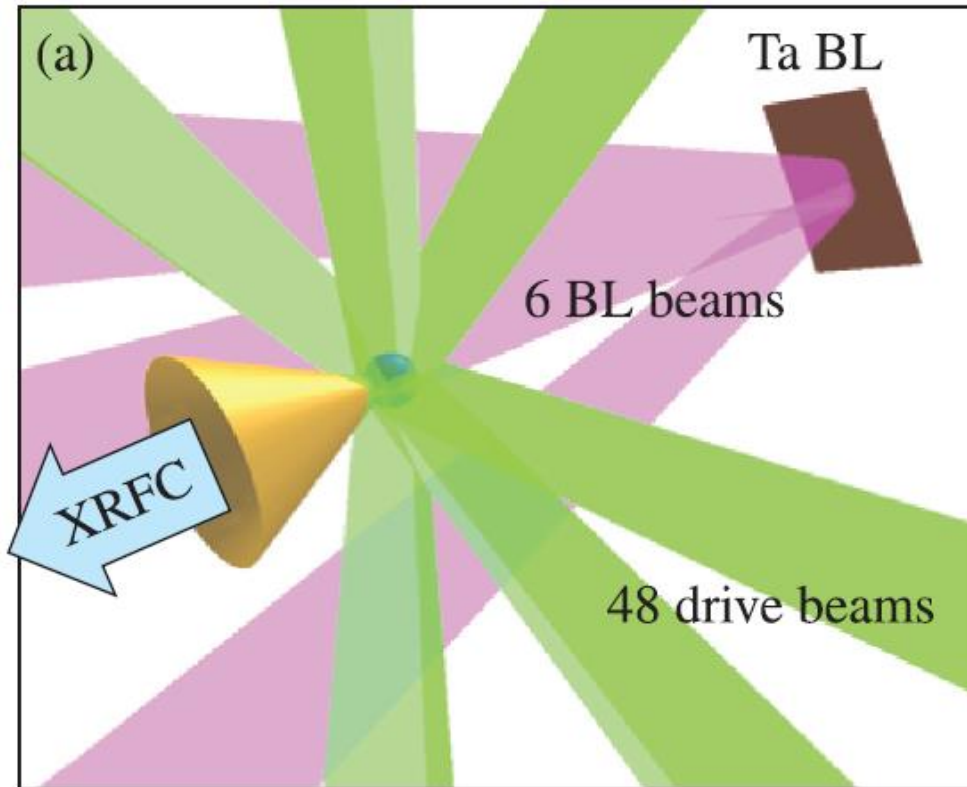


Streak-camera image

Shot 13377



The optical density can be measured using the absorption of a backlighter



$$I = \int I(\varepsilon) \exp(-\mu(\varepsilon) \rho \delta) d\varepsilon$$

$$I = I_{BL} \exp(-\bar{\mu} \rho \delta)$$

$$\ln I = \ln I_{BL} - \mu \rho r$$

X-ray radiography of an X-pinch by using another X-pinch or two X-pinches as point sources of probing radiation

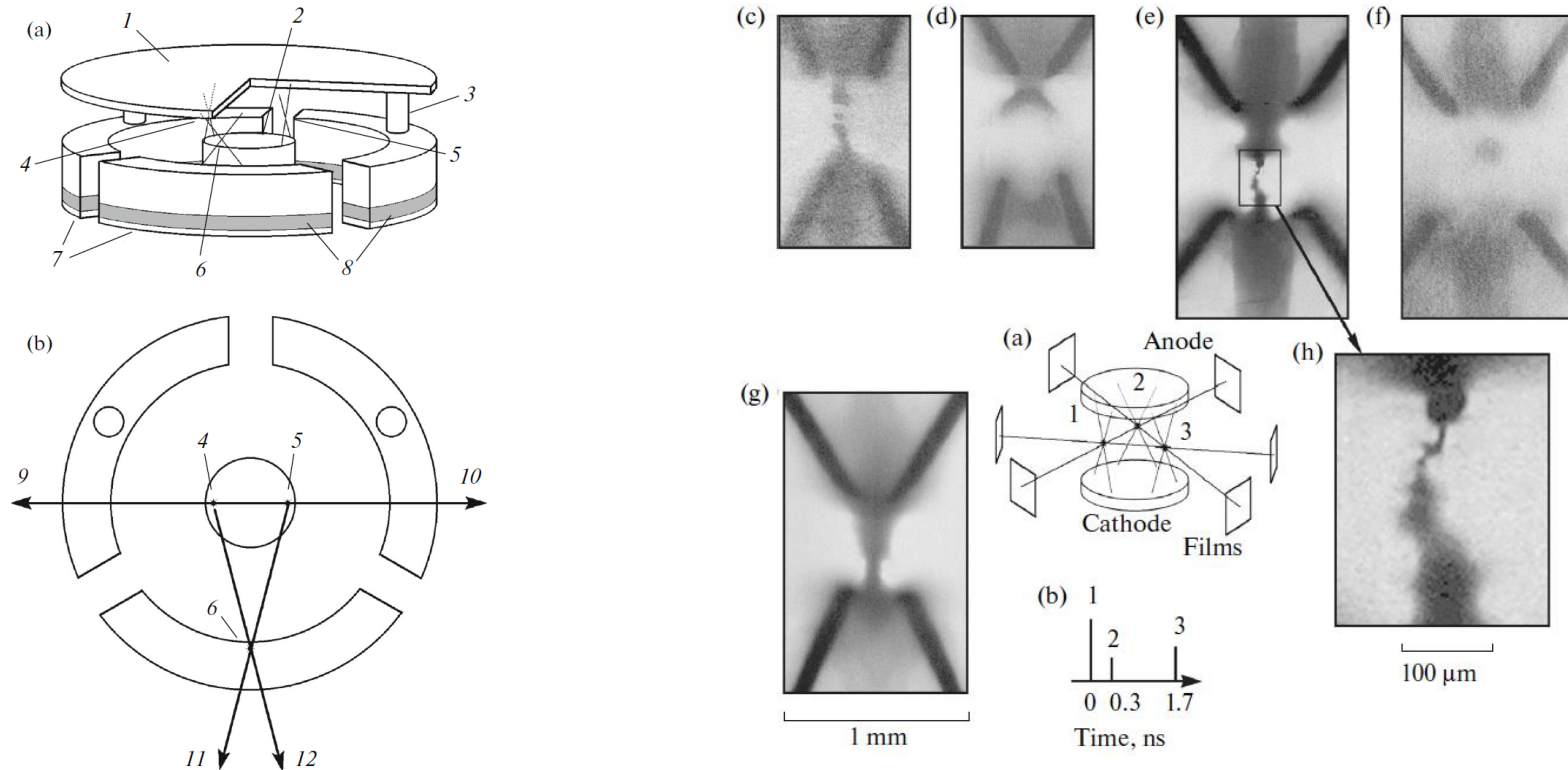
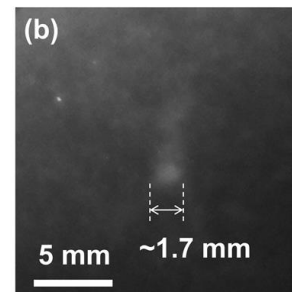
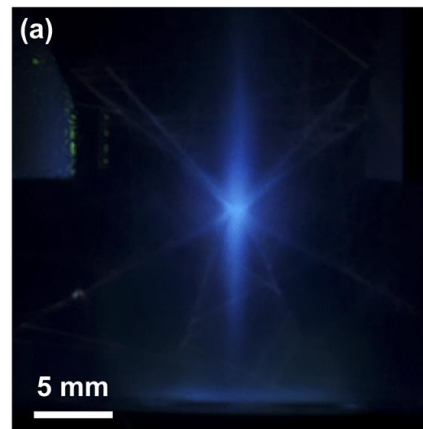
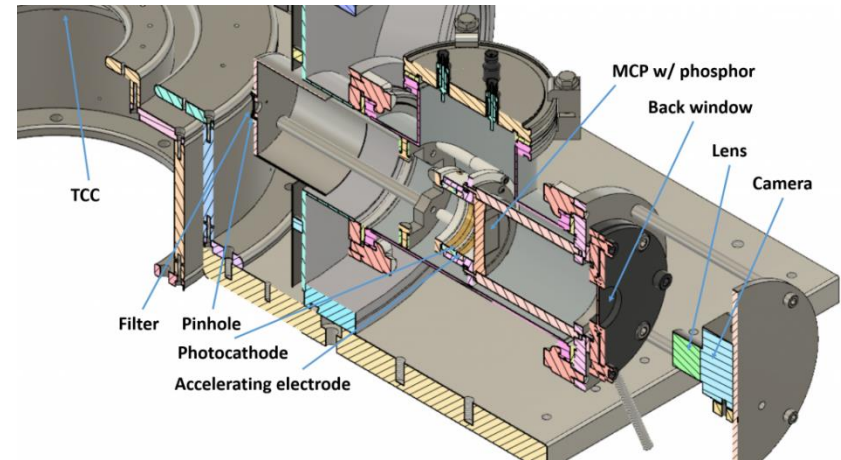
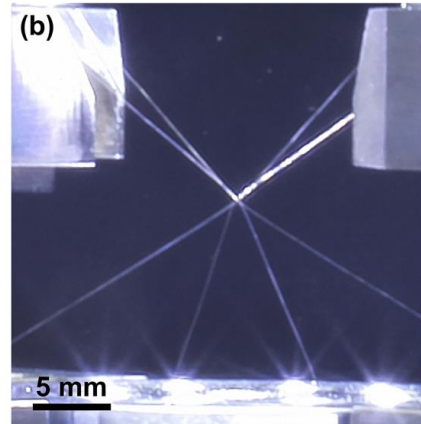
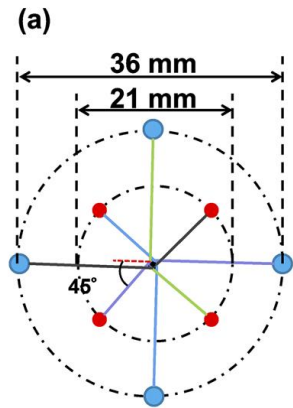
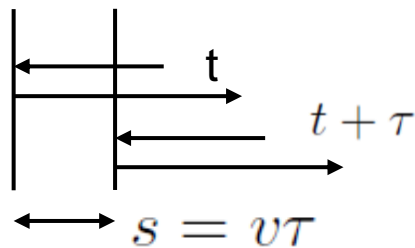
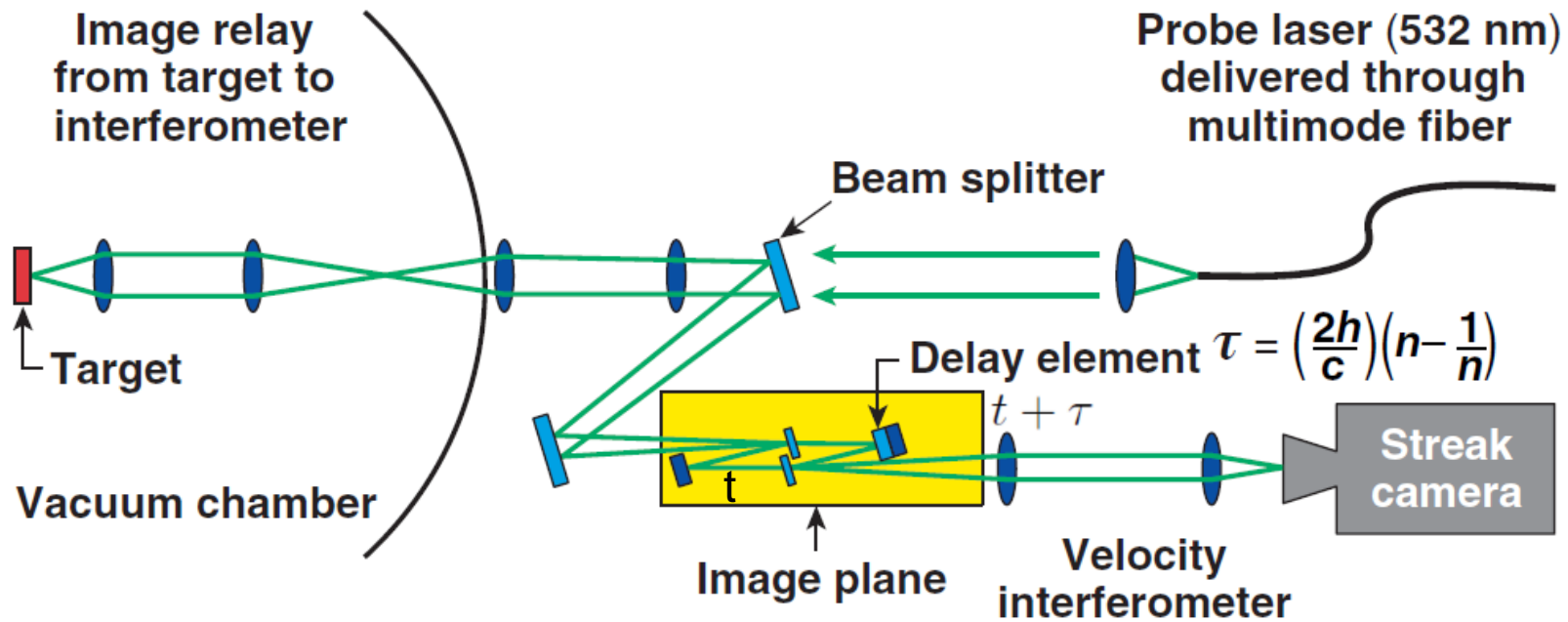


Fig. 44. X-ray radiographs obtained in the system of three parallel $2 \times 12.5\text{-}\mu\text{m}$ Mo X-pinches: (a) arrangement of the pinches and films, (b) temporal positions and relative intensities of probing X-ray pulses, (c) image of X-pinch 1 in the radiation of X-pinch 2, (d) image of X-pinch 1 in the radiation of X-pinch 3, (e) image of X-pinch 2 in the radiation of X-pinch 1, (f) image of X-pinch 2 in the radiation of X-pinch 3, (g) image of X-pinch 3 in the radiation of X-pinch 1 emission, and (h) enlarged fragment of the image.

We demonstrated using x-ray pinhole camera to capture the radiation from an imploded x pinch

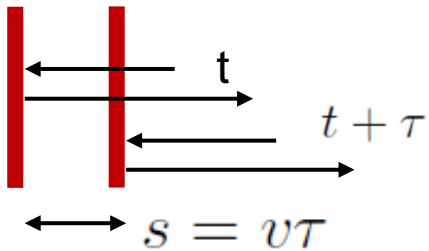
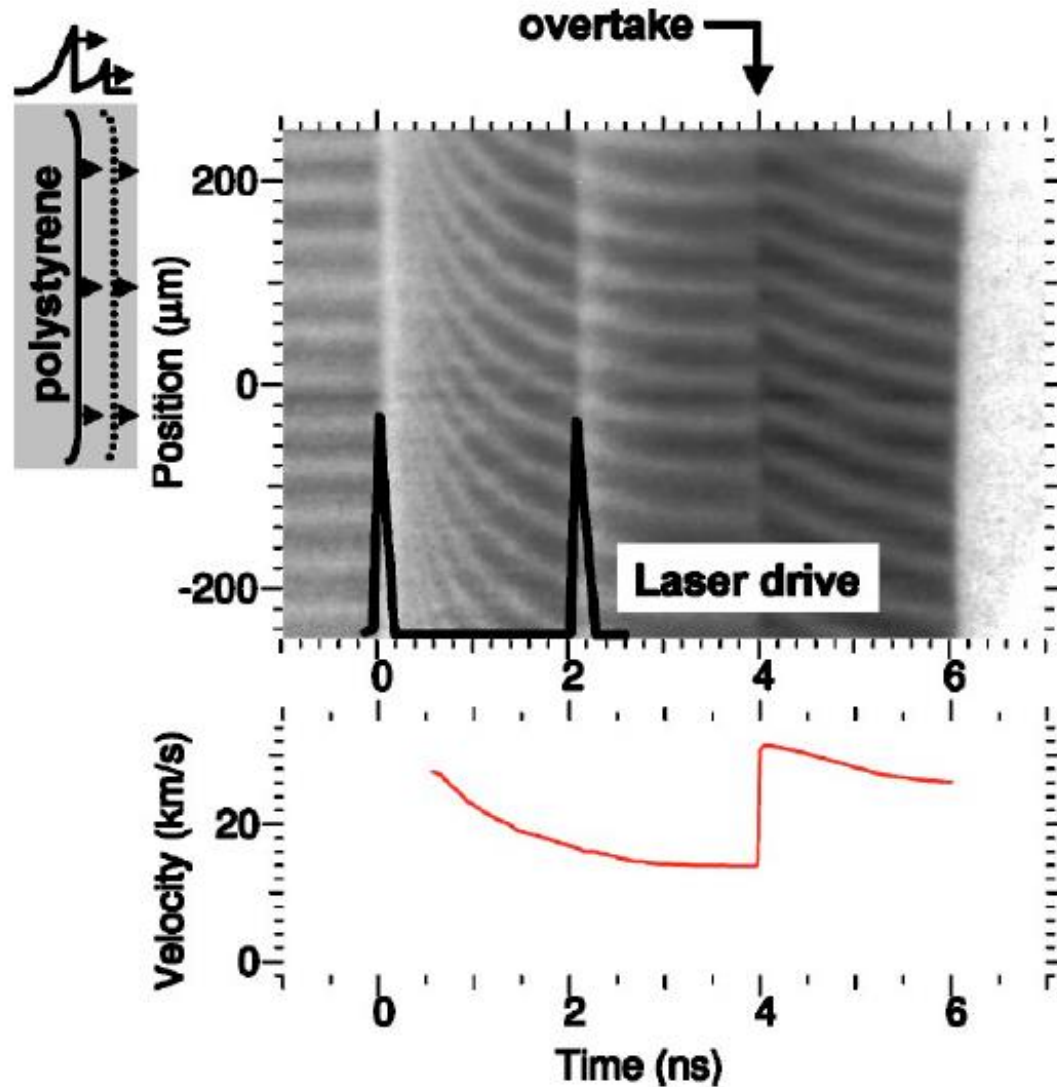


Shock velocities are measured using time-resolved Velocity Interferometer System for Any Reflector (VISAR)

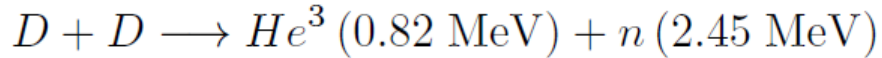
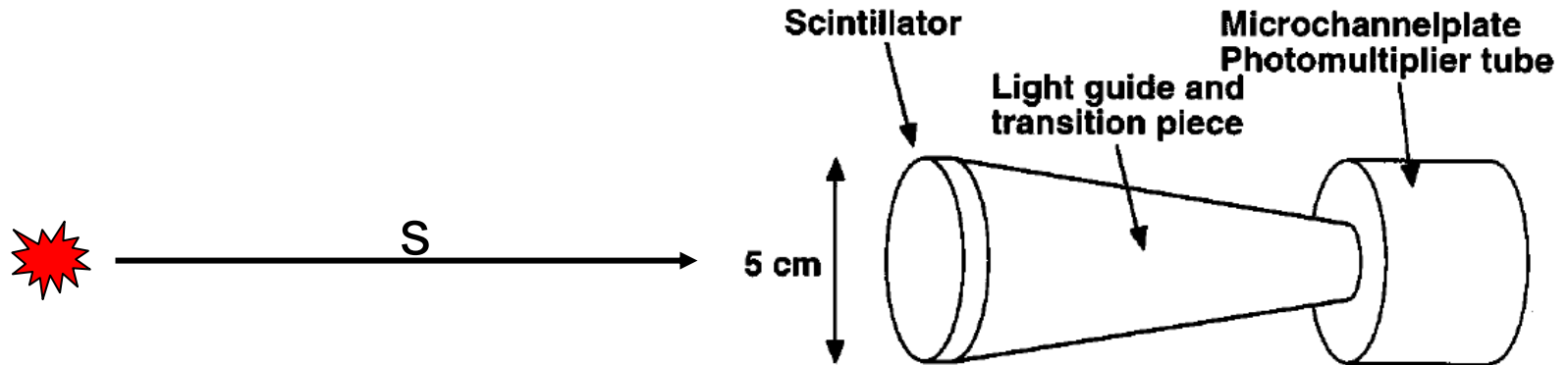


$$\Delta\phi = \frac{vT}{\lambda} \propto v$$

Shock velocities are measured using time-resolved Velocity Interferometer System for Any Reflector (VISAR)

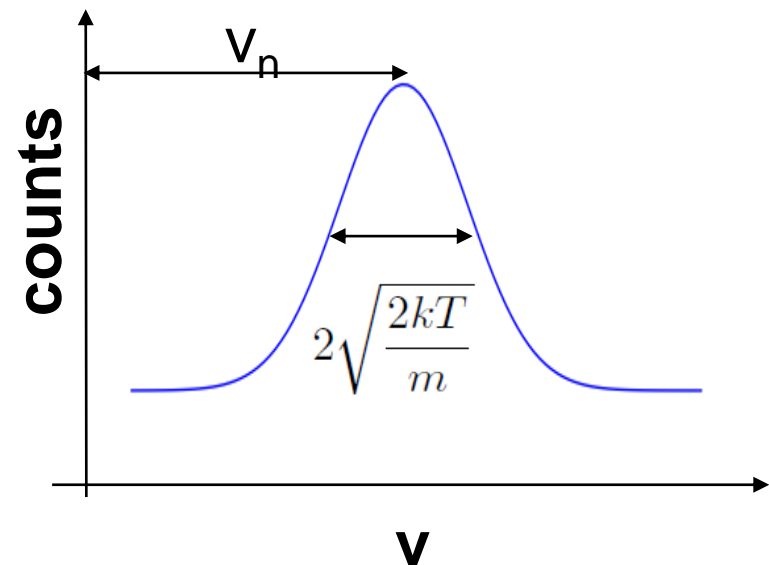


Neutron average temperature is obtained using Neutron Time of Flight (NToF)



$$s = vt \quad v = \frac{s}{t}$$

$$f(v) = \sqrt{\left(\frac{m}{2\pi kT}\right)} \exp\left(-\frac{mv^2}{2kT}\right)$$



The OMEGA Facility is carrying out ICF experiments using a full suite of target diagnostics

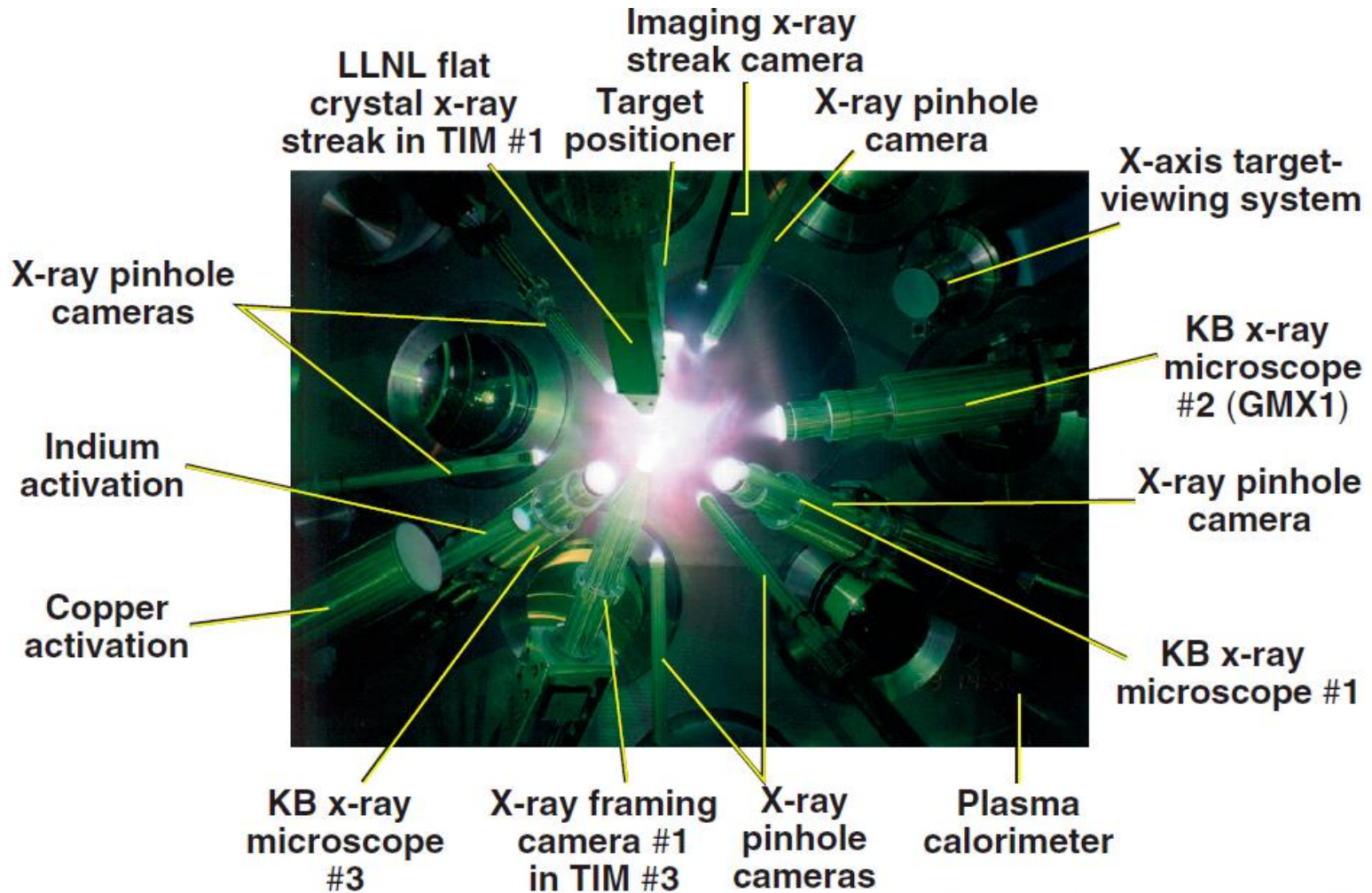
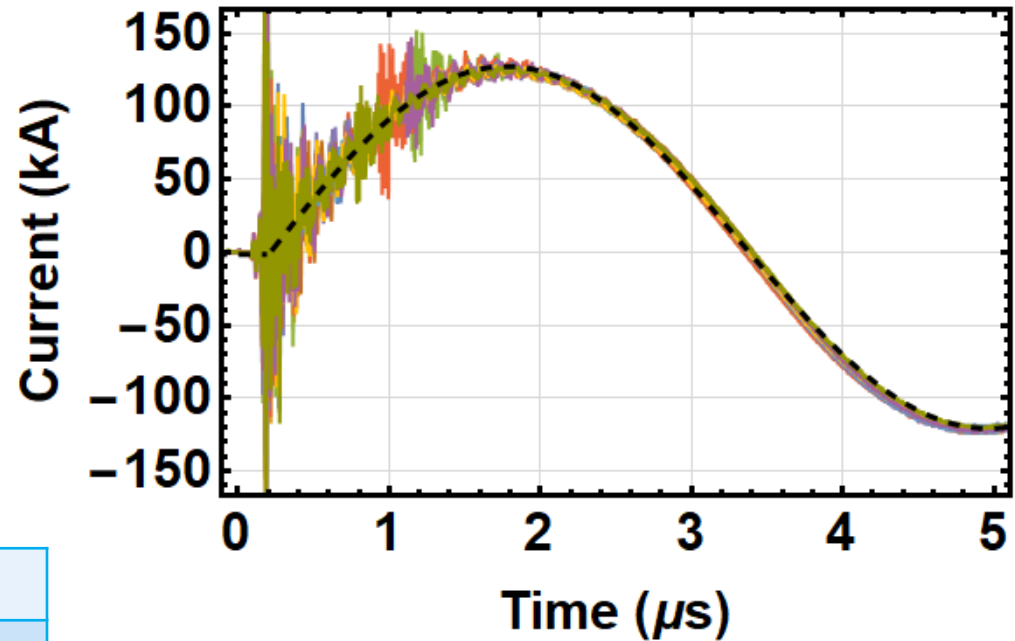
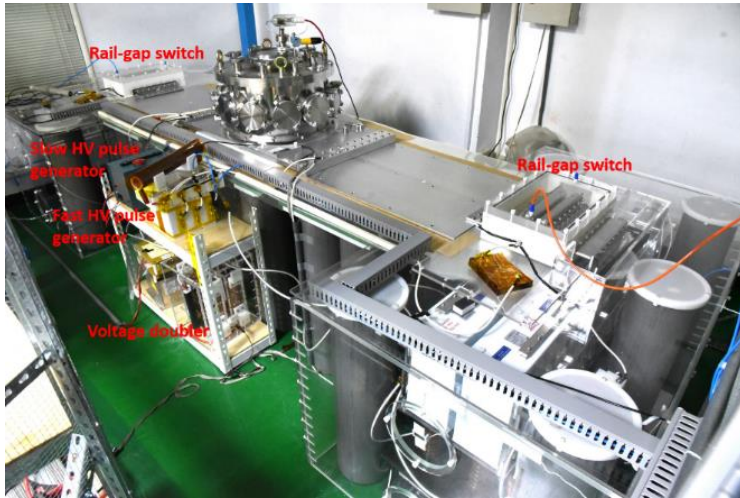


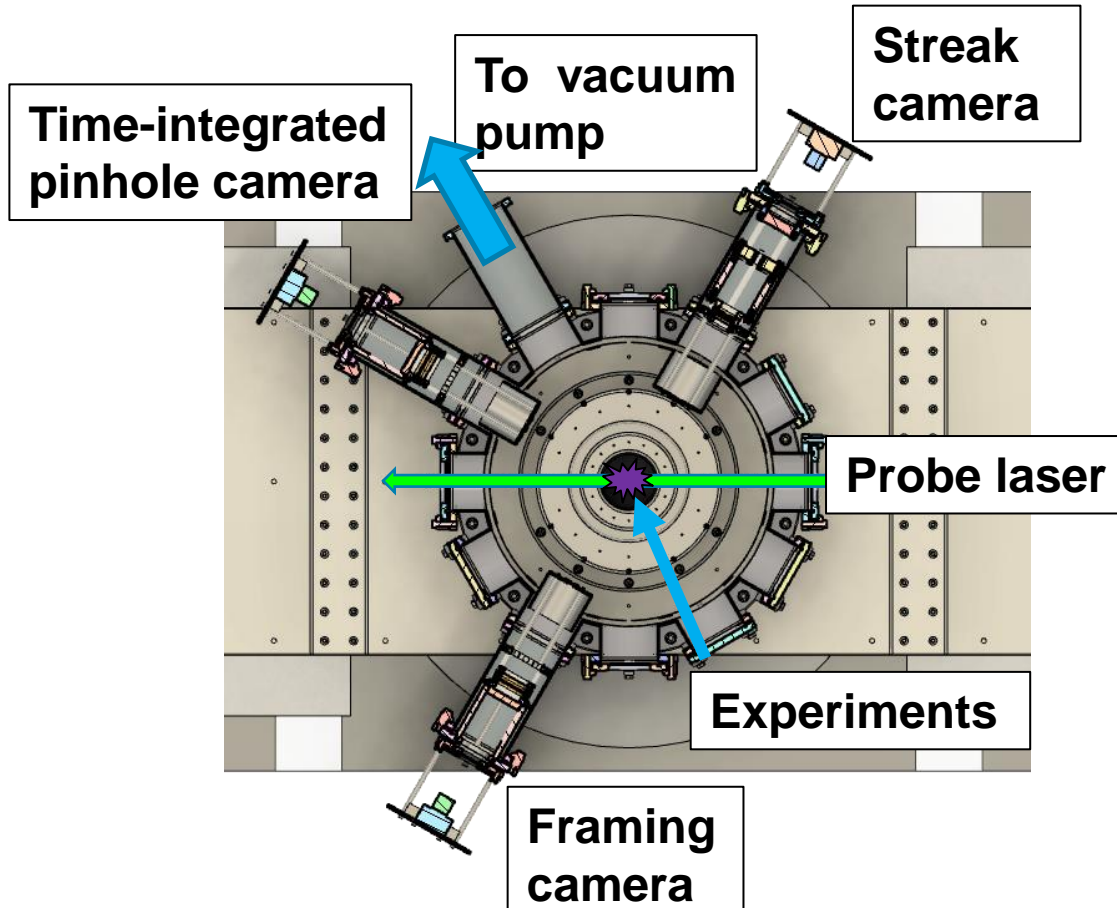
Photo taken from port H11B

A peak current of ~ 135 kA with a rise time of ~ 1.6 μ s is provided by the pulsed-power system



Capacitance (μ F)	5
V_{charge} (kV)	20
Energy (kJ)	1
Inductance (nH)	204 ± 4
Rise time (quarter period, ns)	1592 ± 3
I_{peak} (kA)	135 ± 1

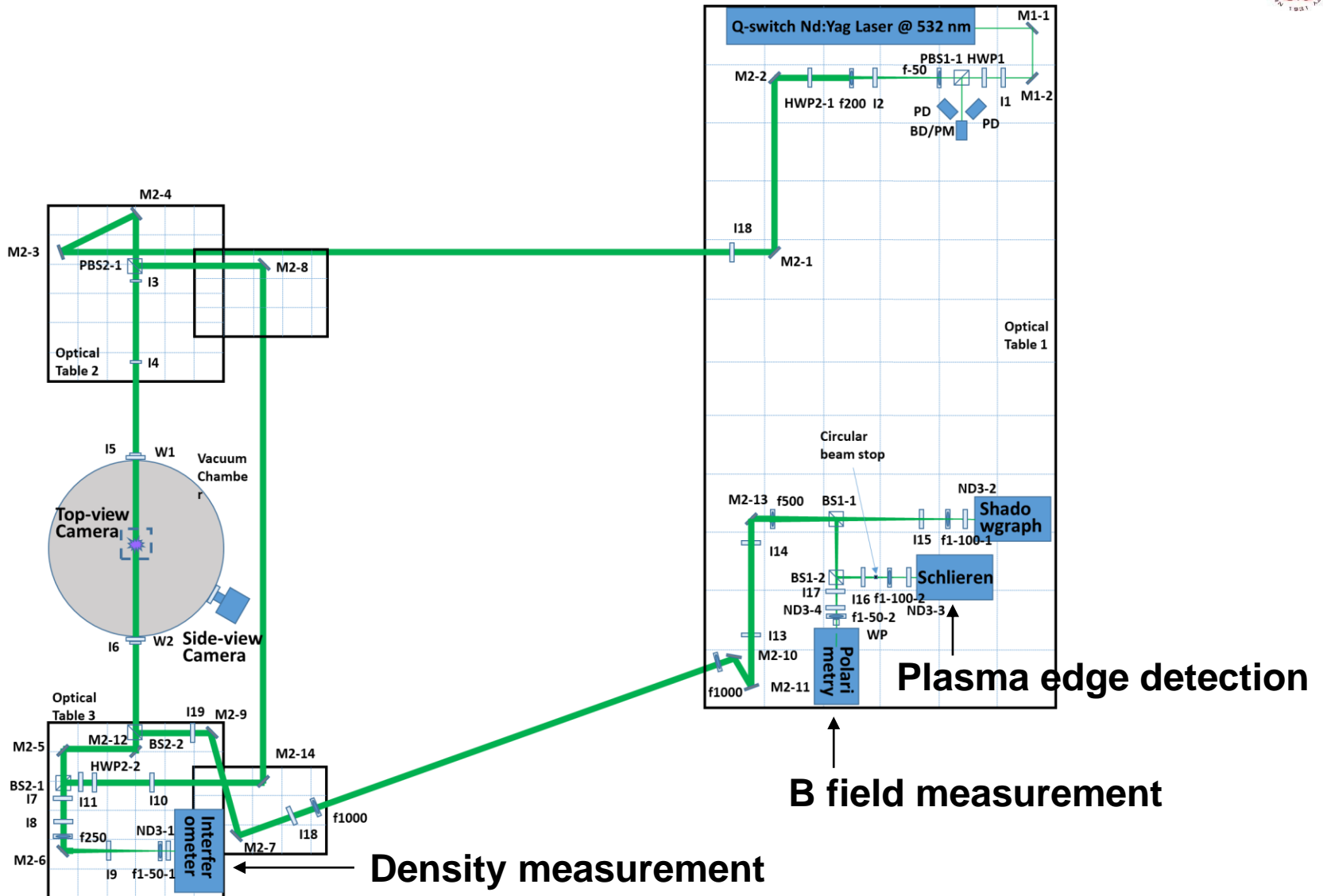
A suit of diagnostics in the range of (soft) x-ray are being built



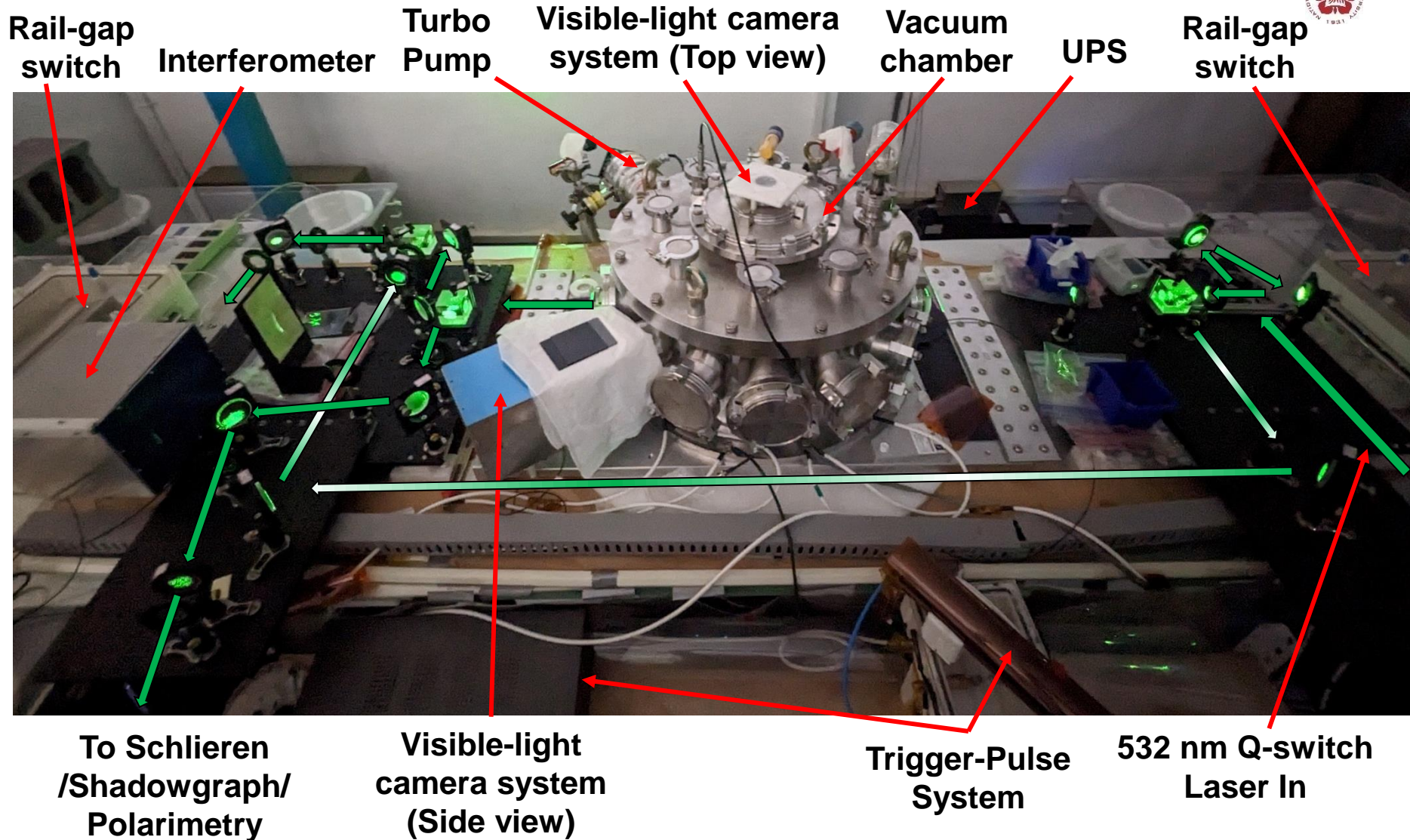
- CsI are used as the photocathode for all x-ray imaging system.
- Au photocathode may be used in the future.

- Pinhole camera:
 - Magnification: 1x
 - Exposure time: 1 μ s
- Streak camera:
 - Magnification: 1x
 - Temporal resolution: 15 ps
- Framing camera:
 - Magnification: 0.3x
 - Temporal resolution: \sim ns using 4 individual MCPs
- Laser probing:
 - For interferometer, schlieren, shadowgraphy, Thomson scattering.
 - Temporal resolution: \sim 300 ps using stimulated brillouin scattering (SBS) pulse compression in water

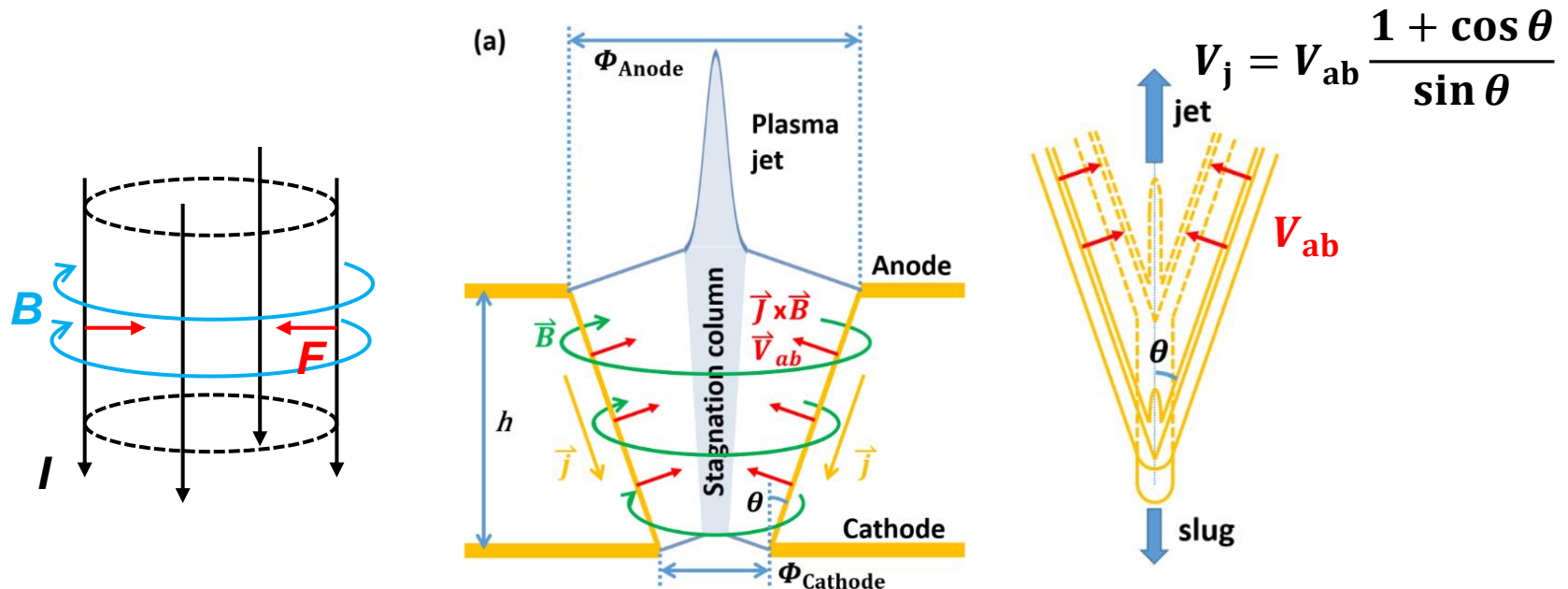
Time-resolved imaging system with temporal resolution in the order of nanoseconds was implemented



Varies diagnostics were integrated to the system

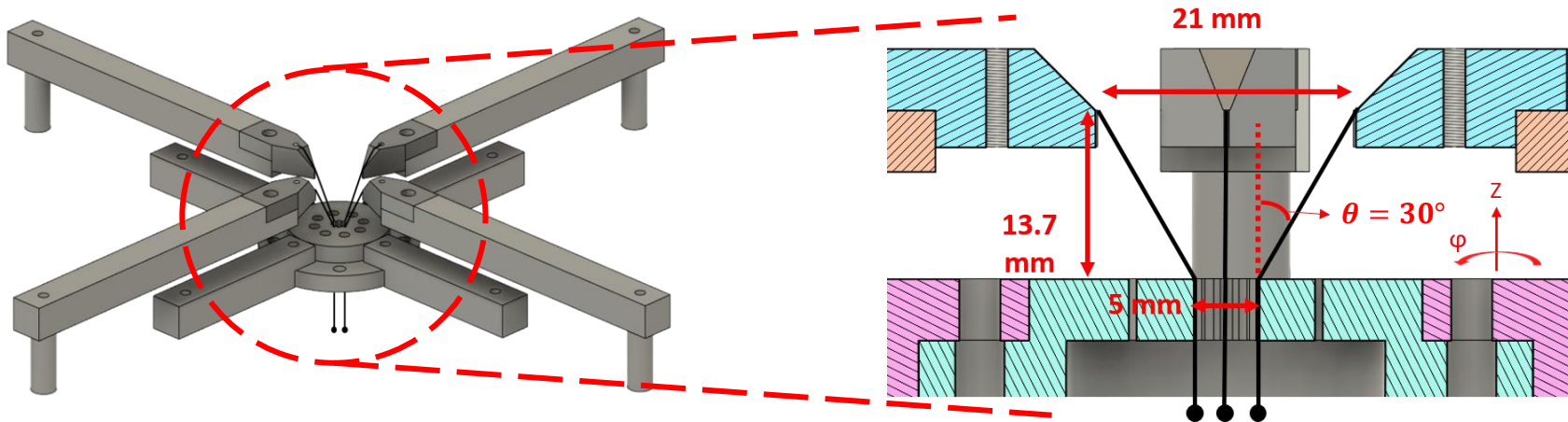


A plasma jet can be generated by a conical-wire array due to the nonuniform z-pinch effect

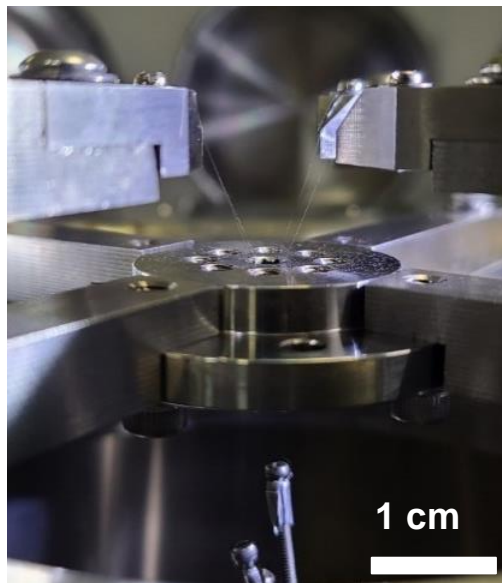
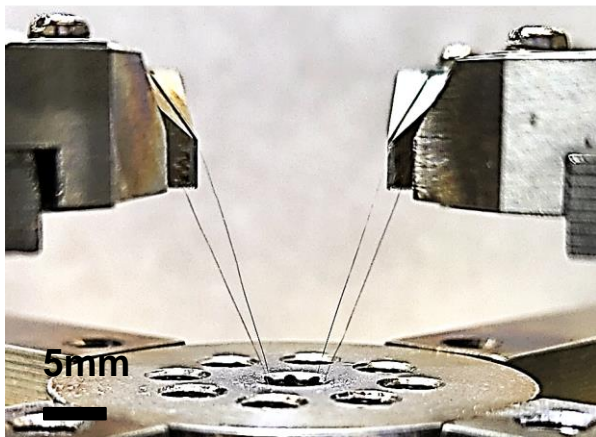


1. Wire ablation : corona plasma is generated by wire ablations.
2. Precursor : corona plasma is pushed by the $\vec{J} \times \vec{B}$ force and accumulated on the axis forming a precursor.
3. Plasma jet is formed by the nonuniform z-pinch effect due to the radius difference between the top and the bottom of the array.

Our conical-wire array consists of 4 tungsten wires with an inclination angle of 30° with respect to the axis



- Conical-wire array

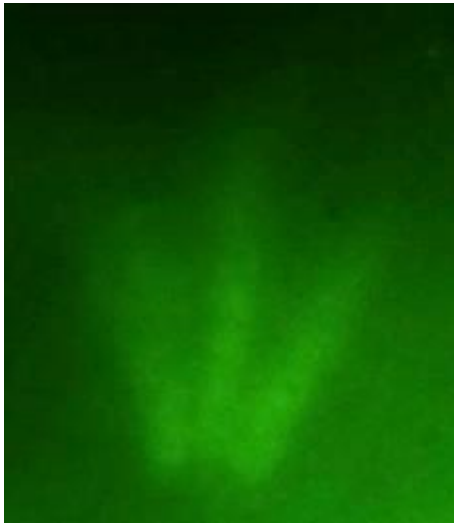


- Material : Tungsten.
- Number of wires : 4.
- Diameter : $20 \mu\text{m}$.

Self-emission of the plasma jet in the UV to soft x-ray regions was captured by the pinhole camera



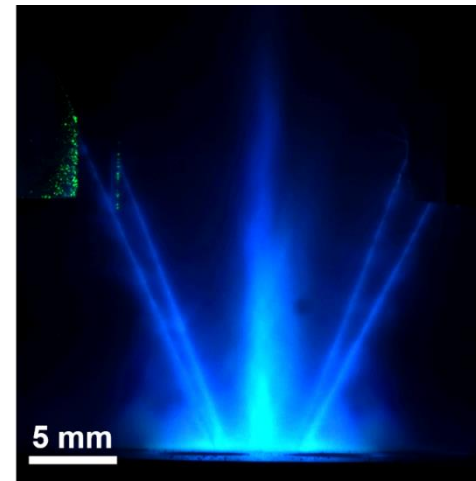
- Image in UV/soft x ray



(Brightness is increased by 40 %.)

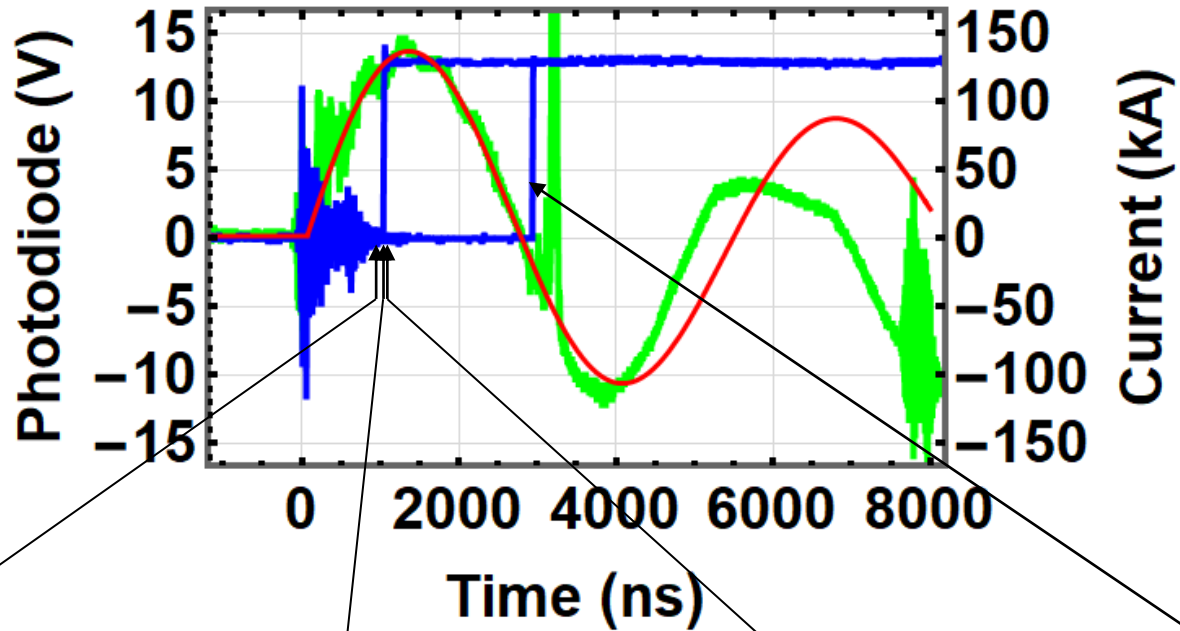
- Pinhole diameter: 0.5 mm, i.e., spatial resolution: 1 mm.

- Image in visible light

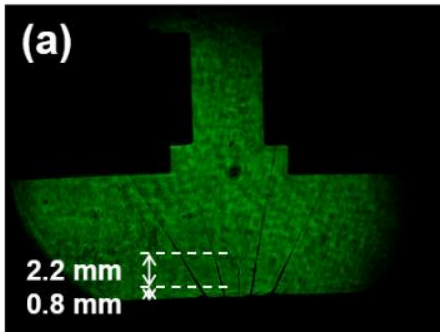


(Enhanced by scaling the intensity range linearly from 0 – 64 to 0 – 255.)

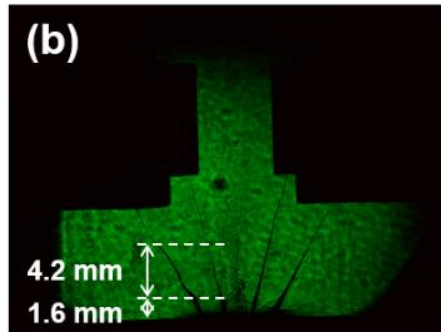
Plasma jet propagation was observed using laser diagnostics



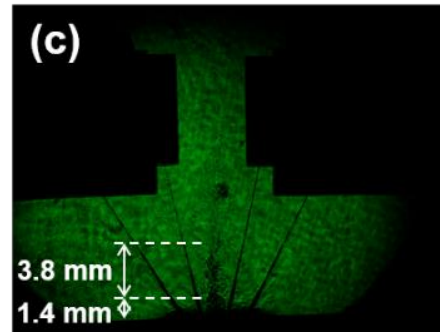
- Shadowgraph images:



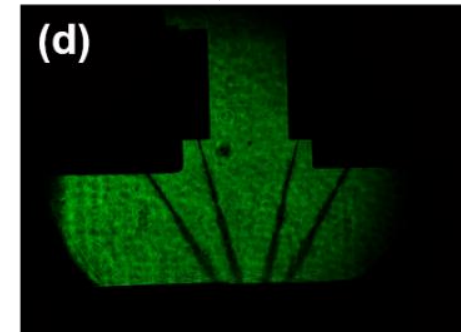
930 ± 20 ns



975 ± 2 ns



985 ± 3 ns

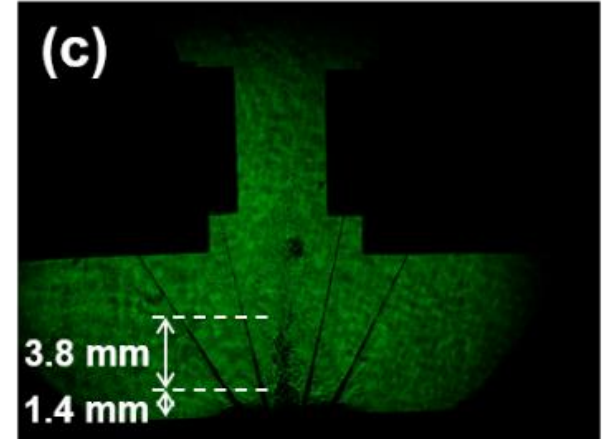
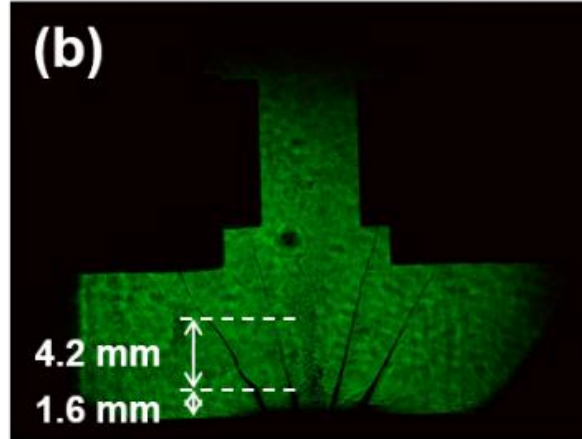
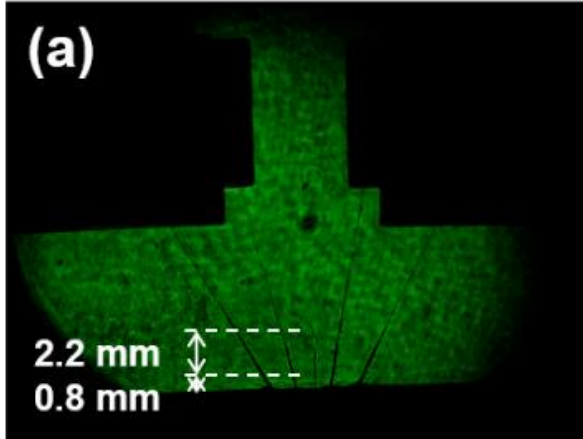


2945 ± 2 ns

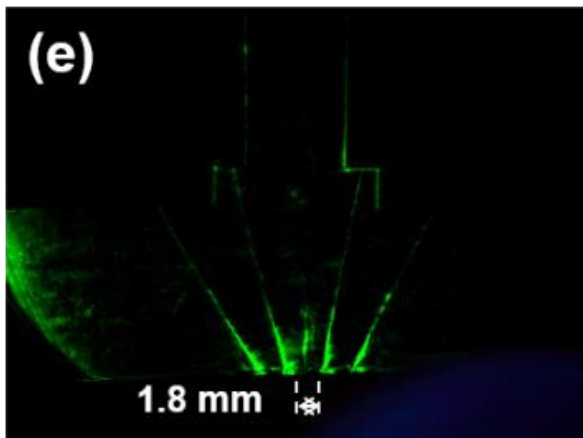
Length of the plasma jet at different time was obtained by the Schlieren images at different times



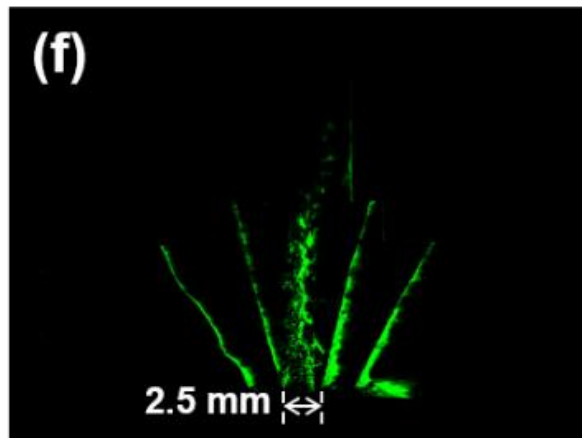
- Shadowgraph images:



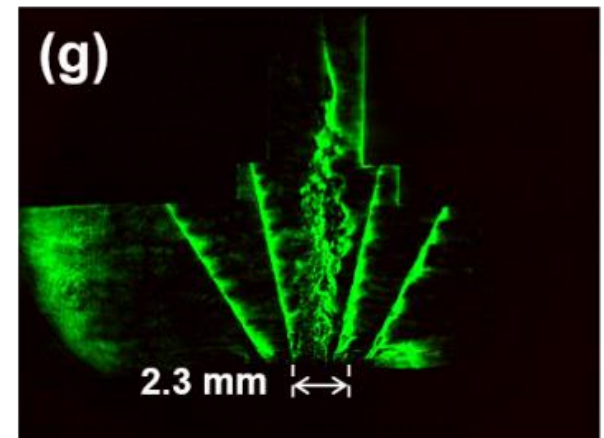
- Schlieren images:



930 ± 20 ns

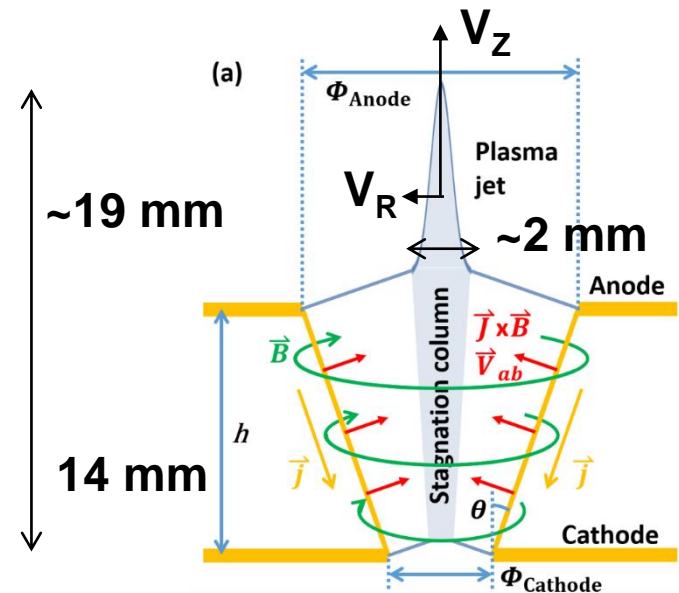
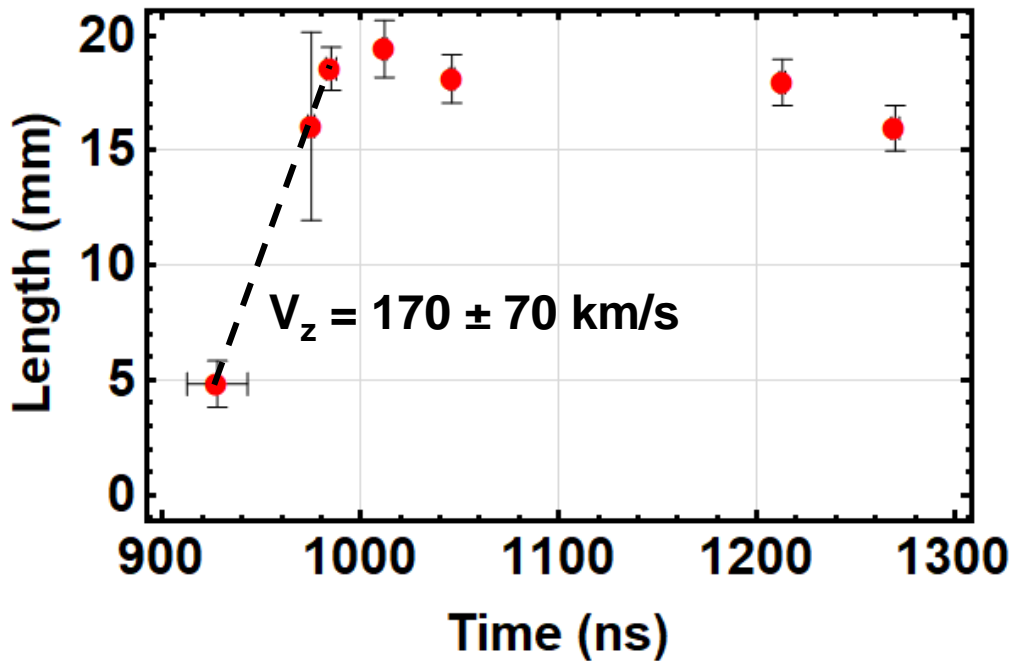


975 ± 2 ns



985 ± 3 ns

The measured plasma jet speed is 170 ± 70 km/s with the corresponding Mach number greater than 5



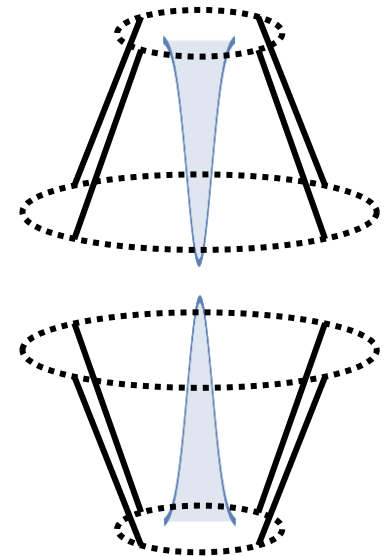
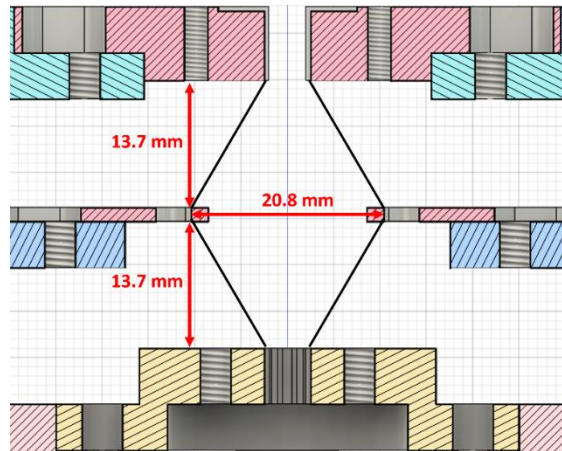
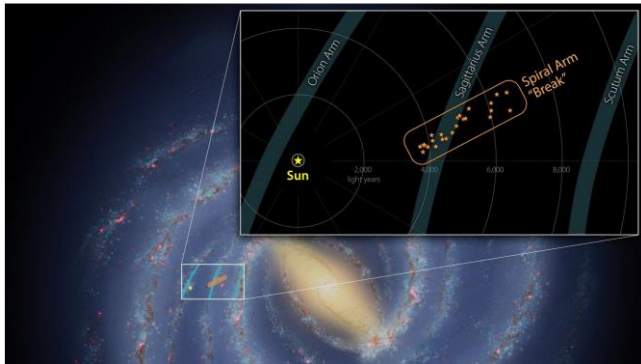
$$M = \frac{V_z}{V_R} \geq \frac{Z}{r} \approx \frac{(19 - 14) \text{ mm}}{\frac{2 \text{ mm}}{2}} = 5$$

$$V_{ab} = V_j \frac{\sin \theta}{1 + \cos \theta} = 50 \pm 20 \text{ km/s}$$

Plasma disk can be formed when two head-on plasma jets collide with each other



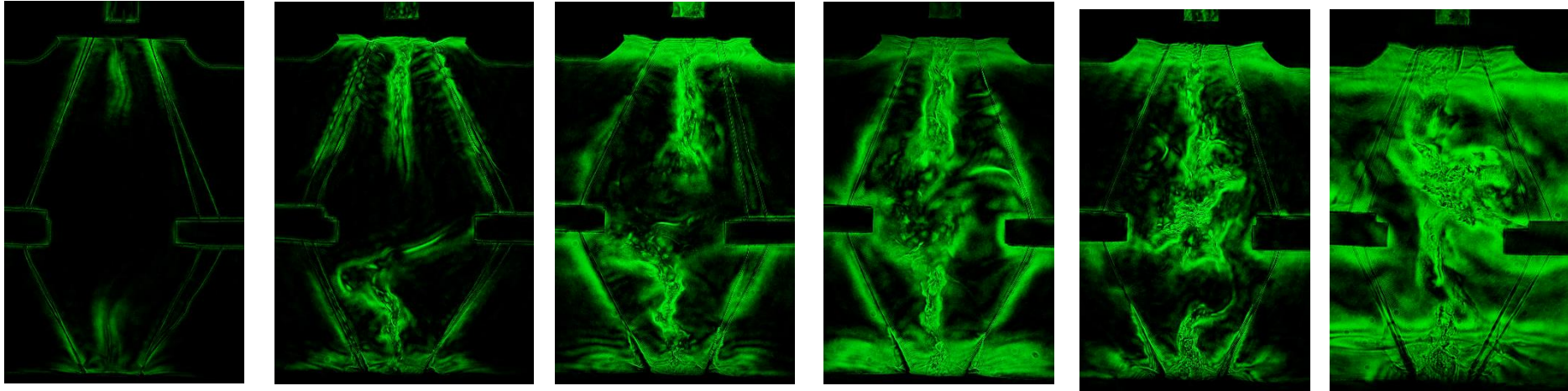
- Astronomers Find a 'Break' in One of the Milky Way's Spiral Arms.



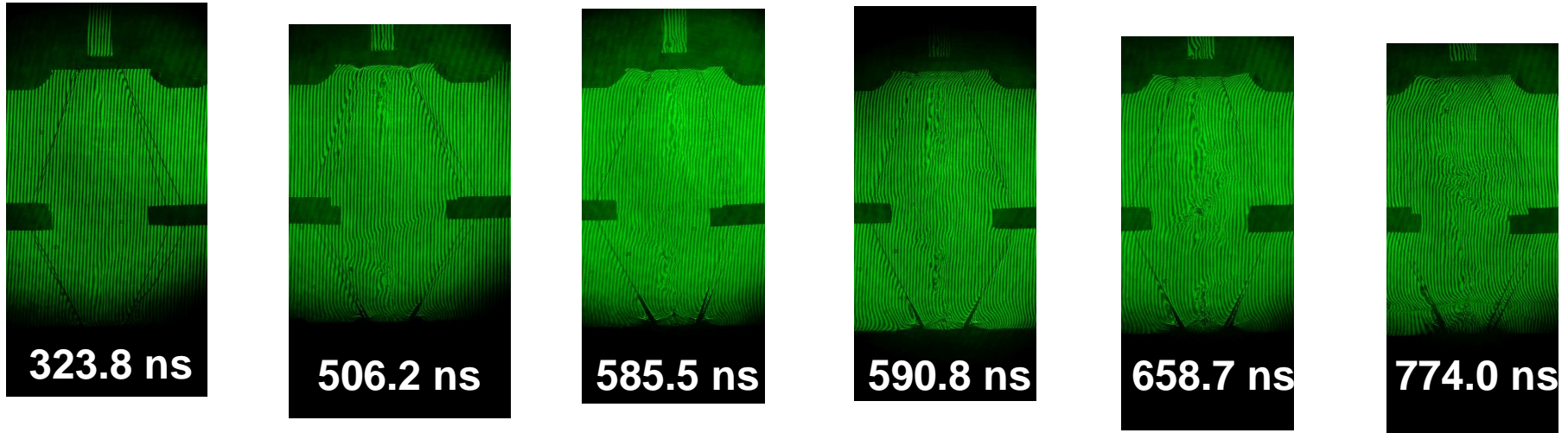
Plasma disk can be formed when two head-on plasma jets collide with each other



Schlieren



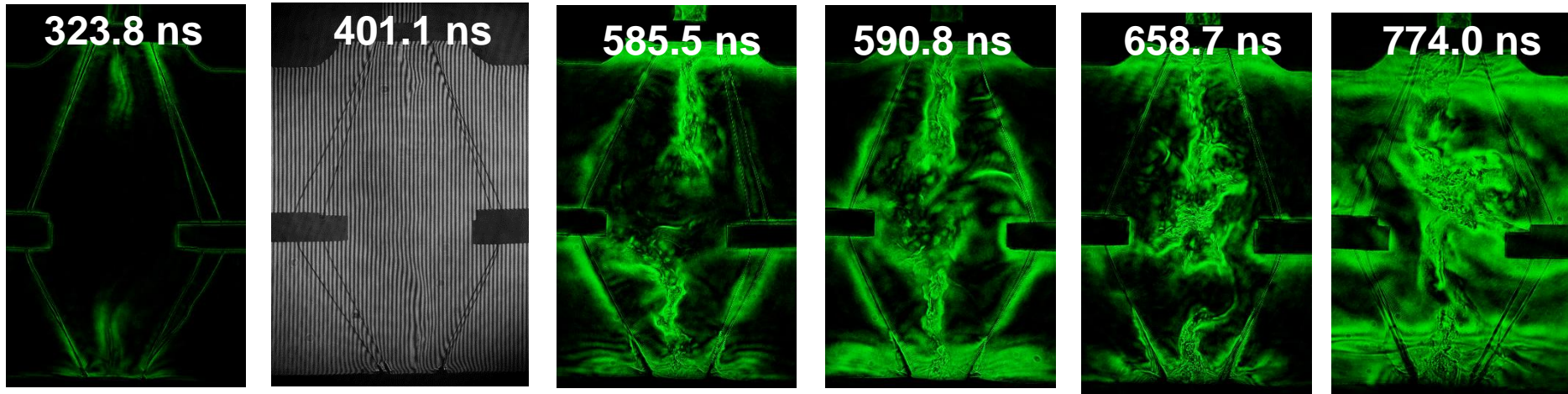
Interferometer



Plasma disk can be formed when two head-on plasma jets collide with each other

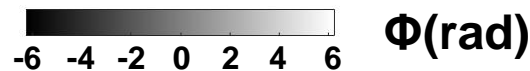
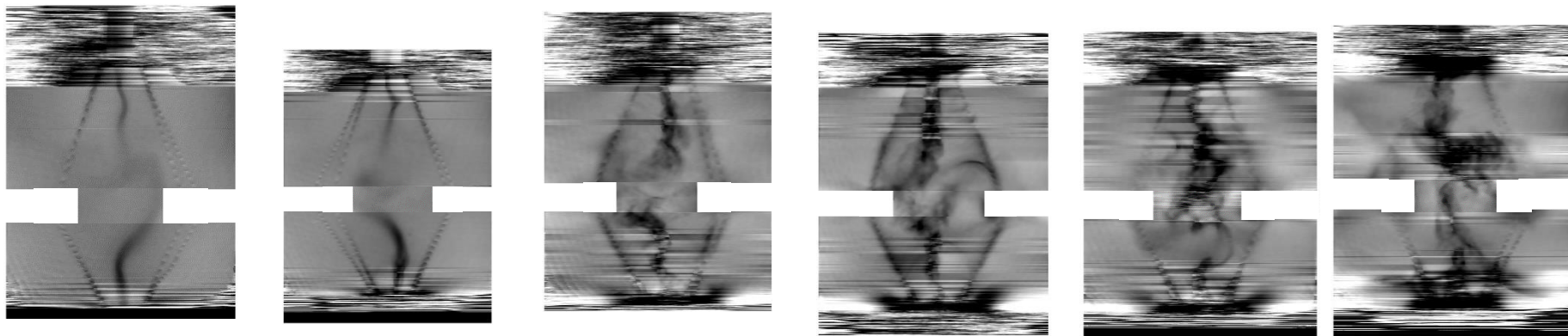


Schlieren



Interferometer

$$-2\pi \sim 2\pi \Rightarrow 0 \sim 4.2 \times 10^{17} \text{ cm}^{-2} \Rightarrow 8.4 \times 10^{17} \text{ cm}^{-3} \text{ for } l = 5\text{mm}$$

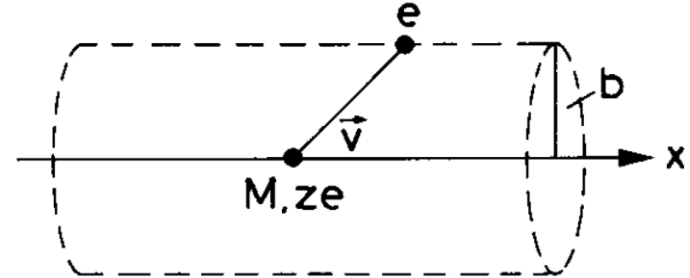


Energetic charged particles losses most of its energy right before it stops



Momentum transfer:

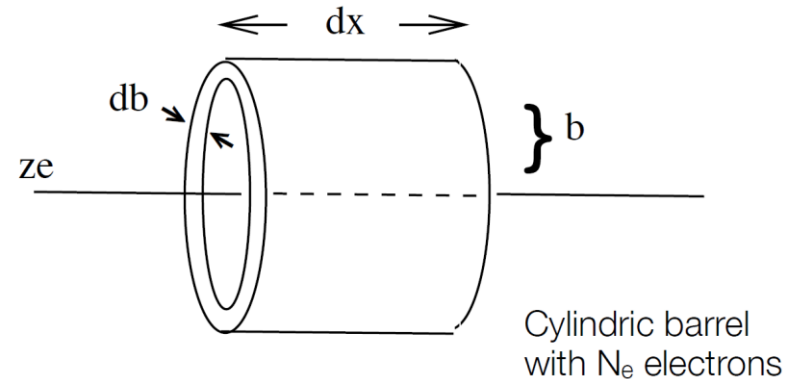
$$\Delta p_{\perp} = \int F_{\perp} dt = \int F_{\perp} \frac{dt}{dx} dx = \int F_{\perp} \frac{dx}{v}$$



$$= \int_{-\infty}^{\infty} \frac{ze^2}{(x^2 + b^2)} \cdot \frac{b}{\sqrt{x^2 + b^2}} \cdot \frac{1}{v} dx = \frac{ze^2 b}{v} \left[\frac{x}{b^2 \sqrt{x^2 + b^2}} \right]_{-\infty}^{\infty} = \frac{2ze^2}{bv}$$

Δp_{\parallel} : averages to zero

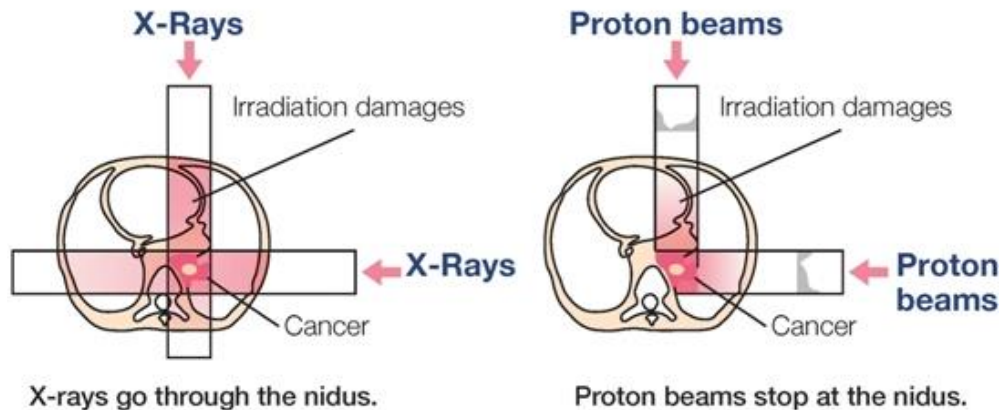
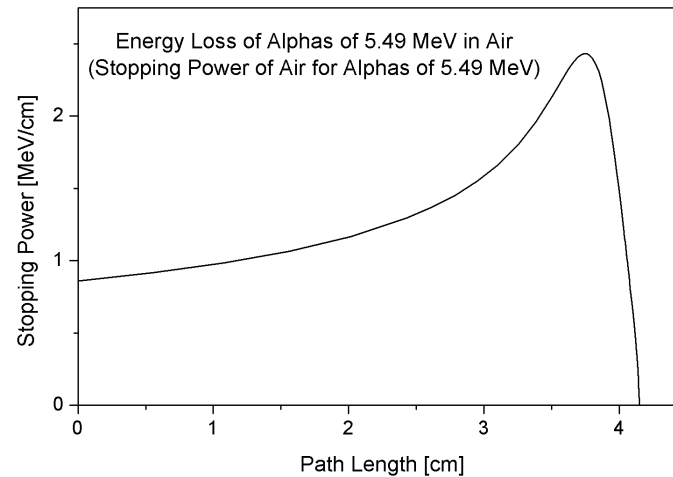
$$\Delta E(b) = \frac{\Delta p^2}{2m_e} \quad N_e = n \cdot (2\pi b) \cdot db dx$$



$$-dE(b) = \frac{\Delta p^2}{2m_e} \cdot 2\pi n b db dx$$

$$-\frac{dE}{dx} = \frac{4\pi n z^2 e^4}{m_e v^2} \cdot \int_{b_{\min}}^{b_{\max}} \frac{db}{b} = \frac{4\pi n z^2 e^4}{m_e v^2} \ln \frac{b_{\max}}{b_{\min}}$$

Proton therapy takes the advantage of using Bragg peak



There are two suggested website for getting the information of proton stopping power in different materials



<http://www.nist.gov/pml/data/star/>

<http://www.srim.org/>

NIST | NIST Time | NIST Home | About NIST | Contact Us | A-Z Site Index | Search

Physical Measurement Laboratory

About PML | Publications | Topic/Subject Areas | Products/Services | News/Multimedia | Programs/Projects | Facilities

NIST Home > PML > Physical Reference Data > Stopping-Power & Range Tables: e-, p+, Helium Ions

NISTIR 4999 | Version History | Disclaimer

Stopping-Power and Range Tables for Electrons, Protons, and Helium Ions

M.J. Berger, J.S. Coursey, M.A. Zucker and J. Chang
(NIST, Physical Measurement Laboratory)

estar * *astar* * *pstar* *

Abstract:
The databases ESTAR, PSTAR, and ASTAR calculate stopping-power and range tables for electrons, protons, or helium ions, according to methods described in ICRU Reports 37 and 49. Stopping-power and range tables can be calculated for electrons in any user-specified material and for protons and helium ions in 74 materials.

Contents:

1. Introduction
2. ESTAR: Stopping Powers and Ranges for Electrons
3. PSTAR and ASTAR: for Protons and Helium Ions (alpha particles)

References
Appendix: Significance of Calculated Quantities

Access the Data:

1. Electrons
2. Protons

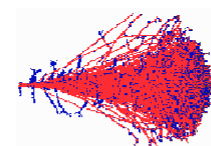
請選擇語言
由「Google 翻譯」技術提供

© Creations/2010 Shutterstock.com

Access the Data
Electrons | Protons | Helium Ions

NIST Standard Reference Database 124
Rate our products and services.
Online: October 1998 - **Last update:** August 2005

Contact
Stephen Saltzer



SRIM Textbook

Software	Science
SRIM / TRIM Introduction	Historical Review
Download SRIM-2013	Details of SRIM-2013
SRIM Install Problems	Experimental Data Plots
SRIM Tutorials	Stopping of Ions in Matter
Download TRIM Manual Part-1, Part-2	Stopping in Compounds
Stopping Range and Dose	Scientific Citations of Experimental Data
High Energy Stopping	

The thickness of a filter can be decided from the range data from NIST website



COPPER

To download data in spreadsheet (array) form, choose a delimiter and use the checkboxes in the table heading. After downloading, save the output by using your browser's Save As feature.

Delimiter:

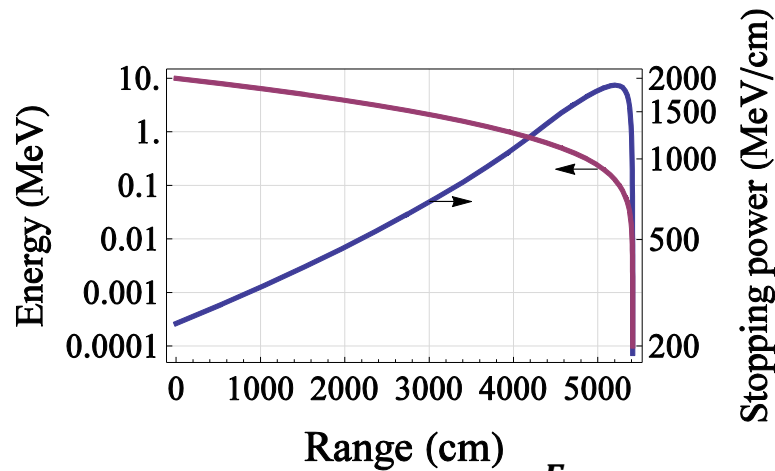
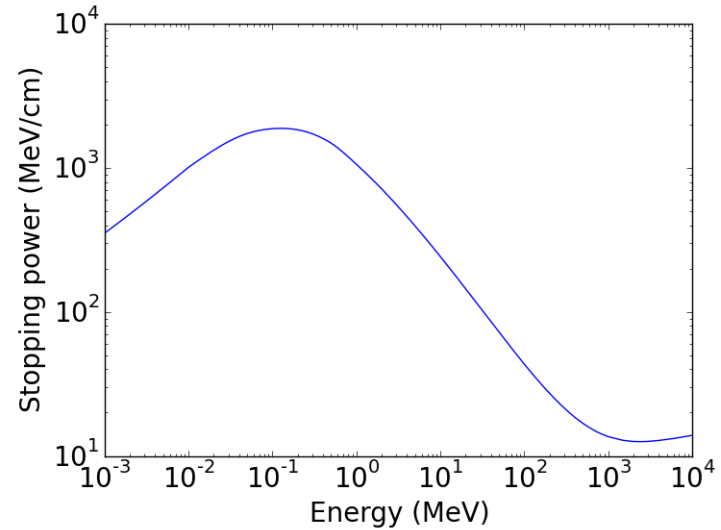
- space
- (vertical bar)
- tab (some browsers may use spaces instead)
- newline

Download data

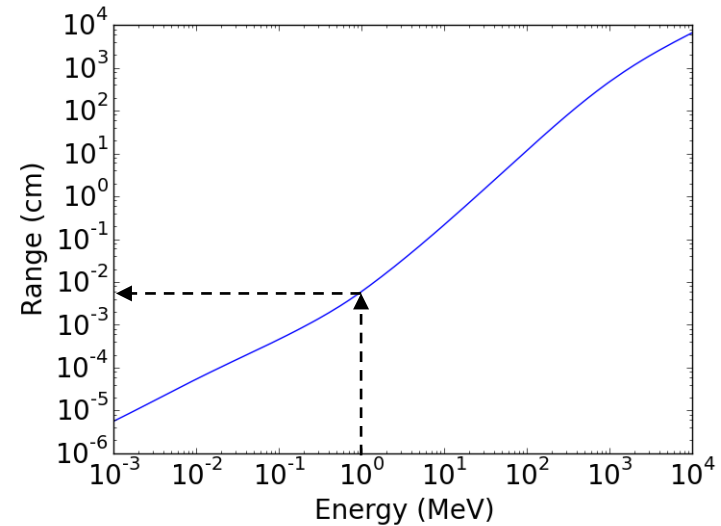
$$\frac{dE}{\rho dx}$$

$$\rho x$$

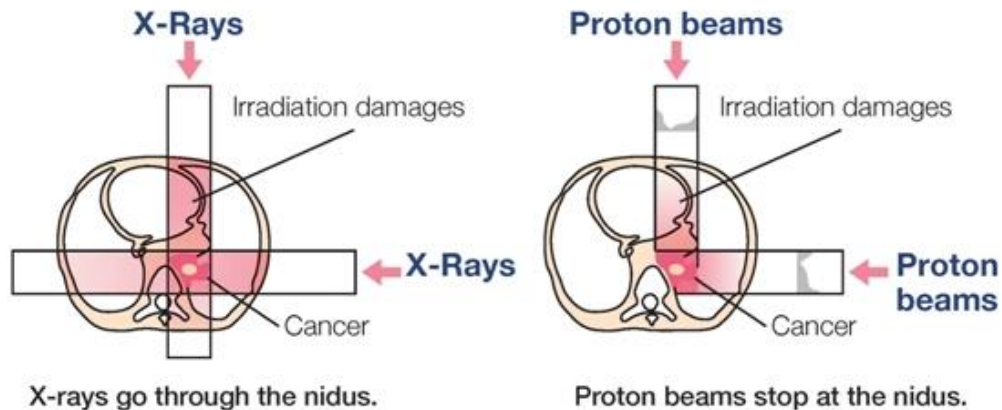
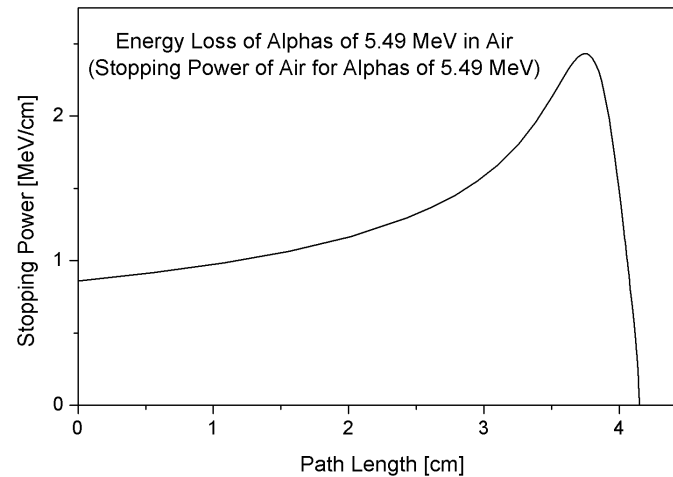
(required) Kinetic Energy (MeV)	Stopping Power (MeV cm ² /g)			CSDA (g/cm ²)	Projected	Detour Factor Projected / CSDA
	Electronic	Nuclear	Total		Range (g/cm ²)	
1.000E-03	3.490E+01	4.408E+00	3.931E+01	4.116E-05	5.620E-06	0.1365
1.500E-03	4.274E+01	4.231E+00	4.697E+01	5.267E-05	8.301E-06	0.1576
2.000E-03	4.935E+01	4.049E+00	5.340E+01	6.263E-05	1.101E-05	0.1759
2.500E-03	5.518E+01	3.876E+00	5.906E+01	7.152E-05	1.374E-05	0.1921
3.000E-03	6.045E+01	3.718E+00	6.416E+01	7.964E-05	1.647E-05	0.2068
4.000E-03	6.980E+01	3.440E+00	7.324E+01	9.419E-05	2.194E-05	0.2329
5.000E-03	7.804E+01	3.207E+00	8.124E+01	1.071E-04	2.739E-05	0.2556
6.000E-03	8.548E+01	3.010E+00	8.849E+01	1.189E-04	3.280E-05	0.2758
7.000E-03	9.233E+01	2.840E+00	9.517E+01	1.298E-04	3.817E-05	0.2940
8.000E-03	9.871E+01	2.692E+00	1.014E+02	1.400E-04	4.347E-05	0.3106
9.000E-03	1.047E+02	2.561E+00	1.073E+02	1.496E-04	4.872E-05	0.3258
1.000E-02	1.104E+02	2.445E+00	1.128E+02	1.587E-04	5.391E-05	0.3398



$$\frac{dE}{dx} = f(E) \Rightarrow x = \int_{E_i}^{E_f} \frac{dE}{f(E)}$$



Proton therapy takes the advantage of using Bragg peak



Saha equation gives the relative proportions of atoms of a certain species that are in two different states of ionization in thermal equilibrium



$$\frac{n_{r+1}n_e}{n_r} = \frac{G_{r+1}g_e}{G_r} \frac{(2\pi m_e KT)^{3/2}}{h^3} \exp\left(-\frac{\chi_r}{KT}\right)$$

- n_{r+1} , n_r : Density of atoms in ionization state $r+1$, r (m^{-3})
- n_e : Density of electrons (m^{-3})
- G_{r+1} , G_r : Partition function of ionization state $r+1$, r
- $g_e=2$: Statistical weight of the electron
- m_e : Mass of the electron
- χ_r : Ionization potential of ground level of state r to reach to the ground level of state $r+1$
- T : Temperature
- h : Planck's constant
- K : Boltzmann constant

Some backgrounds of quantum mechanics



- Planck blackbody function:

$$u(\nu, T) = \frac{8\pi h \nu^3}{c^3} \frac{1}{e^{h\nu/KT} - 1} \quad (W/m^3 \text{ Hz})$$

- Boltzmann formula:

- g_i, g_j : statistical weight

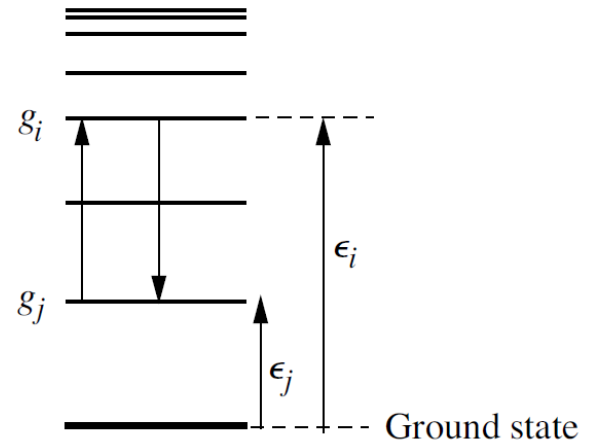
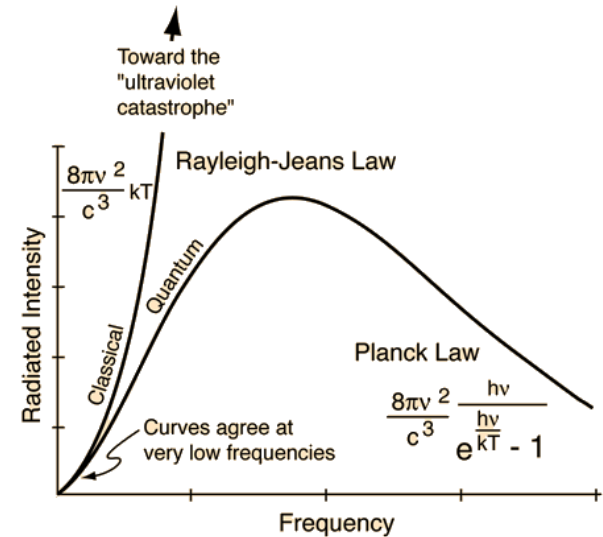
$$\frac{n_i}{n_j} = \frac{g_i e^{-\epsilon_i/KT}}{g_j e^{-\epsilon_j/KT}} = \frac{g_i}{g_j} e^{-h\nu_{ij}/KT} \quad \frac{g_i}{g_j} = \frac{2J_i + 1}{2J_j + 1}$$

(J : angular momenta quantum number)

- Number in the i^{th} state to the total atom:

$$\frac{n_i}{n} = \frac{n_i}{\sum n_j} \equiv \frac{g_i e^{-\epsilon_i/KT}}{G} \quad G \equiv \sum g_j e^{-\epsilon_j/KT}$$

G: partition function of statistical weight for the atom, taking into account all its excited states.



Einstein coefficient



- Probability of electron energy transition:

– Excitation (\uparrow): $P_{ji} = B_{ji}u(\nu, T)$

– De-excitation (\downarrow): $P_{ij} = A_{ij} + B_{ij}u(\nu, T)$

- In thermal equilibrium:

$$n_i(A_{ij} + B_{ij}u) = n_j B_{ji}u$$

$$\frac{g_i}{g_j} e^{-x}(A_{ij} + B_{ij}u) = B_{ji}u$$

$$u = a(e^x - 1)^{-1}$$

$$a \left(e^x B_{ji} - \frac{g_i}{g_j} B_{ij} \right) = (e^x - 1) \frac{g_i}{g_j} A_{ij}$$

$$x \equiv \frac{h\nu}{kT}$$

$$a \equiv \frac{8\pi h\nu^3}{c^3}$$

- The Einstein coefficients are independent of T or ν .

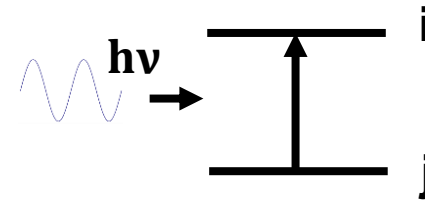
$$x \rightarrow 0, e^x \rightarrow 1$$

$$x \rightarrow \infty, e^x \rightarrow \infty$$

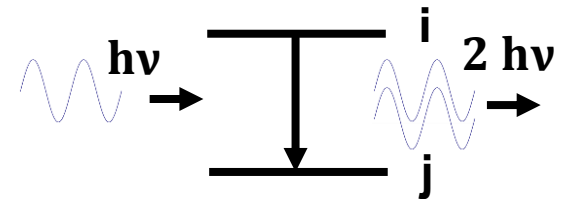
$$\frac{B_{ij}}{B_{ji}} = \frac{g_j}{g_i}$$

$$a B_{ji} = \frac{g_i}{g_j} A_{ij} \quad \frac{A_{ij}}{B_{ij}} = \frac{8\pi h\nu^3}{c^3}$$

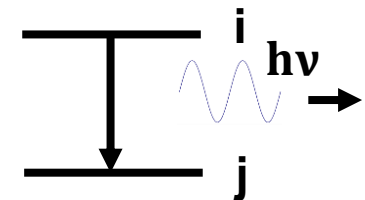
- Photoexcitation:



- Induced radiation:



- Spontaneous radiation:



Saha equation is derived using the transition between different ionization states



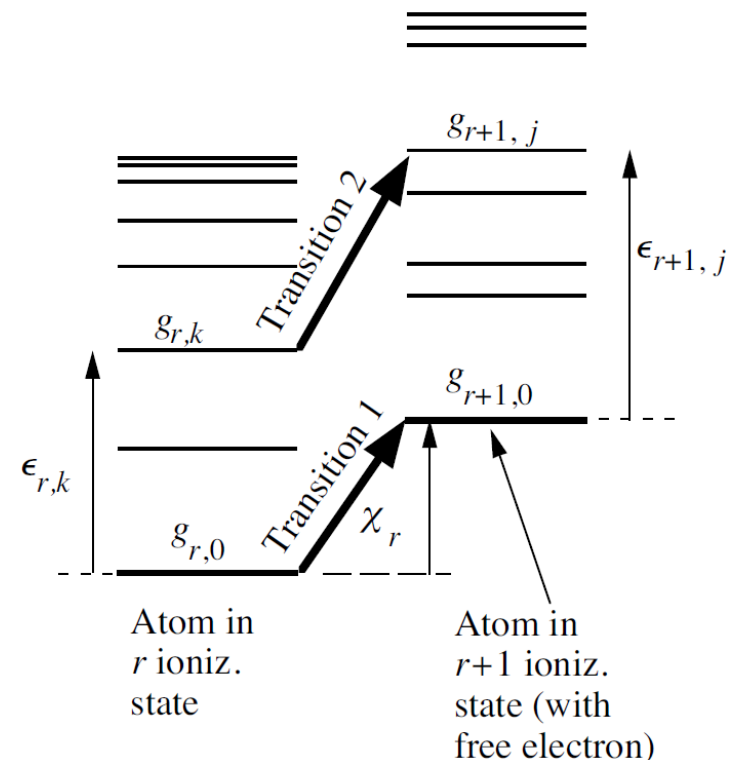
- Required photon energy for transition 1 from the ground state of r ionization state to the ground state of $r+1$ ionization state:

$$h\nu = \chi_r + \frac{p^2}{2m}$$

← Energy of the free electron

- Required photon energy for transition 2 from the energy level k of r ionization state to the energy level j of $r+1$ ionization state:

$$h\nu = \chi_r + \epsilon_{r+1,j} - \epsilon_{r,k} + \frac{p^2}{2m}$$



Saha equation is derived using the transition between different ionization states



- Photoionization:

$$R_{pi} = n_{r,k} u(\nu) B_{r,k \rightarrow r+1,j}$$

- Induced radiation:

$$R_{ir} = n_{r+1,j} n_{e,p}(\rho) u(\nu) B_{r+1,j \rightarrow r,k}$$

- Spontaneous emission:

$$R_{sr} = n_{r+1,j} n_{e,p}(\rho) A_{r+1,j \rightarrow r,k}$$

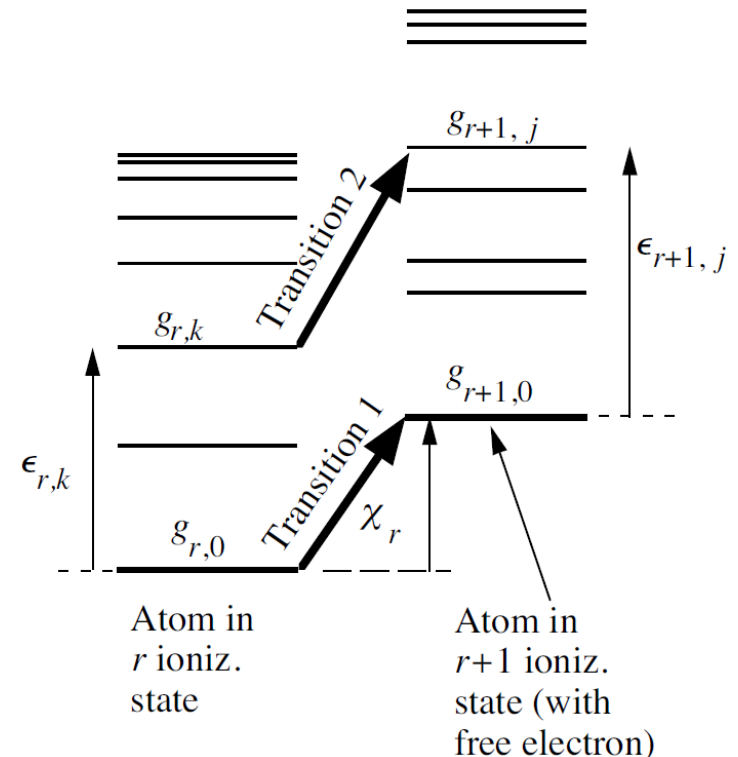
- In thermal equilibrium:

$$\begin{aligned} n_{r+1,j} n_{e,p} A_{r+1,j \rightarrow r,k} + n_{r+1,j} n_{e,p} u B_{r+1,j \rightarrow r,k} \\ = n_{r,k} u B_{r,k \rightarrow r+1,j} \end{aligned}$$

- Einstein coefficients:

$$\frac{B_{r,k \rightarrow r+1,j}}{B_{r+1,j \rightarrow r,k}} = \frac{g_{r+1,j}}{g_{r,k}} \frac{g_e 4\pi p^2}{h^3}$$

$$\frac{A_{r+1,j \rightarrow r,k}}{B_{r+1,j \rightarrow r,k}} = \frac{8\pi h\nu^3}{c^3}$$



Saha equation - continued



$$n_{r+1,j}n_{e,p}A_{r+1,j \rightarrow r,k} + n_{r+1,j}n_{e,p}uB_{r+1,j \rightarrow r,k} = n_{r,k}uB_{r,k \rightarrow r+1,j}$$

$$n_{r+1,j}n_{e,p} \frac{A_{r+1,j \rightarrow r,k}}{B_{r+1,j \rightarrow r,k}} + n_{r+1,j}n_{e,p}u = n_{r,k}u \frac{B_{r,k \rightarrow r+1,j}}{B_{r+1,j \rightarrow r,k}}$$

$$\frac{n_{r+1,j}n_{e,p}}{n_{r,k}} = \left(\frac{A_{r+1,j \rightarrow r,k}}{uB_{r+1,j \rightarrow r,k}} + 1 \right)^{-1} \frac{B_{r,k \rightarrow r+1,j}}{B_{r+1,j \rightarrow r,k}}$$

$$\frac{B_{r,k \rightarrow r+1,j}}{B_{r+1,j \rightarrow r,k}} = \frac{g_{r+1,j}}{g_{r,k}} \frac{g_e 4\pi p^2}{h^3}$$

$$n_{e,p}(p) = \frac{n_e 4\pi p^2}{(2\pi mKT)^{3/2}} \exp\left(-\frac{p^2}{2mKT}\right)$$

$$\frac{A_{r+1,j \rightarrow r,k}}{B_{r+1,j \rightarrow r,k}} = \frac{8\pi h\nu^3}{c^3}$$

$$\frac{n_{r+1,j}n_e}{n_{r,k}} = \frac{(2\pi mKT)^{3/2}}{4\pi p^2} \exp\left(\frac{p^2}{2mKT}\right) \left[\frac{c^3}{8\pi h\nu^3} (e^{h\nu/KT} - 1) \frac{8\pi h\nu^3}{c^3} + 1 \right]^{-1} \frac{g_{r+1,j}}{g_{r,k}} \frac{g_e 4\pi p^2}{h^3}$$

$$\frac{n_{r+1,j}n_e}{n_{r,k}} = \frac{(2\pi mKT)^{3/2}}{h^3} \frac{g_{r+1,j}g_e}{g_{r,k}} \exp\left[\frac{1}{KT} \left(\frac{p^2}{2m} - h\nu\right)\right]$$

Saha equation - continued



$$\frac{n_{r+1,j}n_e}{n_{r,k}} = \frac{(2\pi mKT)^{3/2}}{h^3} \frac{g_{r+1,j}g_e}{g_{r,k}} \exp\left[\frac{1}{KT} \left(\frac{p^2}{2m} - hv\right)\right]$$

$$\frac{n_{r+1,j}n_e}{n_{r,k}} = \frac{(2\pi mKT)^{3/2}}{h^3} \frac{g_{r+1,j}g_e}{g_{r,k}} \exp\left[\frac{1}{KT} \left(\frac{p^2}{2m} - \chi_r - \epsilon_{r+1,j} + \epsilon_{r,k} - \frac{p^2}{2m}\right)\right]$$

$$\frac{n_{r+1,j}n_e}{n_{r,k}} = \frac{(2\pi mKT)^{3/2}}{h^3} \frac{g_{r+1,j} \exp\left(-\frac{\epsilon_{r+1,j}}{KT}\right) g_e}{g_{r,k} \exp\left(-\frac{\epsilon_{r,k}}{KT}\right)} \exp\left(-\frac{\chi_r}{KT}\right)$$

$$\frac{n_{r,k}}{n_r} = \frac{g_{r,k} e^{-\epsilon_{r,k}/KT}}{G_r}$$

$$G_r = \sum g_{r,k} e^{-\epsilon_{r,k}/KT}$$

$$\frac{n_{r+1,j}}{n_{r+1}} = \frac{g_{r+1,j} e^{-\epsilon_{r+1,j}/KT}}{G_{r+1}}$$

$$G_{r+1} = \sum g_{r+1,j} e^{-\epsilon_{r+1,j}/KT}$$

$$\frac{n_{r+1}n_e}{n_r} = \frac{G_{r+1}g_e}{G_r} \frac{(2\pi m_eKT)^{3/2}}{h^3} \exp\left(-\frac{\chi_r}{KT}\right)$$

Saha equation – example: hydrogen plasma of the sun



- Photosphere of the sun – hydrogen atoms in an optically thick gas in thermal equilibrium at temperature $T=6400$ K.

- Neutral hydrogen (r state / ground state)

$$G_r = \sum g_{r,k} = g_{r,0} + g_{r,1} \exp\left(-\frac{\epsilon_{r,1}}{KT}\right) + \dots = 2 + 8 \exp\left(-\frac{10.2\text{eV}}{0.56\text{eV}}\right) + \dots \\ = 2 + 9.8 \times 10^{-8} + \dots \approx 2$$

- Ionized state (r+1 state)

$$G_{r+1} = \sum g_{r+1,j} = g_{r+1,0} + g_{r+1,1} \exp\left(-\frac{\epsilon_{r+1,1}}{KT}\right) + \dots \approx 1$$

- Other information: $g_e = 2$ $\chi_r = 13.6\text{eV}; KT = 0.56\text{eV}$ $n_{r+1} = n_e$

$$\frac{n_{r+1}^2}{n_r} = 2.41 \times 10^{21} \frac{1 \times 2}{2} (6400)^{3/2} \exp\left(-\frac{13.6}{0.56}\right) = 3.5 \times 10^{16} m^{-3}$$

It is mostly neutral in the photosphere of the sun



- Assuming 50 % ionization:

$$n_{r+1} = n_r = 3.5 \times 10^{16} m^{-3} \quad n = n_{r+1} + n_r = 7 \times 10^{16} m^{-3}$$

- At higher densities n at the same temperature, there should be more collisions leading to higher recombination rate and thus the plasma is less than 50 % ionization.
- In the photosphere of the sun:

$$\rho \sim 3 \times 10^{-4} \text{ kg}/m^3 \rightarrow n = 2 \times 10^{23} m^{-3} \gg 7 \times 10^{16} m^{-3}$$

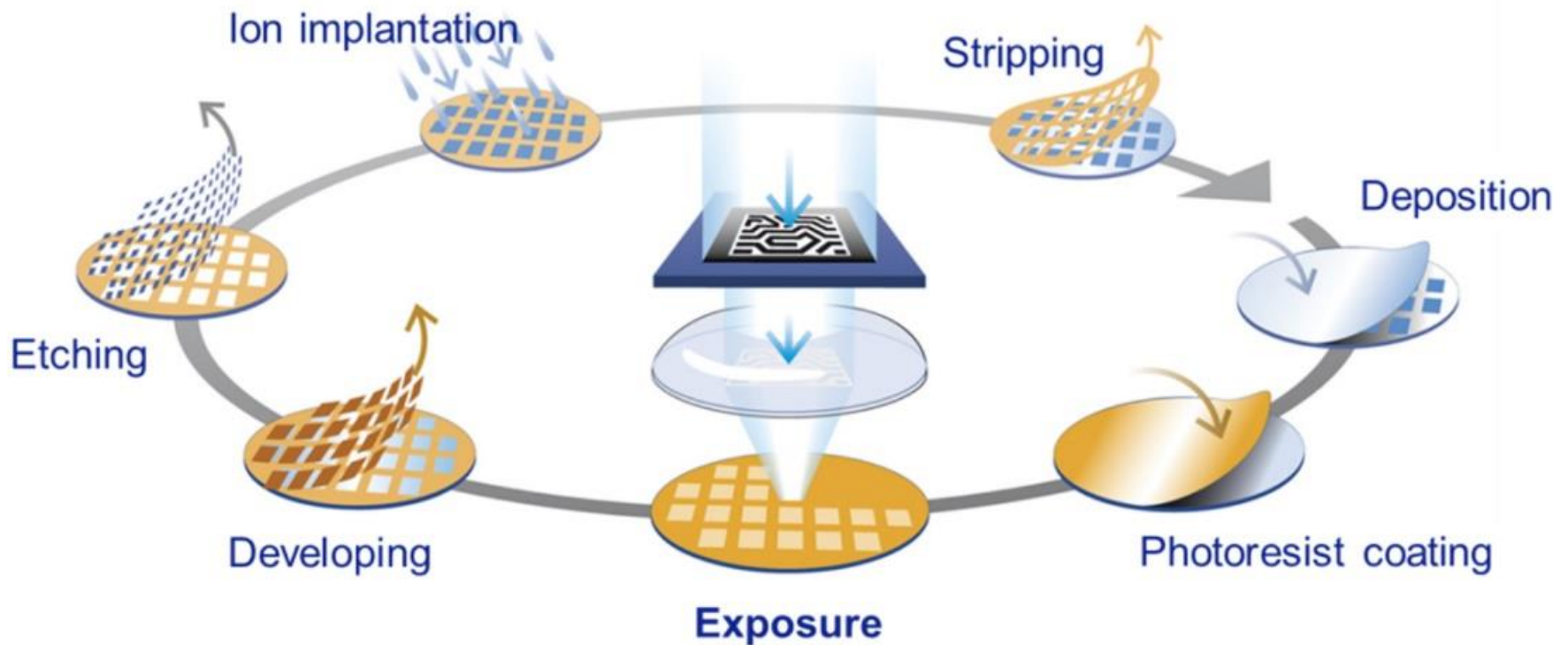
⇒ Less than 50 % ionization

- Use the total number density to estimate the ionization percentage:

$$n_{r+1} + n_r = 2 \times 10^{23}$$

$$\frac{n_{r+1}}{n_r} = 4 \times 10^{-4} @ 6400K$$

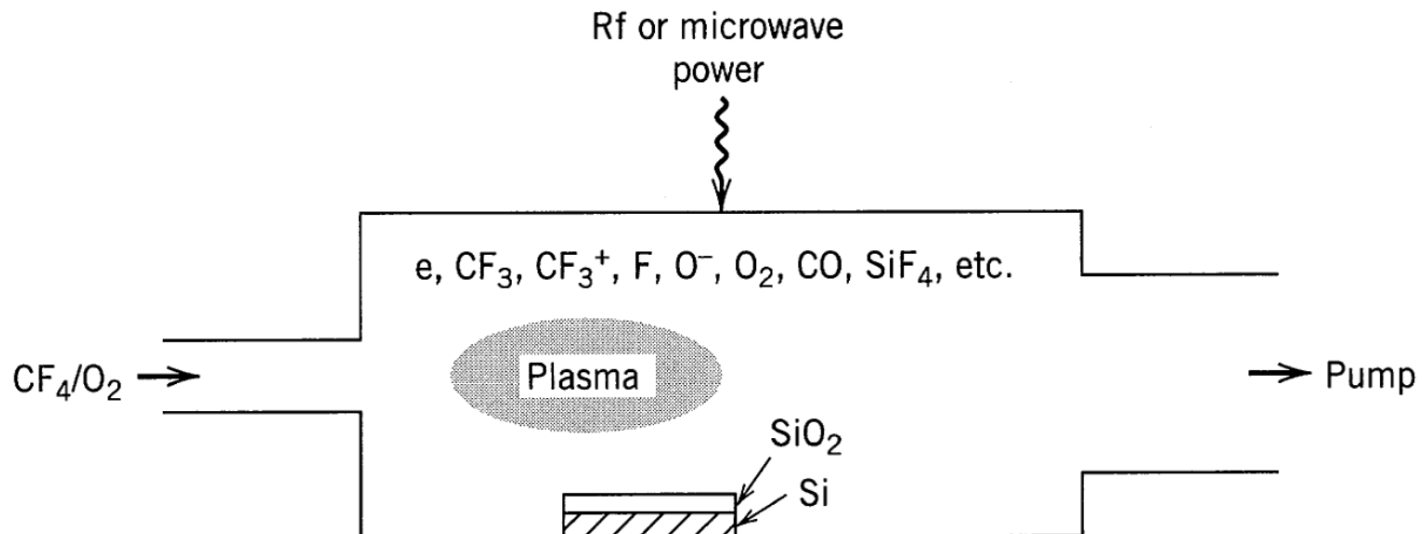
A semiconductor device is fabricated by many repetitive production process



Reference for material processing



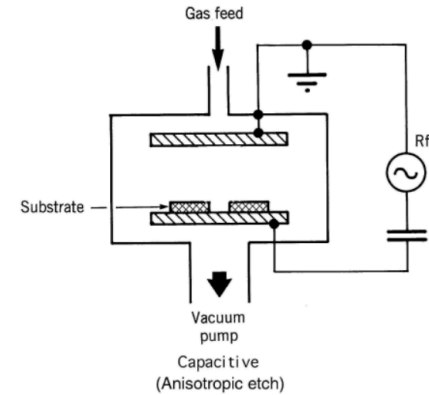
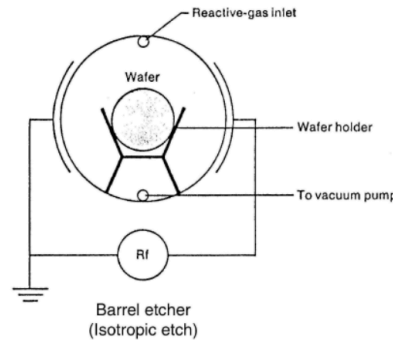
- **Principles of plasma discharges and materials processing, 2nd edition, by Michael A. Lieberman and Allan J. Lichtenberg**
- **<http://www.eecs.berkeley.edu/~lieber/>**
- **Materials science of thin films, 2nd edition, by Milton Ohring**
- **Plasma etching, by Dennis M. Manos and Daniel L. Flamm**
- **Industrial plasma engineering, volume 1, by J. Reece Roth**



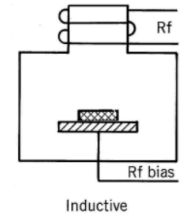
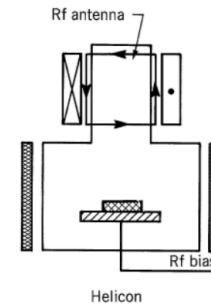
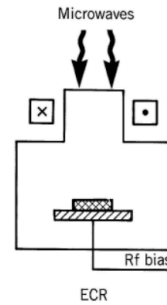
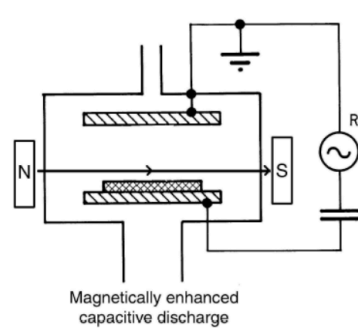
Evolution of etching discharges



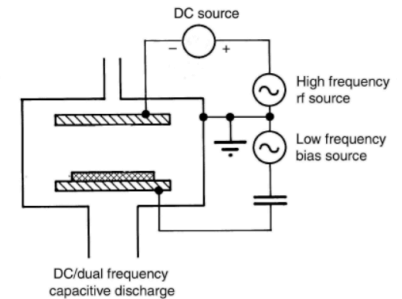
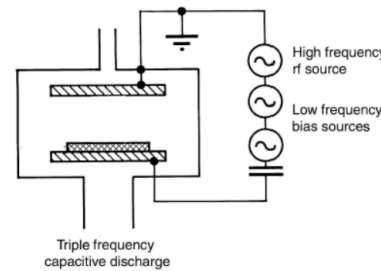
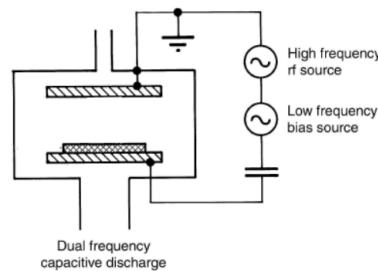
1st generation
(1 source, multi-wafer,
low density)



2nd generation
(2 sources, single-wafer,
high density)



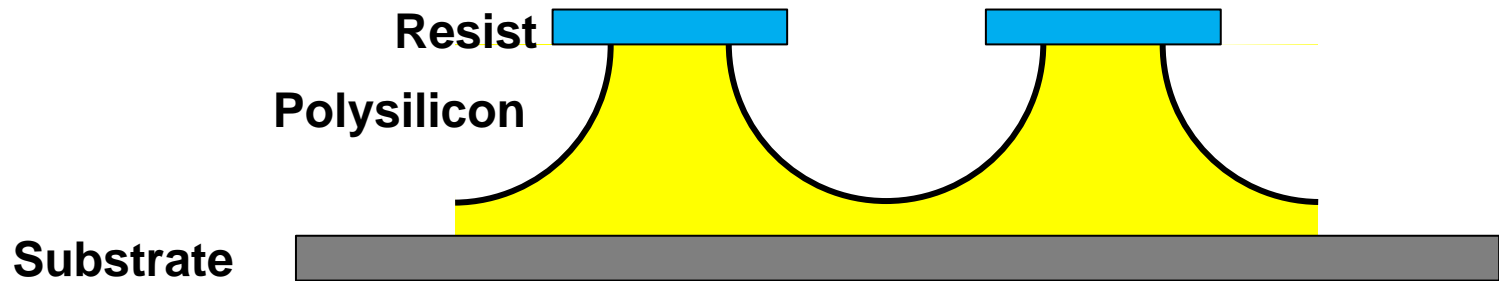
3rd generation
(multi-sources, single-
wafer, moderate density)



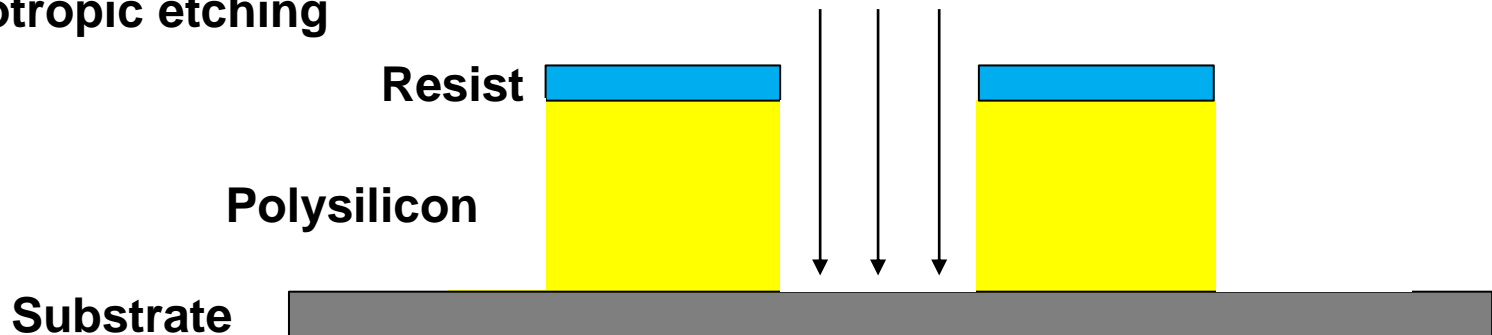
There are two types of etching: isotropic vs anisotropic



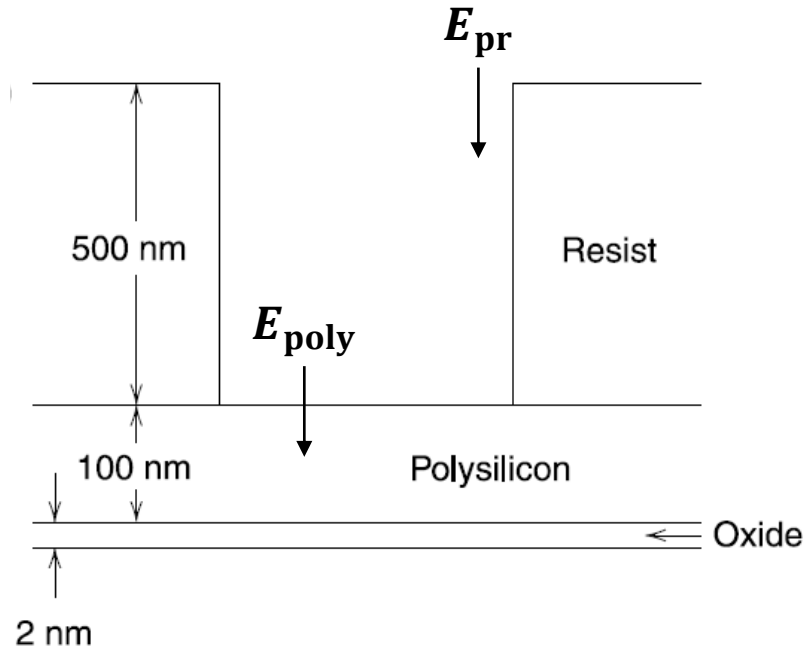
- Isotropic etching



- Anisotropic etching



Plasma etch requirements – etch rate

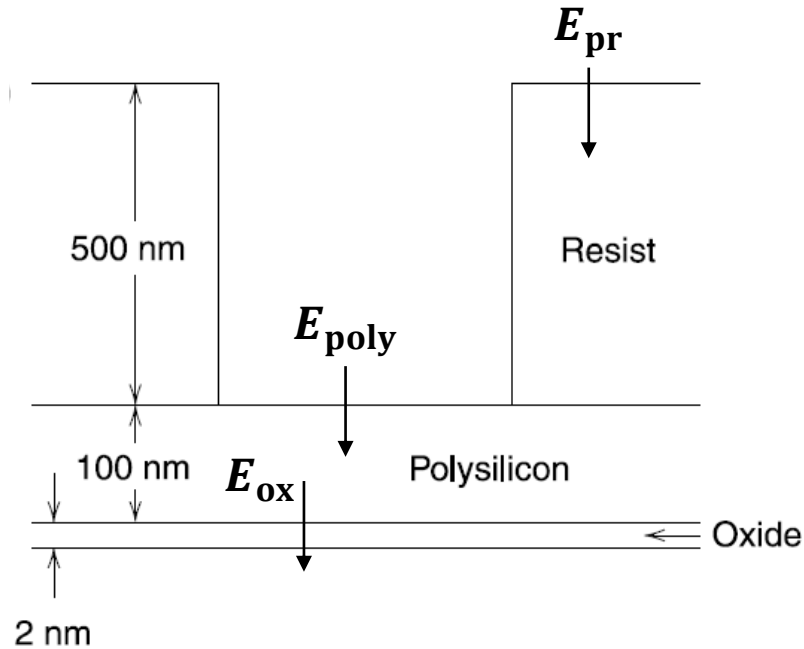


- Etch time needs to be within a few minutes:

$$E_{pr} \geq 250 \text{ nm/min}$$

$$E_{poly} \geq 50 \text{ nm/min}$$

Plasma etch requirements - selectivity



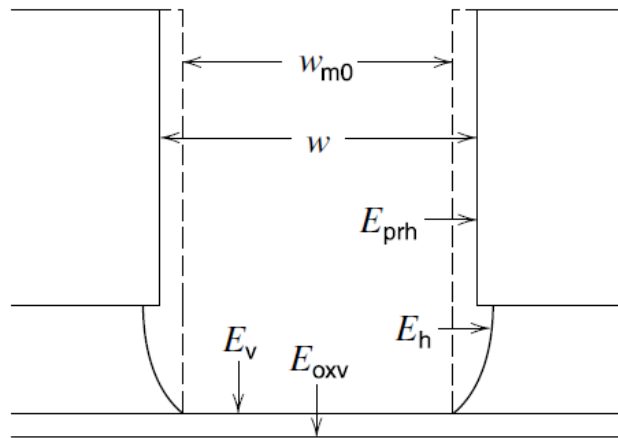
- **Selectivity between polysilicon and resist:**

$$s = \frac{E_{poly} \Delta t}{E_{pr} \Delta t} \gg \frac{100\text{nm}}{500\text{nm}} = 0.2$$

- **Assuming 20% non-uniformity on the wafer:**

$$s = \frac{E_{poly} \Delta t}{E_{ox} \Delta t} \gg \frac{20\% \times 100\text{nm}}{2\text{nm}} = 10$$

Plasma etch requirements – Anisotropy



- Anisotropy**

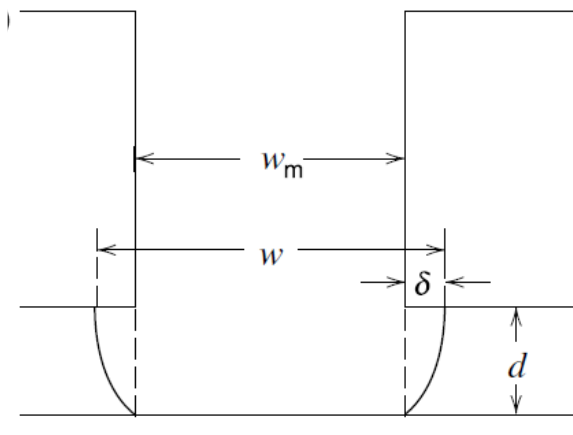
$$a_h = \frac{E_v}{E_h} = \frac{d}{\delta}$$

$$w = w_m + 2\delta$$

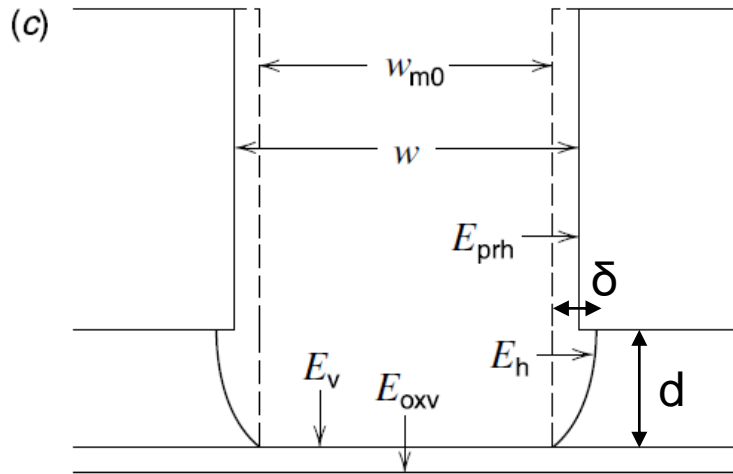
$$a_h \geq \frac{2d}{w - w_m}$$

- The smallest feature size where $w_m=0$:**

$$w \approx \frac{2d}{a_h}$$



Plasma etch requirements – Anisotropy including etching on photoresist

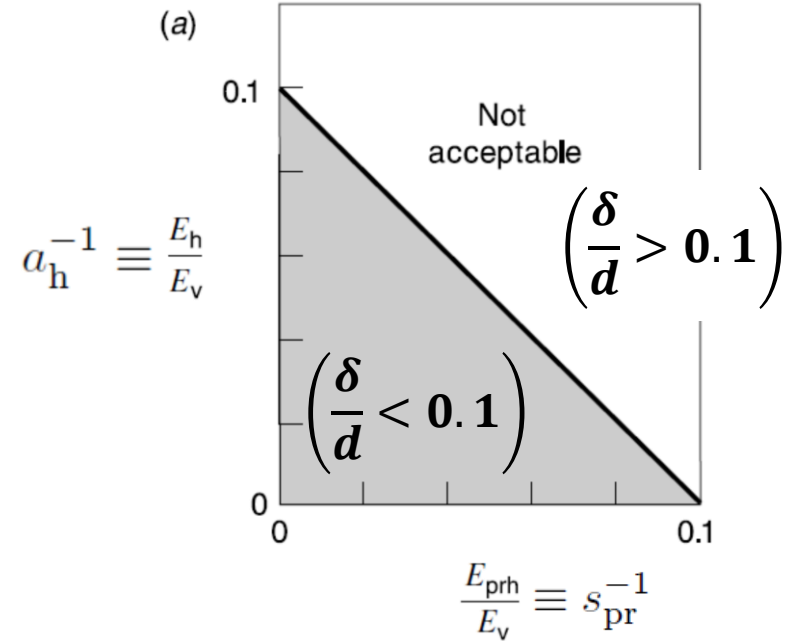


$$\delta \approx (E_h + E_{prh}) t$$

$$t = \frac{d}{E_v}$$

$$\delta \approx d \frac{E_h + E_{prh}}{E_v}$$

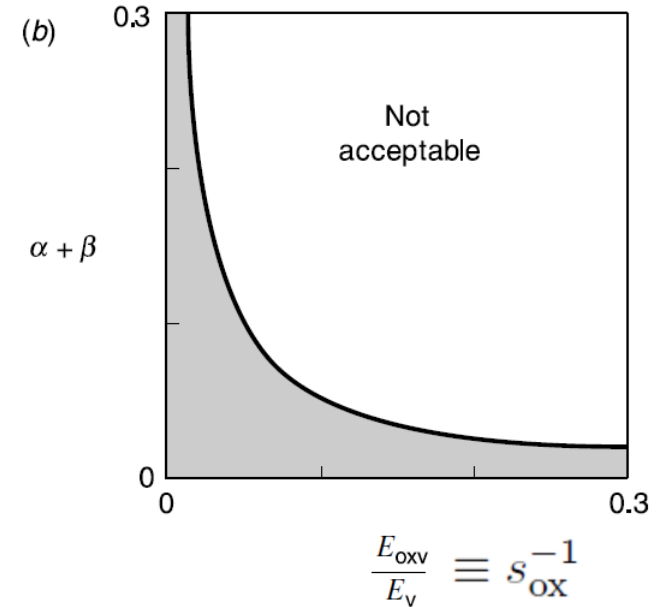
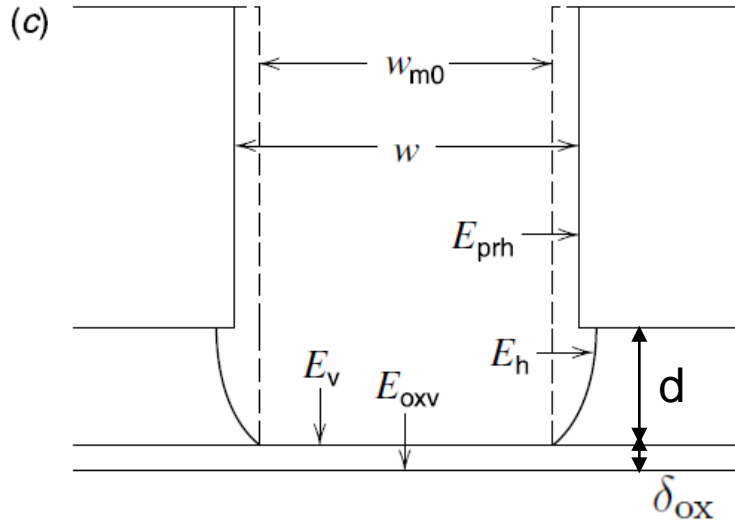
$$\frac{E_h + E_{prh}}{E_v} \approx \frac{\delta}{d}$$



$$\frac{E_h}{E_v} + \frac{E_{prh}}{E_v} = a_h^{-1} + s_{pr}^{-1} \approx \frac{\delta}{d} \equiv 0.1$$

- The contribution of the horizontal etching is from both E_h and E_{prh} .

Plasma etch requirements – Uniformity on selectivity and anisotropy



$$d \rightarrow d(1 \pm \alpha) \quad E_v \rightarrow E_v(1 \pm \beta)$$

where α , β are variations.

$$t_{\max} = \frac{d(1 + \alpha)}{E_v(1 - \beta)} \approx \frac{d}{E_v} (1 + \alpha + \beta)$$

$$t_{\min} = \frac{d(1 - \alpha)}{E_v(1 + \beta)} \approx \frac{d}{E_v} (1 - \alpha - \beta)$$

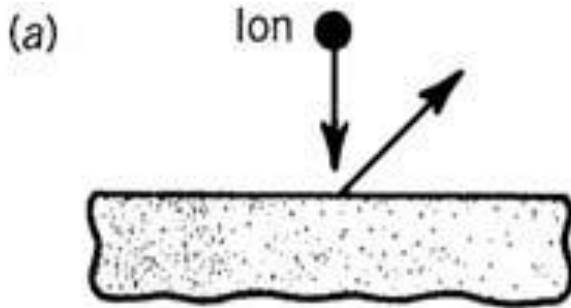
$$\begin{aligned} \delta_{\text{ox}} &= (t_{\max} - t_{\min})E_{\text{oxv}} \\ &= \frac{d}{E_v} 2(\alpha + \beta)E_{\text{oxv}} \end{aligned}$$

$$2(\alpha + \beta) \frac{E_{\text{oxv}}}{E_v} = \frac{\delta_{\text{ox}}}{d}$$

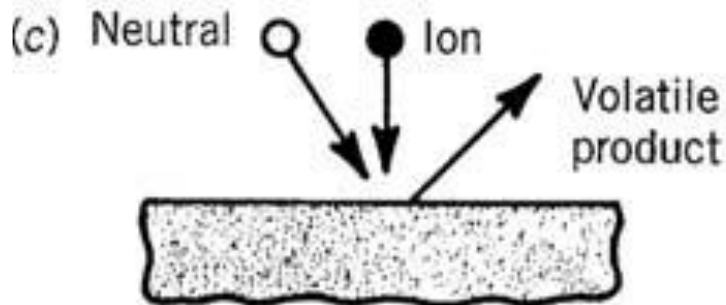
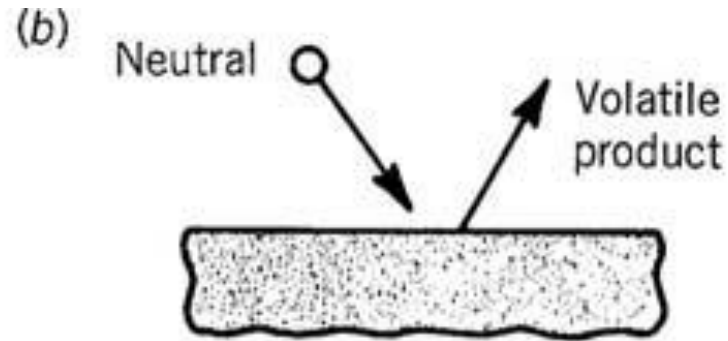
There are four major plasma etching mechanisms



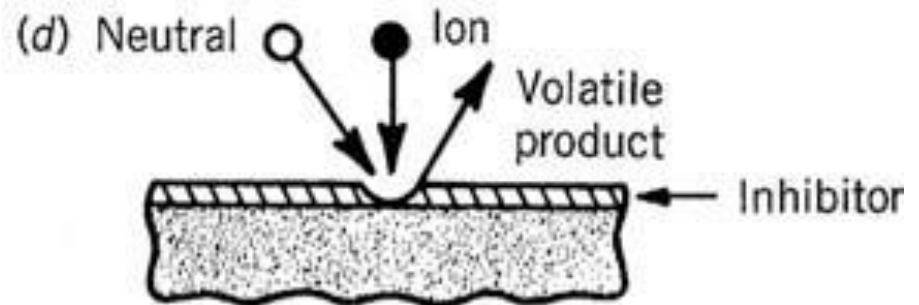
- **Sputtering**



- **Pure chemical etching**



- **Ion energy-driven etching**

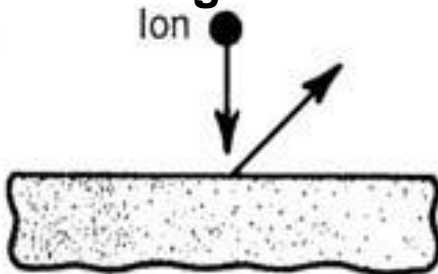


- **Ion-enhanced inhibitor etching**

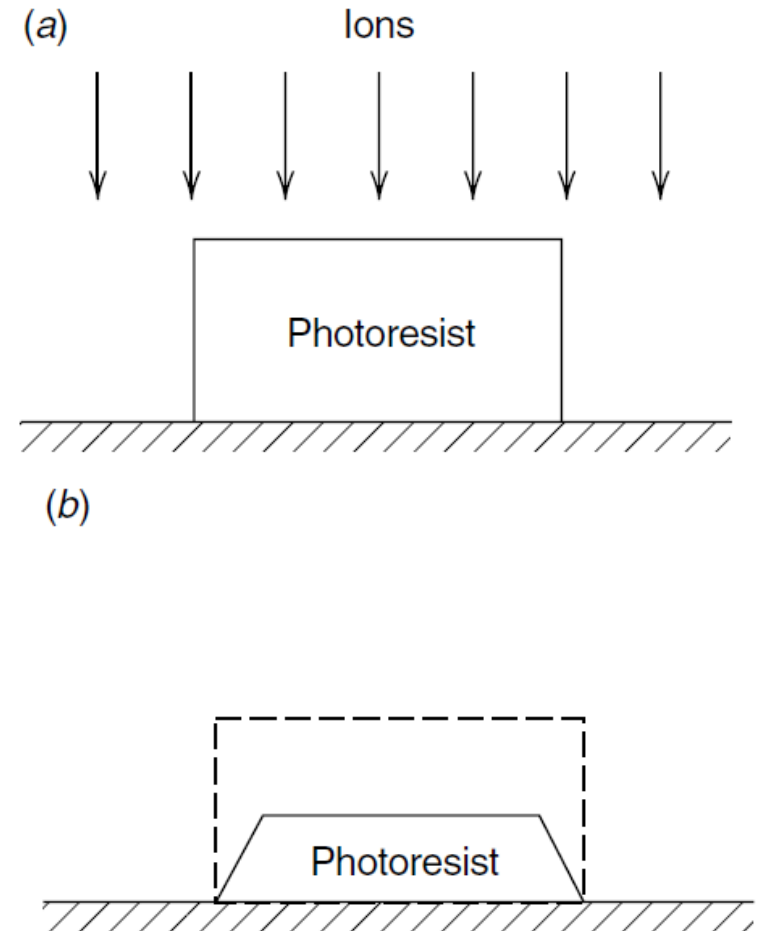
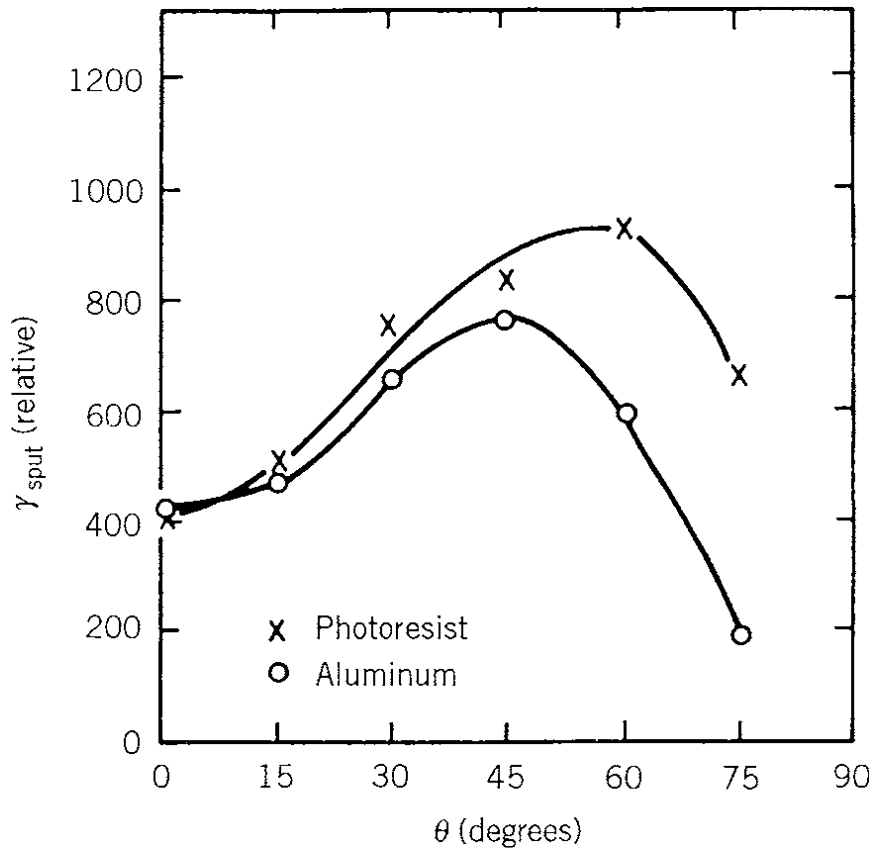
Sputtering is an unselective but anisotropic process



- Unselective process.
- Anisotropic process, strongly sensitive to the angle of incidence of the ion.
- Sputtering rates of different materials are roughly the same.
- Sputtering rates are generally low because the yield is typically of order one atom per incident ion.
- Sputtering is the only one of the four etch processes that can remove nonvolatile products from a surface.
- The process is generally under low pressure since the mean free path of the sputtered atoms must be large enough to prevent redeposition on the substrate or target.



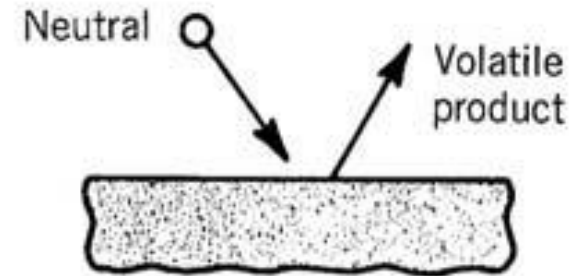
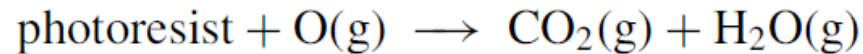
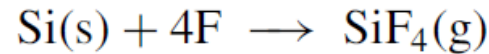
Topographical patterns might not be faithfully transferred during sputter etching



Atoms or molecules chemically react with the surface to form gas-phase products



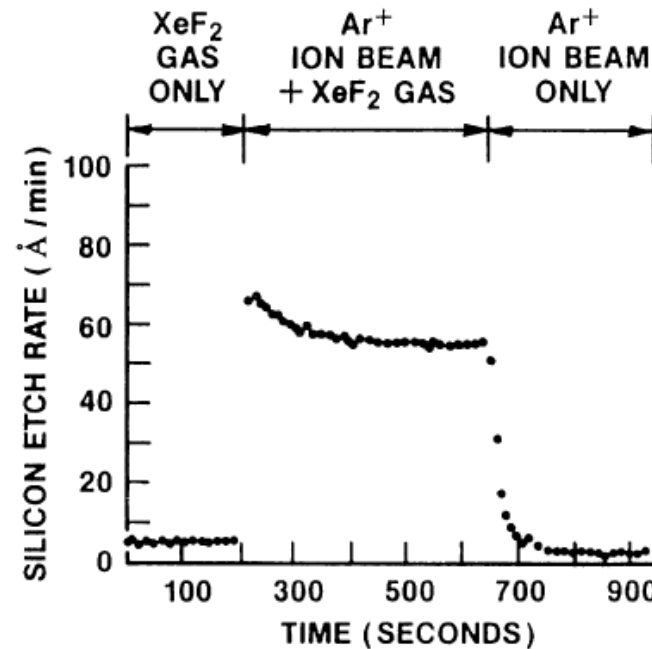
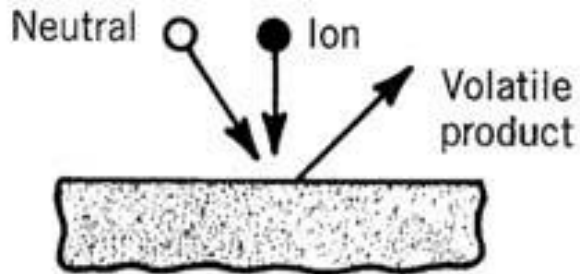
- Highly chemically selective, e.g.,



- Almost invariably isotropic.
- Etch products must be volatile.
- The etch rate can be quite large.
- Etch rate are generally not limited by the rate of arrival of etchant atoms, but by one of a complex set of reactions at the surface leading to formation of etch products.

Ion-enhanced energy-driven etching

The discharge supplies both etchants and energetic ions to the surface



- Low chemical etch rate of silicon substrate in XeF_2 etchant gas.
- **Tenfold increase in etch rate with XeF_2 + 500 V argon ions, simulating ion-enhanced plasma etching.**
- Very low “etch rate” due to the physical sputtering of silicon by ion bombardment alone.

Ion-enhanced energy-driven etching has the characteristic of both sputtering and pure chemical etching



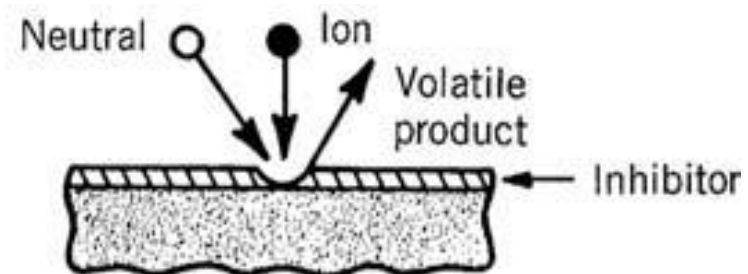
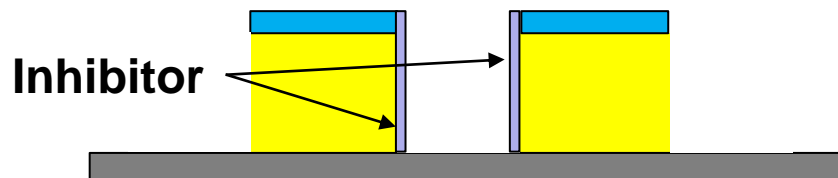
- **Chemical in nature but with a reaction rate determined by the energetic ion bombardment.**
- **Product must be volatile.**
- **Highly anisotropic.**

Ion-enhanced inhibitor etching

An inhibitor species is used



- Inhibitor precursor molecules that absorb or deposit on the substrate form a protective layer or polymer film.
- **Etchant is chosen to produce a high chemical etch rate of the substrate in the absence of either ion bombardment or the inhibitor.**
- Ion bombardment flux prevents the inhibitor layer from forming or clears it as it forms.
- Where the ion flux does not fall, the inhibitor protects the surface (side wall) from the etchant.
- May not be as selective as pure chemical etching.
- A volatile etch product must be formed.
- Contamination of the substrate and final removal of the protective inhibitor film are other issues.



Comparison of different processes



	Sputtering etching	Pure chemical etching	Ion energy-driven etching	Ion-enhanced Inhibitor etching
Selectivity	X	O	O	O
Anisotropic	O	X	O	O
Volatile product	X	O	O	O

TABLE 15.1. Etch Chemistries Based on Product Volatility

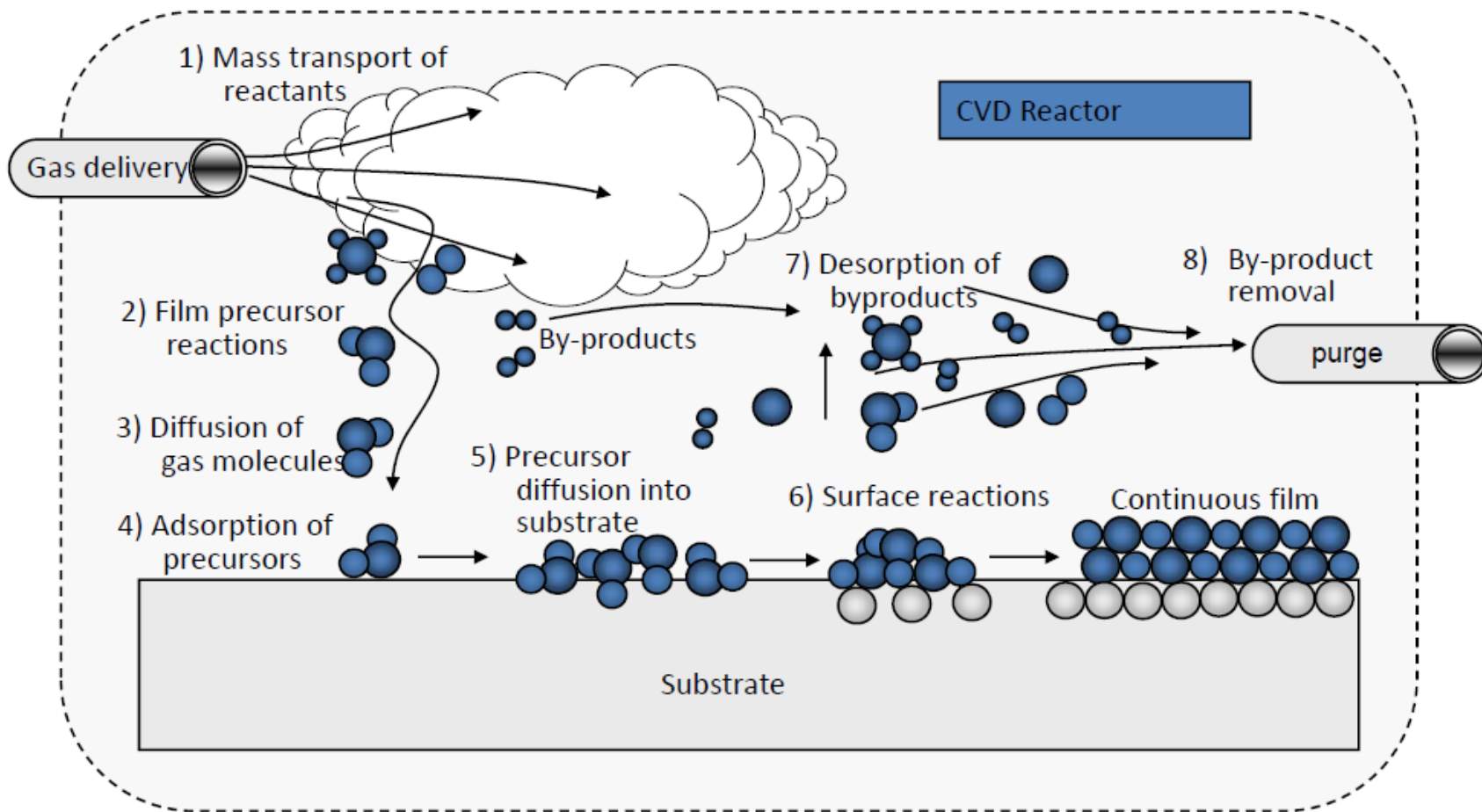
Material	Etchant Atoms
Si, Ge	F, Cl, Br
SiO ₂	F, F + C
Si ₃ N ₄ , silicides	F
Al	Cl, Br
Cu	Cl ($T > 210^{\circ}\text{C}$)
C, organics	O
W, Ta, Ti, Mo, Nb	F, Cl
Au	Cl
Cr	Cl, Cl + O
GaAs	Cl, Br
InP	Cl, C + H

Deposition and implementation

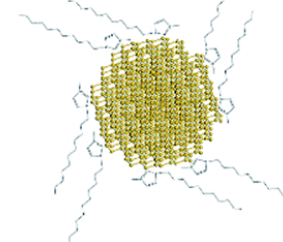
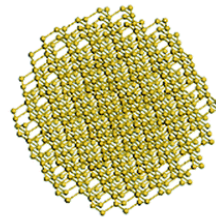
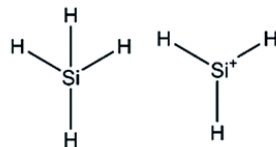
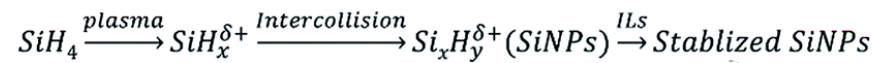
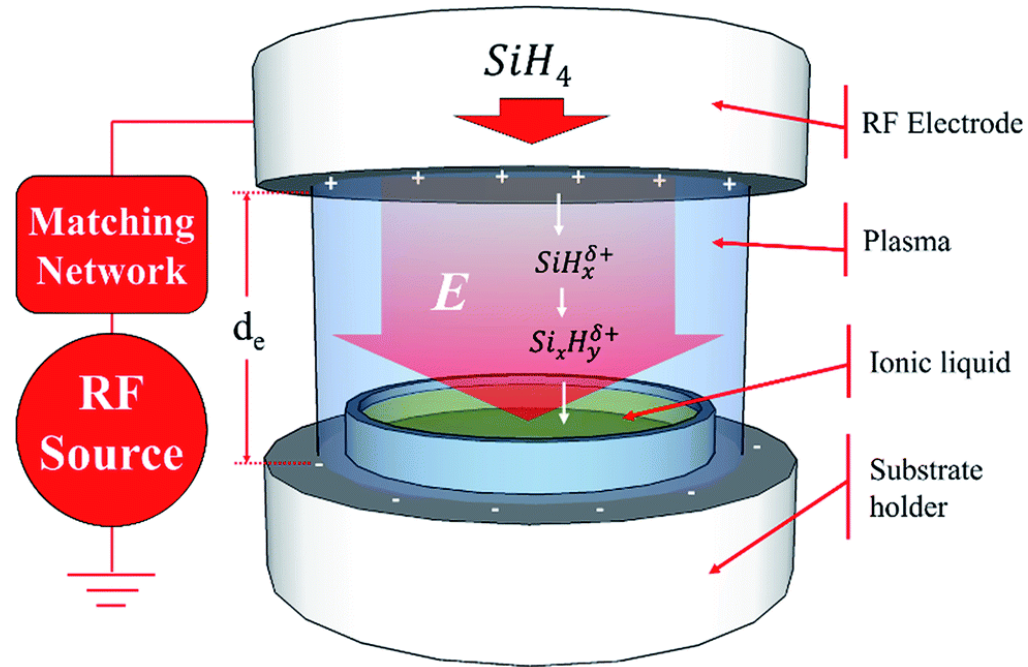


- **Plasma-assisted deposition, implantation, and surface modification are important material processes for producing films on surfaces and modifying their properties**
- **Example processes:**
 - **Plasma-enhanced chemical vapor deposition (PECVD)**
 - **Sputter deposition / physical vapor deposition (PVD)**
 - **Plasma-immersion ion implantation (PIII)**

Chemical Vapor Deposition (CVD)



Plasma-enhanced chemical vapor deposition (PECVD)



Films can be deposited in low temperatures using plasma deposition



- **Device structures are sensitive to temperature, high-temperature deposition processes cannot be used in many cases.**
- **High-temperature films can be deposited at low temperatures.**
- **Unique films not found in nature can be deposited, e.g., diamond.**

Working temperature is determined by the desired film properties

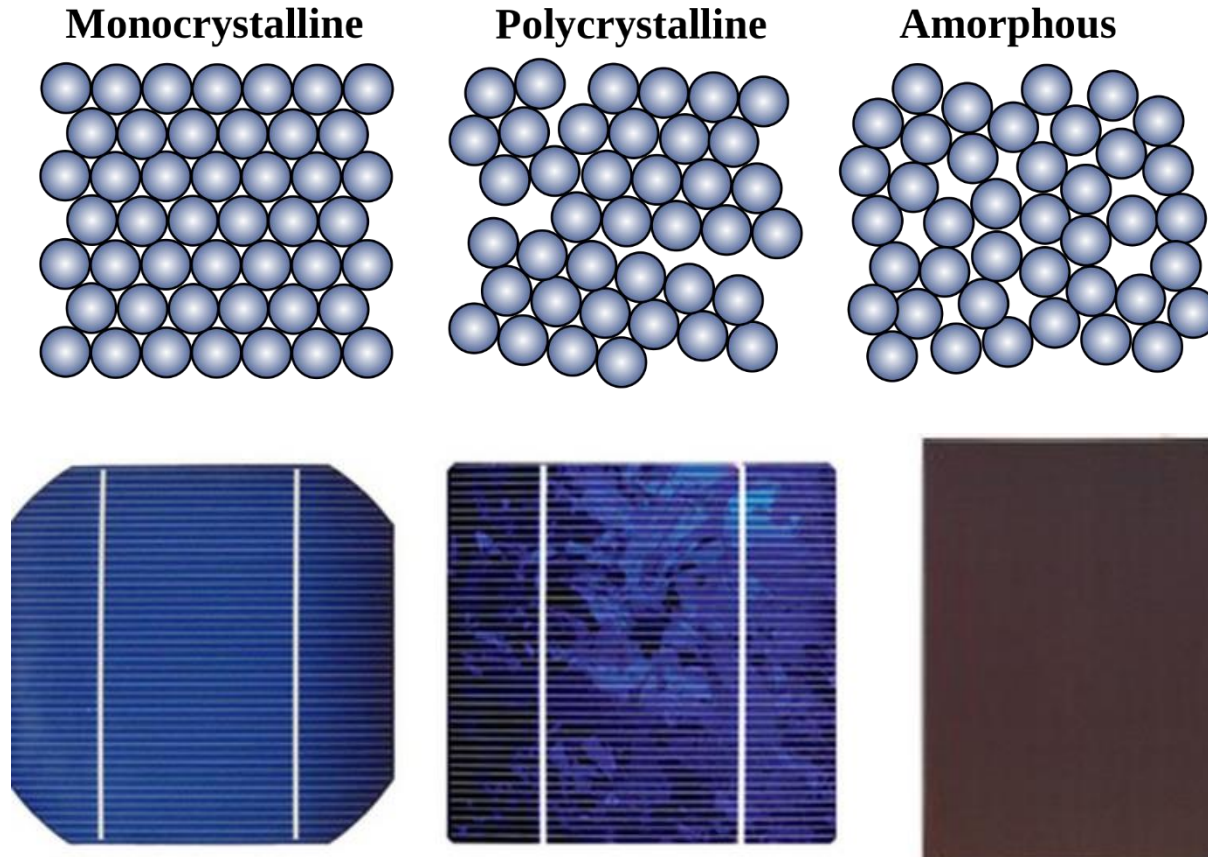


- **CVD – consists of a thermally activated set of gas-phase and surface reactions that produce a solid product at a surface.**
- **PECVD – gas-phase and the surface reactions are controlled or modified by the plasma properties.**
- **$T_e \sim 2-5$ eV in PECVD is much greater than the substrate temperature, the temperature in PECVD is much less than CVD.**
- **Deposition rates are usually not very sensitive to the substrate temperature T .**
- **Film properties such as composition, stress, and morphology, are functions of T .**
- **Low-temperature PECVD films are amorphous, not crystalline, which can more easily be achieved with chemical vapor deposition (CVD).**

Example of using PECVD – amorphous silicon



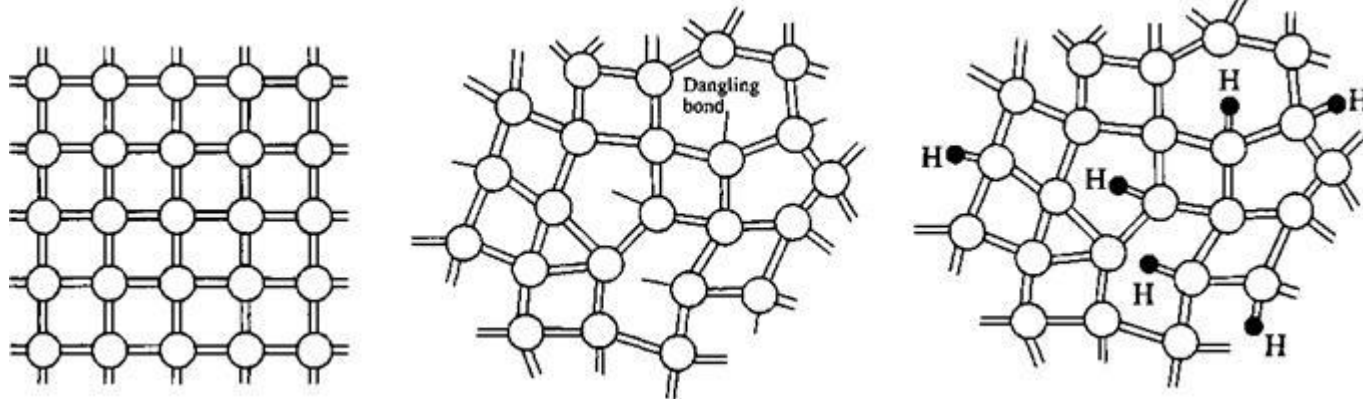
- Amorphous silicon thin films are used in solar cells



Example of using PECVD – amorphous silicon



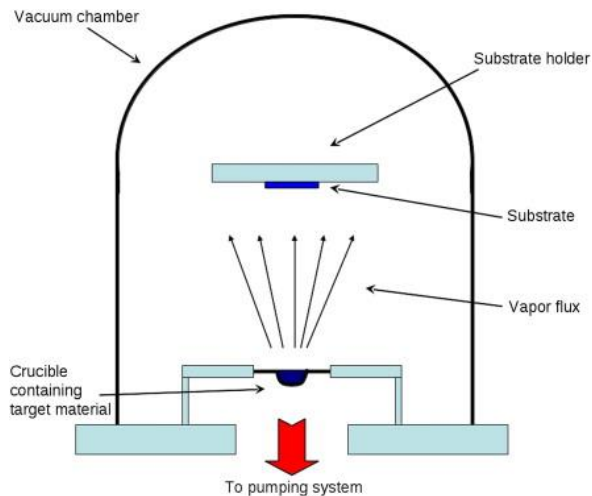
- H is required so that SiH_4 is used
 - For the material to be semiconducting.
 - Terminate the dangling bonds.
 - The dangling bonds are created by ion bombardment (SiH_3^+) which also removes hydrogen from the surface.
 - SiH_3 and SiH_2 radicals are important precursors for film growth while SiH_4 also participates in surface reactions.



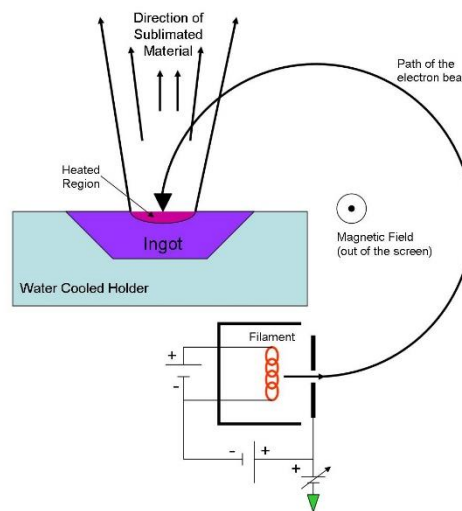
Physical vapor deposition can be achieved by heating the deposited material



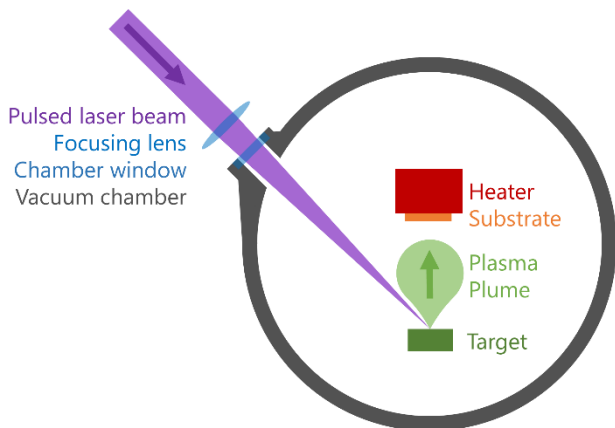
- **Thermal evaporator**



- **Electron-beam evaporator**



- **Pulsed-laser deposition**

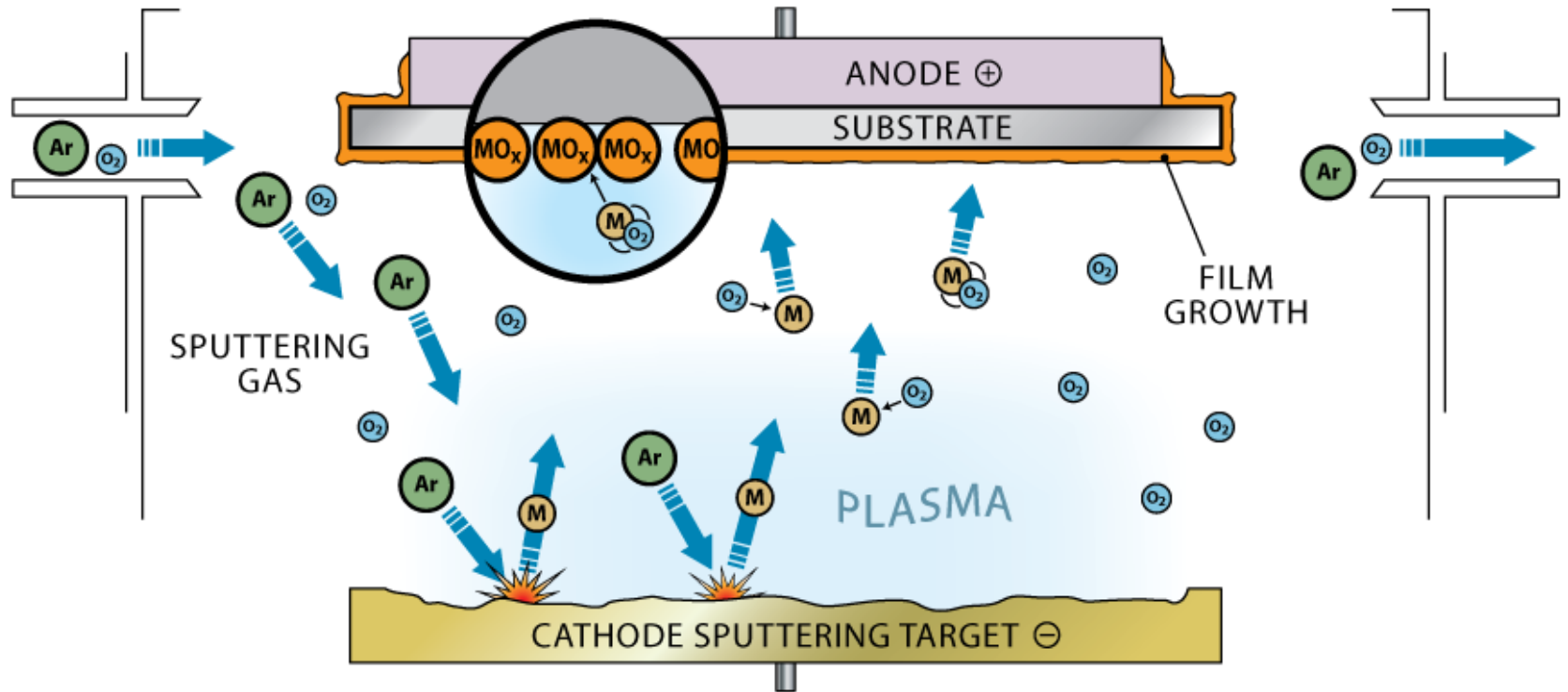


https://en.wikipedia.org/wiki/Pulsed_laser_deposition

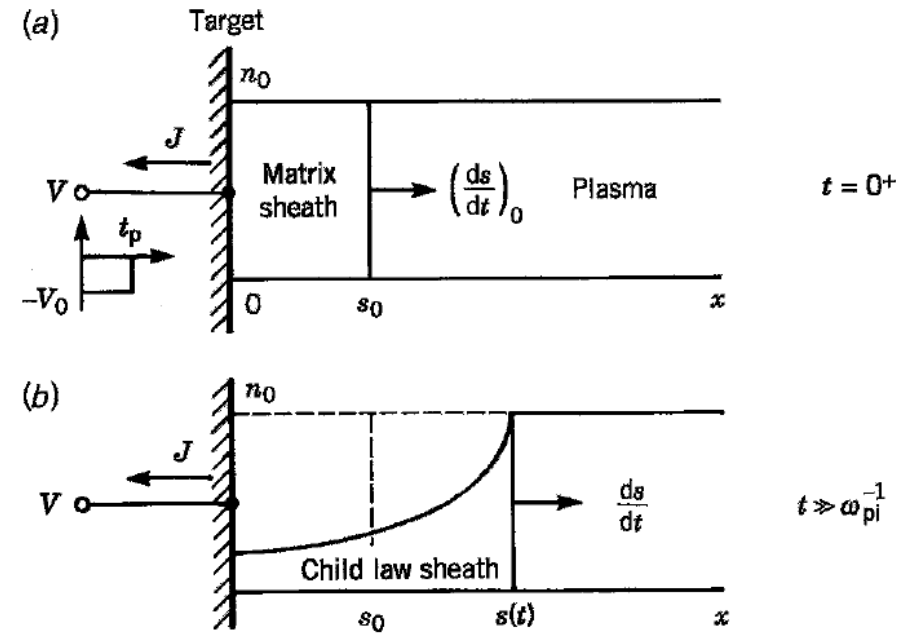
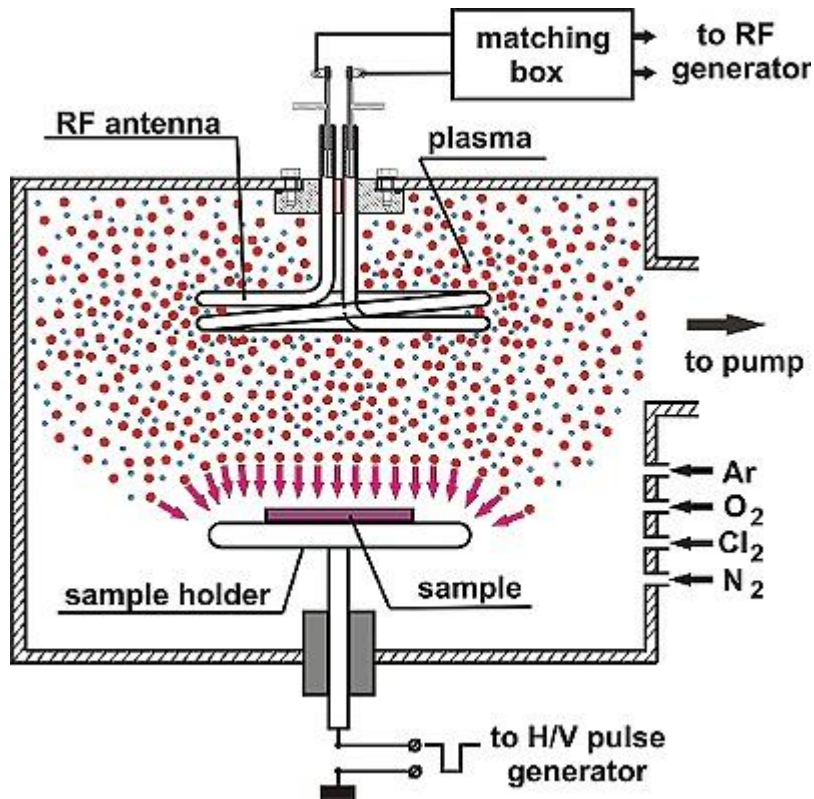
Engineered biomimicry by A. Lakhtakia and R. J. Martin-Palma

https://en.wikipedia.org/wiki/Electron-beam_physical_vapor_deposition

Sputtering deposition

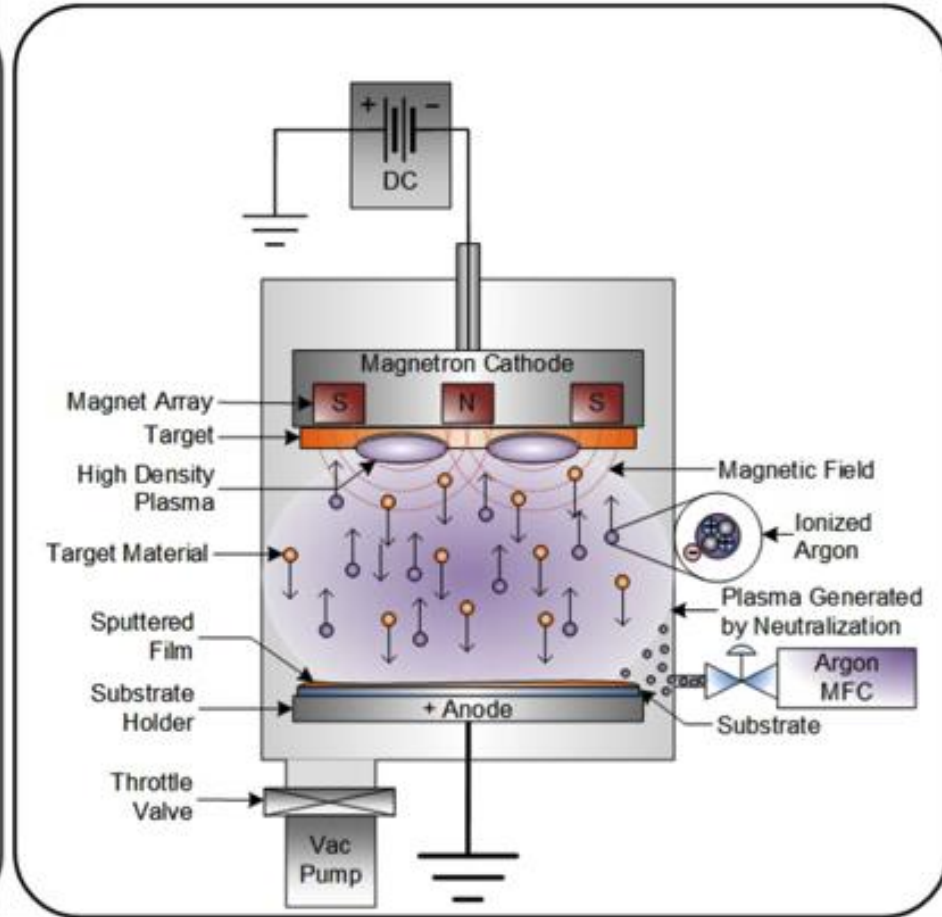
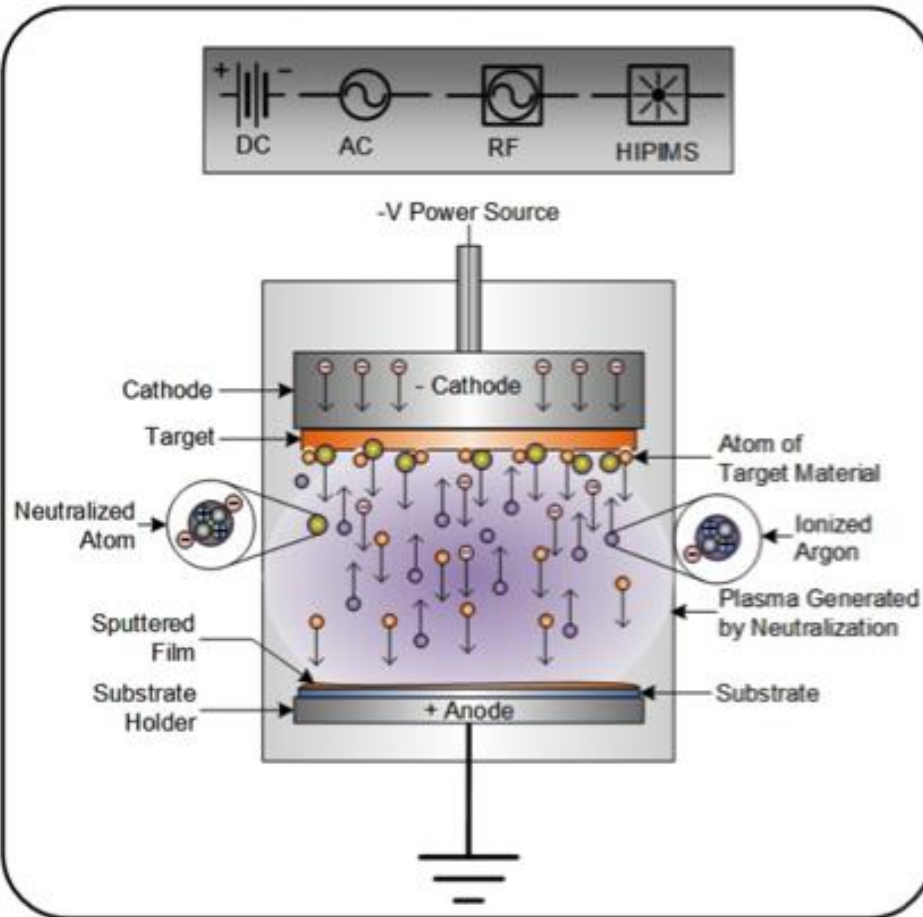


Plasma-immersion ion implantation (PIII)



- Silicon doping – ions such as B, P, As are implanted
- Surface hardening of metals – N, C are implanted

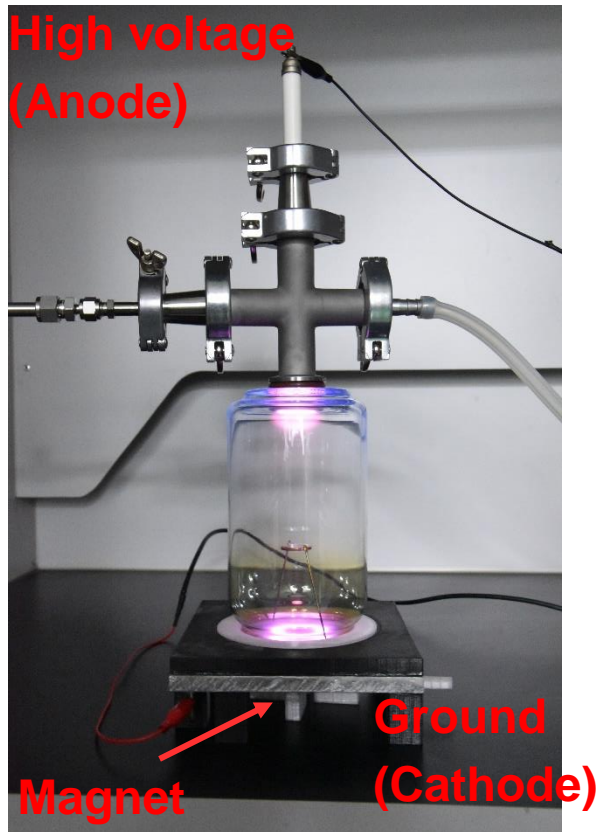
Magnetron sputtering provides higher deposition rates than conventional sputtering



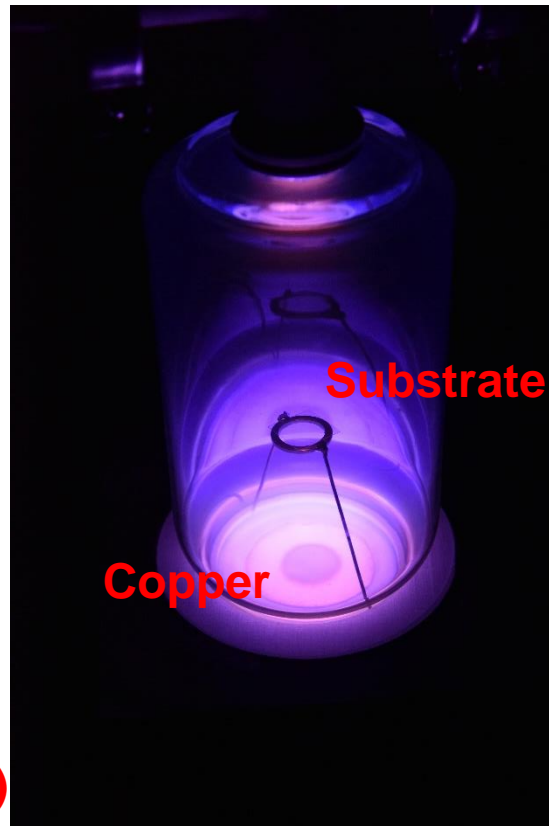
Demonstration experiments – magnetron sputtering



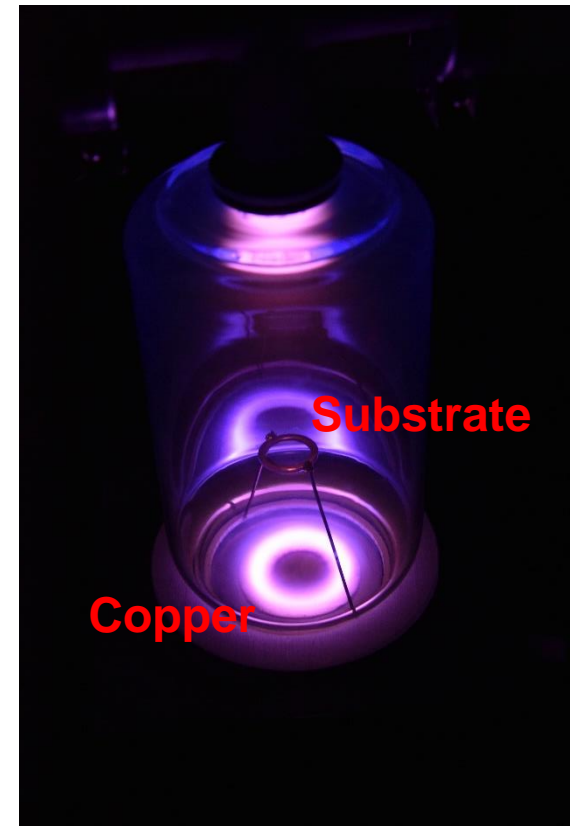
- System



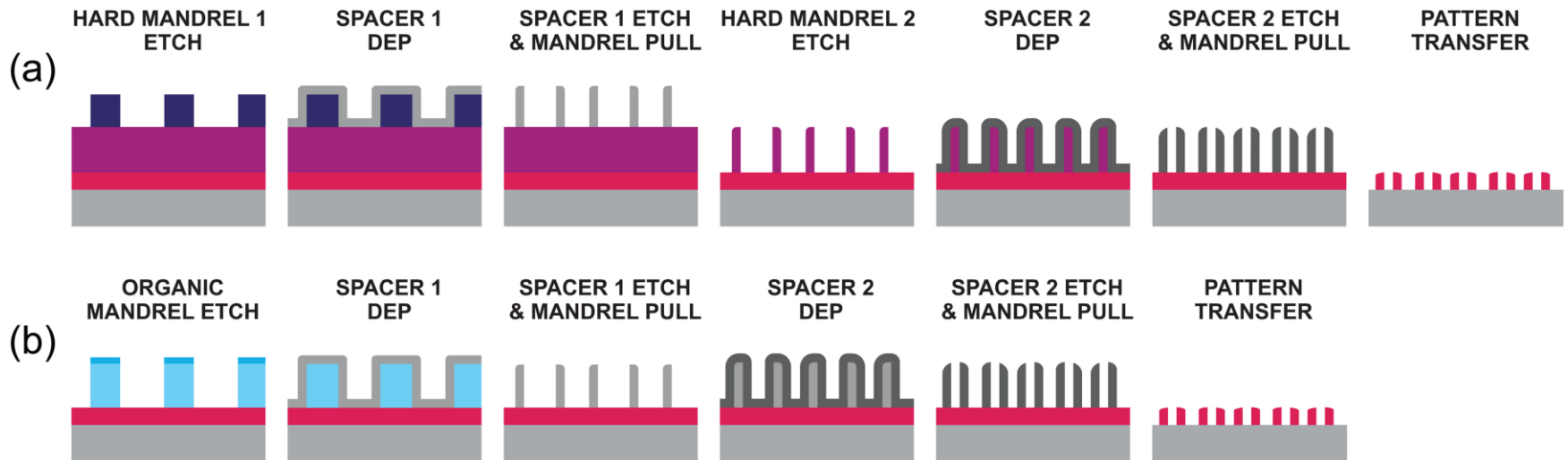
- Without magnet



- With magnet



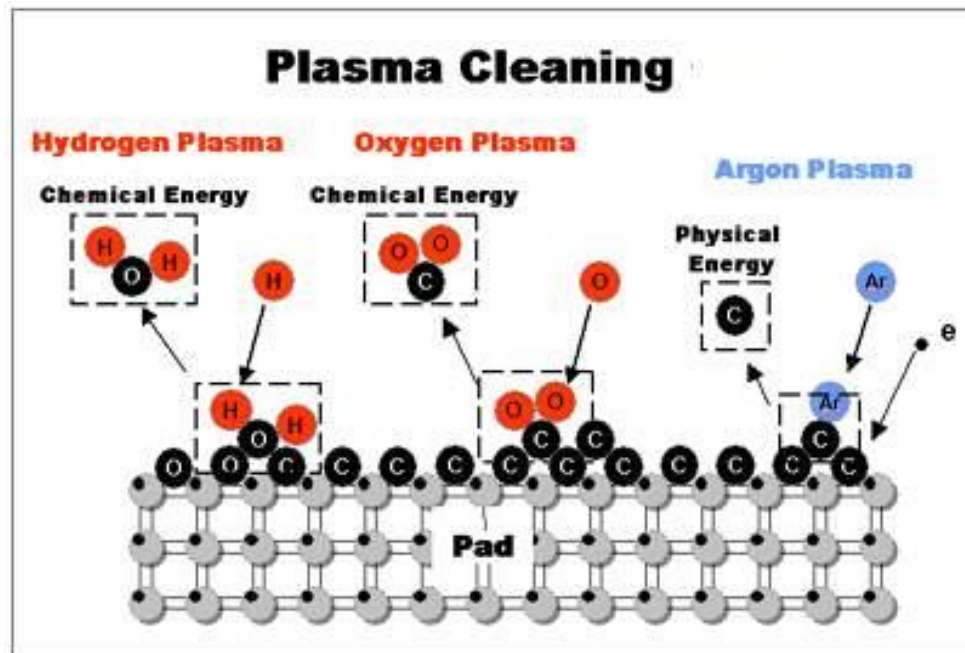
Fine periodic pattern can be made by using self-aligned quadruple patterning



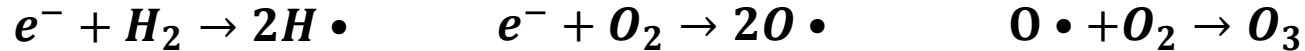
Plasma can be used for cleaning surface



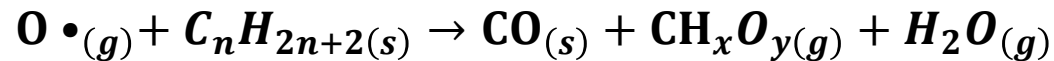
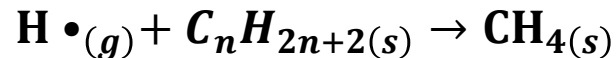
- **Cleaning mechanisms:**
 - **Chemical reactions by free radicals**
 - **Physical sputtering by high energy ions**



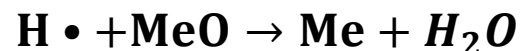
Free radicals are generated and used in chemical reactions



- Highly reactive free radicals generated in plasma may react with the hydrocarbon contaminants of surface oxide.
- Both $H \bullet$ and $O \bullet$ can react with grease or oil on surface to form volatile hydrocarbons.



- $O \bullet$ is more reactive than $H \bullet$. But $O \bullet$ may also react with surface metal to form oxide, deteriorating the material properties. Nevertheless, $H \bullet$ can make metal oxide back to metal.



The effect of chemical reactions is increased as the pressure increases



- **Advantages:**

- **Stable gas products are formed.**
- **No redeposition problem.**
- **High etching selectivity.**

- **Disadvantages:**

- **Higher concentration of H_2 or O_2 is required to ensure an appropriate etching rate.**
- **H_2 safety or O_2 strong oxidation ability needs to be monitored.**

High energy ions are used in physical sputtering cleaning



- Ions generated in plasma can be accelerated toward the substrate to physically bombard away the atoms of contaminants.
- The physical sputtering rate increases as the following quantities increase:
 - Plasma density;
 - Accelerating voltage;
 - Mass of bombardment atoms.
- The physical sputtering is also enhanced by lowering the pressure.
- High cathode bias is used.
- Ar^+ has strong sputtering effect.

The physical sputtering rate increases with higher cathode bias and Ar concentration and lower pressure



- **Advantages:**

- Highly efficient cleaning effect can be achieved.
- Gas consumption rate can be very low.

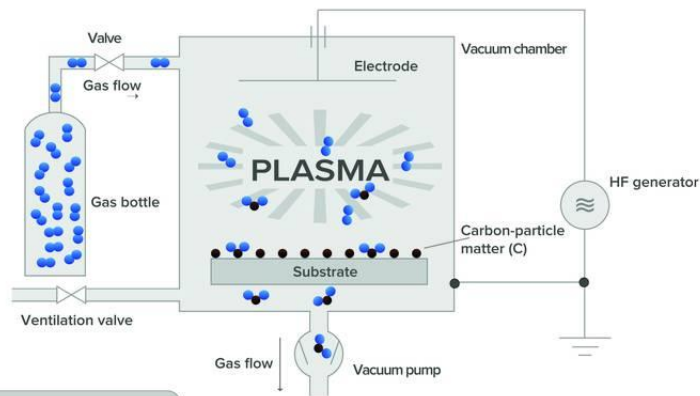
- **Disadvantages:**

- Etching problems – non-selective etching by physical sputtering.
- Redeposition problems: the products sputtered out may be highly unstable and tend to deposit again downstream.

Plasma cleaning examples



Low-pressure plasma system: Generation with a low-frequency or high-frequency generator

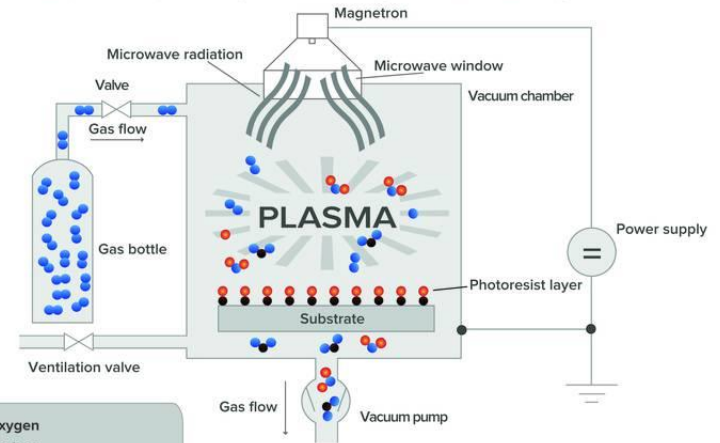


- Oxygen
- Carbon

e.g.: The removal of carbon-particle matter with O₂ plasma
 $C + O^2 \rightarrow CO_2 \uparrow$

Diagram 6

Low-pressure plasma system: Cleaning with a microwave generator



- Oxygen
- Carbon
- Hydrogen

e.g.: Removal of photoresist
 $C + O_2 \rightarrow CO_2 \uparrow$
 $2H + O \rightarrow H_2O \uparrow$

Diagram 7

Plasma cleaning needs to work in the regime of abnormal glow discharge



- Top view



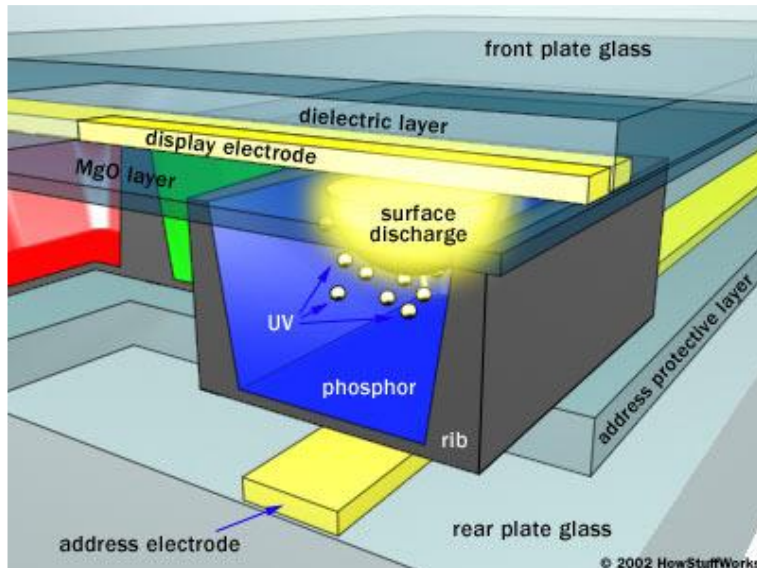
- Side view



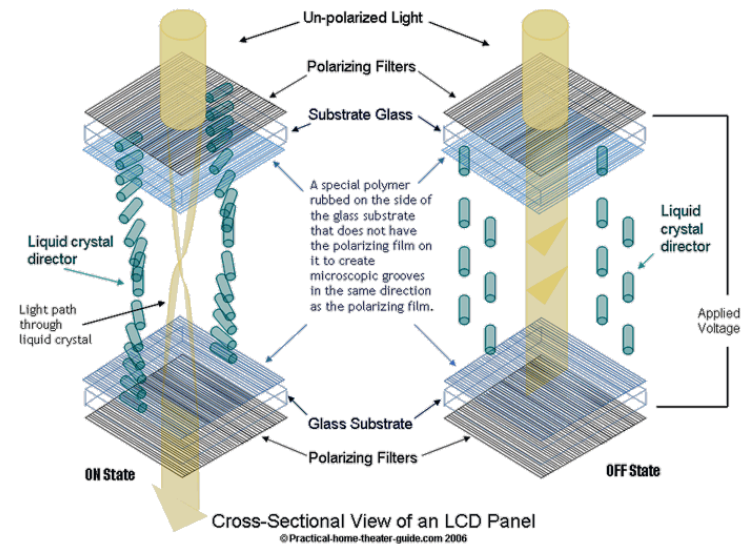
Light source and display systems



Plasma display panel (PDP)



Liquid crystal display (LCD)

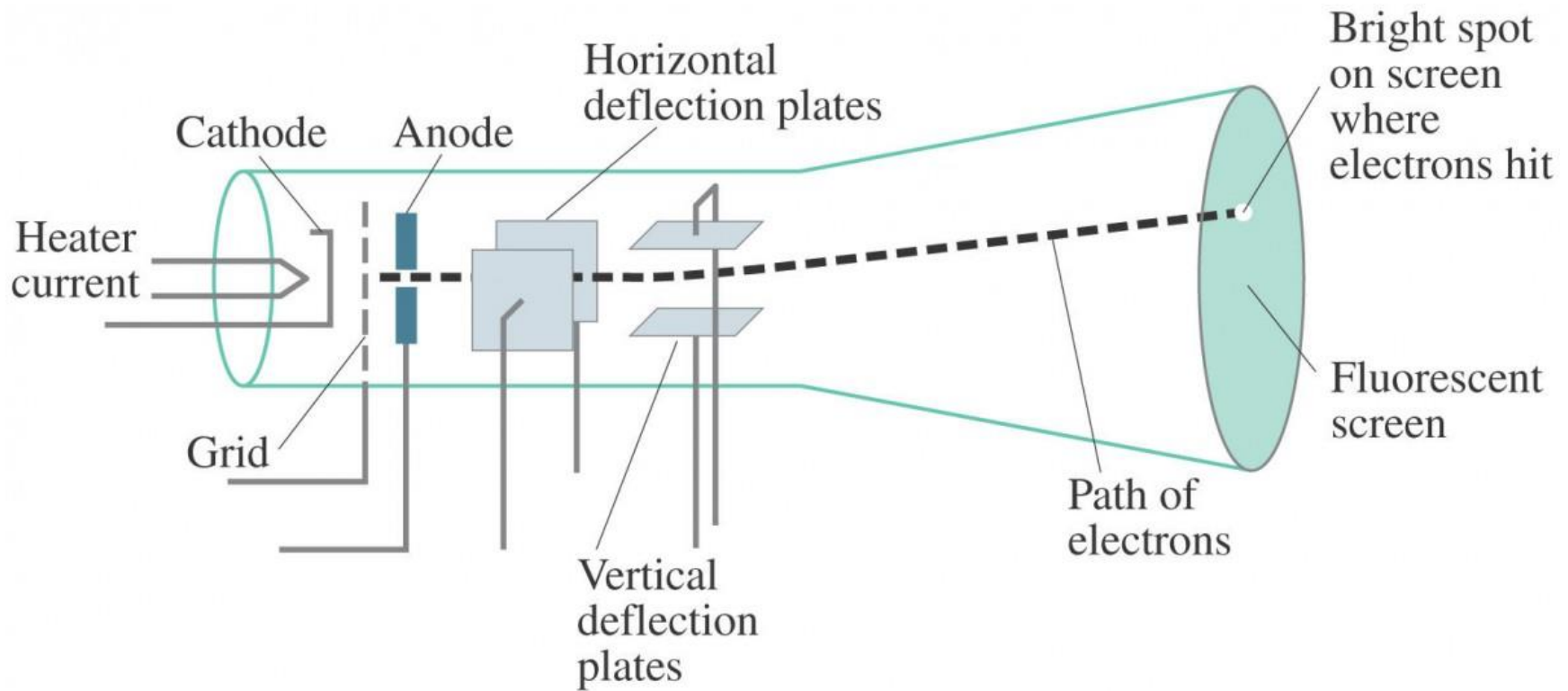


Outlines

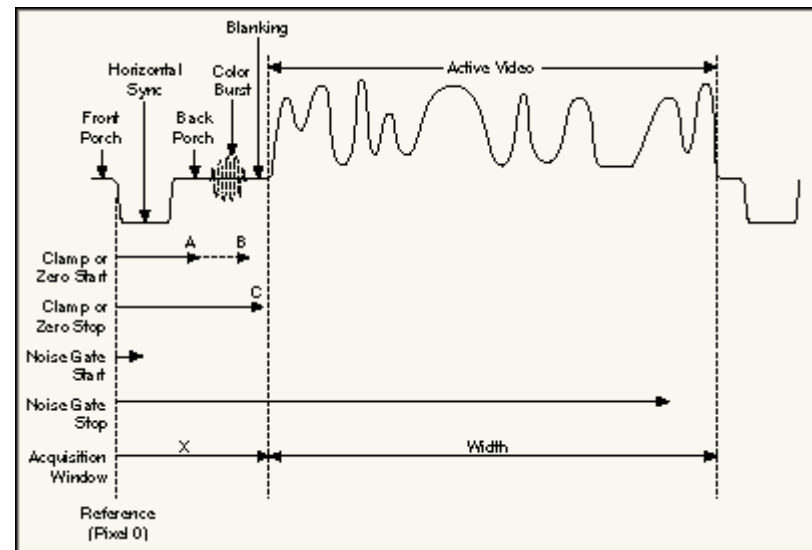
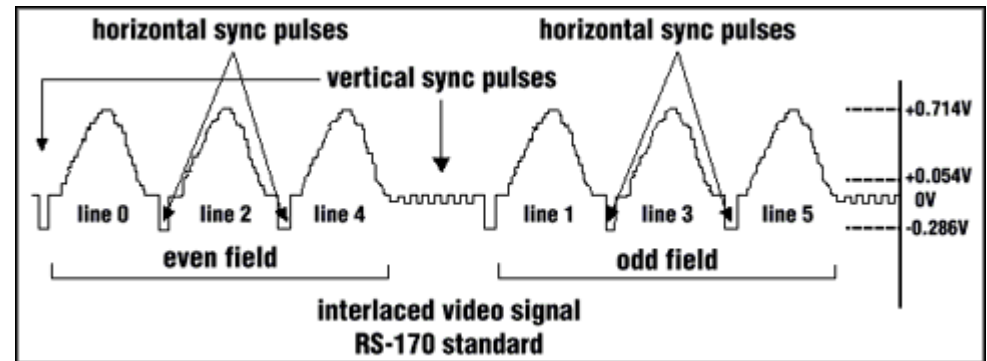
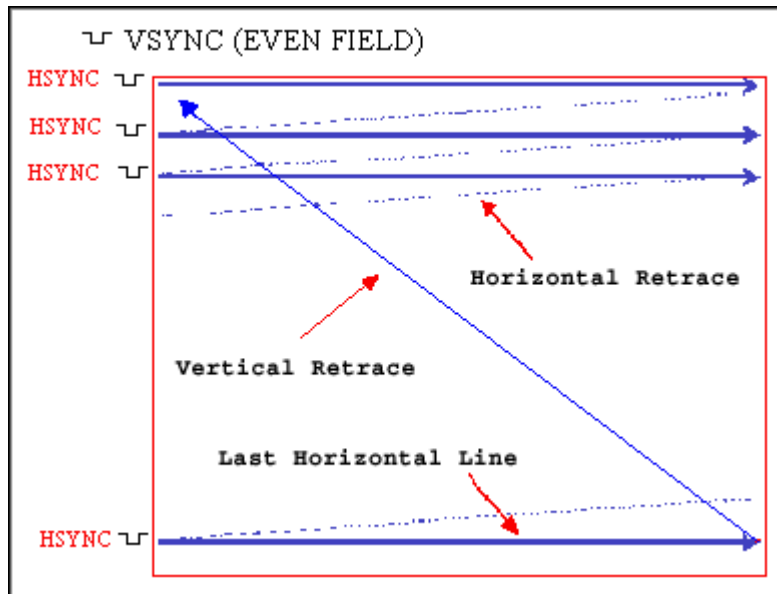


- **Cathode Ray Tube**
- **Color space (CIE 1931 color spaces)**
- **History of plasma display panel (PDP)**
- **Design of PDP**
- **Liquid crystal display (LCD)**
- **LCD vs PDP**

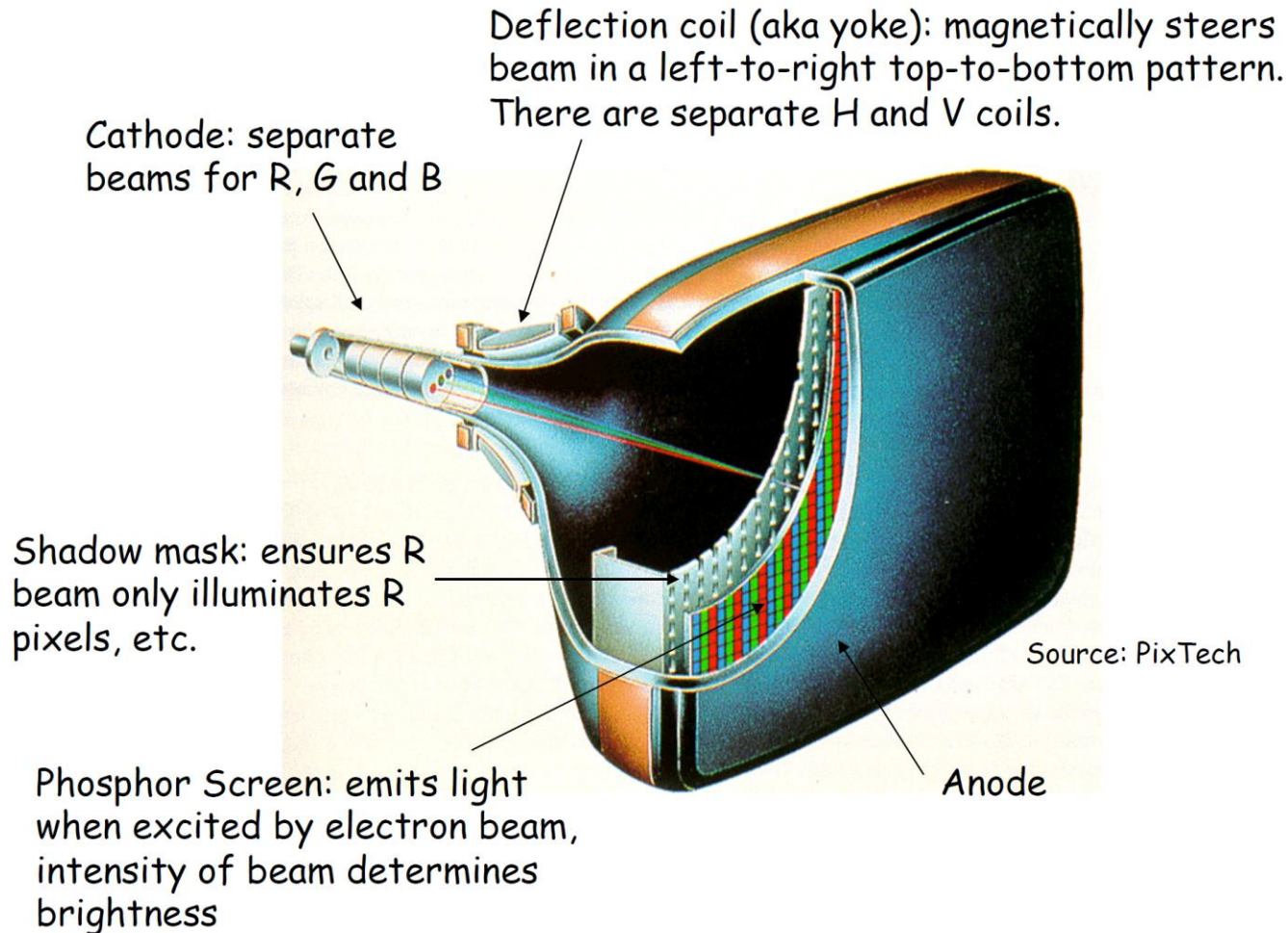
Cathode Ray Tube uses electron beams to light the fluorescent screen



The image is shown by scanning through the whole screen with the single electron beam



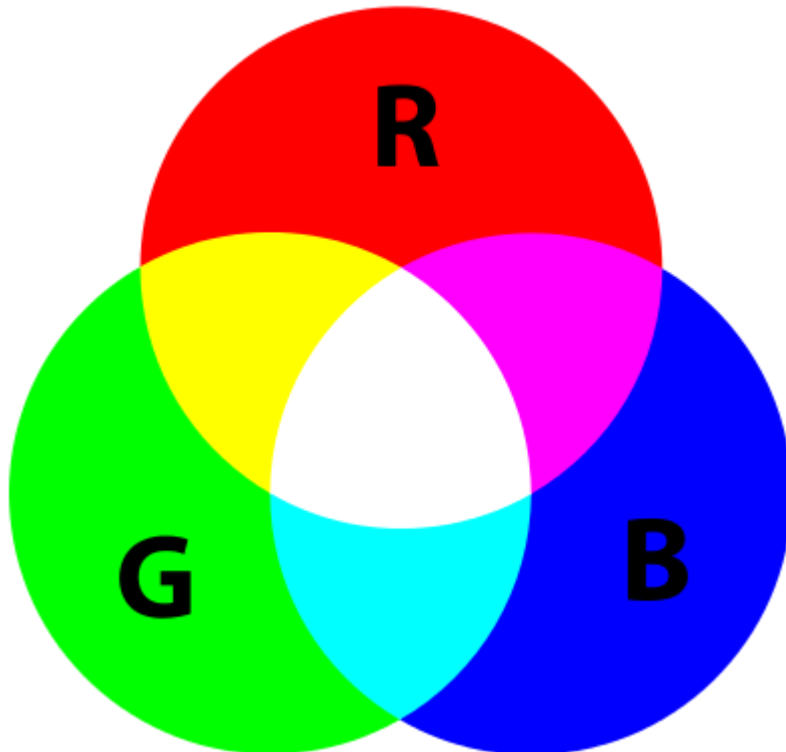
Color image is formed by using three electron beams scanning through three different color channels



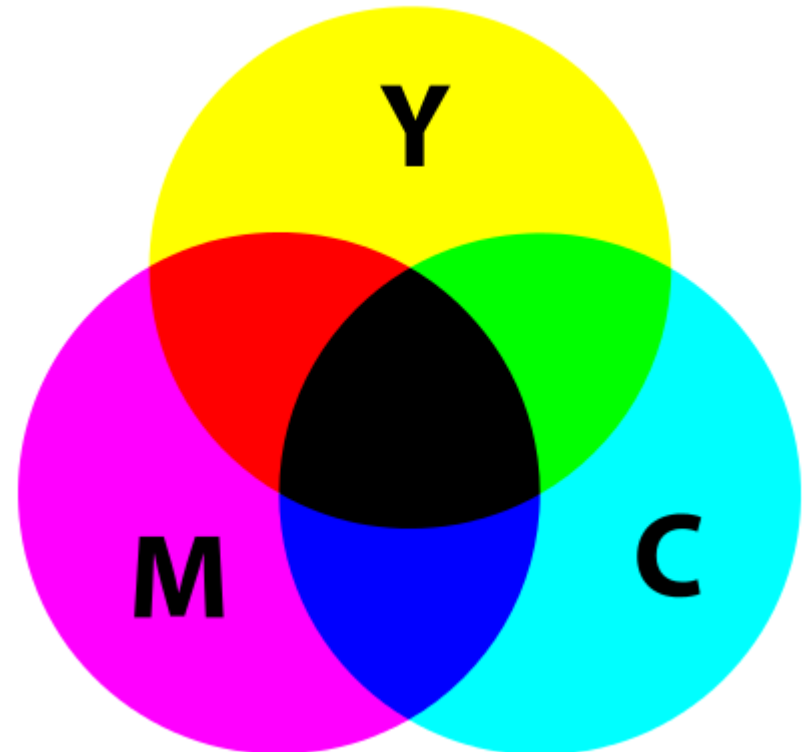
Color can be created using three primary colors



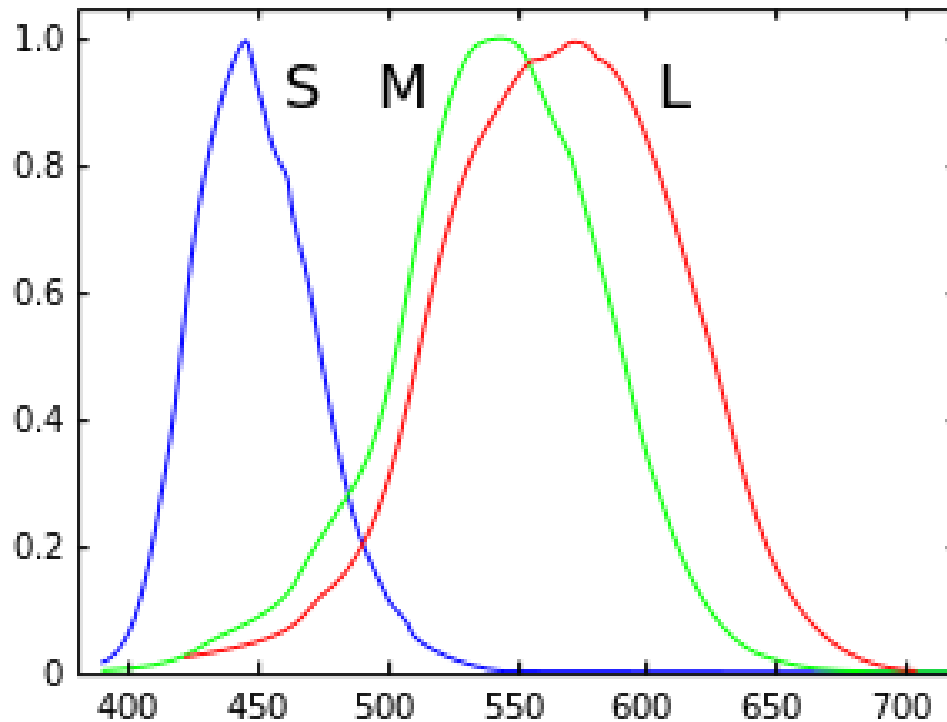
Additive primaries



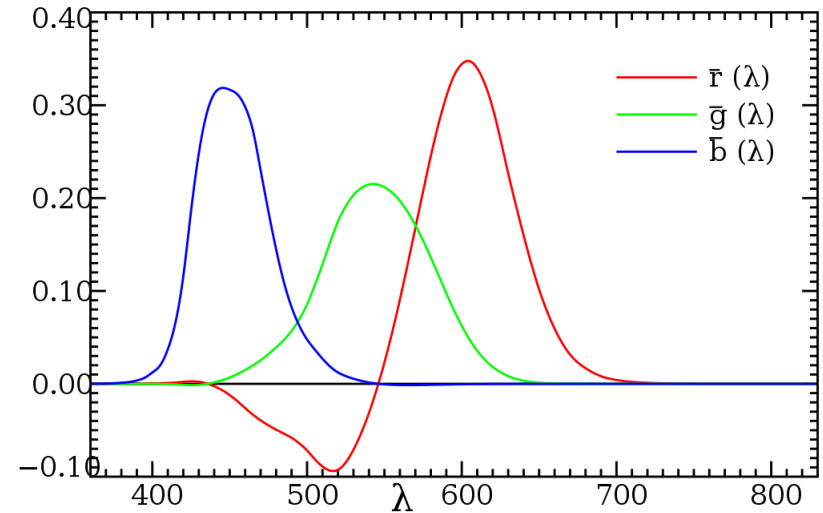
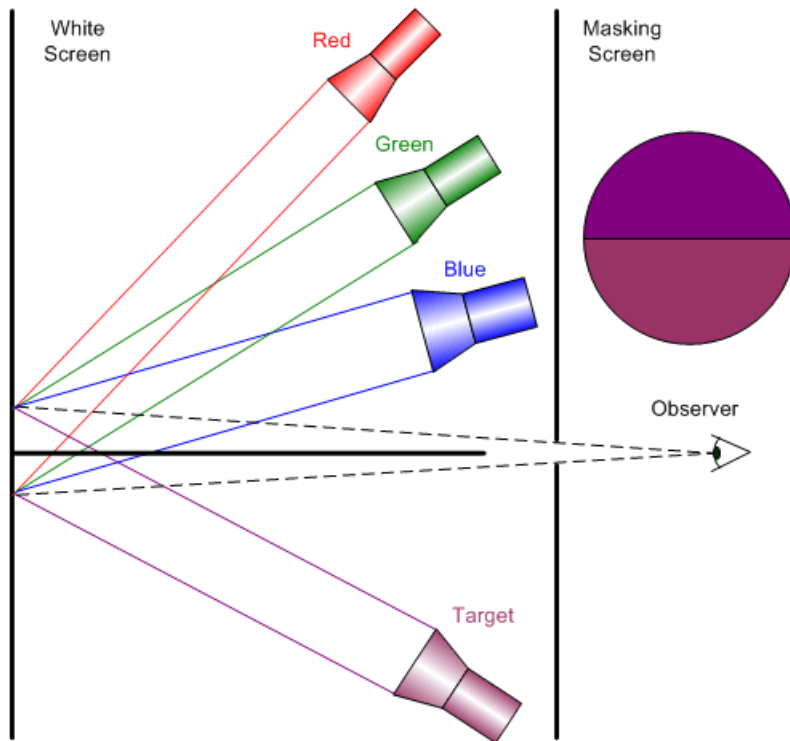
Subtractive primaries



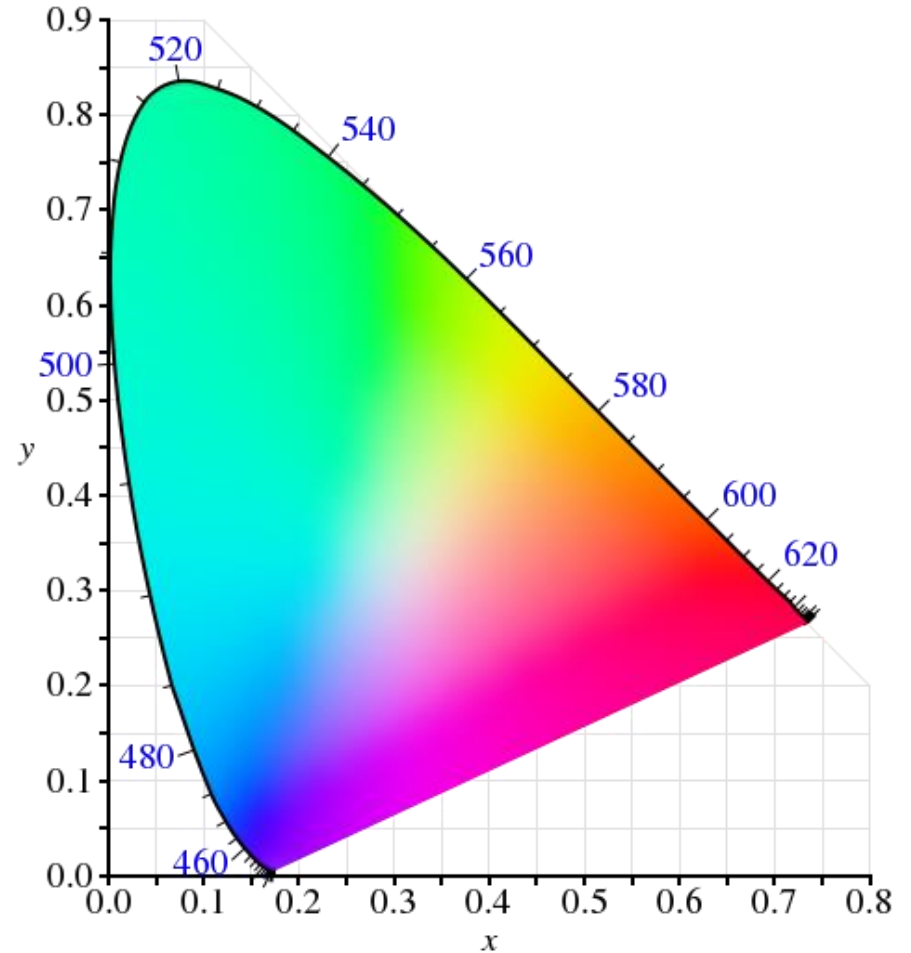
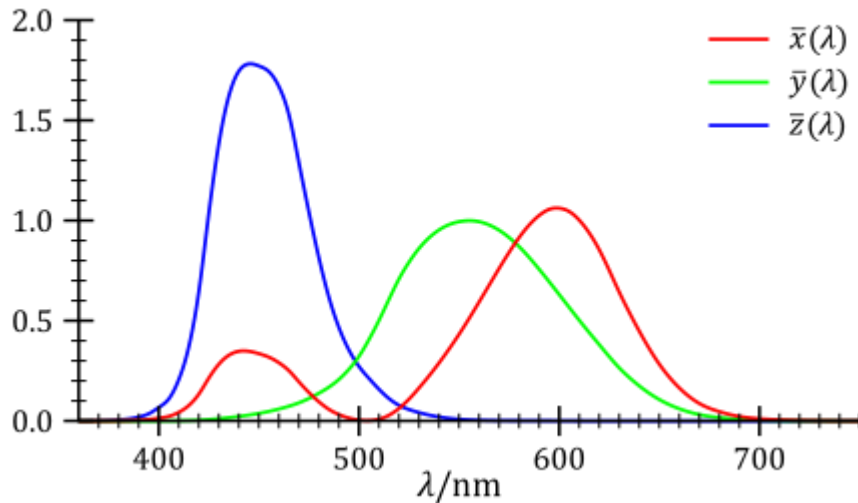
Human retina has three kinds of “cones” that have different spectral response



Spectral response of retina “cones” are tested using light sources with single wavelength

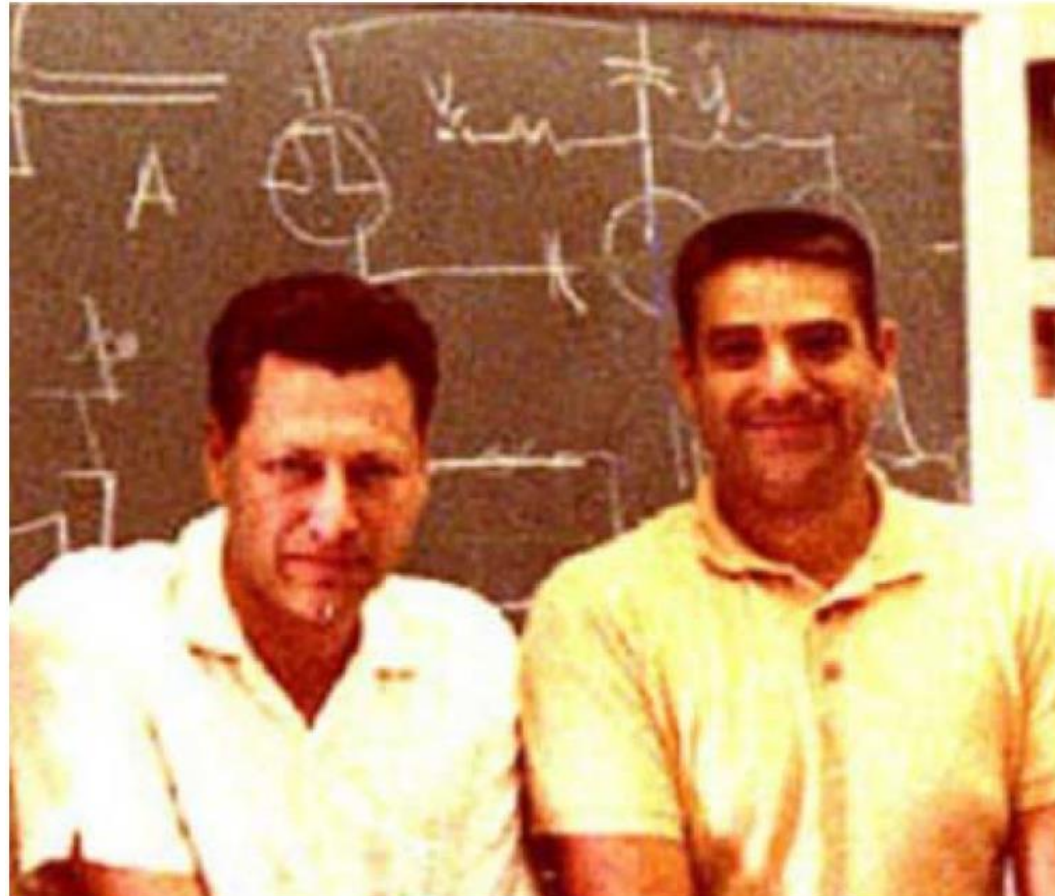


The CIE 1931 color space chromaticity diagram is the standard color space



History of PDP

Plasma display panel was invented at the University of Illinois in 1967



Prof. H. Gene Slottow

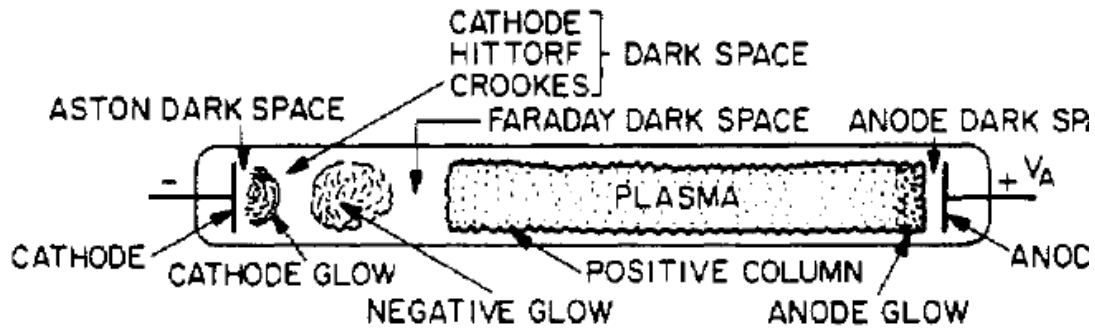
Prof. Donald L. Bitzer

PDP was invented due to a need for Programmed Logic for Automatic Teaching Operations (PLATO) in 1960s



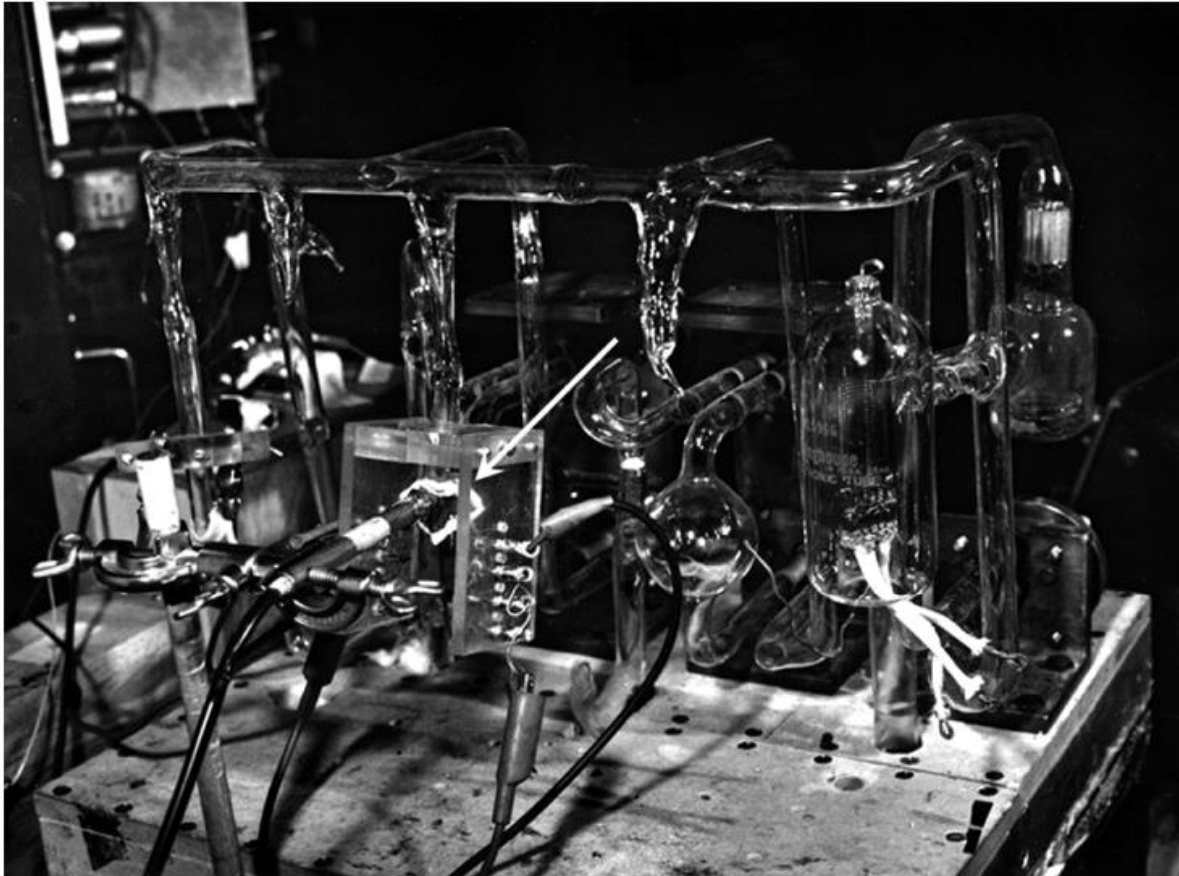
<https://topwallpapers.pw/computer/keyboards-computers-history-teletype-typewriters-desktop-hd-wallpaper-1035981/>
https://en.wikipedia.org/wiki/Punched_tape
[https://en.wikipedia.org/wiki/PLATO_\(computer_system\)](https://en.wikipedia.org/wiki/PLATO_(computer_system))

The positive column in a glow discharge is used to excite phosphors in color PDP



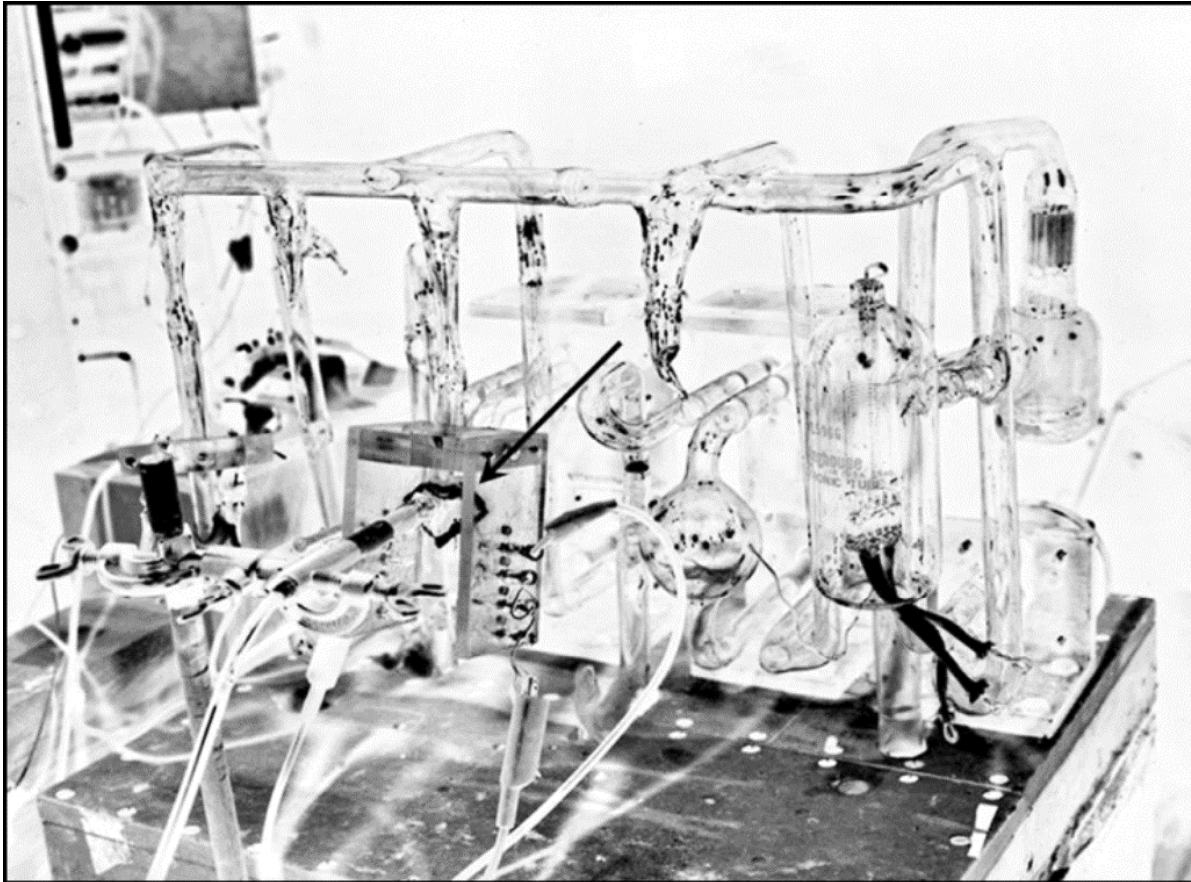
- Majority of monochrome PDPs use the negative glow as the light source
- The positive column is used to excite phosphors in fluorescent lamps and in color PDPs

Early plasma panel (PD) attached to the glass vacuum system used for the first plasma displays at UI



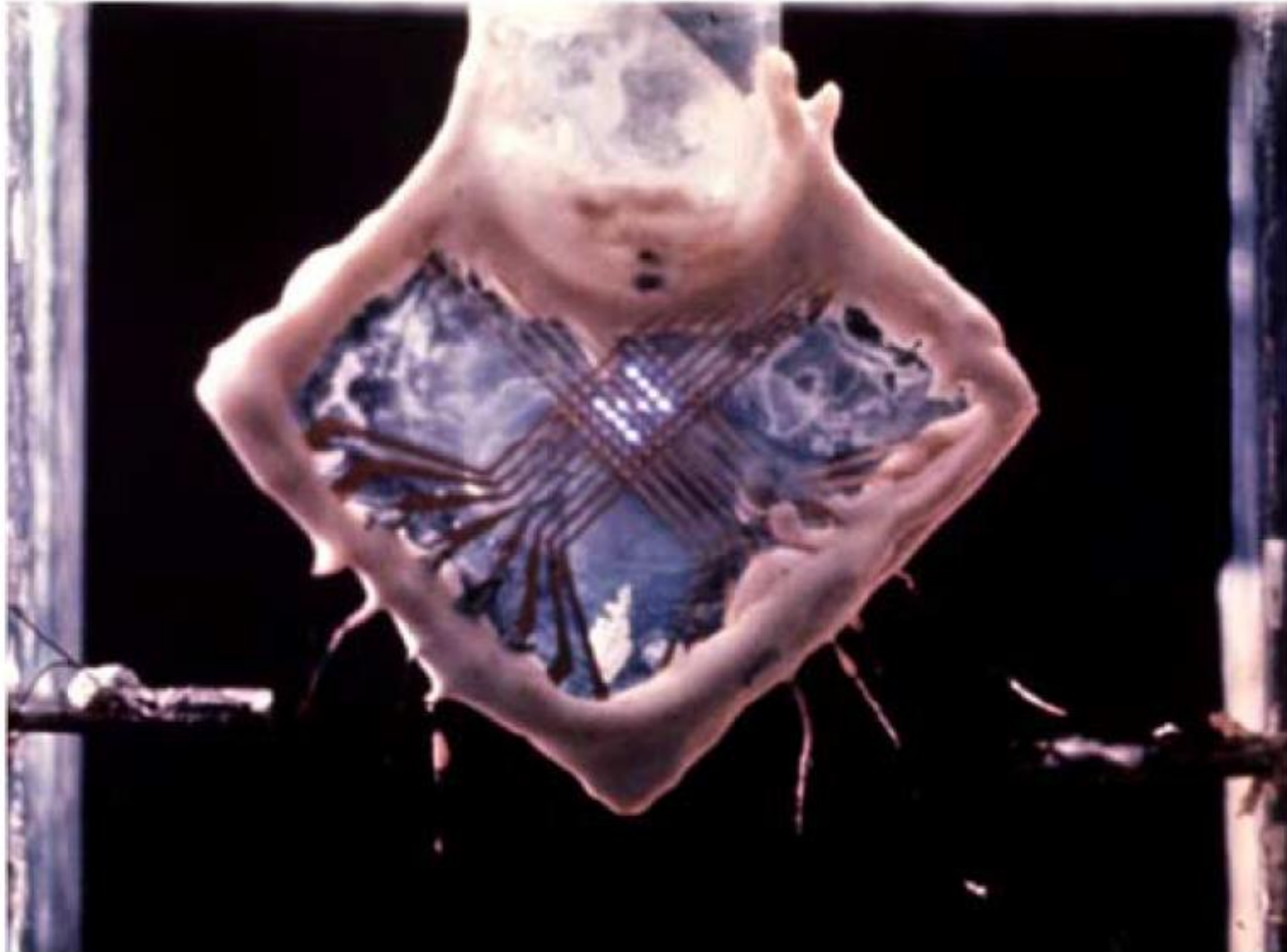
- It had the same alternating sustain voltage, neon, gas, and dielectric glass insulated electrodes that are used for plasma TVs today.

Early plasma panel (PD) attached to the glass vacuum system used for the first plasma displays at UI

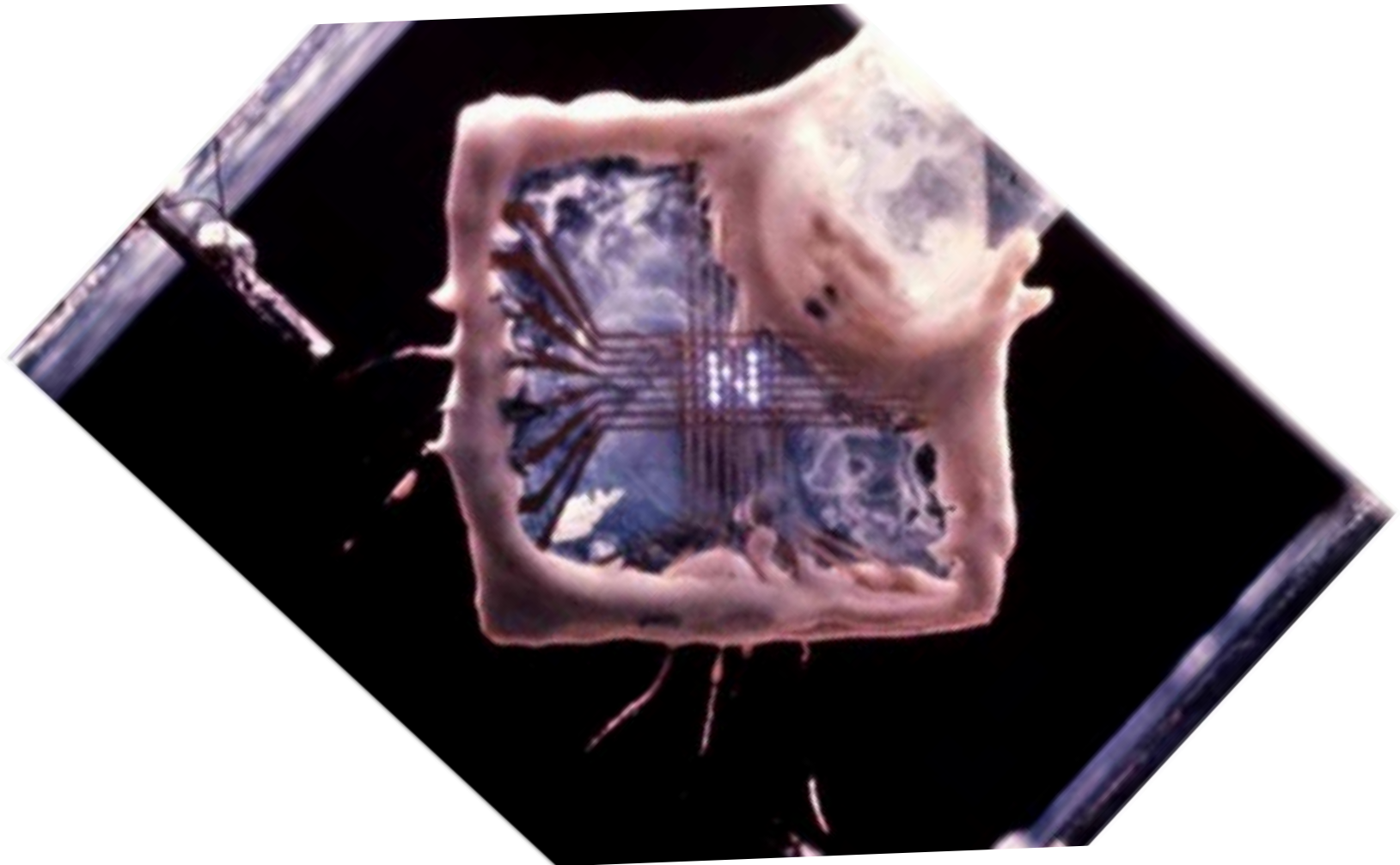


- It had the same alternating sustain voltage, neon, gas, and dielectric glass insulated electrodes that are used for plasma TVs today.

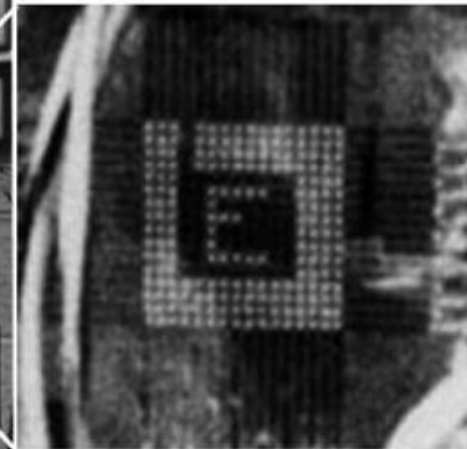
Early 4x4 pixel panel has achieved matrix addressability for the first time



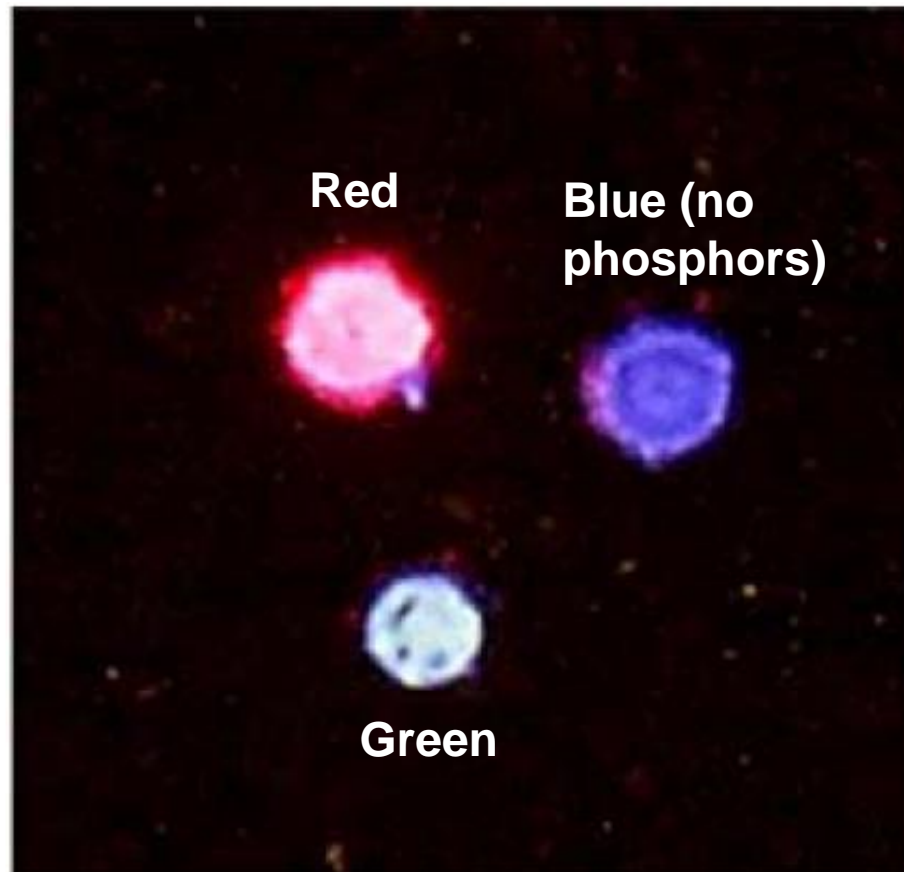
Early 4x4 pixel panel has achieved matrix addressability for the first time



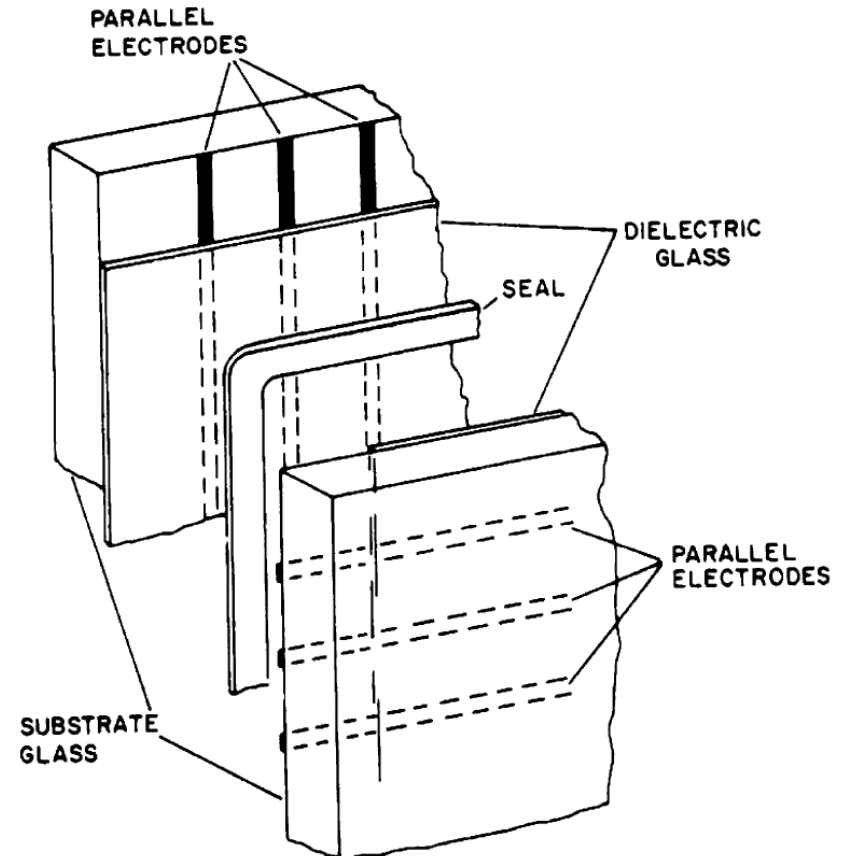
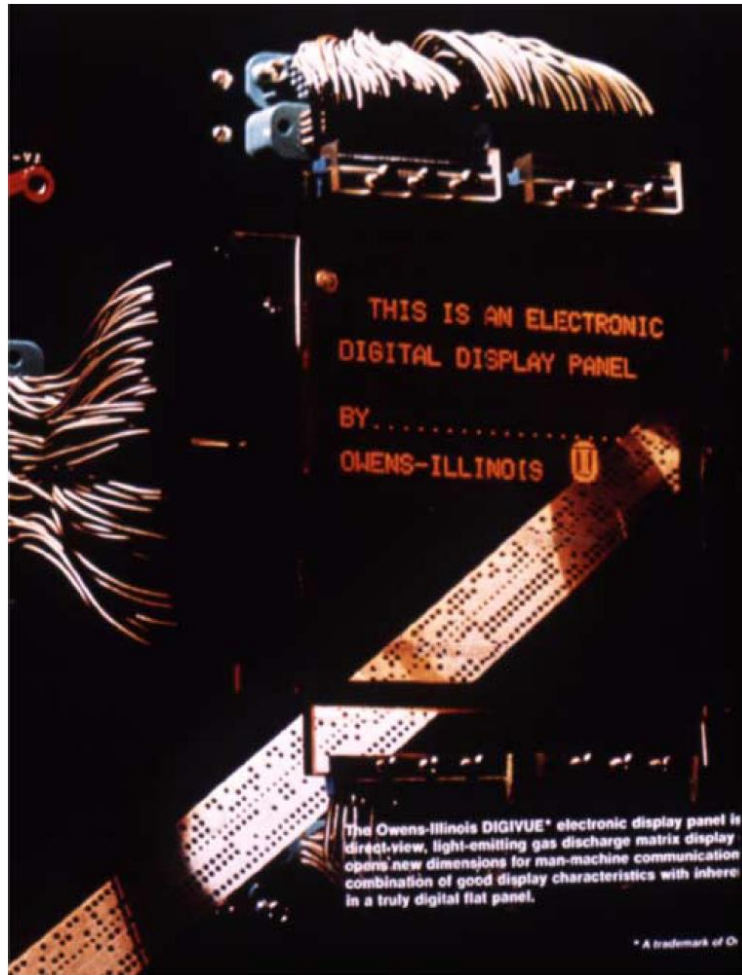
A 16x16 pixel PD, developed in 1967, needed to be addressed manually



First color PD was three cell prototype with red and green color phosphors excited by a xenon gas discharge



Open-cell structure developed in 1968

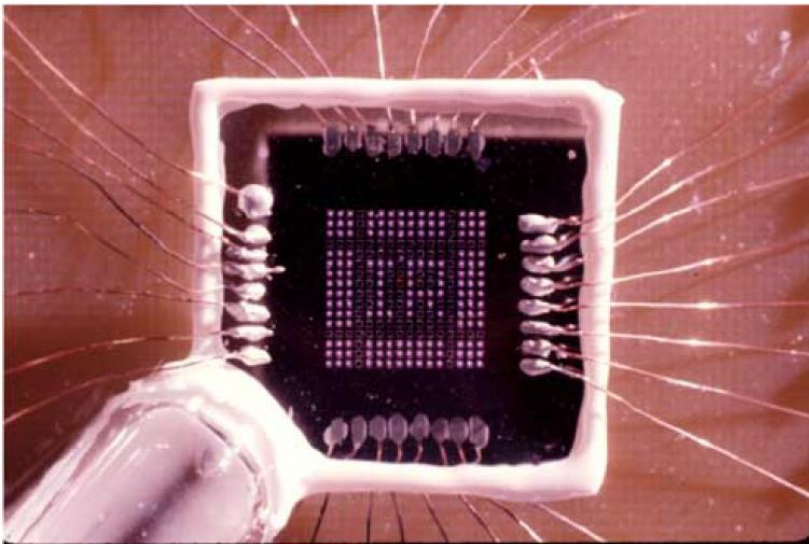


- It could be baked under vacuum at 350 °C to drive out contaminants.

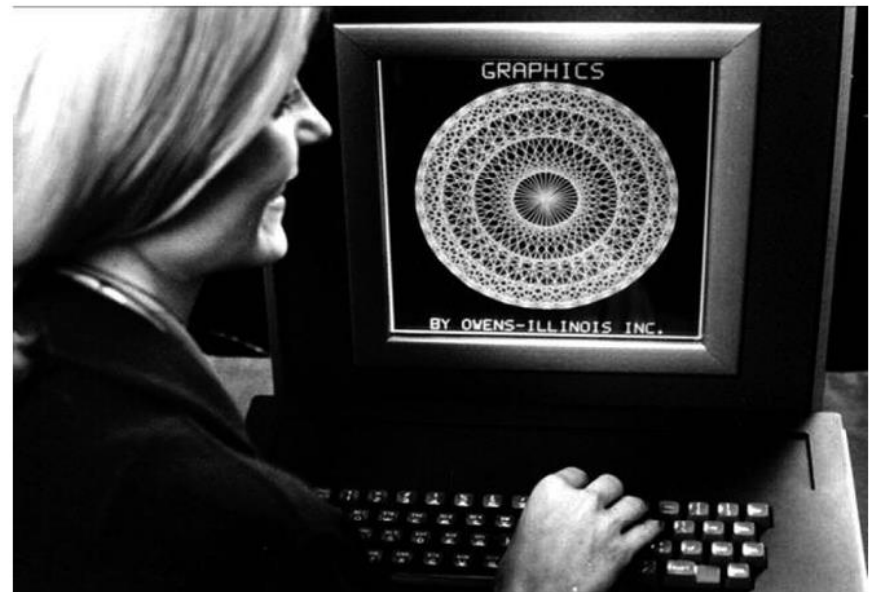
More progress



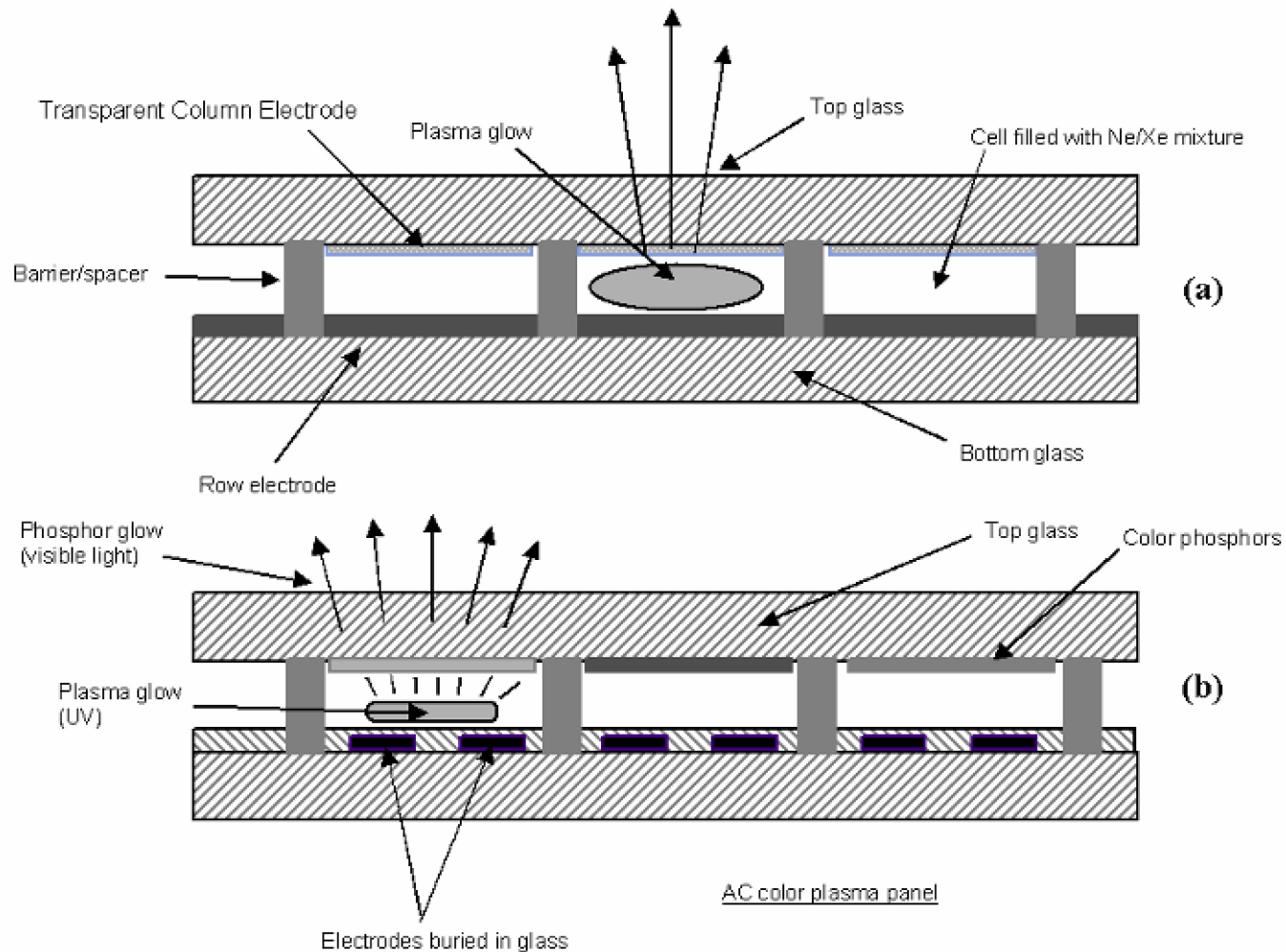
**1968, University of Illinois
16x16 pixels**



**1971, Owens-Illinois
512x512 pixels**

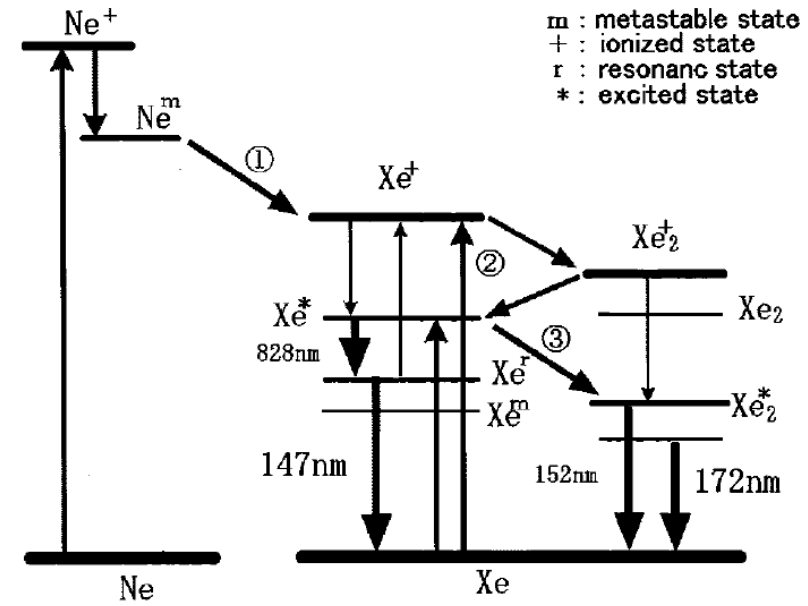
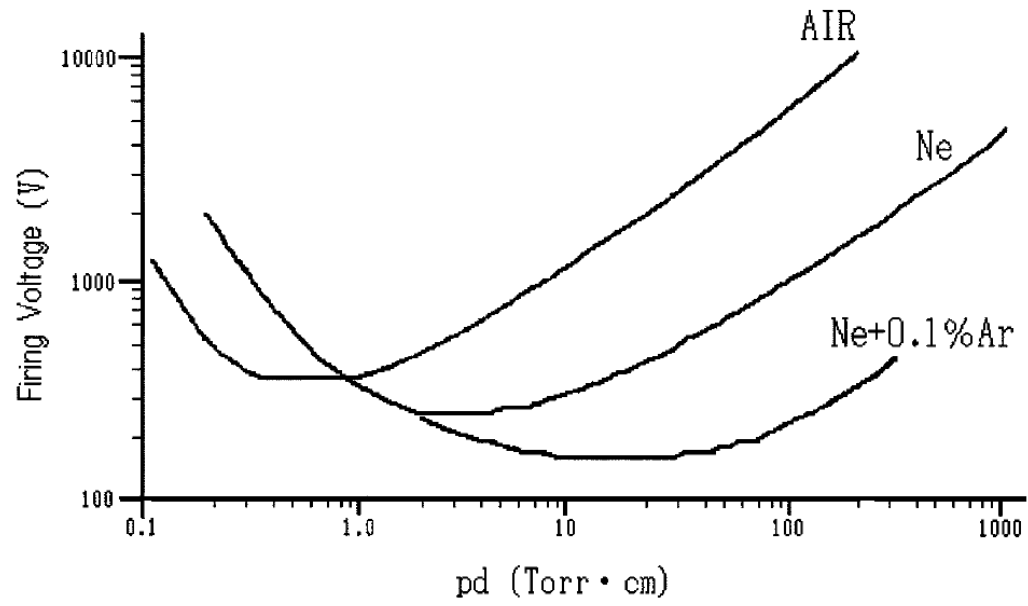


Color PDPs had short display lifetime due to the degradation of color phosphors caused by ion sputtering

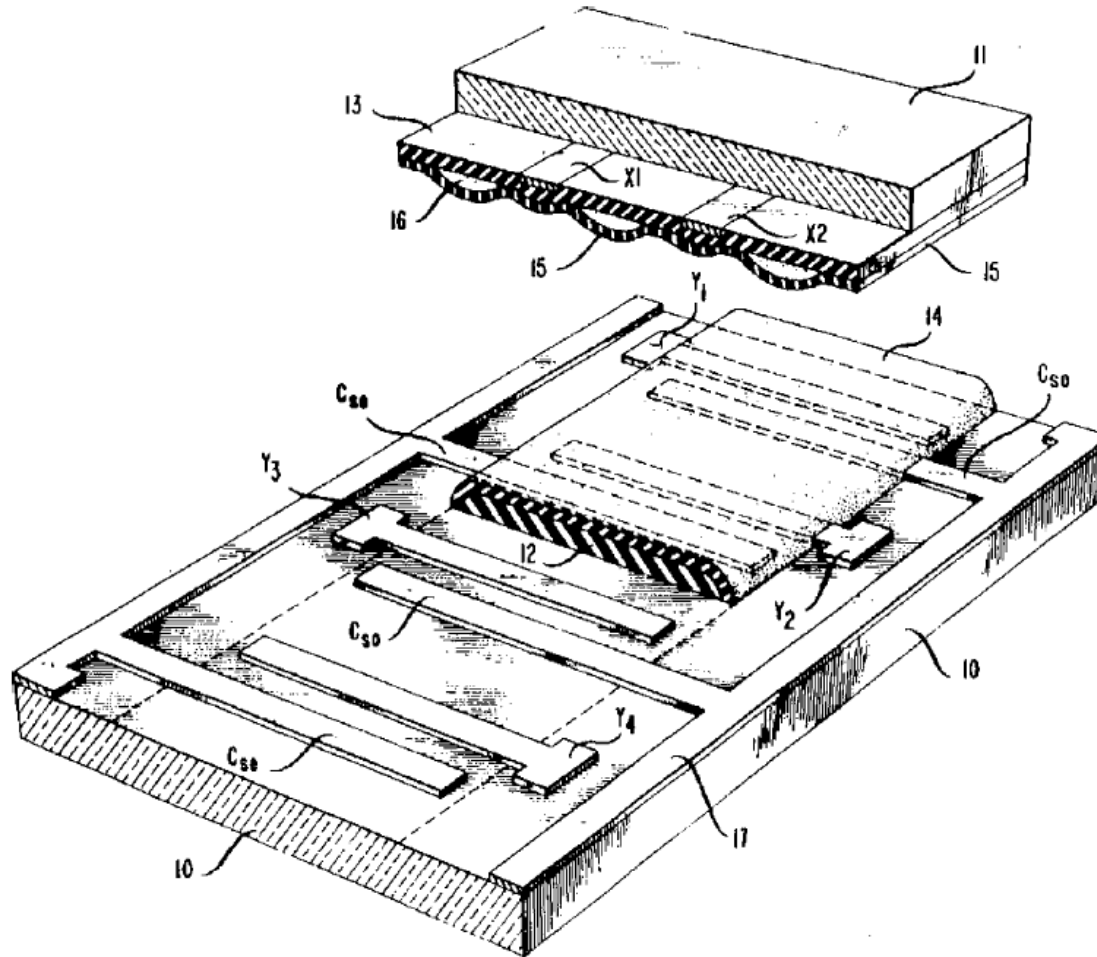


Design of PDP

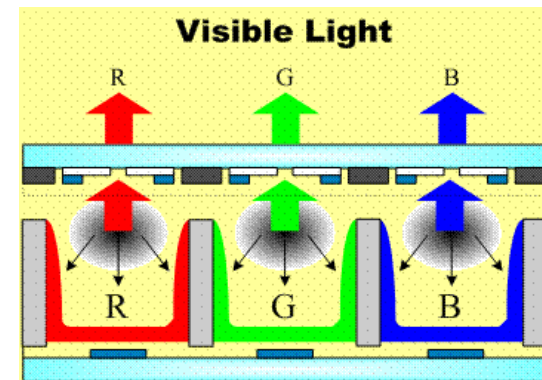
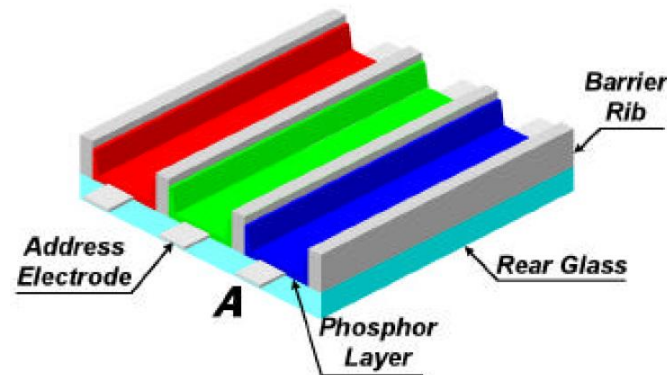
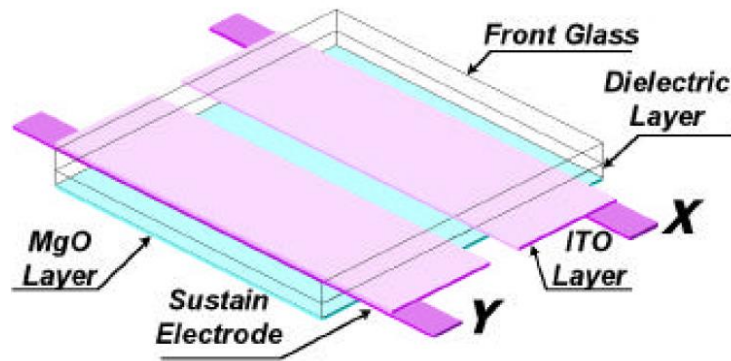
A lower breakdown voltages can be obtained with very small amounts of added gas



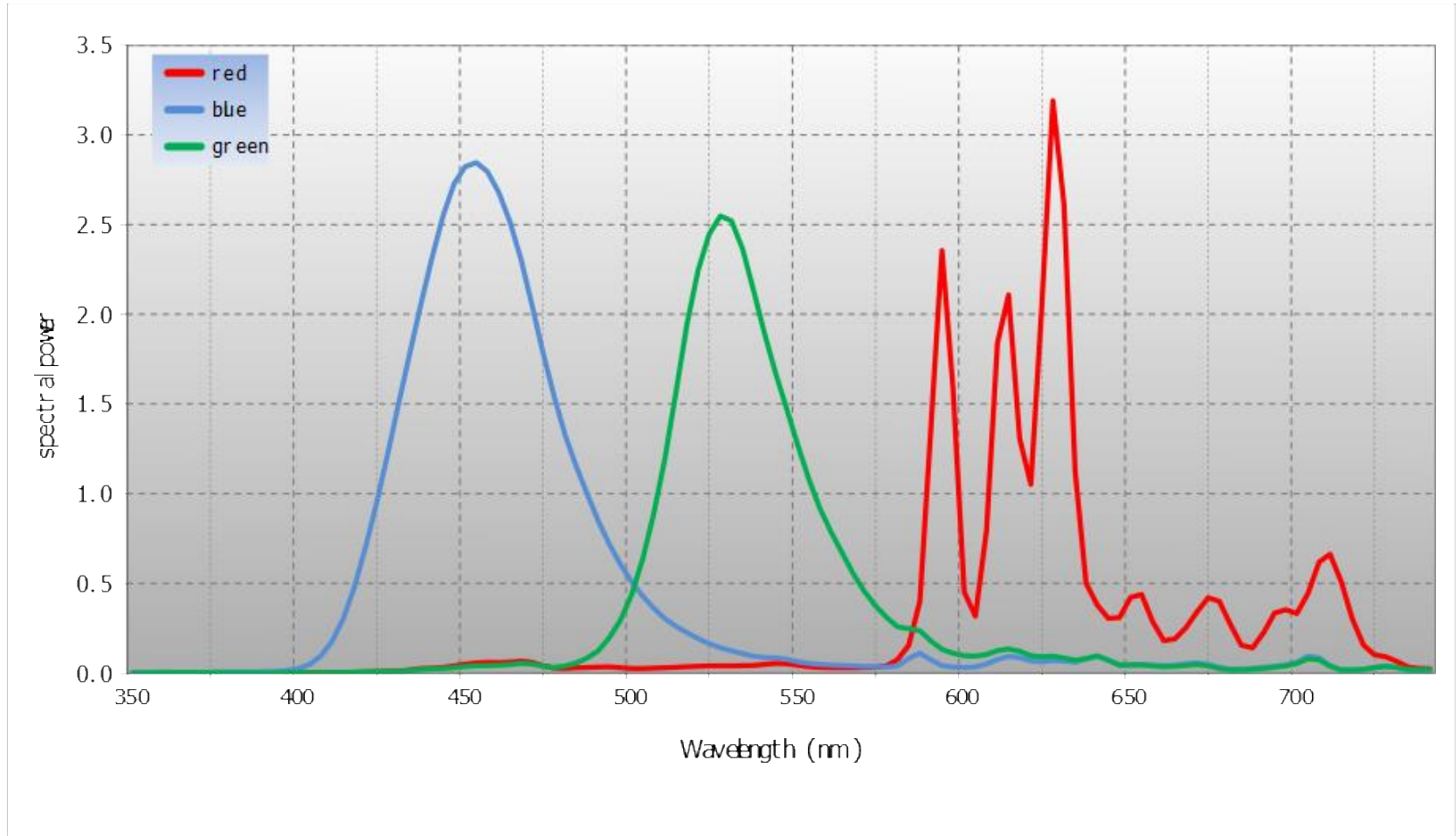
AT&T three-electrode patent



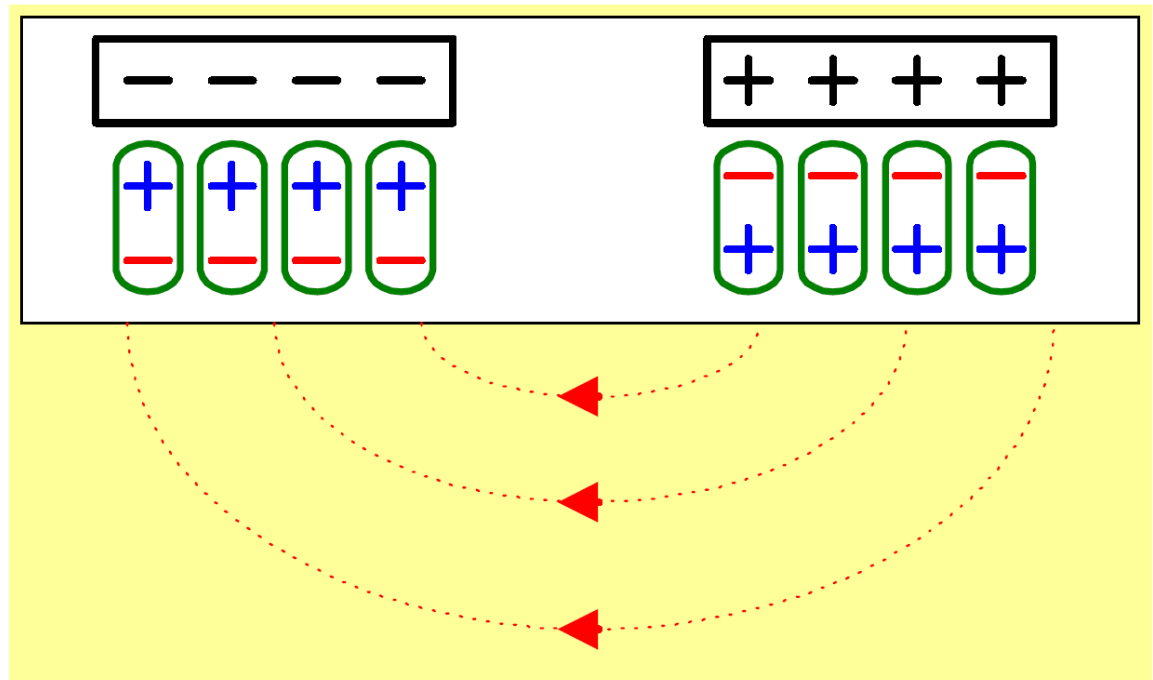
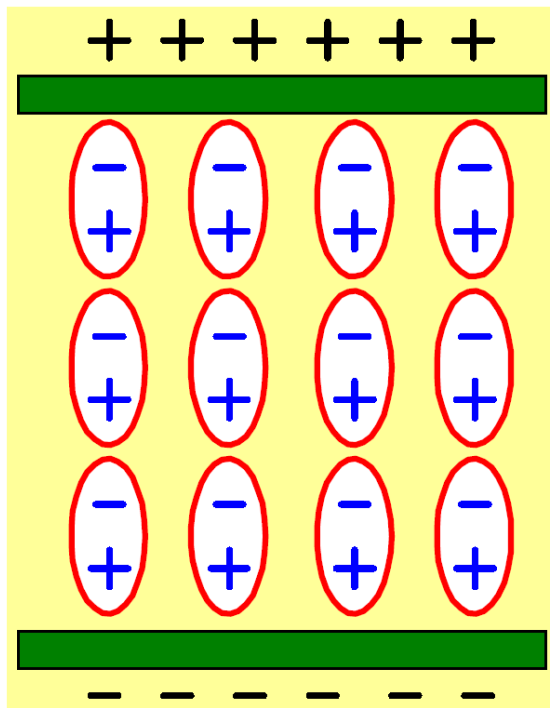
Reflective phosphor geometry is used in most of today's plasma TVs



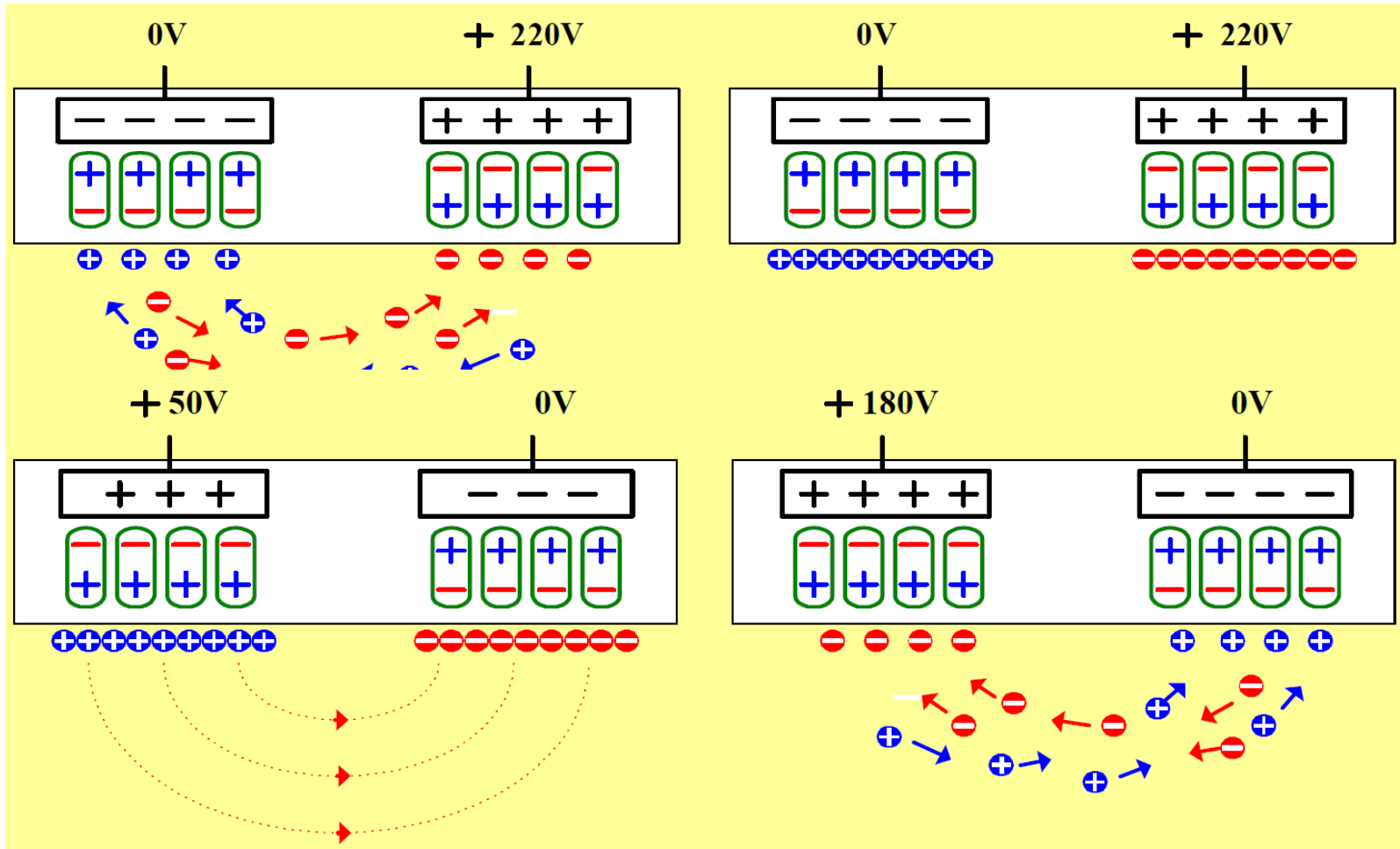
Spectrum of the different phosphors



The foundation of AC discharge

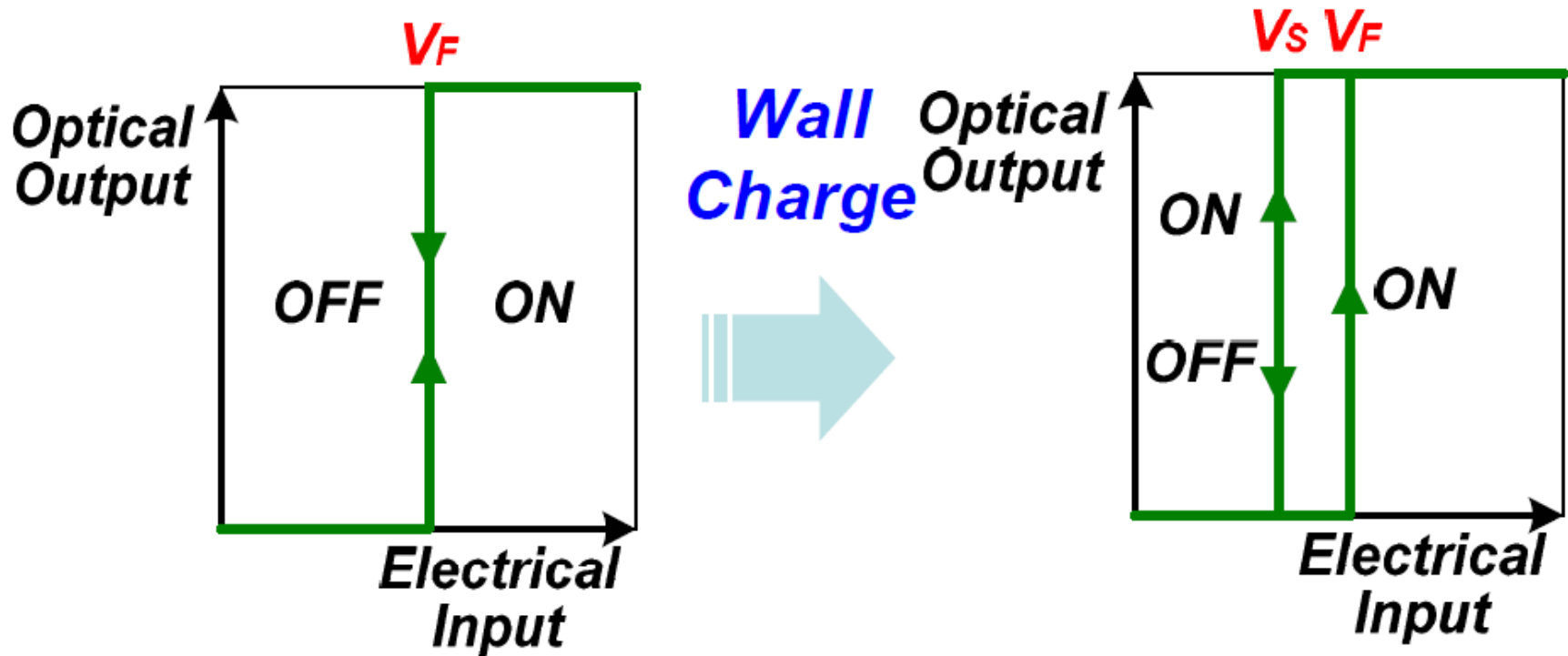


The plasma can be sustained using ac discharged



- **Wall discharge reduced the required discharge voltage**

Wall discharge reduced the required discharge voltage

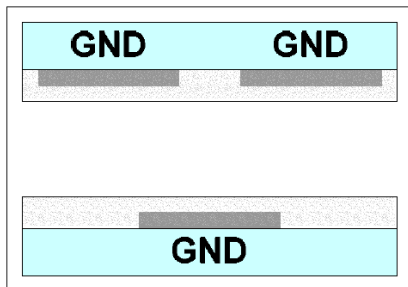


ON/OFF State Selection

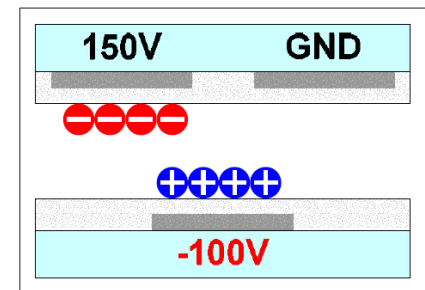
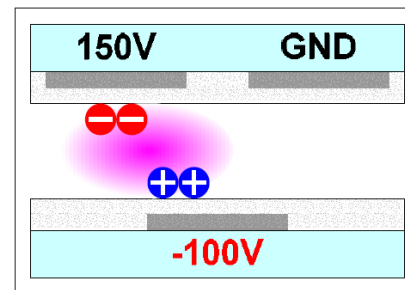
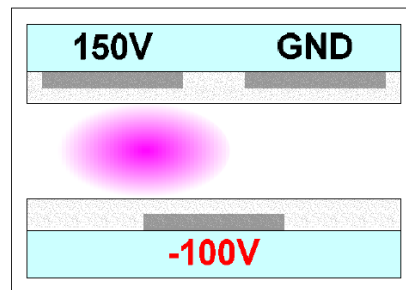


$V_F : 250V$

ON Cell



OFF Cell



(i)

(ii)

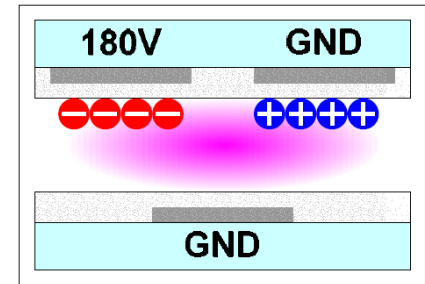
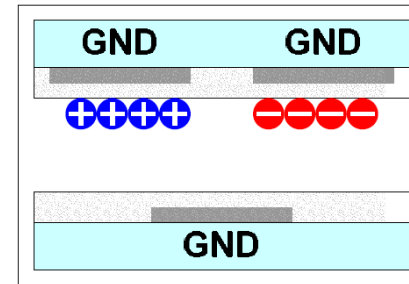
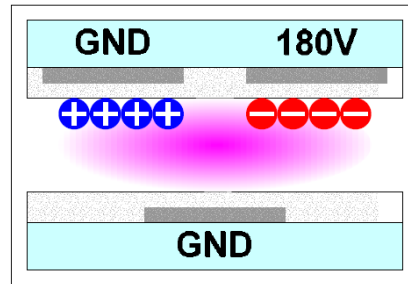
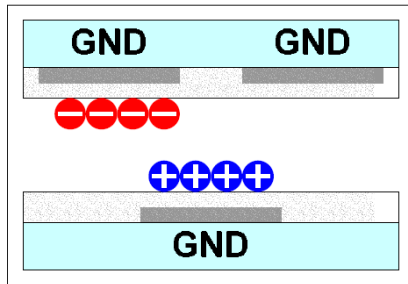
(iii)

(iv)

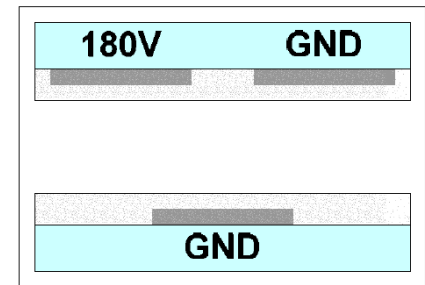
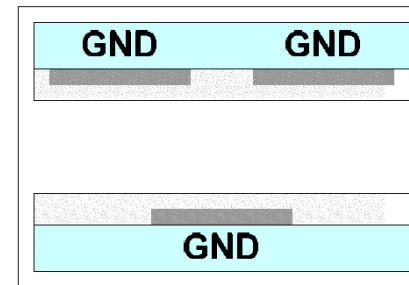
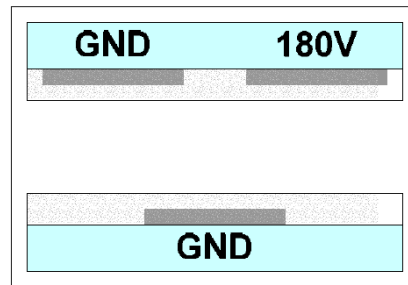
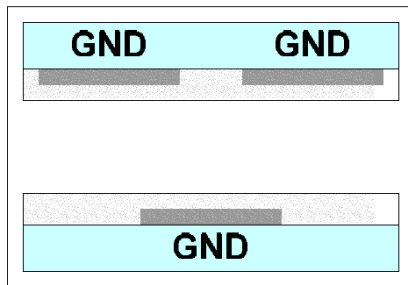
Sustain discharge



ON Cell



OFF Cell



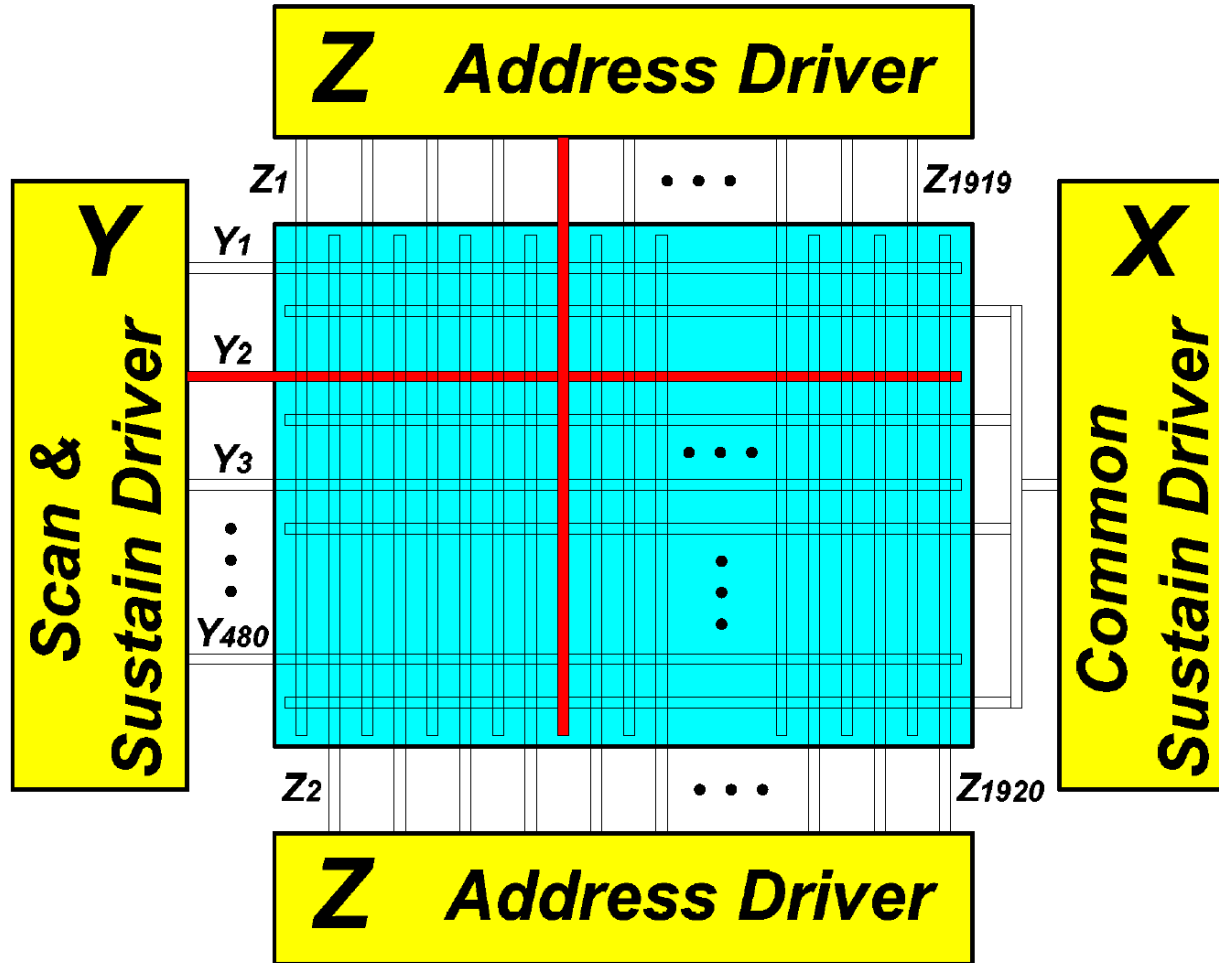
(i)

(ii)

(iii)

(iv)

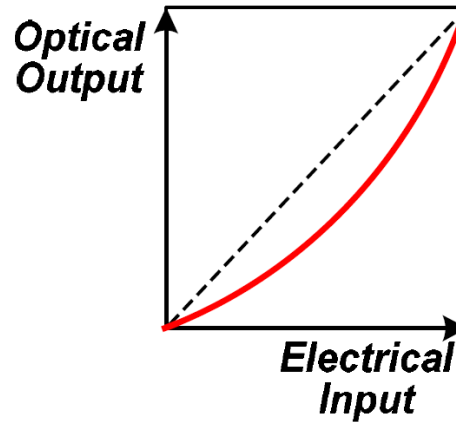
Address and sustain electrodes are connected to different drivers



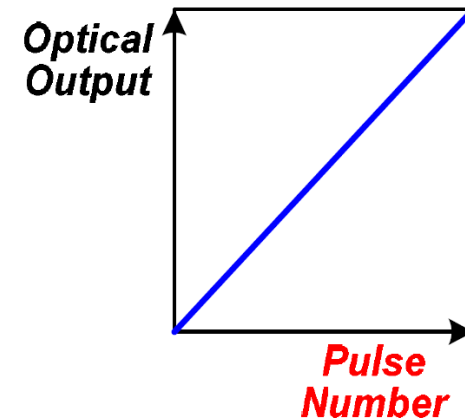
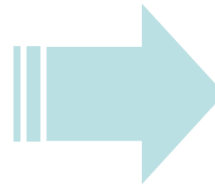
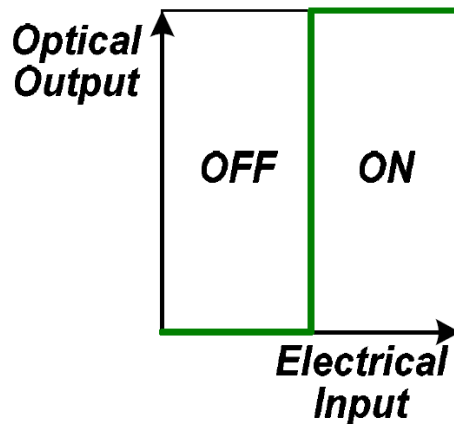
PDP pixel can only be either ON or OFF



- Cathode Ray Tube :



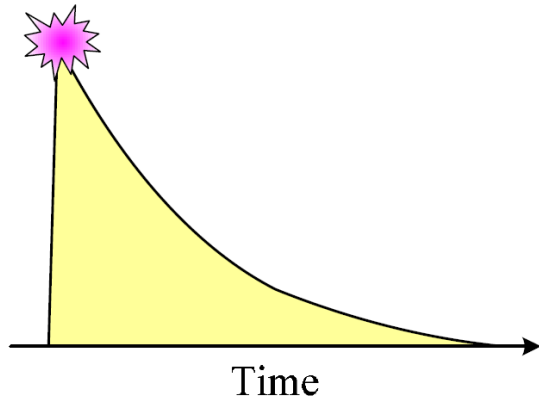
- Plasma Display Panel :



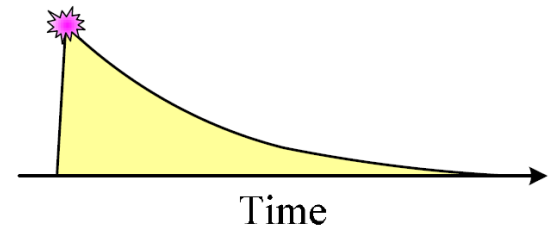
PDP luminance is controlled by using number of light pulses



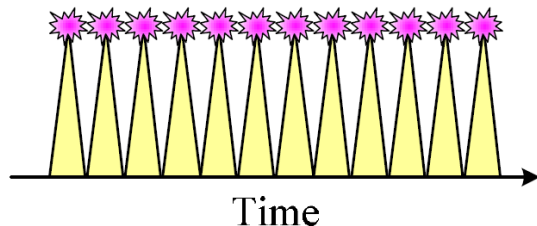
- CRT : Control the Luminance using **Electron Beam Intensity**



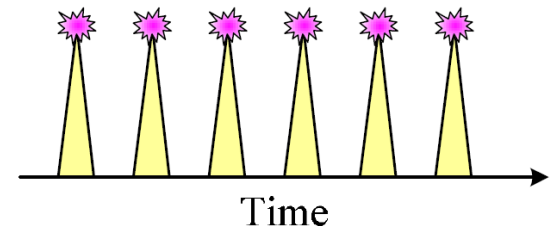
Luminance Ratio
2 : 1



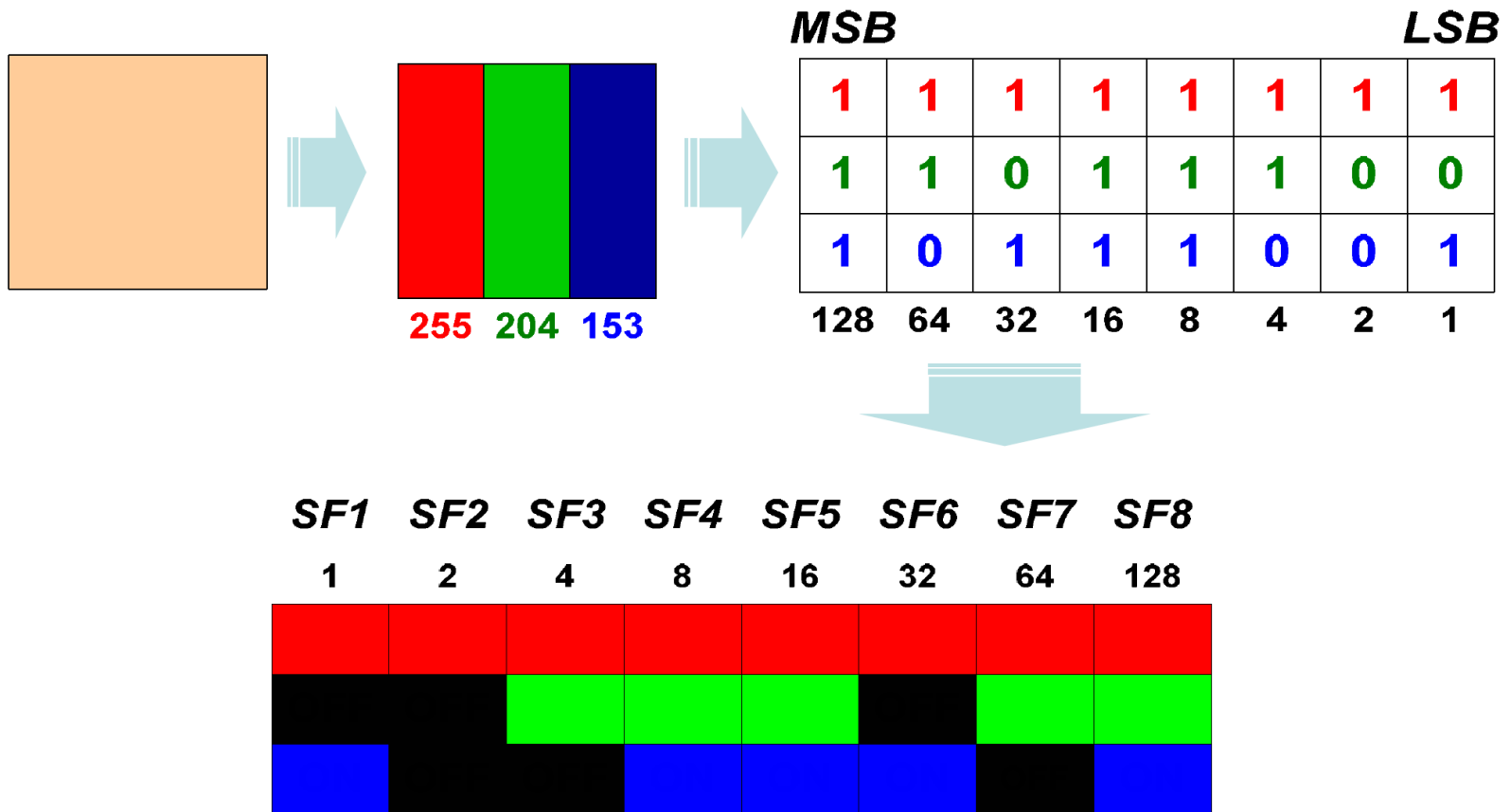
- PDP : Control the Luminance using **Number of Light Pulses**



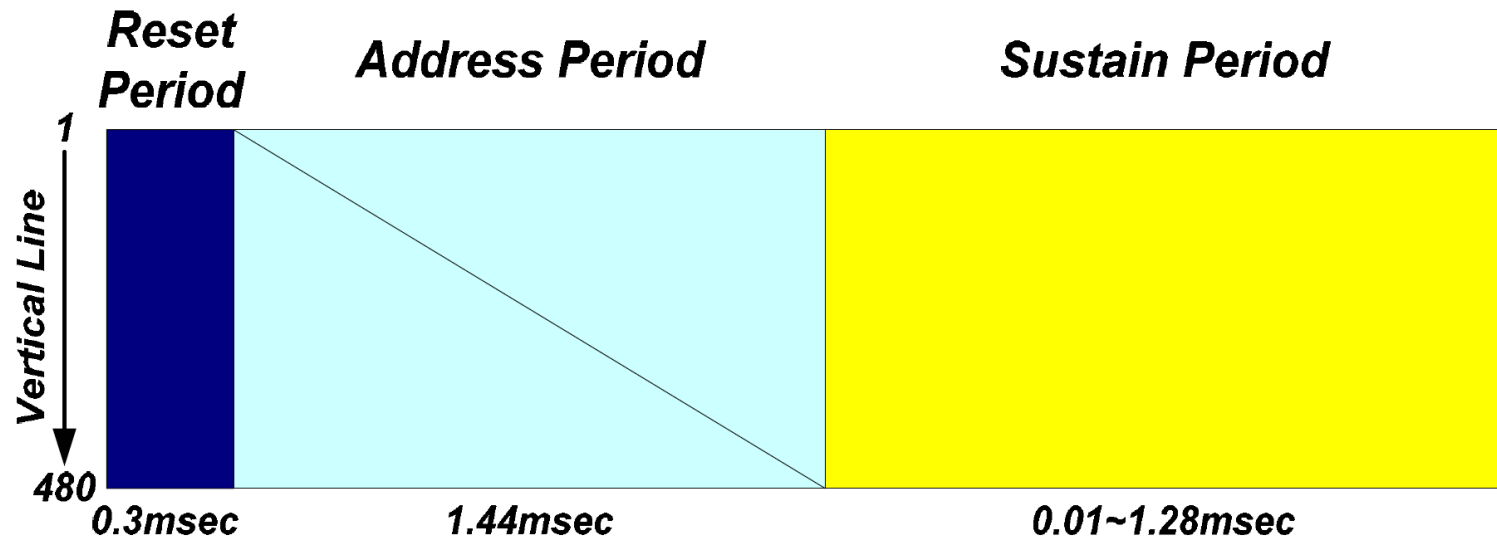
Luminance Ratio
2 : 1



A single field is divided into 8 subfield

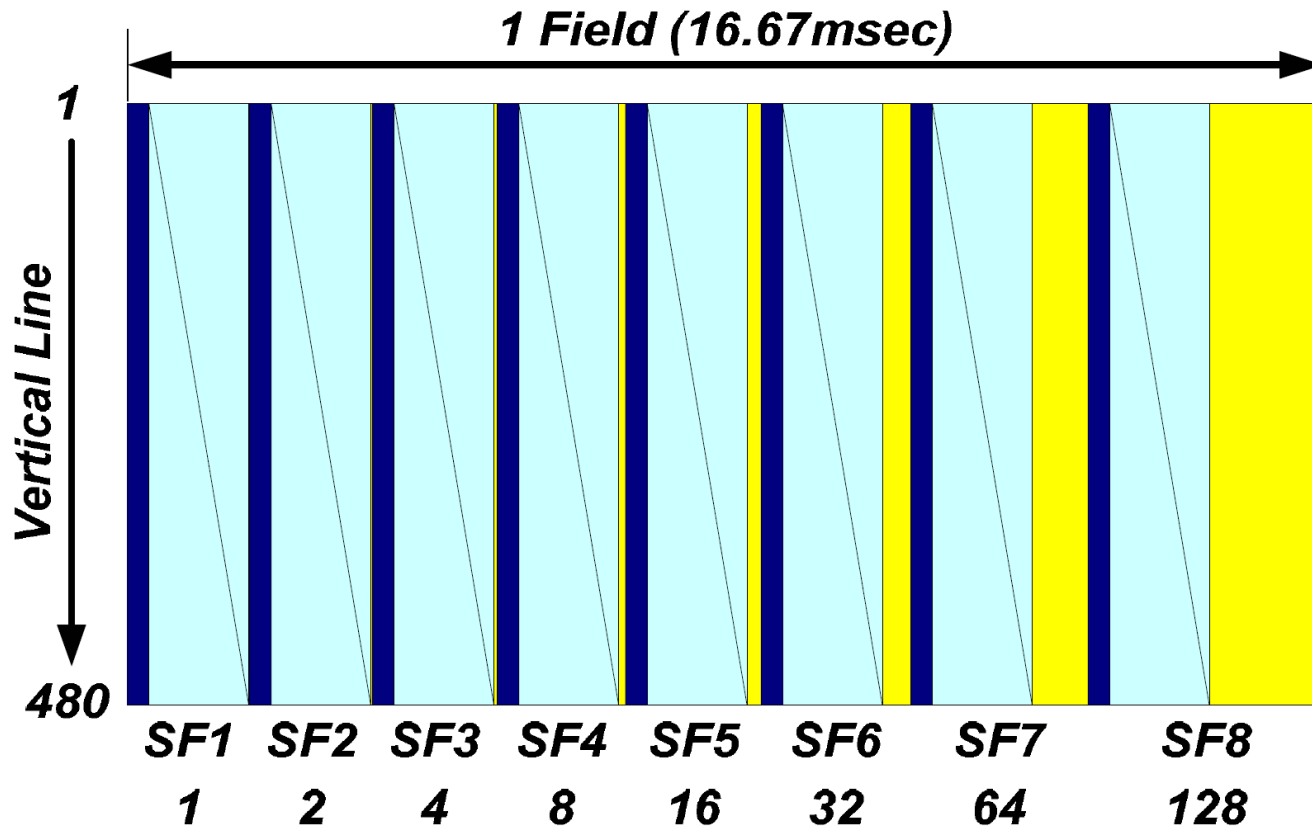


Composition of each subfield



Spec : VGA (640*480)
8 Subfield
0.03msec Address Pulse
100KHz Sustain Freq.

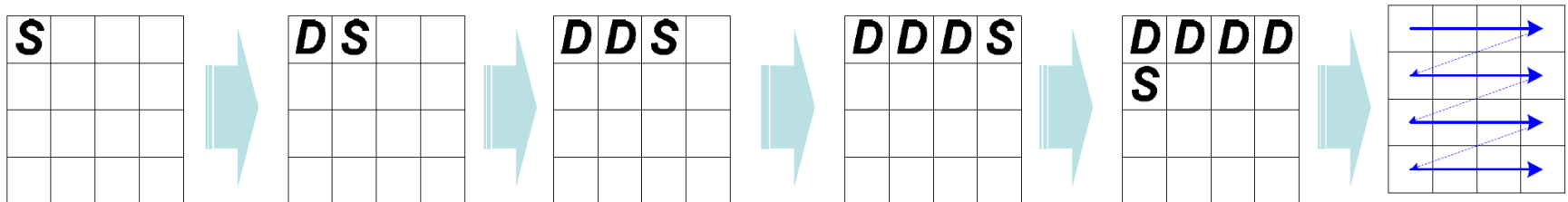
8 subfield in one TV-Field (ADS)



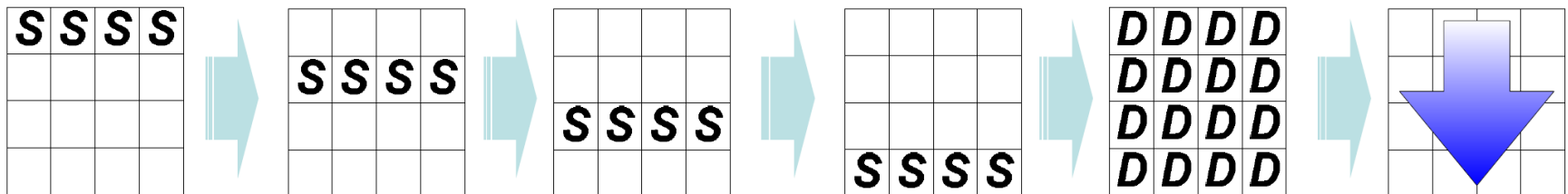
PDP uses line-by-line scanning



- Cathode Ray Tube : Cell-by-Cell Scanning



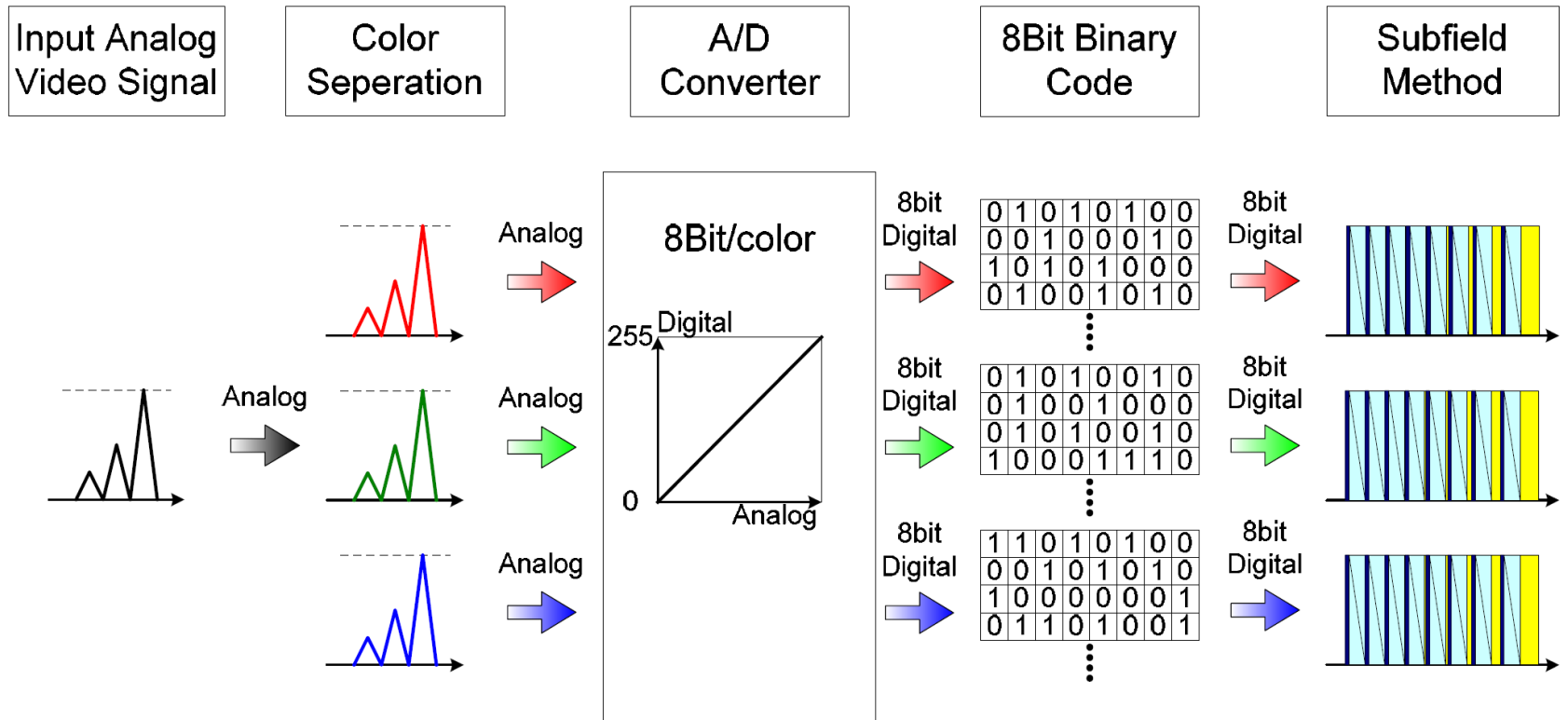
- PDP : Line-by-Line Scanning



Video signal processing



- Analog Video Signal \Rightarrow Digital Pulse Signal



Addressing period



Original Image



SF1



SF2



SF3



SF4



SF5



SF6



SF7

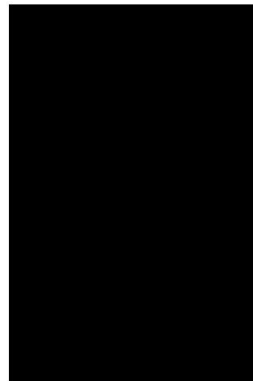


SF8

Displaying period



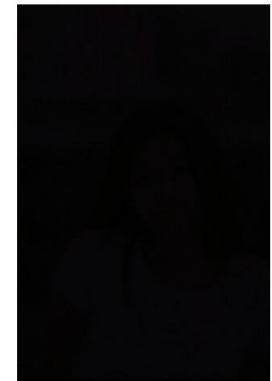
Original Image



SF1



SF2



SF3



SF4



SF5



SF6

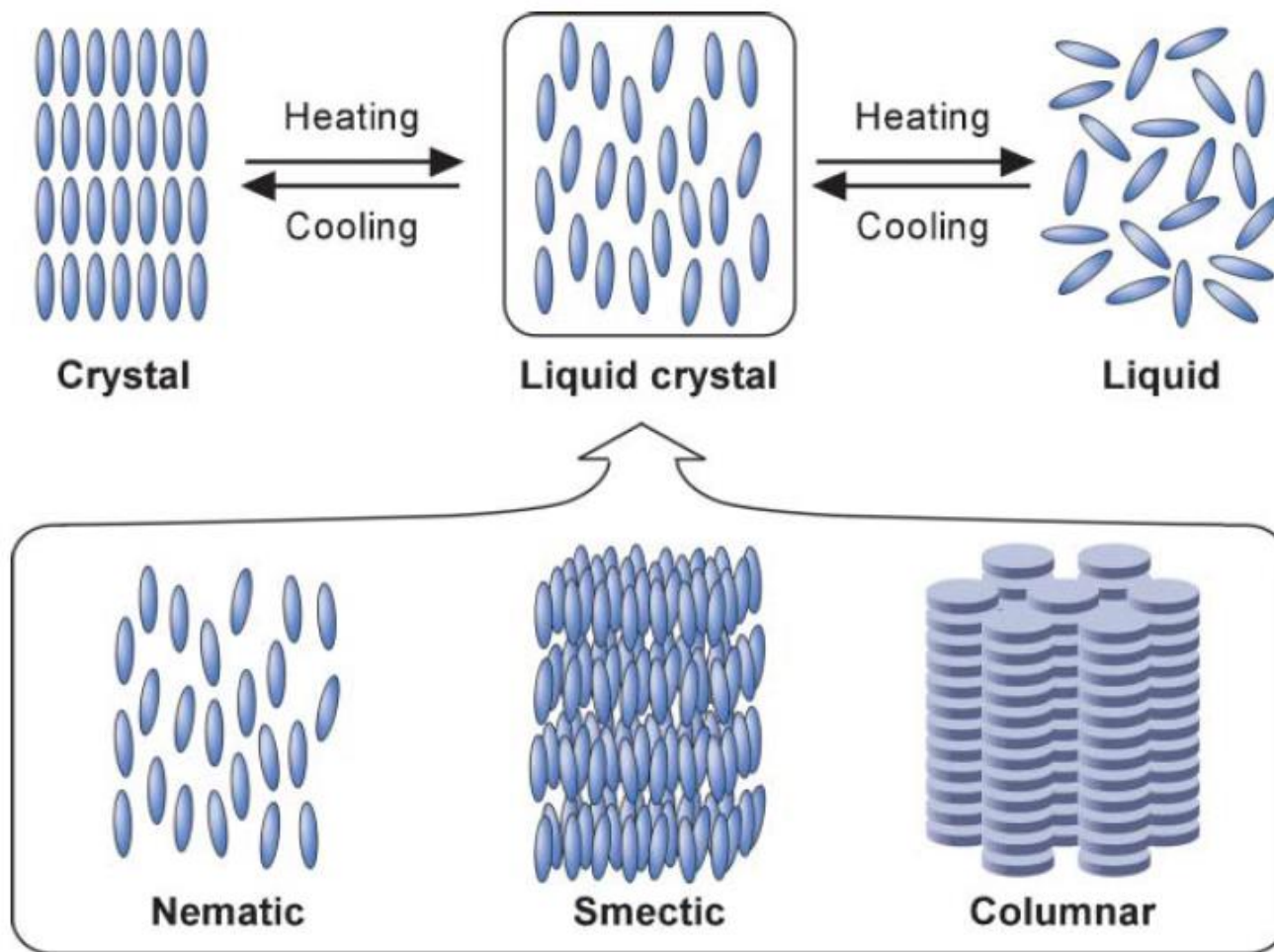


SF7

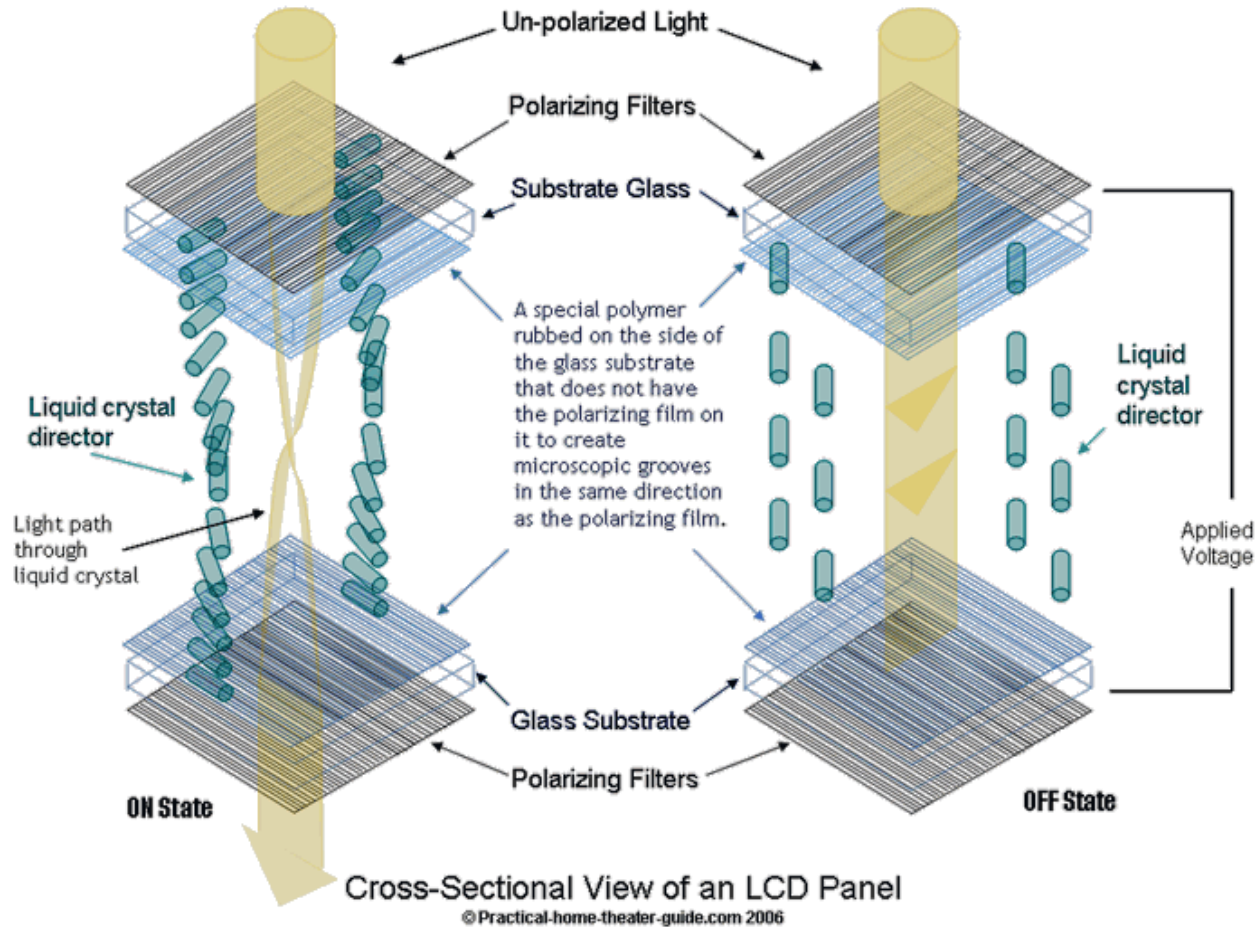


SF8

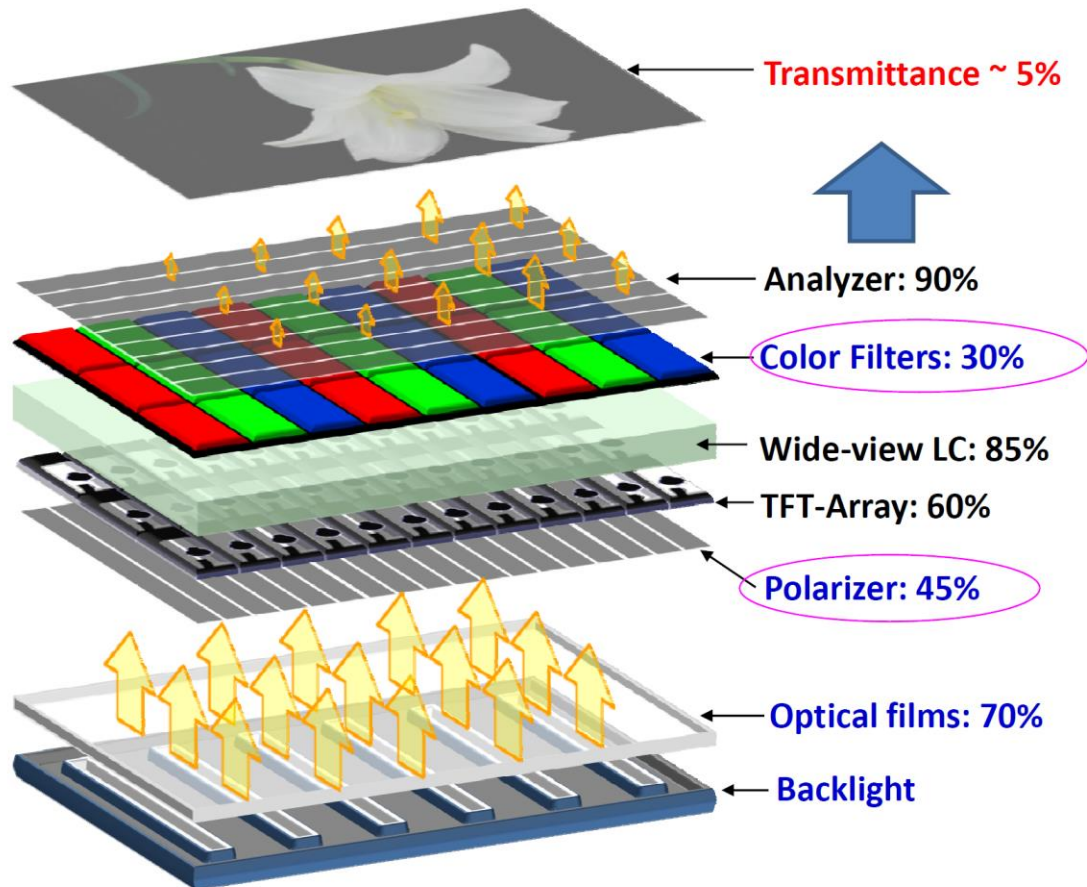
Liquid crystal are a special state of matter between liquid and crystal



Linear polarization of a light can be rotated by miss aligned liquid crystal



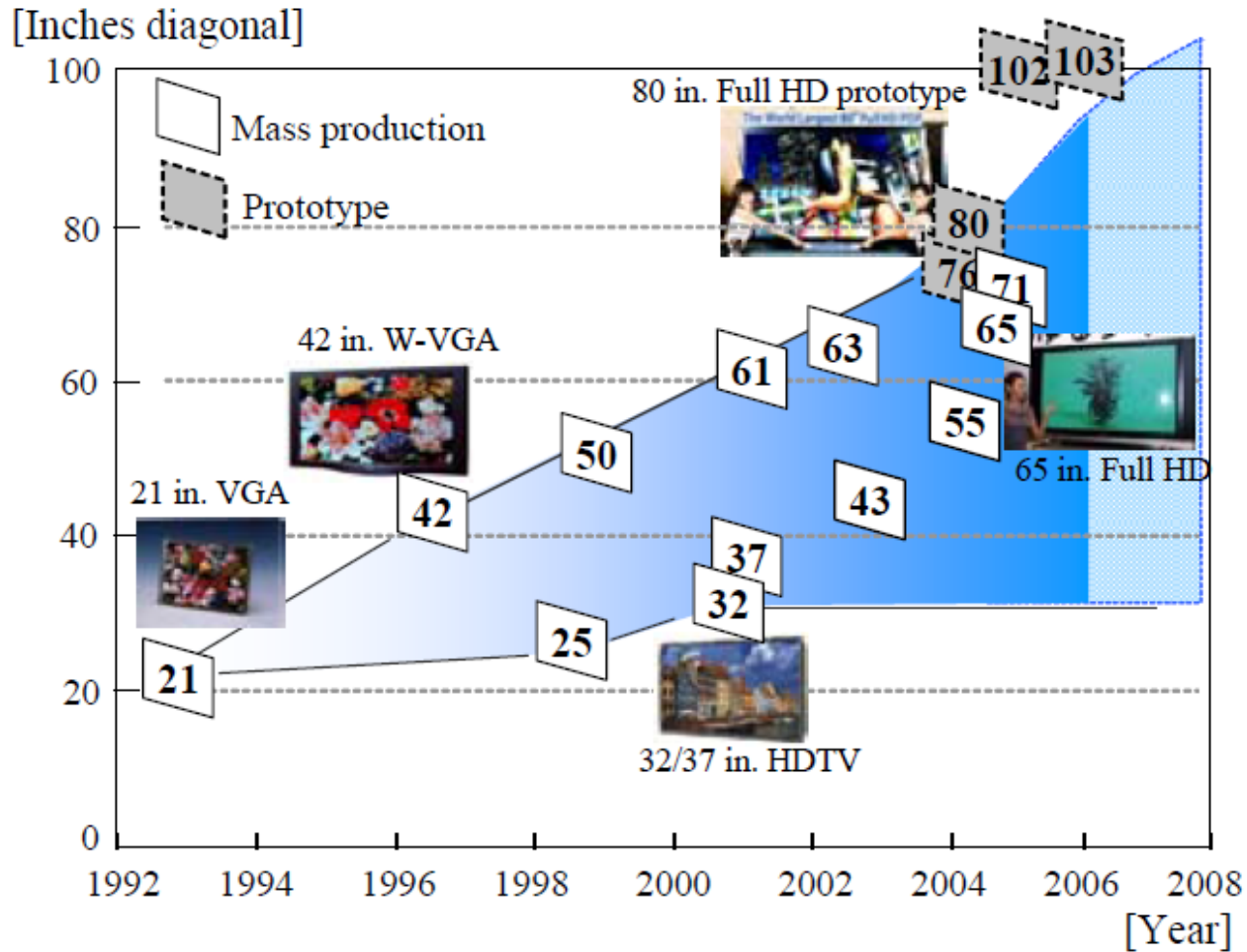
Structure of Liquid crystal display (LCD)



YB Huang, IDRC 2008

Notes from ST Wu, UCF

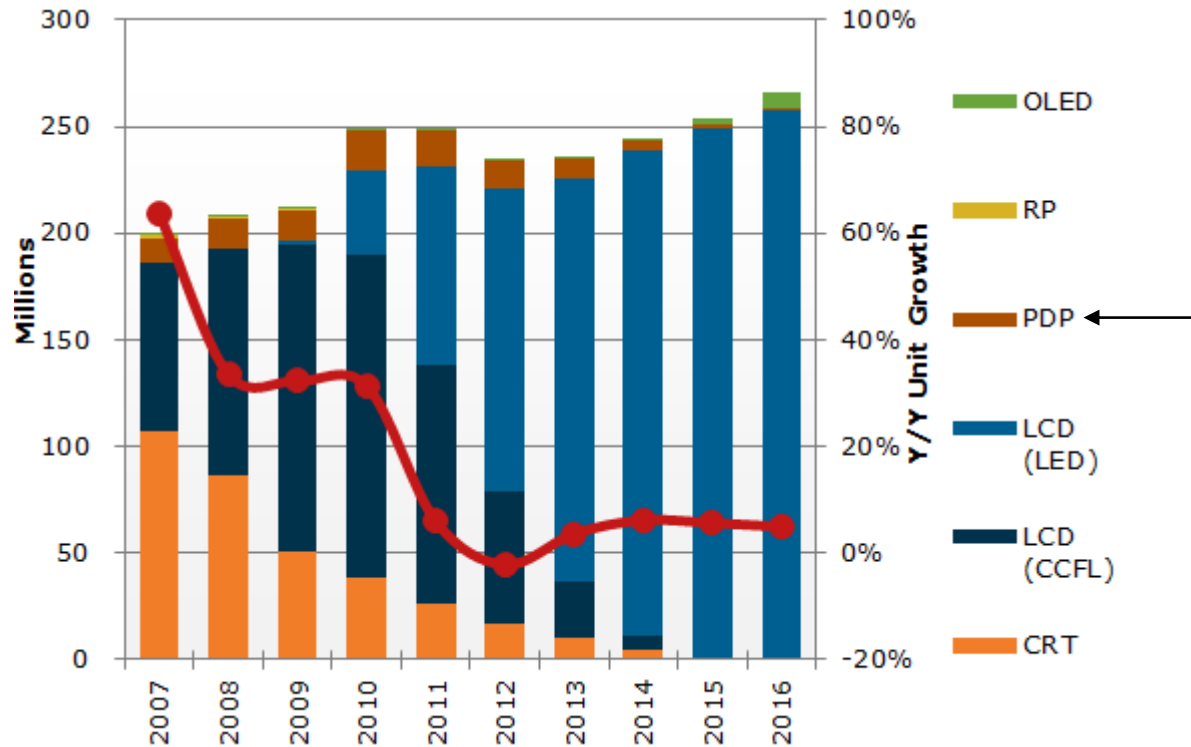
Optimistic projection of PDP market



Reality



TV Shipment Growth by Technology

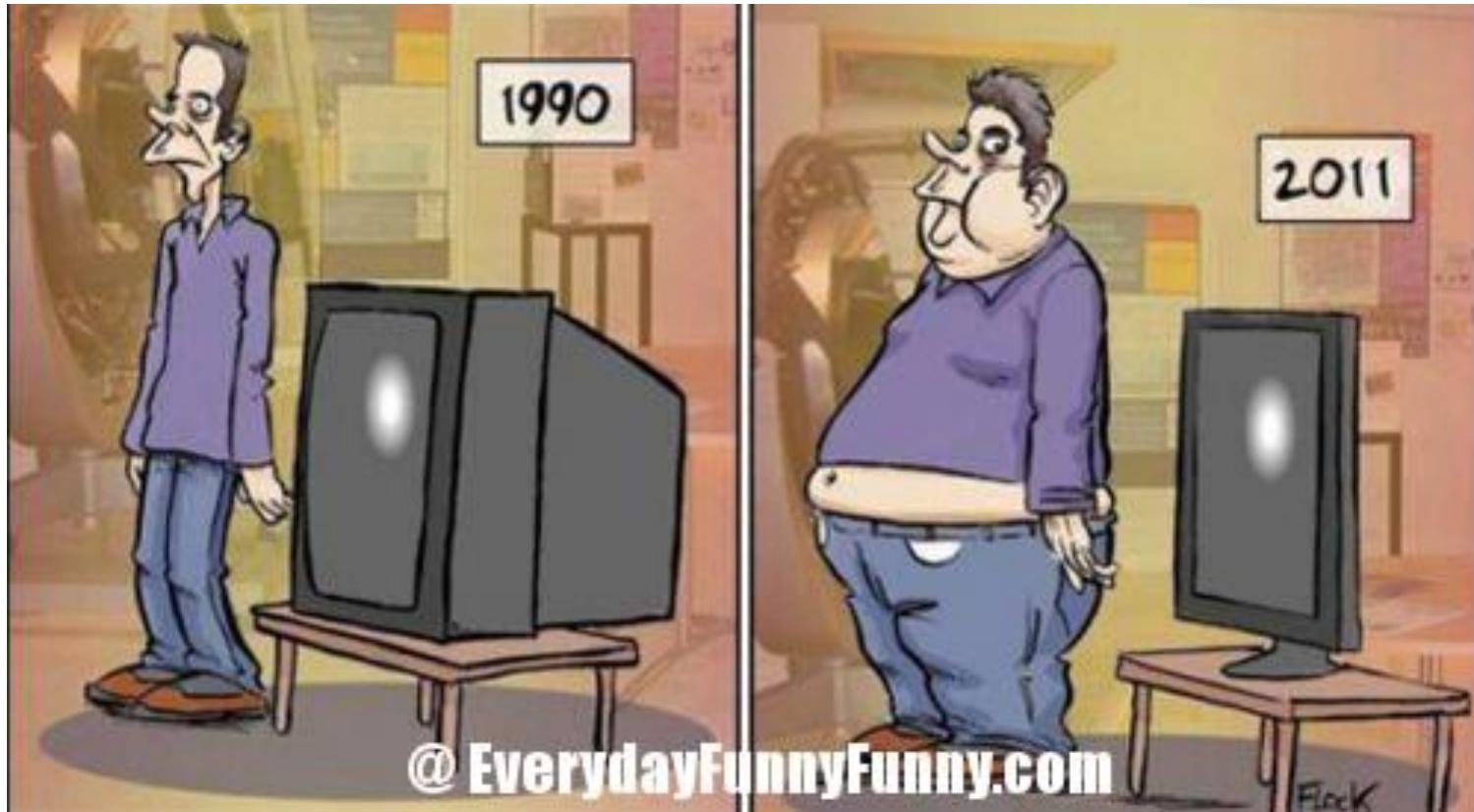


Too many reasons that PDP died!



- **Bright showroom conditions put plasmas at a distinct disadvantage versus LED-lit LCDs**
- **Aesthetics may have played a role in hastening plasma's demise**
- **UHD/4K caught on quickly**
- **Screen-size limitations also played a part in plasmas plight**
- **You can't bend a plasma**
- **Plasmas were harder to deal with than LCDs**
- **While OLED is still in the early stages of development, there's no question it offers greater potential than plasma**
- **Energy efficiency may have played a part in putting plasma out to pasture**
- **Plasma was the original flat-panel technology, People just thought of it as old technology.**
- **Projectors improved in quality and prices dropped**

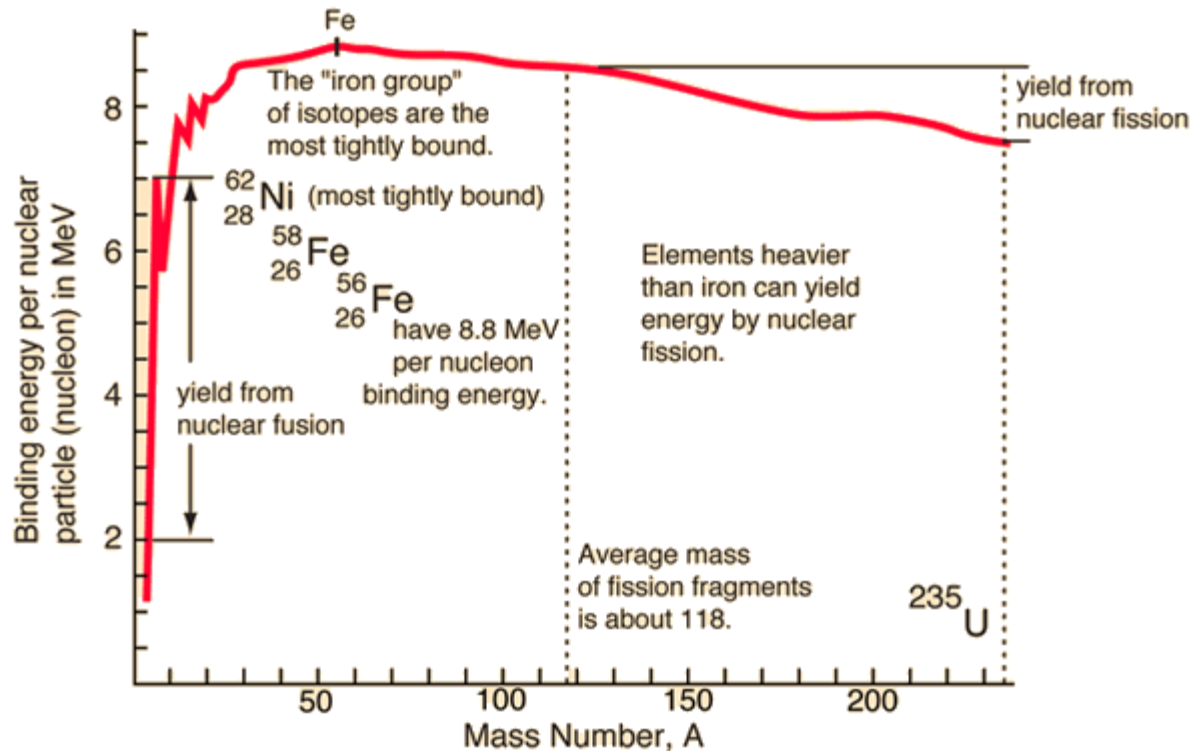
Let's stand up and do exercise!!



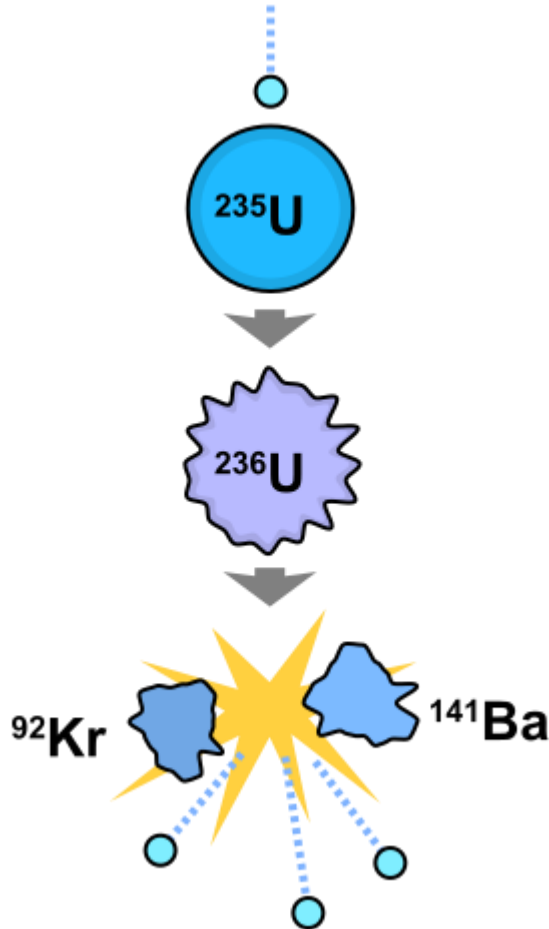
The hydrogen bomb



The “iron group” of isotopes are the most tightly bound

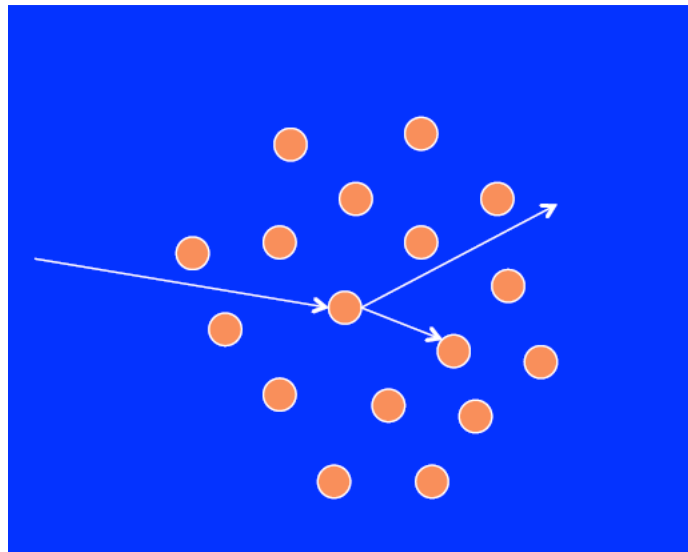


Chain reaction can happen in U^{235} fission reaction

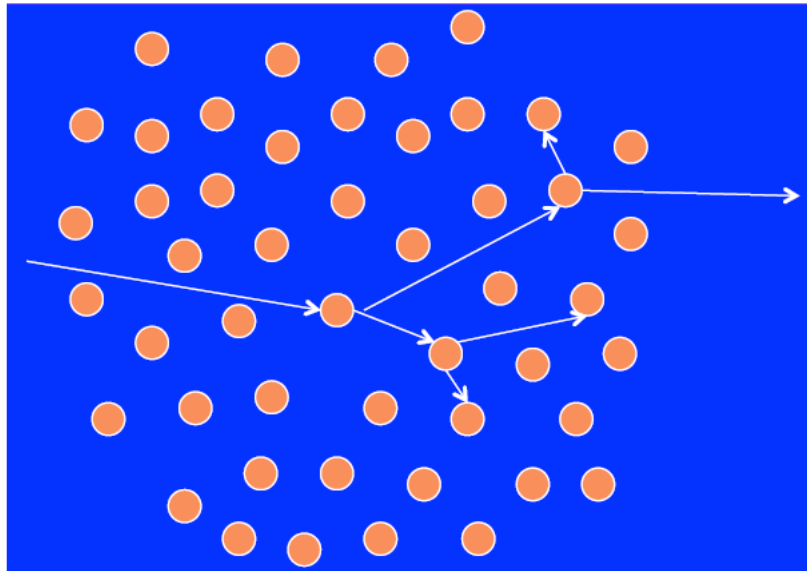


- ~ 200 million electron volts (MeV)/fission, ~million times more than chemical reactions
- Energy for bombs, or for civilian power can generate huge amounts of energy (and toxicity) in a small space with a modest amount of material
- Source of safety, security issues for nuclear power

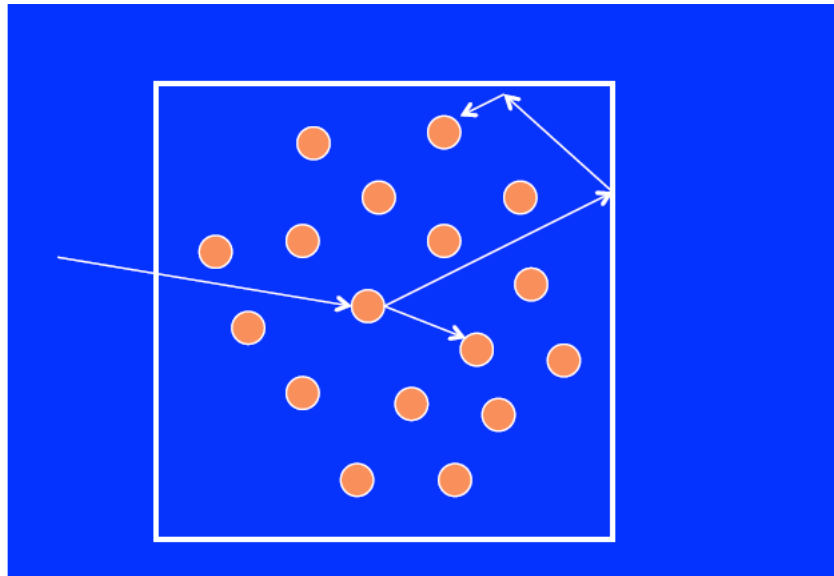
The neutrons are leaking out and stopping the chain reaction in a sub-critical mass



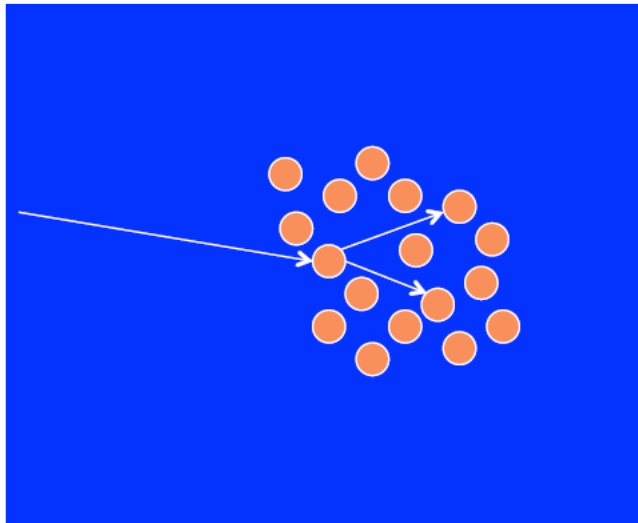
Solution 1: add more material



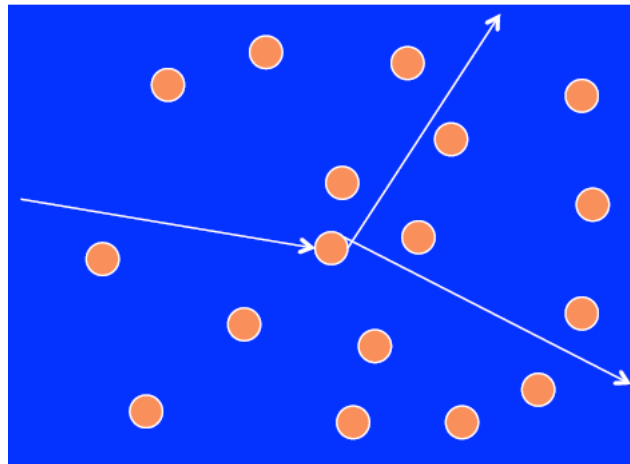
Solution2: reflect the neutron back in



Solution 3: increase the density



How to get the material together before it blows apart?

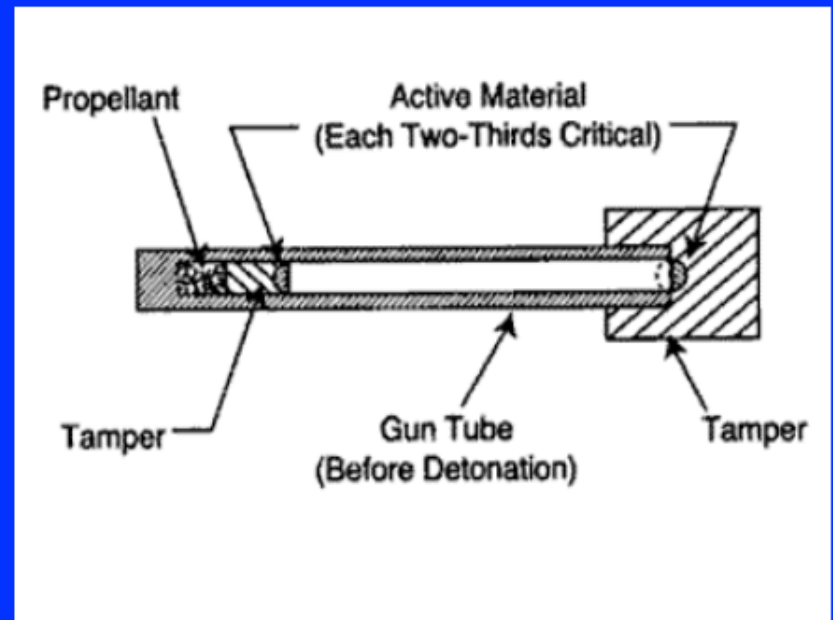


- **There are always neutrons around**
- **Once chain reaction starts, material will heat up, expand, stop reaction**
- **How to get enough material together fast enough?**

Gun-type bomb



- **Simple, reliable – can be built without testing**
- **Highly inefficient – require lots of nuclear material (50-60 kg of 90% enriched HEU)**
- **Can only get high yield with HEU, not plutonium**
- **Hiroshima bomb: cannon that fired HEU projectile into HEU target**

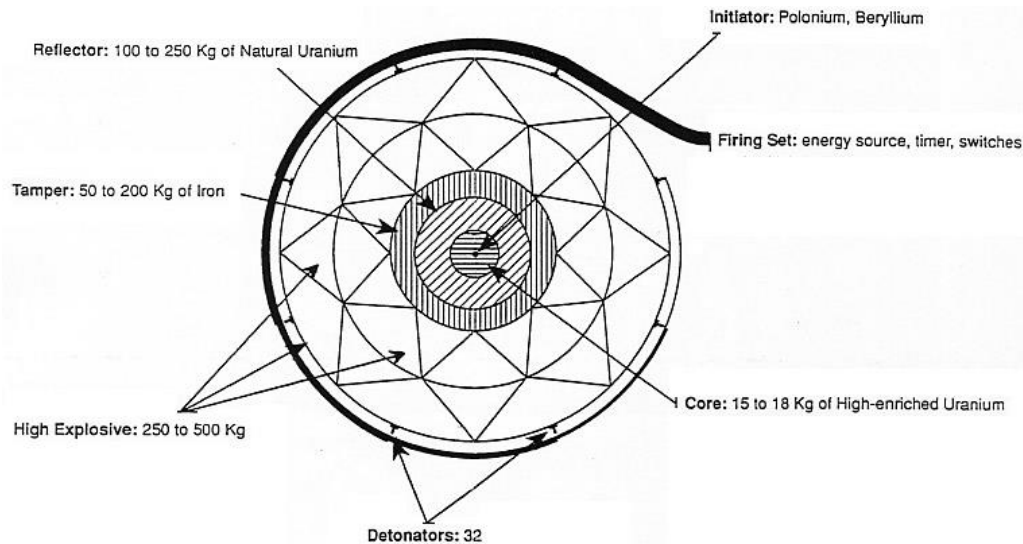


Source: NATO

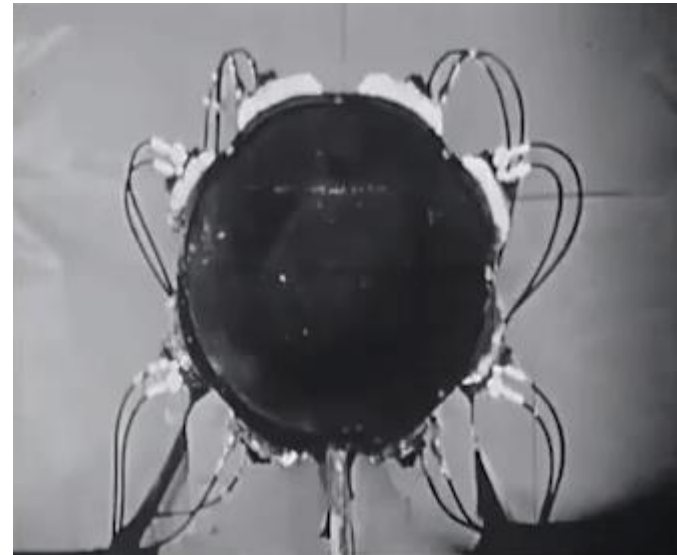
Implosion design



- A schematic diagram of an implosion bomb



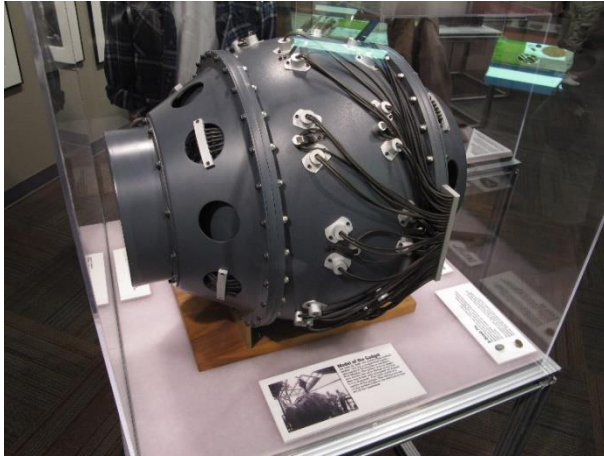
- Small-scale slow-motion cross-section of a shaped charge implosion design



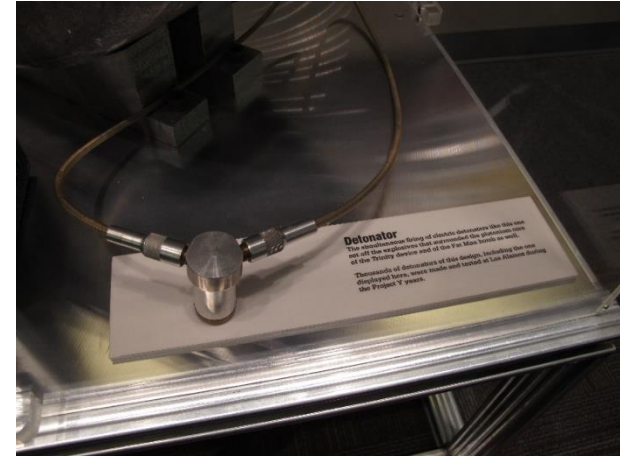
The 1st nuclear bomb: Trinity (Bradbury Science Museum)



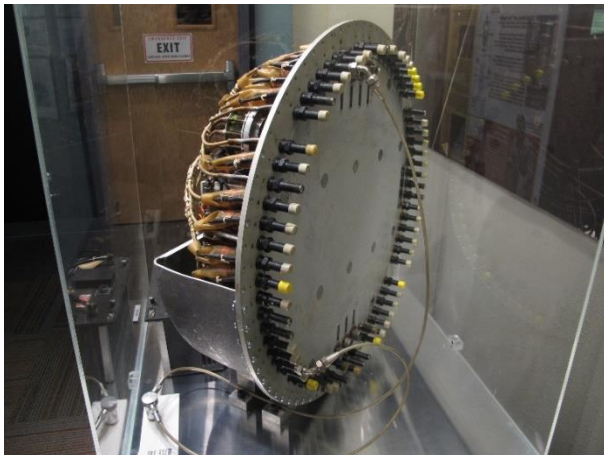
- **Model of the Trinity Gadget**



- **Project Y Atomic Bomb Detonator System**



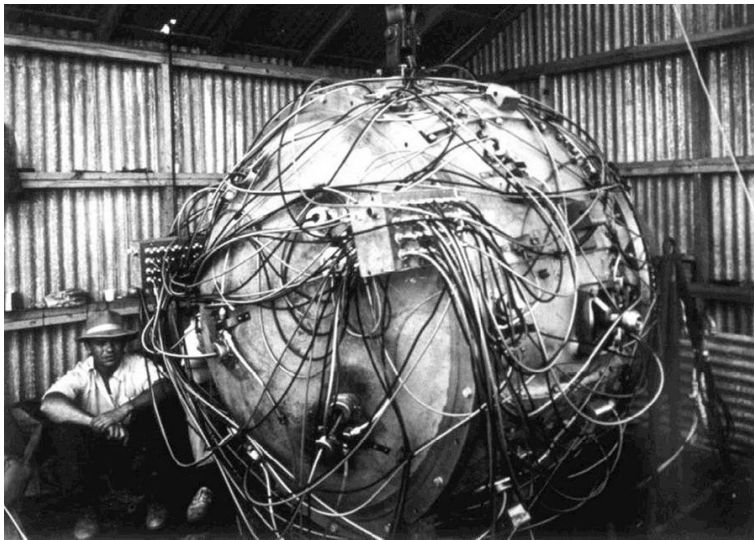
- **Project Y Atomic Bomb Detonator System**



- **Project Y Atomic Bomb Detonator System Spark Gap Switch**

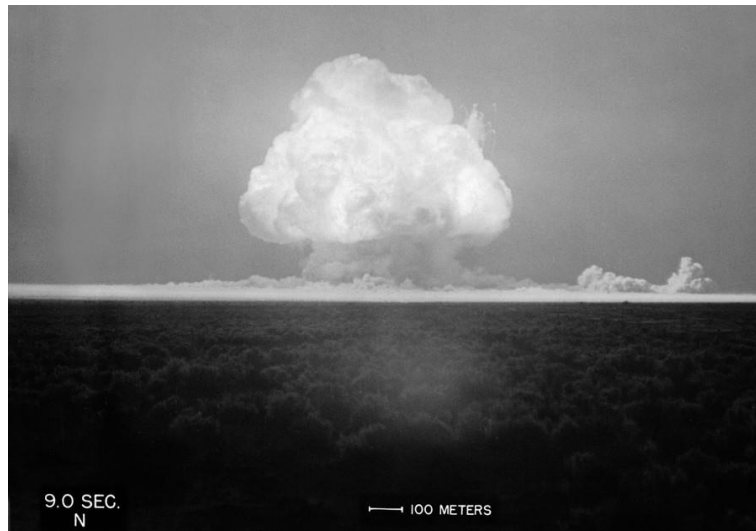
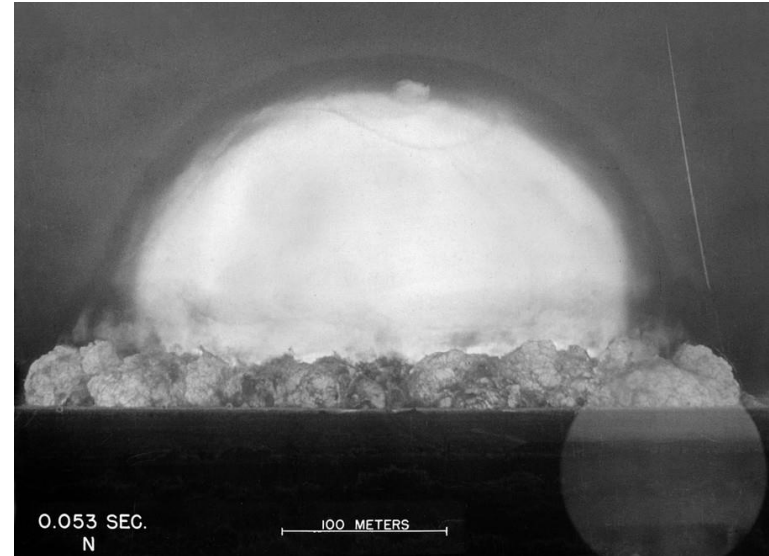
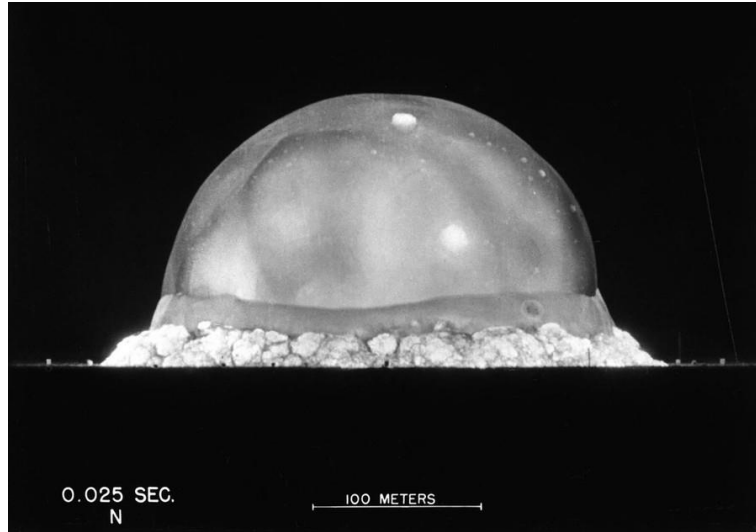


The 1st nuclear bomb: Trinity



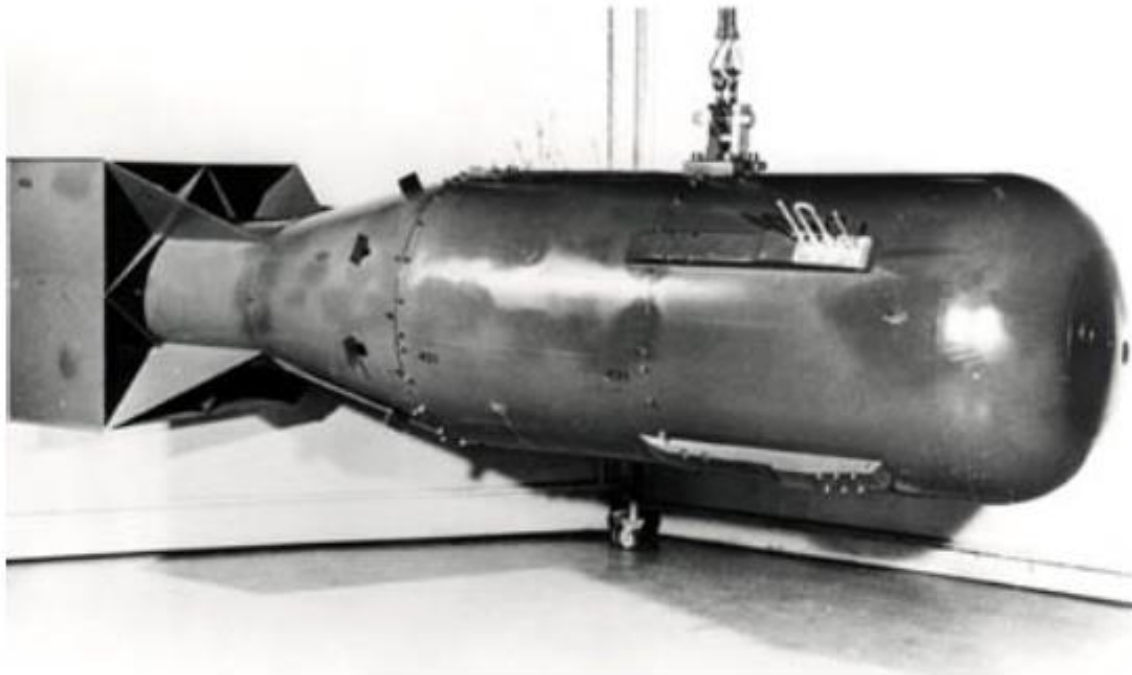
<https://www.theatlantic.com/photo/2015/07/70-years-since-trinity-when-we-tested-nuclear-bombs/398735/>
https://saddlebagnotes.com/arts-and-leisure/tucson-seismographs-detected-first-nuclear-test-at-trinity-n-m/article_b01c5b20-f6fb-11eb-a221-6327df2feaeb.html

Trinity explosion on July 16, 1945



<https://www.theatlantic.com/photo/2015/07/70-years-since-trinity-when-we-tested-nuclear-bombs/398735/>
https://en.wikipedia.org/wiki/Trinity_%28nuclear_test%29

Hiroshima Bomb – “Little Boy”



Gun Type – Easiest to design and build (Hiroshima bomb was never tested)

About 13 kiloton explosive yield

Atomic bomb is very destructive



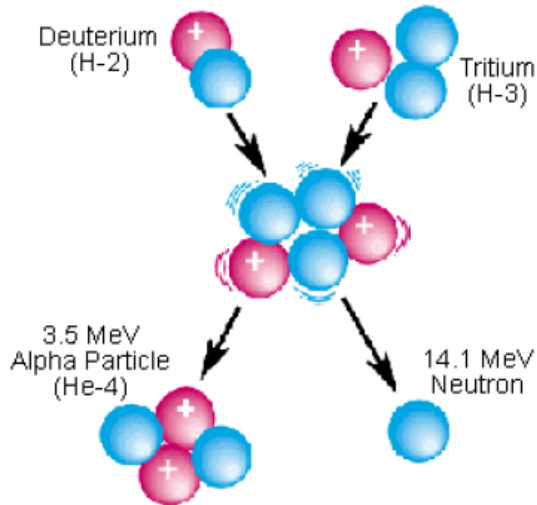
Hiroshima: August 6, 1945



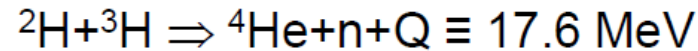
Nagasaki: August 9, 1945



The fusion process

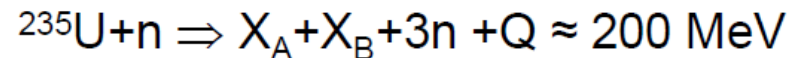
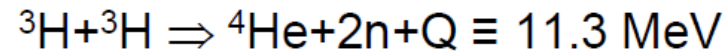
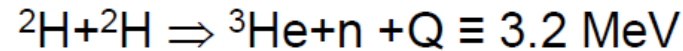
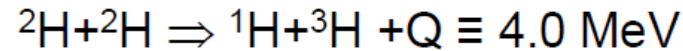


Deuterium-Tritium Fusion Reaction



Energy release $Q=17.6 \text{ MeV}$

In comparison



Fusionable Material, deuterium ${}^2\text{H}$ (D) and tritium ${}^3\text{H}$ (t):

Deuterium: natural occurrence (heavy water) (0.015%).

Tritium: natural occurrence in atmosphere through cosmic ray bombardment; radioactive with $T_{1/2}=12.3 \text{ y}$.

“Advantages” of hydrogen bomb



$$\text{Fusion of } ^2\text{H} + ^3\text{H}: \quad \frac{Q}{A} = \frac{17.6 \text{ MeV}}{(3 + 2) \text{ amu}} = 3.5 \frac{\text{MeV}}{\text{amu}}$$

$$\text{Fission of } ^{235}\text{U}: \quad \frac{Q}{A} = \frac{200 \text{ MeV}}{236 \text{ amu}} = 0.85 \frac{\text{MeV}}{\text{amu}}$$

Fusion is 4 times more powerful than fission
and generates 24 times more neutrons!

$$\text{Neutron production:} \quad ^2\text{H} + ^3\text{H} : \quad \frac{n}{A} = \frac{1}{5} = 0.2$$

$$^{235}\text{U} + n : \quad \frac{n}{A} = \frac{2}{236} = 0.0085$$

Hydrogen bomb uses a fission bomb to initiate the fusion reaction



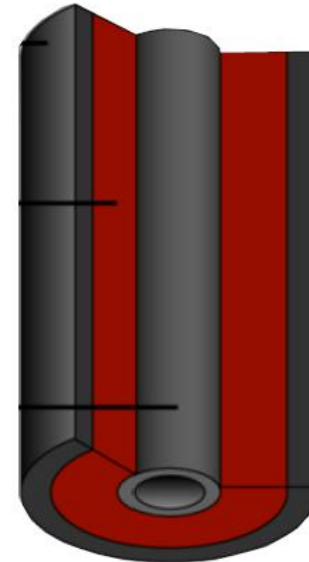
Primary Fission Device

Core: ^{239}Pu , ^{235}U ,
plus $^2\text{H}+^3\text{H}$ booster

Shell: ^{238}U tamper

High explosive lenses

Fuel



Secondary Fusion Device

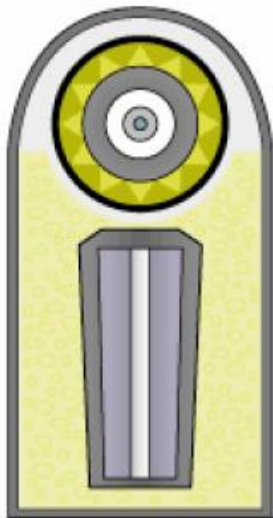
Radiation channel

^{239}Pu sparkplug

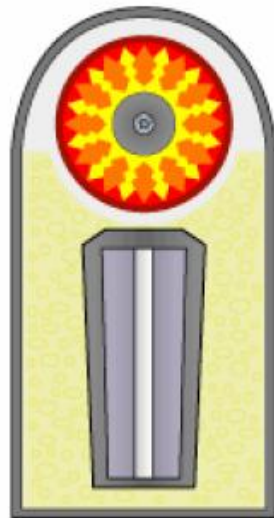
^6Li , ^2H , ^3H fusion cell

^{238}U tamper

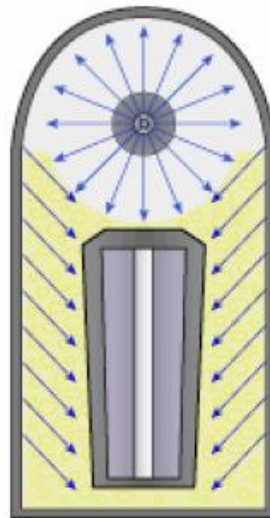
Event sequence



1. Warhead before firing; primary (fission bomb) at top, secondary (fusion fuel) at bottom, all suspended in polystyrene foam.



2. HE fires in primary, compressing plutonium core into supercriticality and beginning a fission reaction.



3. Fissioning primary emits X-rays which reflect along the inside of the casing, irradiating the polystyrene foam.



4. Polystyrene foam becomes plasma, compressing secondary, and plutonium sparkplug begins to fission.



5. Compressed and heated, lithium-6 deuteride fuel begins fusion reaction, neutron flux causes tamper to fission. A fireball is starting to form...

Additional pressure from recoil of exploding shell (ablation)!

You don't want to build a hydrogen bomb!

